

**FIRST
PRINCIPLES
MODELLING
FOR THE PREDICTION OF
THE STRUCTURE AND
THE SPECTROSCOPIC
RESPONSE OF MOLECULAR
MATERIALS**

**DARIA RUTH
GALIMBERTI**
ciclo 28°

Relatore
Dott. MILANI ALBERTO
Tutor e Coordinatore
**Prof. CASTIGLIONI
CHIARA**



POLITECNICO DI MILANO
Dipartimento di Chimica, Materiali, Ing. Chimica "Giulio Natta"
Scuola di Dottorato in Ingegneria dei Materiali

**FIRST
PRINCIPLES
MODELLING
FOR THE PREDICTION OF
THE STRUCTURE AND
THE SPECTROSCOPIC
RESPONSE OF MOLECULAR
MATERIALS**

**DARIA RUTH
GALIMBERTI**
ciclo 28°

Relatore
Dott. MILANI ALBERTO
Tutor e Coordinatore
**Prof. CASTIGLIONI
CHIARA**



POLITECNICO DI MILANO
Dipartimento di Chimica, Materiali, Ing. Chimica "Giulio Natta"
Scuola di Dottorato in Ingegneria dei Materiali

Contents

1	Introduction	1
2	Periodic DFT calculations of the structures and of the spectroscopic response of semicrystalline polymers	5
2.0	Introduction.....	5
2.1	The polymorphism of even Nylon: a subtle interplay between intra- and inter-molecular effects.....	7
	<i>Polymorphism of even nylons revisited through periodic quantum chemical calculations</i> D. Galimberti, C. Quarti and A. Milani <i>Polymer</i> . 67 (2015) 167	
2.2	Crystal structure and spectroscopic assignment of Poly(trimethylene terephthalate)-PTT.....	9
	<i>Crystal Structure and Vibrational Spectra of Poly(trimethylene terephthalate) from Periodic Density Functional Theory Calculations</i> D. Galimberti and A. Milani <i>J. Phys. Chem. B</i> . 118 (2014) 1954	
2.3	$\alpha \rightarrow \beta$ polymorphic transition in Poly(butylene terephthalate): a spectroscopy study.....	11
	<i>Polymorphism of Poly(butylene terephthalate) Investigated by Means of Periodic Density Functional Theory Calculations</i> A. Milani and D. Galimberti <i>Macromolecules</i> . 47 (2014) 1046	
2.4	Crystal Field effects on the spectroscopic properties: the polyethylene test case.....	13
	<i>Modulation of the infrared absorption intensities in solid state. Role of weak intermolecular interactions in the Polyethylene crystal: a computational DFT investigation</i> D. Galimberti, A. Milani and C. Castiglioni -To be submitted	
2.5	Summary and Conclusions.....	15
	Bibliography.....	16
3	Investigating charge distribution and charge mobility from IR intensity parameters: new models and applications	19
3.0	Introduction.....	19
3.1	Deriving the charge fluxes from the second derivatives of the molecular dipole.....	25
	<i>Charge mobility in molecules: Charge fluxes from second derivatives of the molecular dipole</i> D. Galimberti, A. Milani, and C. Castiglioni <i>J. Chem. Phys.</i> 138 (2013) 164115	

3.2	Extension of the model to interacting molecules: hydrogen-bonding interactions.....	27
	<i>Infrared intensities and charge mobility in hydrogen bonded complexes</i> D. Galimberti, A. Milani and C. Castiglioni <i>J. Chem. Phys.</i> 139 (2013) 074304	
3.3	Summary and Conclusions.....	29
	Bibliography.....	30
4	First-Principles molecular dynamics simulations for the prediction of the structure and vibrational spectra of complex systems	35
4.0	Introduction.....	35
4.1	Static vs dynamic DFT prediction of IR spectra of flexible molecules in condensed phase: the (CICF ₂ CF(CF ₃)OCF ₂ CH ₃) molecule as a test case.....	39
	<i>Static vs dynamic DFT prediction of IR spectra of flexible molecules in condensed phase: the (CICF₂CF(CF₃)OCF₂CH₃) molecule as a test case</i> D. Galimberti, A. Milani, M.P. Gaigeot, S. Radice, C. Tonelli, R. Picozzi, C. Castiglioni - <i>To be submitted</i>	
4.2	Combining static and dynamic approaches for the determination of the infrared absorption intensities.....	41
	4.2.0 Introduction.....	41
	4.2.1 Theory.....	43
	4.2.2 Results.....	49
	4.2.3 Band assignment.....	57
	4.2.4 Conclusions.....	60
4.3	Applying FPMD to crystalline polymers: the PE test case.....	63
	4.3.0 Introduction.....	63
	4.3.1 Computational details.....	64
	4.3.2 NVT equilibration with 300Ry plane wave basis set.....	65
	4.3.3 NVT equilibration with 600Ry plane wave basis set.....	71
	4.3.4 NpT equilibration.....	74
	4.3.5 Conclusions and future perspectives.....	75
4.4	Summary and Conclusions.....	79
	Bibliography.....	80
5	Conclusions	85

Chapter 1

Introduction

Molecular and polymeric materials are now an unavoidable ingredient of the everyday life, playing a major role in building our world as we know it. Despite their so well-assessed employments, pure and applied research and technology are still focusing deeply on polymers, providing innovative applications in several fields, ranging from nanotechnology to design, from physics to biomedicine. The development of novel systems is indeed extremely active, as continuously demonstrated by the scientific literature and by new relevant industrial outcomes.

The molecular nature is a common characteristic of this wide family of materials and determines a close correlation between the properties of the materials - at the macroscopic scale - and the material structure at the atomic, mesoscopic and microscopic scale. The macroscopic properties exploited in applications, such as for example the elastic modulus, the transition temperatures, the optical behaviour etc. can be rationalized based on intramolecular effects (e.g. chemical constitution, configuration and conformation of the chains...) and supramolecular phenomena (e.g. specific interactions between chains or macromolecular domains, morphology and solid state packing).

Meaningful examples in this context are polymorphism phenomena, particularly relevant in polymeric materials: they originate from competitive or cooperative intra- and intermolecular effects which can induce different crystalline forms associated to different macroscopic properties for the same material. Such a modulation of the materials response as a function of the molecular structure, i.e. structure-properties correlations, is at the foundations of the whole materials science and has obvious consequences in technological applications.

The close dependence of the properties from the phenomena occurring at the molecular scale allows, in principle, to tune the macroscopic behaviour through a rational design of the nano, micro and mesoscopic structure. Acting on these scales requires a deep knowledge of the molecular and supramolecular architecture of the material and how this architecture can affect the physicochemical properties. Therefore, an investigation at the molecular scale becomes crucial in the development of new nanostructured molecular materials (such as for example polymeric nanofibers, nanocomposites, hybrid organic-inorganic or biomaterials) and requires appropriate characterization techniques.

Both XRD (X-Ray Diffraction) and vibrational spectroscopy techniques have been widely adopted for polymers: IR and Raman spectroscopies have always been used and proved to be very powerful characterization tools for molecular and polymer materials, demonstrating why their use is now widespread also in the industrial environments. Their relevance is not limited to analytical measurements but they have been also used to get information on the whole

architecture of the material and to shed light on the molecular phenomena that rule its behaviour, usually in connection with technological applications. Indeed, the spectra recorded are particularly sensitive to all the subtle intra and intermolecular phenomena.

The impact of vibrational spectroscopy is thus very high and it has fields of applications ranging from the design of new systems to the monitoring of the production procedures. However, due to the complexity of the effects involved at the molecular level (e.g. anisotropic energies of interactions, polymorphism, co-existing amorphous and crystalline domains, local defects, complex morphology, chain folding...), the interpretation of the structural and spectroscopic data on the basis of experimental measurements alone can lead to many uncertainties and ambiguities. Indeed, as an example, it is quite usual to find conflicting suggestions among different authors in the band assignment of vibrational spectra.

In recent years, quantum-chemical modelling become an essential tool in chemical, molecular and materials sciences, as demonstrated by the 2013 Nobel Prize in Chemistry, awarded to Martin Karplus, Michael Levitt and Arieh Warshel "*for the development of multiscale models for complex chemical systems*".

Quantum chemical calculations in particular showed an high accuracy for the prediction of the structural and spectroscopic properties of molecular systems, providing an important support for the characterization of the material. Moreover, their importance is not limited only to the rationalization of the experimental data but their reliability is now so significant that they can be exploited for the design of novel interesting systems.

In this context, the aim of my PhD Thesis work is that of exploring the potentialities of state-of-the-art theoretical and computational tools for the investigation of the structure and spectroscopic response of polymer materials, focusing in particular on those methods which have been never or seldom adopted before for these systems.

By considering many examples and systems, we aimed from one hand at supporting the experimental characterization; on the other hand, we want also to use quantum chemical simulations to shed light on physicochemical properties of molecules and to contribute to the rationalization of the behaviour of the material at the molecular scale.

In addition, the work here presented also gives few outcomes on methodology, since many tests have been required to check computational setups, theoretical methods and numerical algorithms, for systems never investigated before by means of these techniques.

The work focused on three interconnected topics: i) the application to crystalline polymers of periodic DFT calculations through the CRYSTAL code; ii) the development of theoretical models to investigate the molecular charge distribution by means of Equilibrium Charges and Charge Fluxes (ECCF); iii) the application of First-Principles Molecular Dynamics (FPMD) simulations, both on small molecular systems and polymers. In particular we adopted Born-Oppenheimer MD as implemented in the CP2K code.

Topic (i) is the subject of Chapter 2: it describes an investigation of the crystalline phase and of related polymorphism phenomena of polymers belonging to different families. This work shows the advantages offered by CRYSTAL code for the prediction of the structural properties and the spectroscopic response of polymers. Only recently the implementation of this code allowed to run DFT simulations of molecular crystals directly treated as infinite

periodic systems, describing accurately both intra- and intermolecular interactions, which play a fundamental role in macromolecular systems. Indeed, there are few papers in the literature that explore the potentiality of this method for the study of polymer systems, and most of them have been published by the developers of the CRYSTAL code or by our research group.

In Chapter 3 – topic (ii) - we report the development and application of the Equilibrium Charges-Charge Fluxes (ECCF) model for the parameterization of the Cartesian derivatives of the molecular dipole (Atomic Polar Tensor - APT): ECCF provide powerful parameters to study the electronic charge distribution in molecules and for the interpretation of their IR absorption intensities. The theory, developed for small molecules, can be applied also to complex systems which can be described by means of suitable molecular models, allowing to characterize the relevant physicochemical properties of several organic materials: the charge distribution has indeed a direct relationship with both intra- and intermolecular interactions. The development of an efficient method for the description of molecular charge distribution by means of localized parameters (ECCF) is of considerable importance, not only in the field of theoretical and computational chemistry but also in fields ranging from biology, molecular physics and materials science.

In the last years and thanks to the improvements in computational facilities, FPMD simulations - topic (iii) - gained more and more importance for the study of the structural and spectroscopic properties of molecular systems. Compared to the approach usually followed in the framework of DFT simulations, where spectra calculation is carried out for molecular models "*in vacuo*" in double harmonic approximation, i.e. in the hypothesis of small atomic oscillations around the equilibrium geometry, FPMD simulations allow to take into account explicitly the dynamical evolution of the system and the effect of the environment (temperature, pressure, strains, solvent effects etc). Considering in particular the prediction of IR spectra, FPMD simulations take into account automatically the presence of different relevant conformations/complexes in a real environment, while including anharmonicity and, at least in principle, reaching a high degree of accuracy. In Chapter 4, we analyse in details the advantages and limitations of this method, in particular for two cases never approached before with these techniques, such as flexible molecules in liquid phase and polymers in crystalline phase. We test the reliability in the prediction of the IR spectrum of systems characterized by many stable conformations by means of one single FPMD simulation, with respect to the many simulations required for a reliable prediction of the real spectrum, according to more standard approaches. In the same framework, we illustrate and validate a theoretical model for the calculation of the IR spectrum from atomic polar tensors and velocities correlation function, thus avoiding the calculation of the dipole correlation function, which is often very demanding from the view point of the computation. We will show how this new approach allows to overcome some of the current limitations of FPMD for the prediction of spectroscopic properties, thus opening promising perspectives for future investigations through FPMD simulations.

Part of the work, carried out during the PhD Course, has been already published as papers on international journals or is presently in the form of a manuscript to be submitted for publication. Copies of these papers (or manuscripts) are included in the pertaining Chapter of the Thesis. Each paper is preceded by a short summary, aimed to introduce the work; for the detailed discussion of the results, relevant Figures and bibliography we refer to the enclosed paper.

Chapter 2

Periodic DFT calculations of the structure and of the spectroscopic response of semicrystalline polymers

2.0 Introduction

The development of new nanostructured polymer systems and their applications in many fields requires a detailed understanding of their structural behaviour at the nanoscale and of its influence on the physicochemical properties.

As already pointed out, due to the complexity of the intra/intermolecular effects, the interpretation of the structural and spectroscopic data of polymeric materials can be a delicate and tricky task. In this context computational approaches represent powerful tools to give both a deeper insight on the molecular properties of polymer materials and a support to experimental investigations.

In the past, the properties of polymers were theoretically investigated based on suitably derived empirical force fields or by means of semi-empirical calculations or quantum-chemical calculation on short oligomers (oligomer approach). With the exception of very few studies, dealing also with the prediction of IR intensities on the basis of empirical parameters (e.g. ECCF or EOP set derived from suitable experiments on small model molecules, see Chapter 2), the empirical approaches often gave good prediction of the vibrational frequencies, but did not allow to simulate the intensity pattern of vibrational spectra. On the other hand, within the oligomer approach, the use of quantum-chemical calculations can provide an accurate prediction of both the structural parameters and spectroscopic observables (frequencies and intensities of vibrational transitions) of the chosen oligomers. However, molecular properties show sometimes a strong dependence on the chain length, thus requiring very large model molecules for a reliable prediction.

In addition to this limitation, a further one can cause serious problems: when significant intermolecular effects take place (i.e. hydrogen-bonding, crystal field) calculations on clusters of molecules of suitable size are mandatory for a reasonable modeling, usually exceeding the current limits with available resource.

We thus decided to test an alternative strategy with respect to the oligomer approach, making use of Quantum Chemical codes which implement Periodic Boundary Conditions (PBC), for a rigorous description of systems characterized by translational symmetry. In the last years,

new computational approaches have been indeed developed to deal with high level quantum chemical calculation on molecular crystals. The CRYSTAL code in particular has been successfully applied by the developers and by our group to semicrystalline polymers, showing very good results in the prediction of the structural and spectroscopic properties of different polymer systems. In this context, a part of the work during my PhD focused on the employment of the CRYSTAL code to relevant families of polymers, to clarify the role of intra and intermolecular phenomena in modulating the structural and vibrational properties of polymers and in providing information to support and complement experimental work.

Unlike other solid state codes, CRYSTAL adopts a "molecular-oriented" implementation, by using Gaussian Atomic Orbitals basis set to build the Bloch wave function, giving the possibility to adopt or adapt the basis sets used in usual molecular calculations. Moreover, CRYSTAL allows to carry out DFT calculations by using hybrid functionals and introducing Grimme correction for the dispersion interaction, which are not correctly taken into account by common (LDA,GGA or hybrid) functionals.

These interactions are fundamental for macromolecular systems as demonstrated in the case of polyethylene where dispersion interaction are the only responsible for the crystal packing (see Section 2.4).

The advantages illustrated above are particularly meaningful with respect to other codes when dealing with molecular materials, as for instance plain waves codes.

As a second example of the application of the CRYSTAL code in this context, we will demonstrate how the marked polymorphism of even nylons is due to a suitable balance of conformational effects, hydrogen bonding and Van der Waals forces between CH₂ units of different chains (see Section 2.1).

Finally, another significant advantage of CRYSTAL is that, in addition to the correct treatment of the translational symmetry by means of PBC, the code exploits the whole space group symmetry of the crystal. Beyond the significant saving of computational time, the use of symmetry is crucial also in the solution of the vibrational problem, because it directly provides the assignment of the vibrational modes (phonons) to the correct symmetry species. This allows an easier rationalization of the experimental spectral pattern.

In the following, different cases will be presented, starting from even nylons, to a couple of aromatic polyesters, never investigated before by quantum chemical methods, and to polyethylene.

2.1 The polymorphism of even Nylon: a subtle interplay between intra- and inter-molecular effects

Nylons (the commercial name for polyamides) are an emblematic case of polymers that, despite their employment in everyday life, are still widely investigated for new innovative applications, as demonstrated by the case of nylon based nanocomposites or electrospun nanofibers, with applications in many different fields.

The close connection of nylons properties with the phenomena taking place on a molecular scale allow, in principle, to modify the macroscopic behaviour through a rational design of the nano, micro and mesoscopic structure.

At the nanoscale, polymorphism is one of the key phenomena ruling the properties of polyamides, being one the main actors governing the structure/property correlations (eg. the modulation of the mechanical response depending on the crystal phase).

Polymorphism is a subtle and delicate mechanism originating both from intra- and intermolecular effects which can be either cooperative or not.

In the case of even single number nylons (namely $((\text{CH}_2)_{n-1} \text{CONH})_x$, n even number), experimental results show that two polymorphs, with different macroscopic properties, can be stable at room temperature. The relative stability of the two forms change with the number of CH_2 units between the amide groups (see Figure 2.1) : the α phase is more stable for NY6 and shorter nylons (NY4) while the γ phase is more stable for NY8 and longer chains nylons.

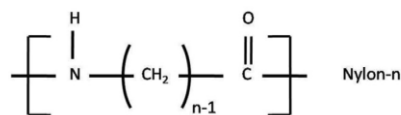


Fig. 2.1 Chemical structure of Nylon-n

By means of a computational approaches, mainly based on classical molecular dynamic simulations, different authors proposed that the relative stability of the crystal packing in the two polymorphs could be related to competitive intermolecular effects. However a clear picture was still lacking, due also to the intrinsic limitations of the computational tools adopted.

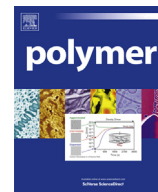
To clarify the role of the different molecular phenomena that modulate the structural properties of nylons polymers, we employed the crystal code to carry out a DFT investigation of the different polymorphs of even nylons. This work aimed to show the importance of this approach for the interpretation of the structural properties of the polymeric materials and to provide insights which are hardly accessible from experiments.

As illustrate in details in the paper "*Polymorphism of even nylons revisited through periodic quantum chemical calculations*" D. Galimberti, C. Quarti, A. Milani, *Polymer*. 67 (2015) 167–173, here enclosed, we carried out a set of DFT calculations with PBC (including Grimme corrections to obtain a reliable description of Van der Waals interactions) on the 3D crystal cells of α and γ polymorphs of even polyamides (ranging from nylon-4 up to nylon-12) and on the infinite

1D polymer chains possessing α and γ conformations. Our scope was to discriminate between inter and intramolecular effects, analysing their different contributions. Moreover, considering the intermolecular term, a procedure has been proposed to investigate the role and the contribution played by the hydrogen bonding and by the Van der Waals packing of CH_2 units.

Our results gave a clear picture of a quite complex behaviour: in NY4 and NY6 hydrogen bonding interactions, promoting the occurrence of the α structure, dominate over the contribution arising from CH_2 interactions and from conformational effects; on the other hand, in NY10 and NY12, the CH_2 packing interactions and the contribution of intramolecular effects, both favouring the γ structure, dominates and explains why a γ structure is experimentally found for these materials. Finally in NY8, intermolecular contributions due to the packing of the CH_2 balance the hydrogen bonds effects and the setting of the γ structure is ruled by conformational energy only.

This work demonstrated how the rationalization of the molecular behaviour of polymers is indeed ruled by a large variety of different, co-existing effects. Despite this complexity, state-of-art quantum-chemical calculations are able to shed light in this phenomena; indeed molecular simulations are now a fundamental tool in polymer science and technology.



Polymorphism of even nylons revisited through periodic quantum chemical calculations



Daria Galimberti, Claudio Quarti ¹, Alberto Milani*

Politecnico di Milano, Dip. Chimica, Materiali, Ing. Chimica "G. Natta", P.zza Leonardo da Vinci 32, 20133 Milan, Italy

ARTICLE INFO

Article history:

Received 13 March 2015

Received in revised form

17 April 2015

Accepted 20 April 2015

Available online 28 April 2015

Keywords:

Polyamides

Density functional theory

Hydrogen bonding

ABSTRACT

Density functional theory calculations with periodic boundary conditions have been carried out for the 3D crystal cells of α and γ polymorphs of even polyamides (ranging from nylon-4 up to nylon-12) in order to investigate the relative stability of the two forms. The infinite 1D polymer chains possessing α and γ conformations have been also simulated to shed light on the intramolecular effects taking place in these systems and to discriminate the intermolecular effects in terms of hydrogen bonding and packing of CH₂ units. The results of this analysis allowed to give a detailed interpretation of the polymorphism properties observed in even nylons, predicting a larger stability for the α form in nylon-4 and nylon-6 and a stabilization of the γ phase from nylon-8 up to nylons having a larger number of CH₂ unit in the chain.

© 2015 Elsevier Ltd. All rights reserved.

1. Introduction

Nylons, the commercial name for polyamides, are a family of polymeric materials that are now part of our everyday life [1]. Beyond their common availability, innovative and promising applications are currently under investigation by the scientific community, as in the case of electrospun nanofibers [2–6], nanocomposites [7,8] or applications as biomaterials in nanomedicine.

At the nanoscale, polymorphism is one of the key phenomena ruling the properties of polyamides, being the main actor in the set up of the structure/property correlations that determine a different tensile response, Young modulus or a different thermal response, as for example in the case of Nylon 6 (NY6) where two main α and γ polymorphs co-exist at room temperature. Moreover, depending on the particular class of nylons considered (even, odd, even–even etc.) polymorphism can show a different behavior and peculiar characteristics [1,9]. However, in spite of its importance, the rationalization of the polymorphic phenomena in nylons is a not completely solved issue and it has been investigated also by means of computational approaches, including both classical and quantum chemical simulations [10–14]. The complexity of these phenomena

is related to the variety of molecular effects that characterize polyamides and that are related to a subtle balance among different concurrent intermolecular effects (e.g. hydrogen bonding and vdW interactions) and intramolecular effects (e.g. conformational energy, intramolecular non-bonded electrostatic interactions). Since the stabilization of a given polymorph implies peculiar trends of the macroscopic properties a careful understanding of the crystal structure, of its evolution under the external parameters and of the energetics ruling these phenomena is mandatory for a rationalization of the behavior of the material also at the macroscale.

Even, single-numbered nylons NY_n here investigated have a $-(NH)-(CH_2)_{n-1}-(C=O)-$ chemical structure ($n = 4, 6, 8, 10, 12$): NY6 and NY8 crystallize in two different polymorphs, the α and the γ form (sketched in Fig. 1 in the case of NY6), with the former phase that is more stable for NY6 and shorter nylons (NY4) while the latter is more stable for NY8 and longer chains nylons. The two polymorphs are quite different. They possess different space group symmetry and different chain conformation, with the α form showing an all trans conformation and the γ form showing a quasi-extended skew conformation of the CH₂ units adjacent to the amide group.

It has been proposed [1,10–12] that the different crystal packing in the two polymorphs could be related to competitive intermolecular effects: theoretical studies, mainly resorting to classical molecular dynamics simulations [10,11] or quantum chemical simulations carried out on small molecular models [12] have been already reported in the literature, to investigate this behavior; however, a comprehensive investigation on the topic, based on

* Corresponding author.

E-mail address: alberto.milani@polimi.it (A. Milani).

¹ Current address: Université de Mons, Laboratory for Chemistry of Novel Materials, Place du Parc 20, 7000 Mons, Belgium.

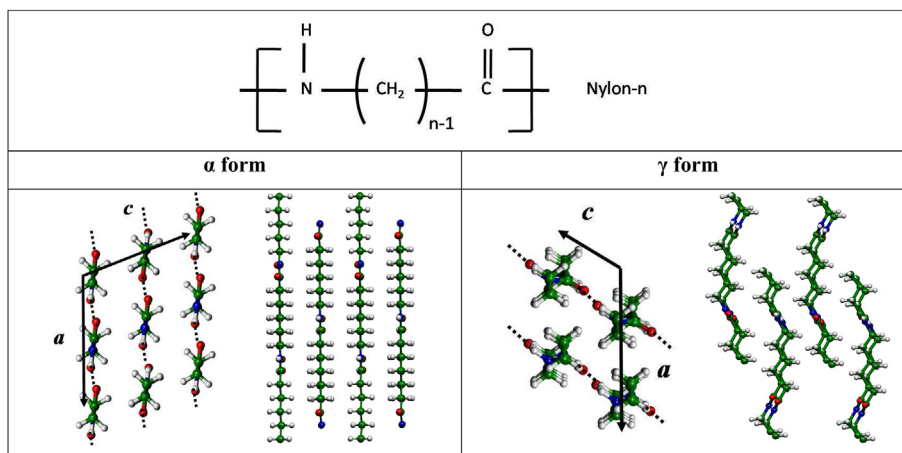


Fig. 1. Structural formula of even nylons-*n*. Sketches of the crystalline structures of the α and γ polymorphs. Carbon atoms are in green, hydrogen atoms in white, oxygen atoms in red and nitrogen atoms in blue; hydrogen bonds are marked with dots. (For interpretation of the references to colour in this figure legend, the reader is referred to the web version of this article.)

accurate, state-of-the-art quantum chemical calculations and on reliable models would be highly coveted.

In very recent years, new computational approaches have been developed and can be applied in polymer science. The CRYSTAL code in particular has been successfully applied to semicrystalline polymers [14–23], revealing very good performances in the reliable prediction of the structural and spectroscopic properties of polymer systems belonging to different families, including polyamides [14,18,23]. The main advantages of this code is that it allows accurate Density Functional Theory (DFT) calculations adopting full periodic boundary conditions and hybrid exchange correlation functionals, at a reasonable computational cost. It is then possible to run simulations both on infinite one dimensional (1D) polymer chains but also on the real three dimensional (3D) crystal unit cell, thus joining the possibility to carry out quantum chemical calculations without arbitrary choices of models (i.e. the real crystalline cell is considered), and so avoiding the limitation of previous approaches. Moreover, the possibility to fully take into account the space group symmetry of the system and to adopt reliable corrections to the implicit limitation of DFT functional in treating the vdW dispersion interactions are further features of peculiar importance for the simulation of molecular materials.

This computational approach is employed in this paper to study the polymorphism in even single-numbered nylons, ranging from nylon-4 (NY4) to nylon-12 (NY12): for each case, simulations on both the α and γ crystal structures have been carried out to determine the equilibrium geometry and related energetics. Based on a detailed analysis of the different intra- and intermolecular contributions, the molecular phenomena ruling polymorphism in this class of materials will be rationalized.

2. Computational details

Full geometry optimization of the crystal structure and chain conformation of the α and γ polymorphs of nylon-4, -6, -8, -10 and -12 have been carried out by means of the CRYSTAL09 code [24,25] in a fully quantum mechanical framework, using DFT including periodic boundary conditions. Different combinations of DFT functionals and basis sets have been adopted employing both the B3LYP [26,27] and PBE0 [28] hybrid exchange-correlation functionals, combined with 6-31G(d,p) and pob-TZVP [29] basis set. Based on previous computational investigations of polyamides [14,18,23], we introduced the empirical correction for dispersion

interaction (DFT-D) proposed by Grimme [30–32] to obtain a more reliable qualitative and quantitative description of van der Waals interactions, which are among the main actors ruling the polymorphism of nylons and which are not correctly described by standard DFT. The parameters chosen for Grimme corrections are reported in Ref. [14]. In all calculations, the atomic positions and the lattice parameters were fully optimized starting from input structures built on the basis of the experimental geometries of α and γ crystals of nylon-6 from XRD [33–35]. In order to explore conformational effects, geometry optimizations have been carried out also on the infinite 1D polymer chains, characterized by the regular conformation shown by the chains in the two crystals (see Fig. 1).

In order to judge about the accuracy of the computations here adopted we report in Table 1 the comparison between DFT computed (B3LYP-D/pob-TZVP) and available experimental cell parameters [33–39] for all the nylons here investigated. As expected a good agreement is found for all the cases, with mean percentage errors which are lower than 3.5% in all the cases, thus supporting the reliability of our computational approach as found also in our previous paper on NY6 polymorphs [14].

However, it should be noticed that, in the case of molecular solids, thermal effects can have a non-negligible role in modulating the cell parameters, as also verified experimentally [40]. Our periodic DFT calculations (but also molecular mechanics approaches [10,11]) refer to a 0 K configuration and do not take into account temperature effects (entropic contributions of phonons, molecular geometry fluctuations of angles); therefore the comparison with the result of a complete cell optimization should be taken with care due to the absence of these thermal effects. Due to the good agreement here obtained with the experiments, we believe that thermal effects could be confidently considered small and could explain the minor discrepancies observed; in any case, we do not expect them to affect the trends observed for the different nylons here analysed.

3. Results

3.1. Relative stability of α and γ polymorphs

The relative stability of the α and γ forms of even nylons has been theoretically investigated in few papers [10–12] by using different computational approaches: Dasgupta et al. [10] developed the MSXX force field to run classical simulations specifically for

Table 1

Comparison between DFT computed (B3LYP-D/pob-TZVP) cell parameters (values of a,b,c parameters are in Å and in degrees for the β angle) of the α and γ polymorphs of even nylons (NYn, n = 4,6,8,10,12). The percentage error (PE) with respect to the experimental data has been calculated as: $PE = (PAR_{theo} - PAR_{exp}) * 100 / PAR_{exp}$, where PAR means the generic cell parameter (a,b,c). Mean percentage errors (MPE) are also reported by averaging on the PE (absolute value) obtained in each case.

		a	b	c	β
α -NY4	B3LYP-D/pob-TZVP	9.47	12.33	7.37	67.8
	Expt. [36]	9.29	12.24	7.97	65.5
	PE	1.96	0.73	-7.54	MPE 3.41
γ -NY4	B3LYP-D/pob-TZVP	8.82	11.80	4.79	125.5
	Expt.	//	//	//	//
α -NY6	B3LYP-D/pob-TZVP	9.50	17.43	7.42	68.0
	Expt. [33,34]	9.56	17.24	8.01	67.5
	PE	-0.68	1.07	-7.41	MPE 3.05
γ -NY6	B3LYP-D/pob-TZVP	8.84	16.94	4.78	126.3
	Expt. [35]	9.33	16.88	4.78	121.0
	PE	-5.26	0.33	0.06	MPE 1.88
α -NY8	B3LYP-D/pob-TZVP	9.52	22.53	7.47	67.6
	Expt. [37]	9.64	22.4	8.03	65
	PE	-1.27	0.58	-6.98	MPE 2.94
γ -NY8	B3LYP-D/pob-TZVP	8.85	22.05	4.77	126.6
	Expt. [38]	9.54	21.9	4.77	120
	PE	-7.25	0.71	0.08	MPE 2.68
α -NY10	B3LYP-D/pob-TZVP	9.53	27.63	7.50	67.2
	Expt.	//	//	//	//
γ -NY10	B3LYP-D/pob-TZVP	8.85	27.17	4.77	126.8
	Expt. [38]	9.56	26.9	4.78	120
	PE	-7.39	0.99	-0.30	MPE 2.89
α -NY12	B3LYP-D/pob-TZVP	9.56	32.73	7.51	66.7
	Expt.	//	//	//	//
γ -NY12	B3LYP-D/pob-TZVP	8.86	32.28	4.76	126.9
	Expt. [39]	9.58	31.9	4.79	120
	PE	-7.54	1.18	-0.68	MPE 3.13

nylon polymers while Aleman and Casanovas [11] adopted both monte carlo simulations and energy calculations by using again a force field approach to investigate the structural properties of very large nylons. In addition to these classical approaches, a pioneering quantum chemical investigation has been presented by Bernadó et al. [12] where the stability of these polymorphs has been evaluated by reconstructing the energy of the whole crystal as the sum of group contributions due to the intermolecular and intramolecular interactions occurring in and between small molecular fragments. Moreover, the same research group carried out further quantum chemical investigations to characterize the peculiar conformational and intramolecular interactions having place in nylon polymers, adopting also in these cases small molecular models (oligomers) of the whole polymer chains [41]. The general results of these studies, confirming the previous interpretations [1], is that the α form is the stable one for nylon-4 and -6 while the γ form is predominant in the even nylons from NY8 up. This behavior has been explained based on the balance between competing intermolecular effects: indeed, in the α form the hydrogen bonds are more efficient than in γ form, at the expense of a non optimum packing of the CH_2 groups; at the opposite, in the γ form the optimum packing of the methylene units dominate over hydrogen bonding. Therefore, in polymers with shorter monomeric units such as NY4 and NY6, hydrogen bonding interactions are predominant and stabilize the α form preferentially. For nylons with larger monomeric units, the increasing number of CH_2 units

progressively increases the contribution due to their efficient intermolecular packing, which becomes predominant starting from nylon-8, thus stabilizing the γ form. Despite the general agreement between the different computational approaches, there are intrinsically some limitations which could prevent a more detailed investigation of the molecular effects ruling nylon polymorphism. On one hand, classical force field approaches bring the implicit arbitrariness related to the choice of empirical potential energy functions and parameters which could not be able to consider properly all the peculiar interactions taking place (such as non standard intramolecular coulomb interactions [41]). Moreover, some discrepancies in the relative stabilities of nylons with very large aliphatic segments have been also observed when carrying out monte carlo simulations with respect to force-field based energy calculations [1]. On the other hand, quantum chemical calculations on small molecular models bring an arbitrariness in the choice of reliable molecular models which could influence the quantitative results or could not describe completely the real interactions having place in a macromolecular crystal. As an example, a dependence of the relative stability of α and γ conformations on the number of residues adopted to generate the oligomer model of an infinite polymer chain have been observed [41]. Our approach, that resorts on a quantum mechanical treatment carried out on the complete crystalline cell, allows to avoid most of these limitations.

In Fig. 2, the energy difference between the α and γ polymorphs ($E_{\alpha-\gamma} = E_{\alpha} - E_{\gamma}$) is reported from NY4 to NY12, as obtained by the geometry optimization of the 3D unit cell of the two forms for different combinations of DFT functional/basis set. Related numerical values are reported in Table 2.

Fig. 2 reveals that for most of the functional/basis set combinations, the α form is predicted as the most stable one in the case of nylon-4 and nylon-6, in agreement with experimental investigations [1]. Only for B3LYP-D/6-31G(d,p), the γ form turns out to be the preferred one in NY4, contrary to previous theoretical

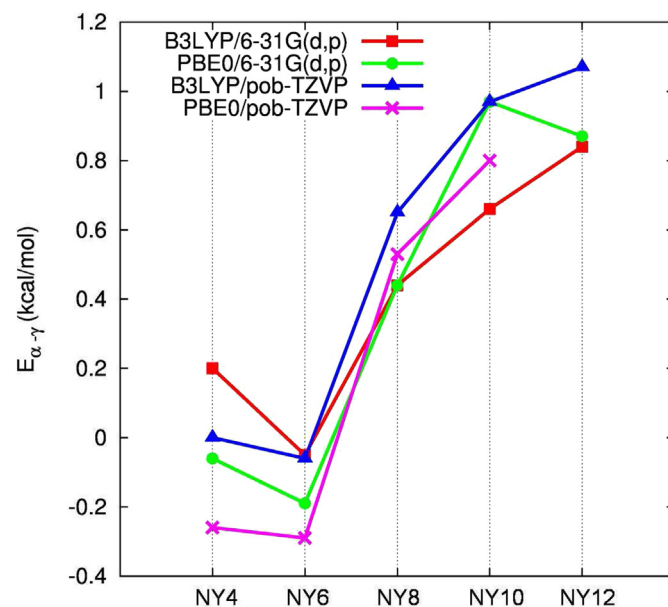


Fig. 2. Relative energies (for single monomer units) of the α and γ polymorphs ($E_{\alpha-\gamma} = E_{\alpha} - E_{\gamma}$) of even, single numbered nylons ranging from NY4 to NY12. Units of kcal/mol. E_{α} , E_{γ} are the DFT computed total energy of the two 3D crystals respectively. The results obtained by using two DFT functionals (PBE0 and B3LYP, with Grimme corrections) and two basis sets (6-31G(d,p) and pob-TZVP) are reported. In the case of PBE0-D/pob-TZVP calculation on NY12, no convergence in the geometry optimization has been obtained and thus no results are indicated. Numerical data are reported in Table 2.

Table 2
Values of the relative energies between α and γ crystals ($E_{\alpha-\gamma} = E_{\alpha} - E_{\gamma}$) per single monomer unit, as obtained for different DFT functionals and basis sets. Units of kcal/mol. In the case of PBE0-D/pob-TZVP calculation on NY12, no convergence in the geometry optimization has been obtained and thus no results are indicated.

3D crystal	B3LYP-D/6-31G(d,p)	PBE0-D/6-31G(d,p)	B3LYP-D/pob-TZVP	PBE0-D/pob-TZVP
NY4	0.20	-0.06	-0.01	-0.26
NY6	-0.05	-0.19	-0.06	-0.29
NY8	0.44	0.44	0.65	0.53
NY10	0.66	0.97	0.97	0.80
NY12	0.84	0.87	1.07	//

studies and structural determinations. It should be noticed, however, that, when investigating supramolecular interaction, computational effects such as basis set superposition error (BSSE) [42], can influence significantly the energetic description of intermolecular interactions. This is the reason why simulations have been also carried out with the more extended (and less BSSE sensitive) pob-TZVP basis set which should give more accurate quantitative values of the relative energies. The stabilization of the α form in NY4 and NY6 found in the other calculations is in agreement with previous investigations [10]: in the case of NY6, the relative energy $E_{\alpha-\gamma}$ ranges from -0.05 to -0.29 kcal/mol per monomer chain in agreement with the -0.323 kcal/mol [10] and -0.50 kcal/mol [12] values previously suggested. With the exception of B3LYP-D/6-31G(d,p) in the case of NY4 the relative energy $E_{\alpha-\gamma}$ ranges from -0.01 to -0.26 kcal/mol and in all the cases it is smaller in magnitude than for NY6. This result is again in agreement with previous molecular mechanics calculations on nylon polymers [10] where a relative $E_{\alpha-\gamma}$ energy of -0.272 kcal/mol is found for NY4 with respect to the -0.323 kcal/mol value found for NY6. Considering nylons with increasing number of CH₂ units, the γ form becomes the most stable one already for NY8 ($E_{\alpha-\gamma}$ ranging from 0.44 to 0.65 kcal/mol) and its stability increases for NY10 ($E_{\alpha-\gamma}$ ranging from 0.66 to 0.97 kcal/mol) and NY12 ($E_{\alpha-\gamma}$ ranging from 0.84 to 1.07 kcal/mol). These trends are in agreement both with the experimental evidences and with previous investigation [10–12]: in Ref. [12] in particular, the results of quantum chemical calculations on small model systems predicted an $E_{\alpha-\gamma}$ energy of 0.63 and 0.82 kcal/mol respectively for NY8 and NY10, showing a very similar trend to the one here presented (0.53 and 0.80 kcal/mol is found at the PBE0-D/pov-TZVP level). It should be noticed that in the case of NY12 while B3LYP-D calculations always predict a larger $E_{\alpha-\gamma}$ energy with respect to NY10, a lower value (0.87 vs 0.97 kcal/mol) is found for PBE0-D/6-31G(d,p) calculation. In Ref. [11], based on monte carlo simulations, a decreasing trend in $E_{\alpha-\gamma}$ has been predicted starting from NY12, suggesting that the preferential stability of the γ form would decrease for nylon possessing a very large number of CH₂ units in the chain. Unfortunately, we could not reach in any way convergence in the geometry optimization of NY12 at PBE0-D/pob-TZVP level and thus we cannot check if our results are due to some computational effects, as the afore-mentioned BSSE, or if they are describing some physicochemical effects which are best described by PBE0 functional with respect to B3LYP.

Aside from these details, our computational study confirms that the α form is the preferred one for nylon-4 and -6, while γ form results to be more stable starting from nylon-8. In previous investigations, this behavior has been interpreted mainly in the light of intermolecular effects, and in particular as due to the balance between hydrogen bonding effects (more efficient in the α form) and optimum packing of CH₂ units (more efficient in the γ form). On the other hand, the present authors have already pointed out the role of the conformational potential of the isolated chain on the polymorphism of NY6 [14]. In the following sections, both the intramolecular interactions ruling the conformational behavior and

intermolecular interactions due to hydrogen bonding and packing of CH₂ chains will be analyzed in detail.

3.2. Conformational effects

An intramolecular/conformational investigation has been carried out by means of geometry optimization and energy evaluation of infinite 1D chains possessing respectively the transplanar conformation, typical of the α polymorph, and the skew conformation of the CH₂ units adjacent to the amide group, typical of the γ polymorph (see Fig. 1). The relative energies are plotted in Fig. 3 and related numerical values are reported in Table 3. As a first result, we found that the typical conformations observed in the two crystals (i.e. a fully extended structure for the α form and the quasi-extended structure for γ form) are maintained after the optimization carried out on the isolated infinite chain, that is in absence of any intermolecular interactions. In other words, these two conformations correspond to real minima of the torsional potential of the chain and they are not ruled by the packing effects taking place in the crystal.

Considering the relative energy of the two conformations as reported in Fig. 3 and Table 3, it is interesting to notice that the quasi-extended γ conformation is the most stable one for all the considered nylons, independently of the computational method employed: when adopting the more extended pob-TZVP basis set the relative energy is found to be about one half of that obtained by

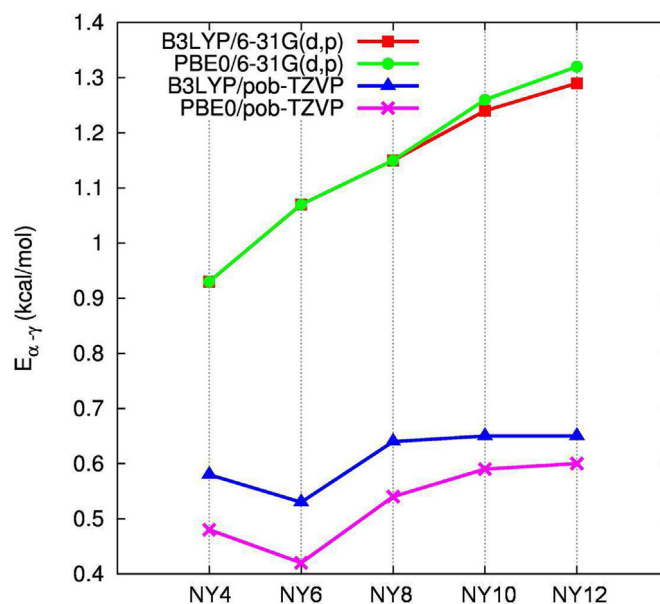


Fig. 3. Plot of the relative energies per single monomer unit $E_{\alpha-\gamma}^{1D} = E_{\alpha}^{1D} - E_{\gamma}^{1D}$ with E_{α}^{1D} , E_{γ}^{1D} being the DFT computed total energy of the two 1D infinite chains possessing respectively α and γ conformation. Units of kcal/mol. The results obtained by using two DFT functionals (PBE0 and B3LYP, with Grimme corrections) and two basis sets (6-31G(d,p) and pob-TZVP) are reported. Numerical data are reported in Table 3.

Table 3

Values of the relative energies per single monomer unit between 1D infinite chains possessing α and γ conformation ($E_{\alpha-\gamma}^{1D} = E_{\alpha}^{1D} - E_{\gamma}^{1D}$), as obtained for different DFT functionals and basis sets. Units of kcal/mol.

1D chain	B3LYP-D/6-31G(d,p)	B3LYP-D/pob-TZVP	PBE0-D/6-31G(d,p)	PBE0-D/pob-TZVP
NY4	0.93	0.58	0.93	0.48
NY6	1.07	0.53	1.07	0.42
NY8	1.15	0.64	1.15	0.54
NY10	1.24	0.65	1.26	0.59
NY12	1.29	0.65	1.32	0.60

6-31G(d,p) basis set but in any case γ conformation is the preferred one. Moreover, its stability is found to slightly increase with the number of CH₂ units in the chain, already giving a possible explanation of the fact that, starting from NY8, the γ polymorph becomes the most stable one and its stability grows when considering NY10 and NY12. Interestingly, for NY6, the stability of the γ conformation is slightly lower than in NY4 and this behavior can be one of the factors explaining why the α polymorph in NY6 is more stable than in NY4.

The most important result of this analysis is that peculiar intermolecular effects play a significant role in the case of NY4 and NY6: supramolecular packing interactions tend to stabilize the α structure in these two polymers, despite the preference of their single chains to adopt the quasi-extended γ conformation. On the other hand, for the other nylons with $n > 6$, intramolecular interactions cooperate with the intermolecular ones in stabilizing the γ form.

From the computational perspective, it is interesting to compare the results obtained here for infinite 1D chains with regular conformations with the results presented in a previous work [41] where conformational effects in nylons have been investigated by using finite length molecular models of the polymeric chains. In that work indeed, while the γ conformation has been found to be always the preferred one for nylons NY n with $n > 6$; the α conformation was found to be the most stable for $n \leq 6$, depending on the number of residue adopted in the molecular models. This demonstrates that the arbitrariness in the choice of the finite-length molecular model adopted (not required in our approach) could influence significantly the final results and interpretations.

3.3. Analysis of intermolecular packing interactions

The next step in the understanding of the polymorphic behavior of even nylons requires a detailed investigation of intermolecular interactions.

A net evaluation of these interactions can be carried out by calculating the cohesive energy of each crystal as the difference between the energy of the 3D crystal and the energy of the isolated 1D chain, both normalized on one monomeric unit. The trends so obtained are reported in Fig. 4 and associated numerical data in Table 4 referred to B3LYP-D/pob-TZVP calculations. In the following discussion we will adopt this computational method in order to obtain numerical values as accurate as possible and to carry out stable calculations for all the systems investigated.

Cohesive energies show a very clear and peculiar behavior: given the larger dimension of the monomeric units and the increasing number of interacting CH₂ units, these energies obviously linearly decrease moving from NY4 to NY12. However, the slope of the two lines associated respectively to α and γ polymorphs is different and it is larger in particular for the latter. Indeed, the cohesive energy is larger for the α form in the case of NY4, they are almost equal for NY6 and NY8 in particular and then it becomes larger for the γ form in NY10 and NY12. For NY8 in particular, the two energies are practically the same, thus

indicating that NY8 is the turning point where a transition in the relative stability of α and γ crystals could take place due to intermolecular effects, stronger in the α form for NY4 and NY6 and in γ form for NY10 and NY12.

In order to give a deeper interpretation of the trend observed and thus of the relative stabilities of α and γ polymorphs (where both intra- and intermolecular effects co-exist), we have to go further in the detailed investigation of supramolecular effects, explicitly considering the different contributions (hydrogen bonding vs close packing of CH₂ groups) taking place.

It is well-known that commonly-used exchange-correlation functionals (such as B3LYP) lack the description of van der Waals (vdW) dispersion interactions, that are an essential ingredient in all molecular materials and of special importance in our present cases. For this reason, the correction proposed by Grimme (based on a semiempirical approach) [30–32] has been adopted in our calculations, as explained in the computational details. According to this approach, a two-body potential energy contribution of the type ($-C_6/R^6$) is added to the total DFT energy to recover the correct description of vdW interactions. This correction further allows to estimate the contribution due to the intermolecular vdW interactions between CH₂ units. We indeed carried out two types of new calculations: in the first one no Grimme corrections are introduced on all the atoms while in the other one they are

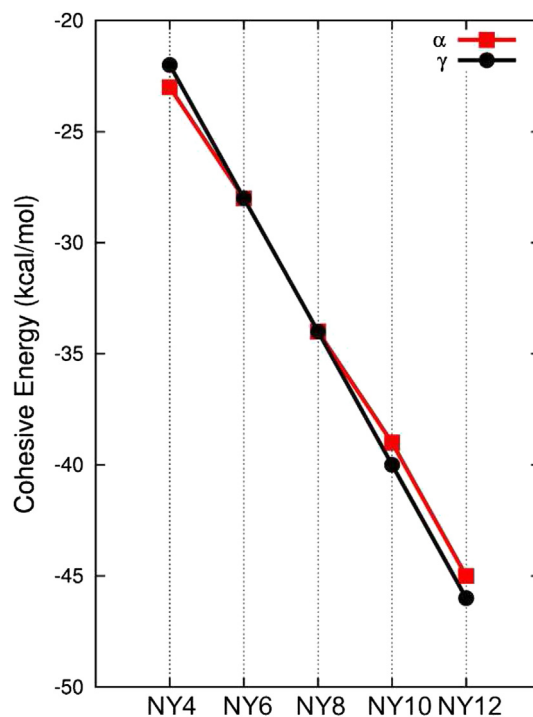


Fig. 4. DFT computed (B3LYP-D/pob-TZVP) cohesive energies $E_{\text{coh}} = E^{3D} - E^{1D}$ (kcal/mol per single monomer unit) with E^{3D} , E^{1D} being the total energy of the crystal and of the infinite isolated chain.

Table 4
Values of cohesive energies per single monomer unit, Grimme intermolecular vdW energy contribution of CH₂ units, Grimme intermolecular vdW energy contribution of CH₂ units normalized on a single CH₂ group, and H-bonding energy contribution. Units of kcal/mol. The definition of the different terms is reported in the text. These data have been obtained by means of B3LYP-D/pob-TZVP calculations. Units in kcal/mol residue.

	Cohesive energy	Grimme intermolecular Vdw contribution all CH ₂	Grimme intermolecular Vdw contribution per CH ₂	H-bonding contribution
α-NY4	-23.02	-5.66	-1.89	-17.37
γ-NY4	-22.44	-5.96	-1.99	-16.48
α-NY6	-28.90	-10.93	-2.19	-17.97
γ-NY6	-28.30	-11.69	-2.34	-16.61
α-NY8	-34.17	-16.62	-2.37	-17.54
γ-NY8	-34.18	-17.60	-2.51	-16.58
α-NY10	-39.80	-22.57	-2.51	-17.23
γ-NY10	-40.12	-23.54	-2.62	-16.58
α-NY12	-45.65	-28.62	-2.60	-17.03
γ-NY12	-46.07	-29.51	-2.68	-16.56

introduced only on CH₂ groups. The differences in the total energies of these simulations give an estimation in each case of the total (intermolecular + intramolecular) vdW interaction energies between CH₂ units belonging to the different adjacent polymer chains. In order to obtain the intermolecular contributions only, intramolecular vdW interactions have to be removed. These terms can be evaluated by using a similar procedure: indeed their values can be evaluated for each case by carrying out two single point calculations for the infinite isolated polymer chains where Grimme's correction is either added on CH₂ groups only or it is completely missing. The energy difference between the latter and the former gives the intramolecular vdW contributions between CH₂ groups which should be subtracted from the total vdW energies to isolate only the intermolecular terms, reported in Table 4. The results obtained immediately give a clear description: in all the cases the contribution due to the packing of CH₂ groups is slightly larger (more negative) in the case of the γ form, thus supporting the fact that in this crystal a better arrangement between CH₂ units is obtained. It is also interesting to verify that, for increasing number of CH₂ units, this vdW contribution, normalized per each single CH₂ group, increases with the length of the methylenic part of the chains. In other words, the bigger is the number of CH₂ in the chain, the more efficient is their packing, both in the case of α and γ crystals. This is probably due to the larger freedom of CH₂ groups in monomeric units of larger length.

Having now demonstrated that vdW interactions between CH₂ groups are more efficient for the γ form, it is necessary to get information about the energetic of the hydrogen bonding in each case.

The cohesive energy E_{coh} , can be considered the sum of different intermolecular interactions:

$$E_{\text{coh}} = E_{\text{H-bond}}^{\text{DFT}} + E_{\text{CONH}}^{\text{grimme}} + E_{\text{CH}_2\text{-CONH}}^{\text{grimme}} + E_{\text{vdW}}^{\text{DFT}} + E_{\text{CH}_2}^{\text{grimme}} \quad (1)$$

where $E_{\text{H-bond}}^{\text{DFT}}$ is due to the DFT contribution of the hydrogen-bonding, $E_{\text{CONH}}^{\text{grimme}}$ is the Grimme vdW contribution of the amide groups (that is the dispersion interaction term in hydrogen-bonding not taken into account by DFT), $E_{\text{CH}_2\text{-CONH}}^{\text{grimme}}$ is the Grimme vdW contribution of the amide groups interacting with CH₂ groups of the adjacent chains, $E_{\text{CH}_2}^{\text{grimme}}$ is the Grimme intermolecular vdW contribution of CH₂ units analyzed previously and $E_{\text{vdW}}^{\text{DFT}}$ is the DFT contribution due to VdW interactions.

The global energy associated to the hydrogen bonding ($E_{\text{H-bond}}$) between neighboring chains has been calculated

subtracting from this cohesive energy the Grimme vdW contribution of CH₂ units:

$$E_{\text{H-bond}} = E_{\text{coh}} - E_{\text{CH}_2}^{\text{grimme}} = E_{\text{H-bond}}^{\text{DFT}} + E_{\text{CONH}}^{\text{grimme}} + E_{\text{CH}_2\text{-CONH}}^{\text{grimme}} + E_{\text{vdW}}^{\text{DFT}} \sim E_{\text{H-bond}}^{\text{DFT}} + E_{\text{CONH}}^{\text{grimme}}$$

We already commented that DFT alone cannot take into account properly vdW interactions and thus we can straightforwardly assume the last term $E_{\text{vdW}}^{\text{DFT}}$ as negligible. Moreover, due to the large distance, also the Grimme vdW contribution between CH₂ groups and the amide groups $E_{\text{CH}_2\text{-CONH}}^{\text{grimme}}$ is of secondary importance. The difference so calculated ($E_{\text{coh}} - E_{\text{CH}_2}^{\text{grimme}}$) can be thus related mainly to the contribution of hydrogen bonding ($E_{\text{H-bond}}^{\text{DFT}} + E_{\text{CONH}}^{\text{grimme}}$) and it is reported in the last column of Table 4. Also in this case a very clear trend is obtained: in all the cases the H-bonding contribution is larger for the α form, indicating that in this polymorph the structure maximizes this interaction while CH₂ groups are less efficiently packed.

A last indication on the intermolecular interactions taking place in the two different polymorphs and of their relative importance can be obtained by evaluating the energy difference between the vdW CH₂ and H-bonding contribution in the α and γ forms (Table 5). These differences, together with the energy contribution of intramolecular (conformational) interactions, will be important to predict the relative stability of α and γ polymorph.

It is evident from the energy differences, reported in Table 5, that the CH₂ interactions, dominant in the γ form (positive energy difference), become more for this polymorph for greater number of CH₂ units, thus increasing the tendency to assume a γ structure. On the other hand, the H-bonding stabilization, dominant in the α form (negative energy difference) lowers from NY6 to NY12, therefore decreasing the tendency of the polymer to assume the α structure. Both these trends suggest again an evolution towards the γ structure for increasing number of CH₂ units and it will be the balance

Table 5
Energy differences per single monomer unit between α and γ crystals of the total Grimme vdW energy contribution of CH₂ units and H-bonding energy contribution reported in Table 4 (column 3 and 5). Units of kcal/mol residue. Data obtained at the B3LYP-D/pob-TZVP level of theory.

	ΔE _{α-γ} CH ₂ contribution	ΔE _{α-γ} H-bonding contribution
NY4	0.30	-0.88
NY6	0.76	-1.36
NY8	0.97	-0.96
NY10	0.97	-0.65
NY12	0.88	-0.47

among these intermolecular terms and the intramolecular energy that will determine the most stable crystal structure observed for even nylons, as discussed in the next section.

4. Discussions

As a final analysis it is now interesting to compare the intermolecular energies reported in Table 5 with the conformational energies reported in Table 3 in order to give a final interpretation of the relative stability of even nylons polymorphs based on the interplay between intra- and supramolecular interactions. Starting from NY4, it can be seen indeed that hydrogen bonding tends to stabilize the α form since it gives a dominant contribution of about 0.6 kcal/mol with respect to CH₂ packing interactions that would stabilize the γ form. However, the γ conformation (i.e. the intramolecular contribution) is found to be more stable of practically the same amount of energy (see Table 3), thus balancing net intermolecular effects: this explains why, according to B3LYP-D/pob-TZVP simulations, these two polymorphs are predicted to be almost isoenergetic. For NY6, the intermolecular effects would still promote the occurrence of the α polymorph by, again, a contribution of 0.6 kcal/mol. In this case however, the intramolecular contribution is slightly less than in NY4, thus showing that the stabilization energy associated to the γ conformation of the chain is not able to overcome the intermolecular stabilization resulting by packing in the α structure. Moving now to NY8, we can verify that the H-bonding and CH₂ packing contribution are practically the same and balance one another; therefore the tendency of this polymer to adopt a γ structure is mainly promoted by the larger stability of the γ conformation. NY8 is the turning point in the polymorphic behavior of nylons: indeed considering now NY10 and NY12 the larger intermolecular contribution due to CH₂ packing interactions tend to promote a γ structure concurrently with conformational effects.

5. Conclusions

Thanks to state-of-the-art DFT calculations we revisited the polymorphic behavior of even nylons to shed light on the associated intra and intermolecular phenomena. In NY4 and NY6 hydrogen bonding interactions, that promote the occurrence of the α structure, dominate over CH₂ packing interactions and conformational effects both more favorable to the γ structure. On the other hand, in NY10 and NY12 CH₂ packing interactions dominates and the joint contribution of intramolecular effects explains why a γ structure is found for these materials. In NY8, instead, intermolecular contributions balance by packing of the alkyl chains and hydrogen bonds and the setting on of the γ structure is ruled by conformational effects only.

Beyond clarifying the role of subtle molecular phenomena in modulating the structural properties of nylons polymers, the present study shows the importance of molecular modeling in the understanding of structure-properties correlations in polymer materials, providing information which is of fundamental importance for their characterization and hardly accessible from experiments.

Even if the infinite crystal does not take into account the existence of finite dimension effects (e.g. the lamellar morphology of polymers, chain folds ecc) which could influence the relative stability of polymorphs, in any case it is an unavoidable starting point for the modeling of crystalline polymers.

The additional possibility to compute the spectroscopic response [14–23], paves the way to the application of quantum chemical calculations in different branches of polymer science and technology. Furthermore, it should be noticed that the current accuracy of these methods paves the way to use molecular modeling as a design tool, to predict the response of the material prior to wider and expensive experimental investigations.

Acknowledgments

The authors would like to gratefully thank Chiara Castiglioni (POLIMI) for the useful discussion and suggestions during the writing of the manuscript.

References

- [1] Kohan MI. Nylon plastics handbook. New York: Hanser; 1995.
- [2] Lee KH, Kim KW, Pesapane A, Kim HY, Rabolt JF. *Macromolecules* 2008;41:1494–8.
- [3] Bianco A, Iardino G, Manuelli A, Bertarelli C, Zerbi G. *Chem Phys Chem* 2007;8:510–4.
- [4] Liu Y, Qi L, Guan F, Hedin NE, Zhu L, Fong H. *Macromolecules* 2007;40:6283–90.
- [5] Zussman E, Burman N, Yarin AL, Khalfin R, Cohen Y. *J Polym Sci Part B Polym Phys* 2006;44:1482–9.
- [6] Milani A, Casalegno M, Castiglioni C, Raos G. *Macromol Theory Simul* 2011;20:305–19.
- [7] Loo LS, Gleason KK. *Macromolecules* 2003;36:2587–90.
- [8] Chen G, Shen D, Feng M, Yang M. *Macromol Rapid Commun* 2004;25:1121–4.
- [9] Kinoshita Y. *Makromol Chem* 1959;33(1).
- [10] Dasgupta S, Hammond WB, Goddard WA. *J Am Chem Soc* 1996;118:12291–301.
- [11] Aleman C, Casanovas J. *Colloid Polym Sci* 2004;282:535–43.
- [12] Bernadó P, Aleman C, Puiggali J. *Eur Polym J* 1999;35:835–47.
- [13] Li Y, Goddard AG. *Macromolecules* 2002;35:8440–55.
- [14] Quarti C, Milani A, Civalleri B, Orlando R, Castiglioni C. *J Phys Chem B* 2012;116:8299–311.
- [15] Torres FJ, Civalleri B, Meyer A, Musto P, Albuñia AR, Rizzo P, et al. *J Phys Chem B* 2009;113:5059–71.
- [16] Torres FJ, Civalleri B, Pisani C, Musto P, Albuñia AR, Guerra G. *J Phys Chem B* 2007;111:6327–35.
- [17] Ferrari AM, Civalleri B, Dovesi R. *J Comput Chem* 2010;31:1777–84.
- [18] Galimberti D, Quarti C, Milani A, Brambilla L, Civalleri B, Castiglioni C. *Vib Spectrosc* 2013;66:83–92.
- [19] Quarti C, Milani A, Castiglioni C. *J Phys Chem B* 2013;117:706–18.
- [20] Milani A, Galimberti D. *Macromolecules* 2014;47:1046–52.
- [21] Milani A. *Polymer* 2014;55:3729–35.
- [22] Galimberti D, Milani A. *J Phys Chem B* 2014;118:1954–61.
- [23] Milani A. *J Phys Chem B* 2015;119:3868–74.
- [24] Dovesi R, Orlando R, Civalleri B, Roetti C, Saunders VR, Zicovich-Wilson CM. *Z Krist* 2005; 220:571–573.
- [25] Dovesi R, Saunders VR, Roetti C, Orlando R, Zicovich-Wilson CM, Pascale F, et al. *CRYSTAL09 user's manual*. Torino: University of Torino; 2009.
- [26] Becke A. *J Chem Phys* 1993;98:5648–52.
- [27] Lee C, Yang W, Parr R. *Phys Rev B* 1988;37:785–9.
- [28] Adamo C, Barone V. *J Chem Phys* 1999;110:6158.
- [29] Peintinger MF, Oliveira DV, Bredow T. *J Comput Chem* 2013;34:451–9.
- [30] Grimme S. *J Comput Chem* 2004;25:1463–73.
- [31] Grimme S. *J Comput Chem* 2006;27:1787–99.
- [32] Civalleri B, Zicovich-Wilson CM, Valenzano L, Ugliengo P. *Crystengcomm* 2008;10:405–10.
- [33] Holmes DR, Bunn CW, Smith DJ. *J Polym Sci* 1955;17:159–77.
- [34] Simon P, Argay GY. *J Polym Sci Polym Phys Ed* 1978;16:935–7.
- [35] Arimoto H, Ishibashi M, Hirai M. *J Polym Sci Part A Polym Chem* 1965;3:317–26.
- [36] Fredericks RJ, Doyne TH, Sprague RS. *J Polym Sci* 1966;4:899–911.
- [37] Atkins EDT, Hill MJ, Veluraja K. *Polymer* 1995;36:35–42.
- [38] Cojazzi G, Fichera A, Malta V, Zannetti R. *Makromol Chem* 1978;179:509–18.
- [39] Cojazzi G, Fichera A, Garbuglio C, Malta V, Zannetti R. *Makromol Chem* 1973;168:289–301.
- [40] Itho T. *Jpn J Appl Phys* 1976;15:2295–306.
- [41] Bernadó P, Aleman C, Puiggali J. *Macromol Theory Simul* 1998;7:659–64.
- [42] Simon S, Duran M, Dannenberg JJ. *J Chem Phys* 1996;105:11024–31.

2.2 Crystal structure and spectroscopic assignment of Poly(trimethylene terephthalate)-PTT

Aromatic polyesters are a class of polymeric materials showing peculiar intra and intermolecular interactions which are responsible of the modulation of the their structure.

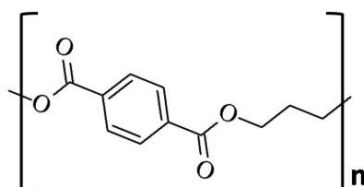


Fig. 2.2 Chemical structure of Poly(trimethylene terephthalate)

Poly(trimethylene terephthalate), PTT, the aromatic polyester containing three methylene units between the aromatic rings, has become available at low cost only recently, paving the way to its technological application for commercial production. Indeed, its physicochemical and mechanical properties, different from those of PET and PBT, show promising potentialities for applications, even if there are several phenomena that still need a complete investigation.

As already pointed out, vibrational spectroscopy is very powerful tool for structural characterization, with the additional advantage of being also used in the industrial environment. However, a correct assignment of the spectral features is mandatory for any analytic application of this technique.

Despite the relative simplicity of PTT, possessing only one stable crystalline phase at room temperature, the contribution of the amorphous phase to the experimental vibrational spectra have made very complex the recognition of marker bands of the crystal generating contrasting interpretations in the literature.

As illustrated in detail in paper "*Crystal Structure and Vibrational Spectra of Poly(trimethylene terephthalate) from Periodic Density Functional Theory Calculations*" (D. Galimberti, A. Milani; J. Phys. Chem. B. 118 (2014) 1954) here attached, in order to solve these ambiguities, we proposed a DFT investigation of the vibrational properties of PTT using the CRYSTAL code.

Before the prediction of the vibrational response, a careful setup and test of the possible variables of the simulations was required, since this family of polymers had been never investigated by means of periodic DFT calculations.

As a first step we fully optimize the geometry testing different computational set-up (B3LYP functional and different basis set). In all calculations the B3LYP functional has been augmented with the empirical correction for dispersion interaction (B3LYP-D2) proposed by Grimme, checking different possible choices for the set of empirical parameters in the model.

As in the case of nylon (see section 2.1), we assessed the accuracy of the computations adopted by means of the comparison of the computed and experimental cell parameters taken from the literature. The computed value reproduce nicely the experimental one in all the case, in particular the combination of the B3LYPD with 6-31G(d,p), adopted in a previous paper on Nylon6 [1], proved to be again the best compromise.

As a second step, we computed the IR spectra and carried out the analysis of the computed vibrational eigenvectors: on this basis, we revised the previous spectral assignments, based on the only experimental investigations and we have been able to propose additional marker bands for the crystalline phase.

Moreover, following the strategy already adopted for other polymeric systems, we compared the spectra obtained for the crystal in its three-dimensional crystalline packing, with those obtained for a infinite chain model to distinguish the bands which are actually marker of the presence of an ordered supra-molecular organization (bands of crystallinity), compared to those bands which are simply markers of chains possessing a "regular" conformation, regardless of the supramolecular organization (regularity bands).

The results obtained for PTT demonstrated the reliability of periodic DFT calculations for the investigation of structural and vibrational properties of polyesters.

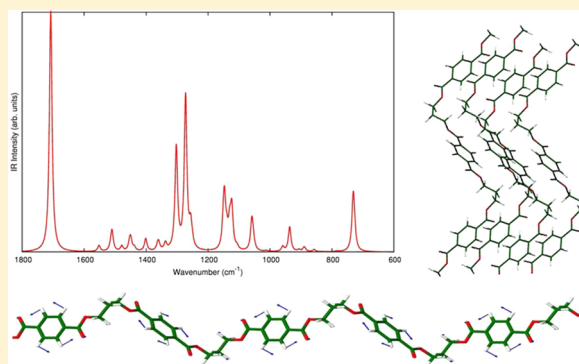
Crystal Structure and Vibrational Spectra of Poly(trimethylene terephthalate) from Periodic Density Functional Theory Calculations

Daria Galimberti and Alberto Milani*

Dipartimento di Chimica, Materiali, Ingegneria Chimica "Giulio Natta", Politecnico di Milano, Piazza Leonardo da Vinci 32, 20133 Milan, Italy

S Supporting Information

ABSTRACT: The crystal structure and the IR spectrum of crystalline poly(trimethylene terephthalate), PTT, have been investigated by means of periodic density functional theory calculations including Grimme's correction for dispersion interactions. Both structural and spectroscopic results have been critically compared to the experimental data taken from the literature, showing very good agreement between theory and the experiments. The previous spectral assignments, based only on experimental investigations, have been revised, and further insights have been obtained. Furthermore, spectroscopic markers of crystallinity or regularity (i.e., of the regular conformation of the polymer chain) have been proposed. In addition to the analysis of the IR spectra, the effect of computational parameters on the crystal structure determination (basis sets and parameters for Grimme's correction) have been analyzed. This work demonstrates that state-of-the-art computational methods can provide an unambiguous description of the structural and vibrational properties of crystalline polymers on the basis of the peculiar intra- and intermolecular interactions occurring in different macromolecular materials.



I. INTRODUCTION

Aromatic polyesters are a well-known class of polymeric materials whose application is now widespread in our everyday life, as witnessed by poly(ethylene terephthalate) (PET) and its countless applications. These polymers show peculiar properties such as even-odd effects depending on the number of methylene units between aromatic rings, resulting in a different conformation and different mechanical behavior for individual members of this family, and even some subtle polymorphic transitions. Indeed, the second member of this family in order of technological importance, poly(butylene terephthalate) (PBT), shows a reversible transition between different crystal structures upon mechanical deformation due to a variation in the conformation of the chain.^{1–6} On the other hand, poly(trimethylene terephthalate), PTT, the aromatic polyester containing three methylene units between the aromatic rings, has received much less attention with respect to PET and PBT. This is mainly due to the fact that it has become available at low cost only recently, paving the way to its technological application for commercial production. The physicochemical and mechanical properties of PTT are different from those of PET and PBT and show promising potentialities for its applications.

As for other classes of polymers, vibrational spectroscopy techniques have been usually adopted to investigate the properties of these polyesters. However, these investigations have been based exclusively on experimental works or

semiempirical calculations, and it is thus quite common to find different interpretations and also some ambiguities in the past literature.

In this context, computational techniques which can give a reliable description of both the structural and vibrational properties of the system became available only very recently.^{7–13}

Therefore, in this work we applied these state-of-the-art techniques to carry out periodic density functional theory (DFT) calculations augmented with an empirical dispersion correction (DFT-D)^{14,15} of poly(trimethylene terephthalate) by using the CRYSTAL09 code,^{16,17} to investigate both the structural and vibrational properties of PTT. Actually, the CRYSTAL code has been successfully applied to a few polymer systems, namely, to the case of polystyrene,^{7–9} polyglycine,¹⁰ nylon 6 polymorphs,¹¹ nylon 6,6,¹² and poly(tetrafluoroethylene),¹³ where it allowed solution of open questions in the interpretation of the structural and vibrational properties, offering computational tools not available before.

Our aims are 2-fold: from one hand, since PTT has been much less studied than PET or PBT, we investigate its structural and vibrational properties to unveil some uncertainties in the interpretation of its IR spectra and to give a

Received: November 25, 2013

Revised: January 16, 2014

Published: January 27, 2014

Table 1. Summary of the Numerical Values Adopted in Calculations (Cases 1–3; See Text) for the Parameters Occurring in Grimme's Correction for Dispersion Interactions^a

	D	s_6	C_6^H	C_6^C	C_6^O	C_6^N	R_{vdW}^H	R_{vdW}^C	R_{vdW}^O	R_{vdW}^N
case 1	20	1.05	0.14	1.75	0.70	1.23	1.001	1.452	1.342	1.397
case 2	20	1.00	0.14	1.75	0.70	1.23	1.3013	1.5246	1.4091	1.4668
case 3	20	1.00	0.14	1.75	0.70	1.23	1.3013	1.70	1.52	1.55

^aIn all cases, a cutoff distance of 25.0 Å was used to truncate direct lattice summation. C_6 are in units of $\text{J nm}^6 \text{mol}^{-1}$ while R_{vdW} are in unit of Å.

contribution for better insight into its properties. On the other hand, due to the absence of polymorphism effects, PTT is the ideal test case to set up the computational parameters before extending the same methodology to much more complicated systems, such as PBT and its polymorphic transitions, which will be the subject of future investigations.

To these aims, in section III.1 the DFT-D computed crystal structure of PTT will be compared with the available experimental data, discussing also the importance of different computational parameters, such as the basis set choice or the parameters adopted in Grimme's correction for dispersion interactions.^{14,15,18} On the basis of this structural investigation, in section III.2 the IR spectra of the PTT crystal will be predicted and compared with previous experimental studies taken from the literature.^{19–26}

II. COMPUTATIONAL DETAILS

Full geometry optimization of the crystal structure and the calculation of the IR spectra of PTT have been carried out by means of the CRYSTAL09 code^{16,17} in the framework of DFT. We adopted the B3LYP^{27,28} hybrid exchange-correlation functional together with the 6-31G(d,p) basis set and the recently developed pob-TZVP²⁹ basis set that has been explicitly parametrized for CRYSTAL periodic calculations. In all calculations the B3LYP functional has been used augmented with an empirical correction for dispersion interaction (B3LYP-D) proposed by Grimme^{14,15} and implemented in CRYSTAL09. Due to the possibility of a choice of different sets of empirical parameters in the model, three different cases have been considered and compared in the present investigation as also done in previous works.^{11–13} The numerical values of these parameters are reported in Table 1: (case 1) parameters proposed by Grimme in his original work;^{14,15} (case 2) parameters proposed by Civalleri et al.;¹⁸ (case 3) same parameters as those in case 2 except van der Waals (vdW) radii of C, N, and O which have been fixed to the standard values reported by Bondi.^{30,31}

In all calculations, the atomic positions and the lattice parameters were fully optimized; default optimization algorithms and convergence criteria were adopted.

In the case of PTT, only one stable form has been found and no other polymorph has been observed: two independent resolved structures have been proposed in the literature by Poulin-Dandurand et al.³² and Desborough et al.,³³ and both agree in predicting a triclinic unit cell with $P\bar{1}$ space group and TGGT conformation on the methylene chain. In our case, as starting guess structure for the calculations, we considered the experimentally determined crystal parameters and atomic coordinates reported by Poulin-Dandurand et al.³² As already proposed in previous works^{11–13} and as explained in section III.2, in order to detect the spectroscopic markers of regularity/crystallinity, we carried out also geometry optimization and frequency calculation on the infinite polymer chain characterized by a regular conformation (one-dimensional (1D)

model chain), taking as the starting structure the conformation shown by the chain in the crystal. The optimized PTT crystal structure is sketched in Figure 1.

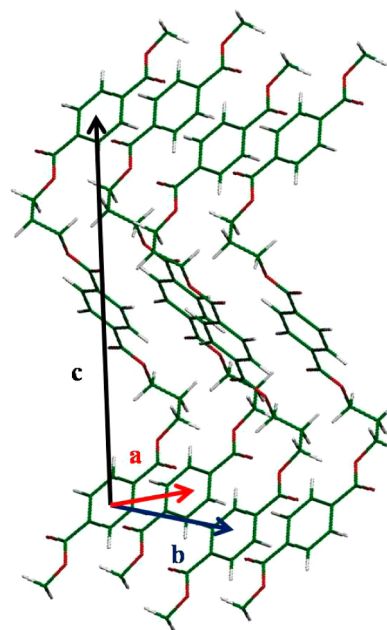


Figure 1. Sketch of the crystalline structure of PTT.

Normal frequency calculations at the Γ point have been carried out on the optimized geometries as achieved by diagonalization of the (numerically calculated) Hessian matrix.

The DFT-D computed spectra have been compared with experimental IR spectra taken from the literature.^{19–26} In these previous works, the authors focused respectively on different frequency ranges when analyzing the vibrational properties of PTT; therefore, when our results are compared with the experimental ones, IR spectra recorded by different authors have been plotted in the different figures depending on the spectral region under investigation.

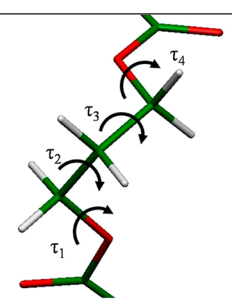
From now on, for the sake of simplicity, we will indicate as B3LYP-D(cX) the DFT calculation carried out by including Grimme's correction using "case X" ($X = 1, 2, 3$) parameters reported in Table 1. To compare the computed and the experimental data, the calculated frequencies B3LYP-D(c3)/6-31G(d,p) (which is the method adopted for the interpretation of the vibrational properties of PTT; see the next section) were scaled by 0.9713. This scaling factor has been determined to put the DFT computed C=O stretching band in correspondence of the experimental reference bands found at 1710 cm^{-1} by many authors,^{19,20,22} and it has been used both for the crystal and the 1D chain model.

Table 2. Experimental^{32,33} and B3LYP-D Computed Cell Parameters for PTT^a

	expt		6-31G(d,p)			pob-TZVP		
	ref 32	ref 33	c1	c2	c3	c1	c2	c3
<i>a</i>	4.637	4.600	4.162	4.331	4.386	4.367	4.461	4.514
<i>b</i>	6.266	6.200	5.983	6.482	6.540	6.089	6.229	6.267
<i>c</i>	18.640	18.300	18.322	18.056	18.377	16.909	17.011	17.191
α	98.400	98.000	96.513	100.982	101.004	98.037	98.906	99.079
β	93.000	90.000	90.609	89.903	89.973	90.172	90.094	90.078
γ	111.100	112.000	112.061	116.218	116.462	112.459	112.218	112.127
	Percent Errors							
<i>a</i>			-10.253	-6.595	-5.410	-5.830	-3.806	-2.652
<i>b</i>			-4.518	3.448	4.371	-2.830	-0.592	0.015
<i>c</i>			-1.706	-3.133	-1.410	-9.287	-8.737	-7.773
α			-1.918	2.624	2.647	-0.369	0.514	0.690
β			-2.571	-3.330	-3.255	-3.041	-3.125	-3.142
γ			0.865	4.607	4.827	1.223	1.006	0.925
	Average Percent Errors							
			3.639	3.956	3.653	3.763	2.963	2.533

^aDistances are in Å; angles, in degrees. Percent errors and the average percent errors with respect to the structure reported in ref 32 are reported for each case.

Table 3. Experimental^{32,33} and B3LYP-D(c3) Computed Dihedral Angles for the Alkyl Sequence of the PTT Chain^a

	Exp. ³²	Exp. ³³	6-31G(d,p)	pob-TZVP	
τ_1	168	167	164	174	
τ_2	60	73	58	62	
τ_3	60	61	67	63	
τ_4	170	152	172	176	

^aAngles in degrees.

III. RESULTS AND DISCUSSION

III.1. Crystalline Structure. In Table 2 we report the values of the cell parameters obtained by full geometry optimization by using different parameters for Grimme's correction and two basis sets (6-31G(d,p) and pob-TZVP). These values are compared to the experimental ones reported by Poulin-Dandurand et al.,³² the percent errors for each case have also been estimated.

In previous papers on Nylon 6¹¹ and Nylon 6,6,¹² a very good agreement has been found with experimental values when the B3LYP/6-31G(d,p) level of theory is employed, and the best results have been reached by using case 3 parameters for Grimme's correction [B3LYP-D(c3)/6-31G(d,p)]. This trend is confirmed for PTT, even if now also B3LYP-D(c1) is a good approximation in addition to B3LYP-D(c3), with an average error over all the cell parameters of 3.639.

Furthermore, our DFT calculations confirm that the PTT chains in the crystal possess a TGGT conformation on the alkyl part as reported in Table 3.

However, it should be noted that B3LYP-D(c1) shows much larger errors if only *a* and *b* parameters are considered: in these cases, the DFT results largely underestimated the experimental values. This trend has been found also in other cases when the parameters proposed by Grimme in his original work (that is B3LYP-D(c1))^{11,12,18} are used; in fact these parameters are

known to overcorrect the dispersion interaction, and *a* and *b* cell parameters are indeed related to the intermolecular weak packing of the chains and are significantly influenced by Grimme's correction.

On this basis, we find again that B3LYP-D(c3) parameters can be considered the best choice of the three. In this work we also repeated the calculations by employing the recently developed pob-TZVP basis set,²⁹ explicitly parametrized to be used in periodic calculations with CRYSTAL09 code. Due to the fact that this basis set is more extended than 6-31G(d,p) and it has been adapted for CRYSTAL calculations, we should expect better agreement with the experimental results.

Actually, when considering B3LYP-D(c2) and B3LYP-D(c3), the average error is further reduced and now B3LYP-D(c3)/pob-TZVP is the best choice among all of the ones here investigated. In particular, the percent errors on *a* and *b* parameters are now almost half with respect to the 6-31G(d,p) case; this result is quite straightforward since a larger basis set such as pob-TZVP largely reduces effects such as basis set superposition error which are more effective on those parameters that are related to intermolecular packing. However, an unexpected result is found in the case of the *c* parameter, associated with the chain axis: when using the pob-TZVP basis set, the percent errors now drastically increase in all cases and are around 7–9%, much larger than the 1.5–3% error found for

the 6-31G(d,p) basis set. The reasons for such discrepancies are unknown, and other systems should be analyzed to verify if some systematic errors are present for this basis set, maybe due to the fact that it has been developed and tested only for ionic solids, semiconductors, and metals.²⁹ Since c parameter is directly related to the chain axis and thus to the intramolecular interactions, the ones which mainly affect the vibrational properties of this system, we preferred to adopt the B3LYP-D(c3)/6-31G(d,p) level of theory for analysis of the IR spectra of PTT rather than the B3LYP-D(c3)/pob-TZVP level. Very good predictions of the IR spectra have been indeed obtained for other polymers already at the 6-31G(d,p) level;^{7–13} the next analysis of IR spectra of PTT will be thus based on B3LYP-D(c3)/6-31G(d,p) data.

III.2. Prediction of the IR Spectra. On the basis of the structural optimization discussed in the previous section, we here analyze in detail the vibrational features of PTT and in particular its IR spectra: in the literature, even if in the case of PTT no polymorphism effect is observed, some discrepancies are present in the spectroscopic assignments. As mentioned above, the DFT spectra reported here are those obtained at the B3LYP-D(c3)/6-31G(d,p) level of theory. In any case, despite the large error on the c parameter, similar results are obtained also when the pob-TZVP basis set is used (see the Supporting Information).

In Figures 2–5, the DFT computed spectra for the PTT crystals are compared in different frequency ranges with the

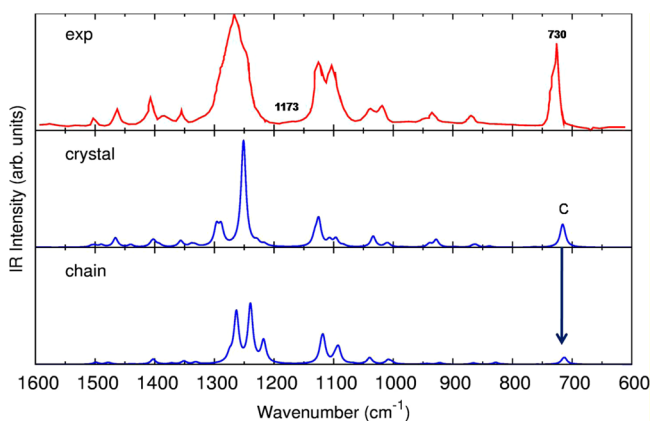


Figure 2. Comparison of the experimental spectrum of Bulkin et al.¹⁹ and the B3LYP-D(c3)/6-31G(d,p) spectra computed for the crystal and the 1D chain model in the frequency range of 600–1600 cm^{-1} .

experimental IR spectra reported in the literature by different authors;^{19,20,25} in addition to the spectrum computed for the crystal, also the spectrum of the regular infinite chain model is shown to discuss the importance of intermolecular interaction on the vibrational properties of crystalline PPT.

Since the birth of polymers' vibrational spectroscopy, the theoretical treatment of the vibrational problem of crystalline polymers has been carried out by choosing a single, infinite chain model possessing the same conformation observed in the crystal (see for example refs 34 and 35 for a general discussion). The rationale behind this choice is related to the fact that the vibrational properties are mostly influenced by intramolecular interactions, while intermolecular interactions can be considered as a small perturbation. Obviously, this approximation can be very crude in some cases (for example hydrogen-bonded polymers) where intermolecular effects can heavily affect the

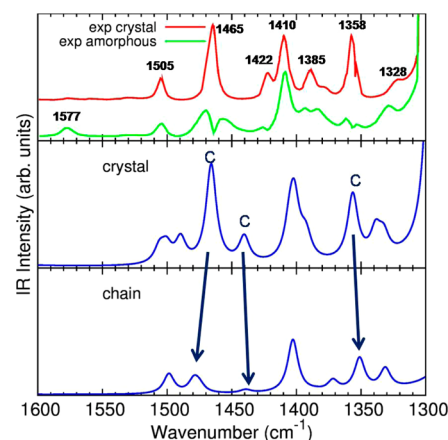


Figure 3. Comparison of the experimental spectra of Kim et al.²⁰ and the B3LYP-D(c3)/6-31G(d,p) spectra computed for the crystal and the 1D chain model in the frequency range of 1300–1600 cm^{-1} .

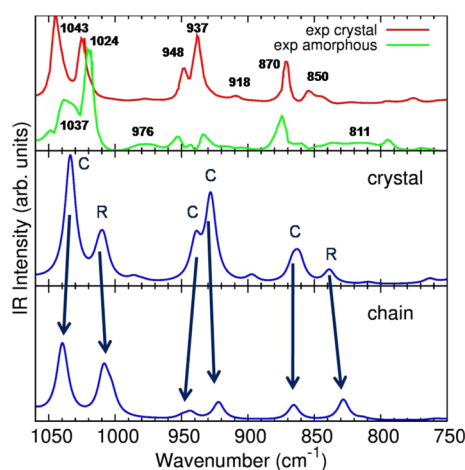


Figure 4. Comparison of the experimental spectra of Kim et al.²⁰ and the B3LYP-D(c3)/6-31G(d,p) spectra computed for the crystal and the 1D chain model in the frequency range of 750–1050 cm^{-1} .

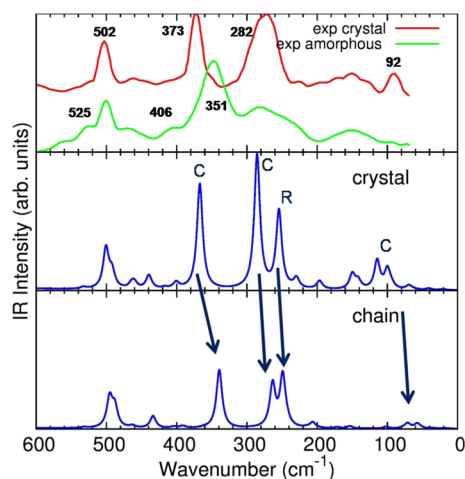


Figure 5. Comparison of the experimental spectra of Vasanthan et al.²⁵ and the B3LYP-D(c3)/6-31G(d,p) spectra computed for the crystal and the 1D chain model in the frequency range of 0–600 cm^{-1} .

vibrational spectra. Furthermore, even some features (e.g., crystal-field splitting) observed in the IR spectrum of the simplest polymer, polyethylene, are due to supramolecular

effects (i.e., the presence of more than one molecule in the unit cell). As a further aspect, in this ground a debate took place in past literature about the so-called “regularity” and “crystallinity” bands: indeed, when considering the vibrational spectra of crystalline polymers, it is important to distinguish between those bands which are effectively due to the presence of a long-range tridimensional order (i.e., crystallinity bands) and those bands which are due only to the fact that the chains possess a regular conformation (i.e., regularity), independently of their supramolecular packing in a crystal lattice. The latter ones cannot be necessarily markers also of the presence of 3D crystals since they are the result only of the intramolecular order. In other words, regularity bands are already present in smectic phases simply characterized by orientational order and by the presence of “elongated” chains with regular conformation (e.g., quenched polypropylene) as well as for stretch oriented polymers where the occurrence of elongated conformations (e.g., transplanar polymethylenes chains or helix conformations) versus coiled chains should be distinguished from recrystallization in 3D lamellar domains. Therefore, these differences have a practical outcome: when using bands for a quantitative estimate of the crystallinity degree, it should be taken into consideration the fact that a regularity band cannot be a true marker of the crystalline phase since it is independent of the molecular packing of the chains and it is only sensitive to the regular intramolecular structure. In order to assign the bands as regularity vs crystallinity bands, the spectrum of the crystal should be compared to the spectrum of the 1D model chain: those bands whose pattern in frequency and/or intensity and/or band shape is markedly different in the two cases are indeed crystallinity bands since they are largely affected by the crystal packing (e.g., the intensification of IR absorptions have been found for hydrogen-bonded polymers such as nylons,^{11,12} and crystal-field band splitting is observed in polyethylene); on the other hand, those bands which have a similar pattern in the two spectra should be considered as regularity bands, since they are only affected by the existence of a peculiar regular conformation of the chains, independently of their intermolecular environment. Also in the case of PTT, we will see that the interactions between the chains in the crystal will influence significantly the IR spectrum, allowing a clear discrimination between crystallinity and regularity bands.

In all of the figures here displayed, very good agreement between experimental and DFT computed spectra is found: the spectrum computed for the crystal actually reproduces the experimental results also in the minor features and provides a detailed interpretation and assignment of the marker bands without taking into account standard empirical correlations which could give place to uncertainties and ambiguities.

In Figure 2 we compare the DFT spectra with the experimental spectrum reported by Bulkin et al.¹⁹ in the frequency range of 600–1800 cm^{-1} : the good agreement between DFT and experimental spectra can be immediately verified. From this general comparison we can already confirm one of the previous assignments: it has been proposed by different authors^{19–22,26} that an experimental band occurring at 1173 cm^{-1} should be assigned to trans conformation in the amorphous phase. In our calculations, no bands are predicting in this range, thus supporting the previous assignment to the amorphous phase. Furthermore, we can also corroborate the suggestion that the band at 730 cm^{-1} receives contributions both from the amorphous and the crystalline phases as stated

by Ward and Wilding,²³ thought it should be remarked that the main contribution comes from the amorphous one.

In order to proceed further in a detailed assignment, in Figures 3 and 4 we analyze separately the 1300–1600 and 600–1050 cm^{-1} frequency ranges, comparing the DFT spectrum of the crystal with the experimental spectra reported by Kim et al.²⁰ who analyzed these regions in detail. The region between 1300 and 1200 cm^{-1} will be not commented on in detail since a very strong and broad band is present in the experimental spectra; this band is due to both crystalline and amorphous domains, and it is thus not significant, neither for the quantitative determination of the amount of the amorphous/crystalline phase in different samples nor to investigate the intra- or intermolecular properties of PTT in different phases.

In the range of 1300–1600 cm^{-1} , the band at 1577 cm^{-1} has been found to decrease with annealing and has been assigned by Kim to the amorphous phase. A similar result has been reported also by other authors:^{22,26} also in this case no bands are predicted, thus supporting this previous assignment.

Considering now the band observed at 1465 cm^{-1} , we can verify that this band is a significant marker of the crystalline phase (computed band at 1466 cm^{-1}). In the experimental spectra, this band actually consistently increases upon annealing while in the amorphous spectra only a broad band with two main components at 1469 and 1458 cm^{-1} is observed.^{19,20,22,26} The comparison between the crystal and the 1D chain model reveals that this band gathers intensity in the crystal and it is thus a true crystallinity band. The intensification that is found for many crystallinity bands of PTT can be related to the existence of quite significant interactions among the chains in the crystals. This is also proved by the red shift predicted for the C=O stretching band at 1710 cm^{-1} of the crystal with respect to the 1D model chain (1750 cm^{-1}): this shift points out the existence of nonnegligible local intermolecular interactions which are responsible for the modulation of the IR spectrum of the crystal. Another band, which usually is assigned as a marker of the crystalline phase, is the strong one observed at 1358 cm^{-1} ; many authors^{19–24,26} assign this feature to a wagging mode of the CH_2 in a TGGT gauche conformation, while Lee et al.²⁴ assigned it as a marker of a GTTG trans conformation. Our calculations indicate that this band (computed at 1356 cm^{-1}) is an evident marker of the PTT crystalline phase and confirm its assignment to the TGGT conformation, which is the one observed in the crystal also in our calculations (the sketch of the normal mode is reported in the Supporting Information). This classification is particularly significant also for practical and analytical purposes since this band has been proposed as a marker to evaluate quantitatively the amount of gauche conformers present in a sample.²² It must be noted that, even if this band is quite strong also in the single chain spectrum, it is intensified by the crystalline field and thus it is a crystallinity band. Another band which has a significant intensity both in the experiments and calculations is the band observed at 1410 cm^{-1} . This feature, associated with aromatic ring vibrations, is predicted by the convolution of two bands calculated at 1405 and 1403 cm^{-1} . This band, however, is present for both amorphous and crystalline phases and should be thus treated as a reference band. Considering then the band experimentally observed by some authors at 1385 cm^{-1} , this band has been usually associated with the amorphous phase^{20–22,24} and in particular with GTTG trans conformers²² or TGGT gauche conformations.²⁴ Kim et al.²⁰ showed that in

Table 4. Classification of Marker Bands of PTT Crystal^a

exptl freq (cm ⁻¹)	previous classification	B3LYP-D(c3)/6-31G(d,p) freq (scaled by 0.9713; cm ⁻¹)	B3LYP-D(c3)/6-31G(d,p) IR intensity (km/mol)	new classification
92	crystal ²⁵	convolution		crystal (crystallinity)
		100	12	
		115	18	
282	crystal ²⁵	254{249}	48{32}	crystal (crystallinity/regularity)
		285	83	
351	amorphous ²⁵			amorphous
373	crystal ²⁵	367	66	crystal (crystallinity)
525	amorphous ²⁵			amorphous
811	amorphous ^{21,22,26}			amorphous
850	crystal ^{20,23}	839{828}	23{36}	crystal (regularity)
870	crystal + amorphous ²⁰	convolution		crystal (crystallinity)
		861	41	
		866	33	
		928	149	
937	crystal ^{19–22,26}	928	149	crystal (crystallinity)
948	crystal ^{19–22,26}	939	68	crystal (crystallinity)
976	amorphous ^{20,22,26}			amorphous
1024	crystal ^{20,22}	convolution		crystal (regularity)
		1009{1003}	59{35}	
		1012{1009}	35{78}	
1173	amorphous ^{19–22,26}			amorphous
1037/1043	crystal ^{20–23,26}	1034	218	crystal (crystallinity)
1328	amorphous ^{20,22,26}	convolution		significant contributions due to crystal
		1332	38	
		1339	49	
		1356	122	
1358	crystal ^{19–24,26}	1356	122	crystal (crystallinity)
1385/1389	amorphous ^{19–22,26} /crystal ²⁰	shoulder		amorphous with small crystal contribution
		1392	38	
1410	reference band ^{19,24}	convolution		reference band
		1403	107	
		1405	56	
		1440	48	
1422	crystal ²⁰	1440	48	crystal (crystallinity)
1465	crystal ^{19,20,22,26}	1466	184	crystal (crystallinity)
1505	crystal, ²¹ ref ^{20,22}	1506	29	contributions due to crystal
1577	amorphous ^{20,22,26}			amorphous
1710	reference band ^{19,22}	convolution		reference band
		1710	1048	
		1711	1024	

^aThe computed frequencies [B3LYP-D(c3)/6-31G(d,p)] refer to the calculation on the crystal. In the case of “regularity” bands the computed value according to the model of the isolated chain (1D model) is also reported in {} brackets. In the Supporting Information the sketch of the normal mode associated with each band is reported.

the same range a band at 1389 cm⁻¹ is observed for the crystal and another one at 1393 cm⁻¹ is observed for the amorphous. The DFT spectrum shows (at 1392 cm⁻¹) a shoulder of the main features at 1405 cm⁻¹ which could indicate indeed that in this region a contribution of the crystalline phase is present. However, due to the simultaneous presence of bands of the two phases, this spectral range is not significant for quantitative measurements. In this frequency range three other bands should be taken into account, observed respectively at 1328, 1422, and 1505 cm⁻¹. The first one is found to decrease with annealing, and therefore it has been assigned to the amorphous phase;^{20,22,26} our calculation reveals that the two bands at 1332 and 1339 cm⁻¹ can be put in correspondence with this frequency value, thus indicating that the experimental band at 1328 cm⁻¹ cannot be assigned uniquely to the amorphous phase.

In the case of the weak band at 1422 cm⁻¹, our calculation corroborates the assignment to the crystalline phase proposed by Kim et al.²⁰ a band is predicted at 1440 cm⁻¹ which can be

put in correspondence with this band; moreover by comparison with the 1D chain model, we can state that it is a true crystallinity band. Finally, the band at 1505 cm⁻¹ has been assigned to the crystal phase by Chuah²¹ and as a reference band by other authors;^{20,22} our calculation reveals that the crystal gives contribution to this band (1506 cm⁻¹).

Another frequency range where significant markers of the crystal and amorphous phase are found is the 600–1050 cm⁻¹ region (Figure 4). Here again very good agreement between experimental and DFT spectra is found. Going into detail, the band at about 1043 cm⁻¹ is assigned to the crystalline phase by many authors (with small differences in frequency (1043^{20,22,23} and 1037 cm^{-19,21,26}) while a shoulder at slightly lower frequency is reported for the amorphous phase.^{20–23,26} DFT calculations confirm its assignment to the crystal phase (band calculated at 1034 cm⁻¹). Comparison with the 1D chain model reveals that this band is enhanced in intensity in the crystal, and it is thus a crystallinity band. A second band is predicted at about 1010 cm⁻¹ (convolution of the two bands computed at

1012 and 1009 cm^{-1}) which can be put in correspondence with the experimental bands at 1024 cm^{-1} . Some authors^{20,22} assigned this band to the crystalline phase; however, at 1018 cm^{-1} another band is observed for the amorphous phase,^{19,20,22} and thus we do not believe that this feature could be used for quantitative measurements of the crystallinity percentage due to this bands overlap. In any case, the band predicted at 1010 cm^{-1} is a regularity band, since its intensity does not show an increase with respect to the corresponding band of the 1D model chain (convolution of two bands predicted at 1003 and 1009 cm^{-1}). The doublet observed at about 940 cm^{-1} is also very well predicted by the calculations. The two experimental bands at 948 and 937/933 cm^{-1} have been assigned in the past as markers of gauche conformations in the crystal phase^{19–22,26} although some discrepancies are found among the authors:^{23,26} at 933 cm^{-1} also a contribution due to the amorphous phase is present, and thus the assignment of this band from experimental data is quite ambiguous. DFT calculations indicate that both bands (calculated at 939 and 928 cm^{-1}) are indeed markers of the crystalline packing.

In the literature, a very important marker of the amorphous phase/trans conformation, which is also used for quantitative analysis, is the band at 976 cm^{-1} :^{20,22,26} our predicted spectra show only a very weak band in this region (986 cm^{-1}), thus confirming the assignment to the amorphous phase. A similar situation occurs for the experimental band at 811 cm^{-1} :^{21–23,26} not predicted by the calculation and thus marker of the amorphous phase. Another doublet is observed at about 860 cm^{-1} with two components at about 850 and 870 cm^{-1} . Based on DFT calculations, both bands (computed at 863 and 839 cm^{-1}) contribute to the crystal spectrum in agreement with previous assignments,^{20,23} even if for the higher frequency components also the contribution of the amorphous takes place.²⁰ However, only the higher frequency band is a true crystallinity band (convolution of two bands at 866 and 861 cm^{-1}) while the one corresponding to the experimental band at 850 cm^{-1} is indeed a regularity band (839 cm^{-1}).

Finally, Yamen et al.²² assigned a band at 918 cm^{-1} to the amorphous phase: in our calculations a weak band is calculated at 897 cm^{-1} which could be put in correspondence with this experimental band, thus indicating that this feature is not only due to the amorphous phase.

The last frequency range here discussed is the far-IR region below 600 cm^{-1} (Figure 5), which has been experimentally investigated by Vasanthan and Yaman.²⁵ Starting from the lower frequency, we confirm that the broad 92 cm^{-1} band, which increases with annealing, is indeed associated with the crystal (115 and 100 cm^{-1} bands). The same behavior is shown by the 282 and 373 cm^{-1} bands which are thus a marker of the crystal phase (computed bands at 285 and 254 cm^{-1} for the experimental 282 cm^{-1} band and 367 cm^{-1} for the 373 cm^{-1} band). In the case of the 92 and 373 cm^{-1} bands the calculation on the 1D model chain reveals that these are actually crystallinity bands while the 282 cm^{-1} band is associated with two contributions, a higher frequency crystallinity one and a regularity one. No features are computed that can be put in correspondence with the 351 and 525 cm^{-1} bands, thus confirming their assignment to the amorphous phase.²⁵ For the experimental band at 502 cm^{-1} taking contribution both from the amorphous and crystalline regions we verified that indeed a large contribution of the crystal can be expected (band computed at 501 cm^{-1}) while the experimental band at 406

cm^{-1} is not uniquely due to the amorphous phase since a weak band is predicted at 401 cm^{-1} for the crystal.

Based on the whole preceding discussion, the final classification of the main IR bands of PTT is reported in Table 4.

IV. CONCLUSION AND PERSPECTIVES

In this work, we investigated the structural and vibrational properties of a terephthalate polyester, poly(trimethylene terephthalate), PTT, by means of state-of-the-art periodic DFT calculations. As for the other polymer systems investigated by a similar methodology,^{7,8,11–13} a detailed interpretation of PTT properties has been obtained, solving the ambiguities and the open questions which are often found in past literature. The attention has been focused here mainly on the vibrational properties of PTT and on the assignment of its IR spectrum: vibrational spectroscopies are indeed extremely sensitive to intra- and intermolecular properties, allowing an investigation of many peculiar phenomena, such as polymorphism and phase transitions. Furthermore vibrational spectroscopy techniques are widely used also in the industrial environment where they are employed both for qualitative and quantitative analyses: the importance of a correct interpretation of the IR spectra is thus well-evident and highlights the significant role played by reliable computational tools. On these grounds, the CRYSTAL code proved to be very powerful in predicting both the crystal structure and the IR spectra of polymer crystals, providing an answer to several open questions.

The present work opens the way to different future possibilities: on one hand, the simple case of PTT demonstrated the reliability of periodic DFT calculations for the investigation of polyesters and they could be extended to the investigation of more subtle phenomena in similar systems, such as for example the polymorphic transitions promoted in poly(butylene terephthalate) by mechanical deformation.^{1–6} On the other hand, based on the very good results obtained for PTT and other different polymers, the same methodology can be extended to any other crystalline polymers, both to give an interpretation of the properties of the material and to carry out an investigation of the molecular phenomena involved or to support experimental techniques in the development and characterization of innovative polymeric systems.

■ ASSOCIATED CONTENT

📄 Supporting Information

Tables listing DFT optimized values of the cell parameters and coordinates of PTT crystal and chain, DFT computed frequencies and IR intensities of PTT crystal and chain, and sketches of the normal modes of vibration of PTT crystal and a figure comparing DFT computed IR spectra by using 6-31G(d,p) and pob-TZVP basis set. This material is available free of charge via the Internet at <http://pubs.acs.org>.

■ AUTHOR INFORMATION

Corresponding Author

*Tel.: +39-02-23993383. E-mail: alberto.milani@polimi.it

Notes

The authors declare no competing financial interest.

ACKNOWLEDGMENTS

We gratefully thank Prof. Chiara Castiglioni (Politecnico di Milano) for very useful suggestions and discussions during the work and the writing of the paper.

REFERENCES

- (1) Yokouchi, M.; Sakakibara, Y.; Chatani, Y.; Tadokoro, H.; Tanaka, T.; Yoda, K. Structures of Two Crystalline Forms of Poly(butylene terephthalate) and Reversible Transition between Them by Mechanical Deformation. *Macromolecules* **1976**, *9*, 266–273.
- (2) Dobrovolny-Marand, E.; Hsu, S.; Shih, C. Spectroscopic Characterization of the $\alpha \rightleftharpoons \beta$ Crystalline Phase Transition in Poly(butylene terephthalate) and Its Copolymers with Poly(tetramethylene oxide). *Macromolecules* **1987**, *20*, 1022–1029.
- (3) Stambaugh, B.; Koenig, J. L.; Lando, J. B. X-ray Investigation of the Structure of Poly(tetramethylene terephthalate). *J. Polym. Sci., Polym. Phys. Ed.* **1979**, *17*, 1053–1062.
- (4) Hall, I. H.; Pass, M. G. Chain Conformation of Poly(tetramethylene terephthalate) and Its Change with Strain. *Polymer* **1976**, *17*, 807–816.
- (5) Desborough, I. J.; Hall, I. H. A Comparison of Published Crystalline Structures of Poly(tetramethylene terephthalate). *Polymer* **1977**, *18*, 825–830.
- (6) Nitzsche, S. A.; Wang, Y. K.; Hsu, S. L. Application of the Molecular Simulation Technique for Clarification of the $\alpha \leftrightarrow \beta$ Phase Transformation in Poly(butylene terephthalate). *Macromolecules* **1992**, *25*, 2397–2400.
- (7) Torres, F. J.; Civalleri, B.; Meyer, A.; Musto, P.; Albuñia, A. R.; Rizzo, P.; Guerra, G. Normal Vibrational Analysis of the Syndiotactic Polystyrene S(2/1)2 Helix. *J. Phys. Chem. B* **2009**, *113*, 5059–5071.
- (8) Torres, F. J.; Civalleri, B.; Pisani, C.; Musto, P.; Albuñia, A. R.; Guerra, G. Normal Vibrational Analysis of a Trans-planar Syndiotactic Polystyrene Chain. *J. Phys. Chem. B* **2007**, *111*, 6327–6335.
- (9) Albuñia, A. R.; Rizzo, P.; Guerra, G.; Torres, F. J.; Civalleri, B.; Zicovich-Wilson, C. M. Uniplanar Orientations as a Tool to Assign Vibrational Modes of Polymer Chain. *Macromolecules* **2007**, *40*, 3895–3897.
- (10) Ferrari, A. M.; Civalleri, B.; Dovesi, R. Ab Initio Periodic Study of the Conformational Behavior of Glycine Helical Homopeptides. *J. Comput. Chem.* **2010**, *31*, 1777–1784.
- (11) Quarti, C.; Milani, A.; Civalleri, B.; Orlando, R.; Castiglioni, C. Ab Initio Calculation of the Crystalline Structure and IR Spectrum of Polymers: Nylon 6 Polymorphs. *J. Phys. Chem. B* **2012**, *116*, 8299–8311.
- (12) Galimberti, D.; Quarti, C.; Milani, A.; Brambilla, L.; Civalleri, B.; Castiglioni, C. IR Spectroscopy of Crystalline Polymers from ab Initio Calculations: Nylon 6,6. *Vib. Spectrosc.* **2013**, *66*, 83–92.
- (13) Quarti, C.; Milani, A.; Castiglioni, C. Ab Initio Calculation of the IR Spectrum of PTFE: Helical Symmetry and Defects. *J. Phys. Chem. B* **2013**, *117*, 706–718.
- (14) Grimme, S. Accurate Description of van Der Waals Complexes by Density Functional Theory Including Empirical Corrections. *J. Comput. Chem.* **2004**, *25*, 1463–1473.
- (15) Grimme, S. Semiempirical GGA-type Density Functional Constructed with a Long-Range Dispersion Correction. *J. Comput. Chem.* **2006**, *27*, 1787–1799.
- (16) Dovesi, R.; Orlando, R.; Civalleri, B.; Roetti, C.; Saunders, V. R.; Zicovich-Wilson, C. M. CRYSTAL: A Computational Tool for the ab Initio Study of the Electronic Properties of Crystals. *Z. Kristallogr.* **2005**, *220*, 571–573.
- (17) Dovesi, R.; Saunders, V. R.; Roetti, C.; Orlando, R.; Zicovich-Wilson, C. M.; Pascale, F.; Civalleri, B.; Doll, K.; Harrison, N. M.; Bush, I. J.; et al. *CRYSTAL09 User's Manual*; University of Torino: Torino, Italy, 2009.
- (18) Civalleri, B.; Zicovich-Wilson, C. M.; Valenzano, L.; Ugliengo, P. B3LYP Augmented with an Empirical Dispersion Term (B3LYP-D*) as Applied to Molecular Crystals. *CrystEngComm* **2008**, *10*, 405–410.
- (19) Bulkin, B.; Lewin, M.; Kim, J. Crystallization Kinetics of Poly(propylene terephthalate) Studied by Rapid-Scanning Raman Spectroscopy and FT-IR Spectroscopy. *Macromolecules* **1987**, *20*, 830–835.
- (20) Kim, K. J.; Bae, J. H.; Kim, Y. H. Infrared Spectroscopic Analysis of Poly(trimethylene terephthalate). *Polymer* **2001**, *42*, 1023–1033.
- (21) Chuah, H. H. Orientation and Structure Development in Poly(trimethylene terephthalate) Tensile Drawing. *Macromolecules* **2001**, *34*, 6985–6993.
- (22) Yamen, M.; Ozkaya, S.; Vasanthan, N. Structural and Conformational Changes During Thermally-induced Crystallization of Poly(trimethylene terephthalate) by Infrared Spectroscopy. *J. Polym. Sci., Part B: Polym. Phys.* **2008**, *46*, 1497–1504.
- (23) Ward, I. M.; Wilding, M. A. Infra-red and Raman Spectra of Poly(m-methylene terephthalate) Polymers. *Polymer* **1977**, *18*, 327–335.
- (24) Lee, H. S.; Park, S. C.; Kim, Y. H. Structural Changes of Poly(trimethylene terephthalate) Film Upon Uniaxial and Biaxial Drawing. *Macromolecules* **2000**, *33*, 7994–8001.
- (25) Vasanthan, N.; Yaman, M. Crystallization Studies of Poly(trimethylene terephthalate) Using Thermal Analysis and Far-Infrared Spectroscopy. *J. Polym. Sci., Part B: Polym. Phys.* **2007**, *45*, 1675–1682.
- (26) Vasanthan, N.; Ozkaya, S.; Yaman, M. Morphological and Conformational Changes of Poly(trimethylene terephthalate) during Isothermal Melt Crystallization. *J. Phys. Chem. B* **2010**, *114*, 13069–13075.
- (27) Becke, A. Density-Functional Thermochemistry. 3. The Role of Exact Exchange. *J. Chem. Phys.* **1993**, *98*, 5648–5652.
- (28) Lee, C.; Yang, W.; Parr, R. Development of the Colle-Salvetti Correlation-Energy Formula into a Functional of the Electron-Density. *Phys. Rev. B* **1988**, *37*, 785–789.
- (29) Peintinger, M. F.; Oliveira, D. V.; Bredow, T. Consistent Gaussian Basis Sets of Triple-Zeta Valence with Polarization Quality for Solid-State Calculations. *J. Comput. Chem.* **2013**, *34*, 451–459.
- (30) Bondi, A. Van Der Waals Volumes and Radii. *J. Phys. Chem.* **1964**, *68*, 441–451.
- (31) Rowland, R. S.; Taylor, R. Intermolecular Nonbonded Contact Distances in Organic Crystal Structures: Comparison with Distances Expected from van Der Waals Radii. *J. Phys. Chem.* **1996**, *100*, 7384–7391.
- (32) Poulin-Dandurand, S.; Pérez, S.; Revol, J.-F.; Brisse, F. The Crystal Structure of Poly(trimethylene terephthalate) by X-ray and Electron Diffraction. *Polymer* **1979**, *20*, 419–426.
- (33) Desborough, I. J.; Hall, I. H.; Neisser, J. Z. The Structure of Poly(trimethylene terephthalate). *Polymer* **1979**, *20*, 545–552.
- (34) Painter, P. C.; Coleman, M. M.; Koenig, J. L. *The Theory of Vibrational Spectroscopy and Its Application to Polymeric Materials*; John Wiley and Sons: New York, Chichester, Brisbane, Toronto, Singapore, 1982.
- (35) Zbinden, R. *Infrared Spectroscopy of High Polymers*; Academic Press: New York, 1964.

2.3 $\alpha \rightarrow \beta$ polymorphic transition in Poly(butylene terephthalate): a spectroscopy study

Poly(butylene terephthalate) (PBT) is another important member of the family of polyesters.

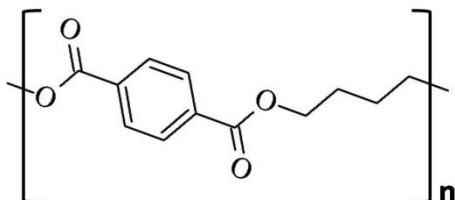


Fig. 2.2 Chemical structure of Poly(butylene terephthalate)

Unlike the case of PTT, where only one stable crystalline phase is found, at room temperature and upon mechanical deformation, PBT shows a reversible transition from the stable α form to a β phase possessing a different conformation of the polymer chain.

The α phase is well known and characterized in literature, whereas the structure of the polymer in the stress-induced β phase is still an open issue. Indeed some discrepancies are found among different authors: Yokouchi et al. [2] report a TSTS'T conformation, but many other authors [3–8] propose an all-trans conformation for the methylene chains in β phase. Due to its sensitivity to the molecular structure, IR spectroscopy has been often used to characterize the materials, but in the case of PBT the experimental investigations alone have not been able to solve the discrepancies in the interpretation of the molecular structure evolution upon deformation.

Therefore, to give a contribution in the understanding of the nature of the β phase, we carried out a DFT investigation of PBT.

As a first step we optimized the crystal structure for the PBT, described as a 3-D crystal starting from the experimental geometry in the α phase and for a TSTS'T conformation (β phase), as described in reference [2]. For the all-trans structure we considered the 1-D chain model, because of the lacking of a resolved 3D crystal structure.

In the case of the α form, the conformation and cell parameter predicted by CRYSTAL are very close to the experimental one, confirming the reliability of the previous interpretations.

In the case of the β form, the DFT calculations shows that the TSTS'T conformation is not a stable minimum of the potential surface. Moreover, a new β^* equilibrium structure with TGTG'T conformation is predicted, different from all the structures previously proposed; our calculations demonstrate also that the all-trans conformation can be indeed a stable minimum.

It is interesting to underline that in the case of PBT, unlike the nylons (see Section 2.1), our calculations demonstrate that intermolecular effects do not modulate the intramolecular structure of the chain: indeed, the same conformation observed for the chains embedded in the crystal in the α and β^* form are found also for the infinite 1D isolated chain model.

Even if these structural data enlighten some new properties of PBT molecular structure, they alone don't allow to draw definitive conclusions about the conformation of the β form. Therefore we decided to take also into account the IR spectra, which had been computed according to the isolated chain models.

As illustrate in details in the paper "*Polymorphism of Poly(butylene terephthalate) Investigated by Means of Periodic Density Functional Theory Calculations*" (A. Milani, D. Galimberti, , *Macromolecules*. 47 (2014) 1046) here attached, the predicted IR spectra give strong indications that β -PBT does possess chains in transplanar conformation: the experimental spectrum of β phase is indeed well predicted by the all-trans chain but not by the β^* conformation.

This is not due to possible deficiencies in our calculation since in the case of the α form, the experimental pattern is nicely reproduced by simulation of the crystal, both in frequency and relative intensity, confirming the reliability of the adopted level of theory.

To further support the all-trans conformation of the chains in the β -PBT, as a last step, the transition from the α to the β form upon mechanical stretching has been simulated, showing a transition of the intramolecular structure from the GTG' conformation found for the α form to the TTT conformation of the strained β form: this findings confirm the spectroscopic results and thus solves all the previous ambiguities. This work is a further step in the application of quantum chemical modeling in material sciences and technology. We verify indeed how the simulations can be applied to give a molecular interpretation of macroscopic properties or process, such as mechanical deformation.

Polymorphism of Poly(butylene terephthalate) Investigated by Means of Periodic Density Functional Theory Calculations

Alberto Milani* and Daria Galimberti

Dipartimento di Chimica, Materiali e Ingegneria Chimica "Giulio Natta", Politecnico di Milano, Piazza Leonardo da Vinci, 32, 20133 Milan, Italy

S Supporting Information

ABSTRACT: The conformation and solid state structure of the two α and β polymorphs of poly(butylene terephthalate) are here studied by means of state-of-the-art first principles calculations, carried out both for the crystals and the infinite one-dimensional chain models. Focusing in details on the debated β form, induced by mechanical deformation, we verified the setting on of an all-trans conformation, as also supported by the simulation of the infrared spectra of the different polymorphs compared to the available experimental spectra. The transition from the α to the β form is also simulated by applying increasing strains to the infinite polymer chain: a peculiar evolution of the intramolecular structure is indeed predicted, showing a transition from the GTG' conformation found for the α form to the TTT conformation of the strained β form.

I. INTRODUCTION

Aromatic polyesters are a class of polymeric materials showing peculiar microstructural properties that can modulate their macroscopic behavior. In this context, phenomena such as different conformational effects and different mechanical behavior for the members of this family, even-odd effects depending on the number of methylene units between aromatic rings, polymorphic transitions among two or more phases etc. are just a few examples. Therefore, despite their technological importance and their widespread application in our everyday life, there are several physicochemical phenomena that still need a complete investigation; furthermore, there are some ambiguities and open questions that still demand an answer.

Poly(butylene terephthalate) (PBT), the second member of this family in order of technological importance after poly(ethylene terephthalate) (PET), shows a reversible transition between different crystal structures upon mechanical deformation, which corresponds to a variation in the conformation of the chain.^{1–22} Many authors have investigated this polymorphic transition by means of different characterization techniques, ranging from X-ray diffraction (XRD)^{1–6,19,21,22} to electron microscopy,²³ vibrational spectroscopy,^{7–10,13–18} nuclear magnetic resonance,²⁴ and molecular mechanics simulations.¹² Despite this large interest, some features are still debated, such as for example the structure of the polymer in the stress-induced β phase: while most of the authors agree in proposing an all-trans structure, other ones have proposed a different conformation for the PBT chains in the crystal. As for other classes of polymers, both XRD and vibrational spectroscopy techniques have been usually adopted to investigate structural properties but they have been based almost exclusively on experimental works, generating sometimes further ambiguities which cannot be easily unravelled. In these grounds, first-principles computational techniques can give a reliable description of both the structural and vibrational properties of the system, even if, to this aim, the suitable computational tools capable of treating periodic molecular

crystal became available only in very recent years.^{25–27} Therefore, in this paper we have applied state-of-the-art techniques to carry out periodic Density Functional Theory (DFT) calculations augmented with an empirical dispersion correction (DFT-D)^{28–30} of poly(butylene terephthalate) polymorphs by means of the CRYSTAL09 code,^{31,32} to investigate and clarify definitively both the structural and vibrational properties of these systems. Very recently, this code has been applied successfully to many other polymeric systems (polystyrene,^{25,26} polyglycine,²⁷ nylon-6 polymorphs,³³ nylon-6,6,³⁴ and polytetrafluoroethylene³⁵) and we used it also for the spectroscopic characterization of poly(trimethylene terephthalate),³⁶ another member of the aromatic polyester class.

In the following, after explaining the computational methodology adopted, we will present the simulation of both the intramolecular and solid-state structure of PBT; then we will proceed to the simulation of its IR spectra, compared to the experimental data available in the literature. At last, the effect of the mechanical deformation will be introduced in the calculation to monitor the evolution of the conformation of the infinite polymer chain.

II. COMPUTATIONAL DETAILS

Full geometry optimization of the crystal structure, chain conformation and the calculation of the IR spectra of PBT have been carried out by means of the CRYSTAL09 code^{31,32} in the framework of Density Functional Theory. We adopted the B3LYP^{37,38} hybrid exchange-correlation functional with the 6-31G(d,p) basis set, introducing also the empirical correction for dispersion interaction (B3LYP-D) proposed by Grimme^{28–30} and implemented in CRYSTAL09. The choice of both the DFT functional and basis set is motivated on the basis of previous computational investigations of polymer systems by means of the CRYSTAL code^{25–27,33–35} where it has been found that this combination can give a very good description

Received: December 19, 2013

Revised: January 14, 2014

Published: January 28, 2014



Table 1. Summary of the Numerical Values Adopted for the Parameters Occurring in Grimme's Correction for Dispersion Interactions^a

d	s_6	C_6^H	C_6^C	C_6^O	C_6^N	R_{vdw}^H	R_{vdw}^C	R_{vdw}^O	R_{vdw}^N
20	1.00	0.14	1.75	0.70	1.23	1.3013	1.70	1.52	1.55

^aA cutoff distance of 25.0 Å was used to truncate direct lattice summation. C_6 are in units of J nm⁶ mol⁻¹ while R_{vdw} are in unit of Å.

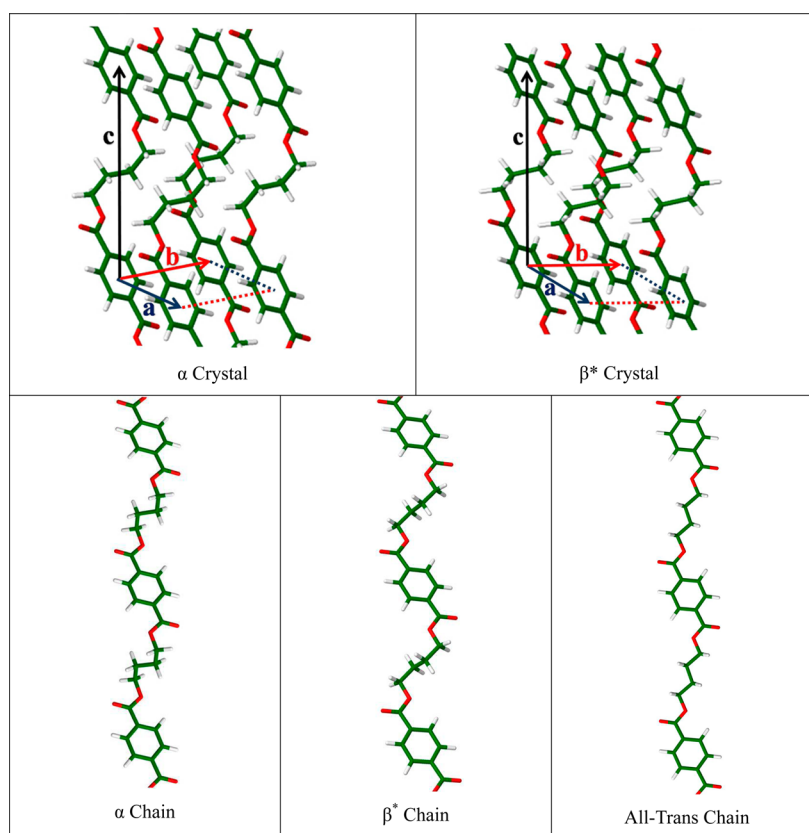


Figure 1. Sketches of the optimized α and β^* crystalline structures of PBT and of the 1D model chains possessing α , β^* and trans conformation. For a definition of β^* see section III.1.

of both the structure and the vibrational spectra. Furthermore, in a very recent paper,³⁶ the case of poly(trimethyl terephthalate) have been investigated by taking into account also the effect of different computational parameters, including both basis set choice and the parameters used for Grimme's corrections: it has been found that B3LYP/6-31G(d,p), combined with the parameters previously adopted for nylon-6 polymorphs³³ and nylon-6,6³⁴ and reported in Table 1, gives indeed the best agreement with the experimental data. This combination is thus used also in the present study.

In all calculations, the atomic positions and the lattice parameters were fully optimized; default optimization algorithms and convergence criteria were adopted. In the case of PBT, two polymorphs have been characterized by different authors:^{1–6,19,21} the α form is the stable one found in the unstrained condition and it shows a GGTG'G' conformation on the O–CH₂ bonds and on the methylene chain. The structural determinations proposed by different authors are in agreement about both the crystal and conformational structure. A second polymorph β is observed for PBT under strain. In this case, non-negligible discrepancies are found among different authors: while Yokouchi et al.¹ report a TSTS'T conformation, many other authors^{4–6,12,19,22} propose an all-trans conformation for the methylene chains in β phase. In all the cases, both the polymorphs have a triclinic unit cell with $P\bar{1}$ space group.

Since Cartesian coordinates of both phases are reported only by Yokouchi et al.,¹ we used these geometries as initial guess for the full geometry optimization of α and β crystals. In addition to the simulation of the whole crystal, we carried out also simulations for

infinite polymer chains (1D model chain); in this case, three structures have been taken into account as starting geometries: the two structures having the conformations observed in α and β crystals and the all-trans chain.

The optimized structures of all these crystals and 1D model chains are sketched in Figure 1.

In all the cases, normal frequencies calculations at the Γ point have been carried out on the optimized geometries as achieved by diagonalization of the (numerically calculated) Hessian matrix.

The DFT-D computed spectra have been compared with the available experimental IR spectra reported by Stambaugh et al.⁷ To compare the computed and the experimental data, the calculated frequencies were scaled by 0.9748: this scaling factor has been determined to put the band computed at 940.7 cm⁻¹ for the 1D model chain of the α polymorph in correspondence of the well-assessed marker band found at 917 cm⁻¹ for the α form.

In addition to the geometry optimization and the prediction of the IR spectra, we also simulate the effect of the mechanical deformation on the conformational structure of a single infinite PBT chain: starting from the geometry of the chain in α conformation ($c' = 23.0166$ Å, chain repeat distance) we progressively increased the value of the repeat distance c' by steps of 0.2 Å until a final value of 28 Å. For each step, a geometry optimization at fixed c' has been carried out and the final structure of each step has been used as input for the next one. The evolution of the conformation has been thus followed for increasing strain to verify the occurrence of the polymorphic transition from the α to the all-trans β conformation.

Table 2. Comparison between DFT-D Computed (B3LYP-D/6-31G(d,p)) Cell Parameters and Those Reported in Previous Investigations for the α Phase of PBT^a

α -PBT	B3LYP-D/6-31G(d,p)	MM ¹²	expt ¹	expt ²	expt ³	expt ⁴	expt ⁶	expt aver. ⁶	errors (%)
<i>a</i>	4.5812	5.343	4.83	4.83	4.87	4.89	4.87	4.86	-5.7
<i>b</i>	5.8684	6.340	5.94	5.96	5.96	5.95	5.99	5.96	-1.5
<i>c</i>	11.8396	10.631	11.59	11.62	11.71	11.67	11.67	11.65	1.6
α	101.0030	98.220	99.70	99.90	100.10	98.90	99.80	99.70	1.3
β	114.2940	117.130	115.20	115.20	116.60	116.60	116.20	116.00	-1.5
γ	111.0675	114.320	110.80	111.30	110.30	110.90	110.90	110.80	0.2

^aValues of *a*, *b*, *c* parameters are in Å and in degrees for the angles. In the last column, the percentage errors (%) of the DFT-D computed values and the average experimental one reported by Desborough et al.⁶ are calculated.

Table 3. Comparison between DFT-D Computed (B3LYP-D/6-31G(d,p)) Cell Parameters and Those Reported in Previous Investigations for the β Phase of PBT^a

β -PBT	B3LYP-D 6-31G(d,p)	MM ¹²	expt ¹	expt ⁴	expt ⁶
<i>a</i>	4.7421	4.874	4.95	4.69	4.73
<i>b</i>	5.9071	6.053	5.67	5.80	5.83
<i>c</i>	12.1937	13.048	12.95	13.00	12.90
α	97.8208	104.650	101.70	101.90	101.90
β	125.9010	125.040	121.80	120.50	119.40
γ	101.5888	103.060	99.90	105.00	105.10

^aValues of *a*, *b*, *c* parameters are in Å and in degrees for the angles. Since different structures have been experimentally resolved, no reference experimental cell parameters can be unambiguously defined to calculate percentage errors with respect to the DFT-D computed data.

III. RESULTS AND DISCUSSION

III.1. Structure and Conformation of PBT Polymorphs.

In Tables 2 and 3, we report the comparison between our computational results and the previous determinations of the crystal structure of α and β polymorphs; a comparison between the conformations observed in the two polymorphs is reported respectively in Tables 4 and 5.

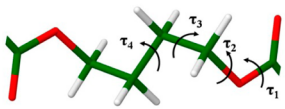
A very good agreement is obtained for the α form. In the last column of Table 2, we report the percentage errors of our DFT-D computed cell parameters with respect to the experimental average parameters reported by Desborough et al.⁶ all the errors are very small and the largest discrepancy is found for the parameter *a*, ruling the van der Waals packing of neighbor chains. This parameter is indeed largely affected by

Table 5. Comparison between DFT-D computed (B3LYP-D/6-31G(d,p)) torsional angles and those reported in previous investigations for the β phase of PBT. A sketch is reported in Table 4 for the definition of these angles. Values are in degrees

β -PBT	B3LYP-D 6-31G(d,p)	MM ¹²	expt ¹	expt ⁴	expt ²²
τ_1 (CCOC)	180	-129	179	-179	-179
τ_2 (COCC)	179	175	-179	-159	-159
τ_3 (OCCC)	71	177	113	162	-166
τ_4 (CCCC)	180	180	180	180	180

the parameters chosen for Grimme's correction from one hand and by temperature effects that are not present in our simulation on the other hand, as also pointed out in previous works.^{33,34} In any case, the absolute deviation of the DFT-D value from the experimental one is small (0.28 Å). If we compare our DFT-D results with the cell parameters computed by Nitsche et al.¹² by means of molecular mechanics (MM) simulations (second column of Table 2) we can verify that DFT-D calculations give a better agreement with the experiments, even if the effect of temperature is not included. This is true in particular for the *c* parameter (chain repeat distance), underestimated by about 1 Å by MM simulations and overestimated only by 0.19 Å by our calculations. In any case, it should be noted that all the data reported for the α form show a very good agreement. Such an accordance is also found when considering the conformation of the chain (Table 4): all the authors indeed propose a GG'TG'G' sequence on the O-CH₂ bonds and on the methylene chain and again our calculations predict values of the torsional angles which are very close to the experimental ones, in particular to the angles reported in refs 2

Table 4. Comparison between DFT-D Computed (B3LYP-D/6-31G(d,p)) Torsional Angles and Those Reported in Previous Investigations for the α Phase of PBT^a

α -PBT					
	B3LYP-D 6-31G(d,p)	MM ¹²	expt ¹	expt ⁴	expt ²
τ_1 (CCOC)	180	152	178	-178	178
τ_2 (COCC)	-94	-68	-88	-94	-91
τ_3 (OCCC)	-67	-61	-66	-79	-88
τ_4 (CCCC)	180	180	180	180	180

^aA sketch is also reported for the definition of these angles. Values are in degrees.

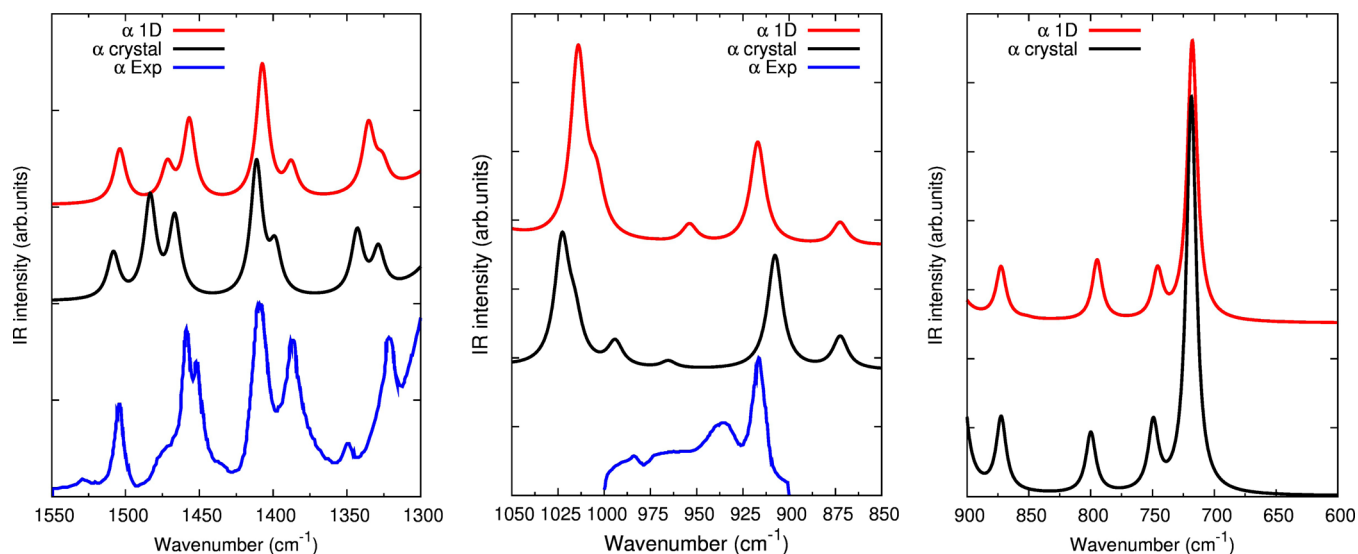


Figure 2. Comparison of DFT-D computed (B3LYP-D/6-31G(d,p)) IR spectra of the crystal and of the infinite polymer chain (1D model chain) of the α phase with the experimental spectra reported in ref 7. The computed frequencies are scaled by 0.9748.

and 4. Also, in this case, our accuracy is larger with respect to MM simulations, where τ_1 and τ_2 angles in particular show a non-negligible difference from the experimental data.

In the case of the β phase, differences are found among the various authors (see Tables 3 and 5): most of them^{4–6,12,19,22} agree in proposing an all-trans conformation for this phase, contrary to the previous proposal to TSTS'T by Yokouchi et al.¹ ($\tau_3 = 113^\circ$). MM simulations¹² predict cell parameters in good agreement with refs 4 and 6 and confirm a trans conformation on the central methylene units, even if a value of -129° is anyway computed for τ_1 contrary to the T angles experimentally observed by all the other authors.

In this context, our calculation predicts a further new equilibrium structure; indeed, a TGTG'T is computed ($\tau_3 = -71^\circ$) which is different from all the previous proposals, both from the all-trans structure and the conformation containing skew torsional angles. Our chain is thus more contracted, resulting in a smaller c parameter, in our case equal to 12.194 Å, contrary to the experimental values of about 13 Å. Because of this difference and to avoid any confusion, from now on we will indicate our DFT-D optimized structure as β^* form.

In order to clarify in deeper details these differences, we carried out DFT-D calculation also for 1D model chains, i.e. single infinite polymer chains possessing the conformation observed in α and β^* crystals and also all-trans conformation. In the case of the " α chain" and of the " β^* chain" torsional angles of 178° , 85° , 57° , 159° and 178° , 167° , -68° , 180° , respectively, are found, thus giving the same conformation observed also in the crystal and excluding the role of any intermolecular effect in modulating the intramolecular structure of the polymer.

Further information can be obtained by calculating the relative energies of the two phases: as expected the β^* crystal is less stable by 3.86 kcal/mol (referred to the unit cell, 56 atoms) with respect to the α form. When considering the infinite chains, this value becomes 2.29 kcal/mol, thus showing that both the intramolecular structure and the intermolecular packing are energetically more efficient in the α form. Interestingly, the all-trans chain is less stable by 3.61 kcal/mol with respect to the α chain and it appears to be also less stable with respect to the β^* chain. However, to give a more

reliable description of the structural evolution of the conformation upon mechanical deformation, we need to include explicitly the effect of the strain in our simulation, as described in section III.3 and which introduces a perturbation with respect to 1D model chains treated as completely isolated systems.

On the basis of the computational study here reported, we are not able yet to confirm any of the previous proposal for the structure of the β polymorph; moreover, based on our first-principles calculations the conformational properties of PBT seems to be even more complicated. In order to solve all these discrepancies, we need to take into account also other properties of PBT: the vibrational properties are the ideal ground to obtain other structural information, due to the extreme sensitivity of IR and Raman spectra to both intra- and intermolecular phenomena. Indeed, also in previous papers,^{25–27,33–35} IR spectroscopy has been widely used to this aim and we demonstrated how the computational method adopted in the current work is very powerful and allows to answer many open questions concerning the spectroscopic characterization of different polymers, including PTT. Also in the case of PBT, no computational studies have been reported yet about the interpretation of the vibrational properties and the assignment of its IR spectrum. In the next section, we will verify that the comparison between experimental and DFT-D computed spectra will allow to clarify which is the structure of the so-debated β polymorph.

III.2. IR Spectroscopy of PBT Polymorphs. As a first step in the analysis of the spectra of PBT we have to check if our DFT-D calculations can give a reliable prediction of the IR spectra. To this aim, in Figure 2, we compare the spectra computed for the crystal and the 1D model chain of the α phase with the experimental spectra reported by Stambaugh et al.⁷ The agreement between the experimental and DFT-D spectra is good and demonstrate the reliability of the computational method adopted. By looking in particular to the first panel, we can verify that the experimental pattern is correctly described by the calculation on the crystal, both in frequency and relative intensity. The 1D model chain shows IR spectra which are very similar to the crystal and the only discrepancy that occurs concerns the relative intensity of the

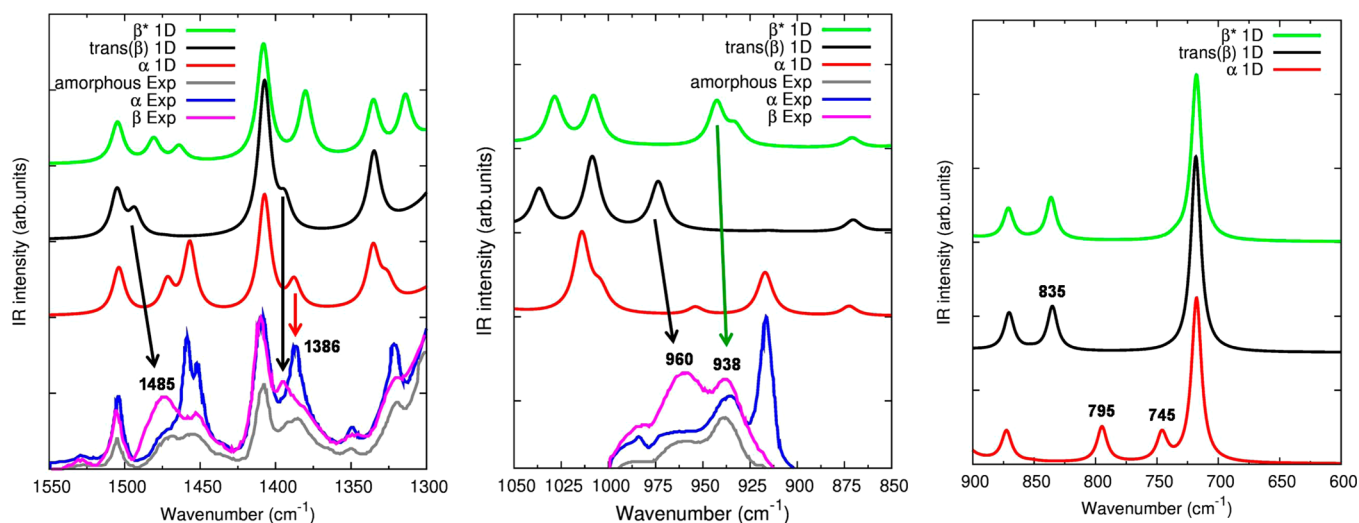


Figure 3. Comparison of DFT-D computed (B3LYP-D/6-31G(d,p)) IR spectra of the 1D chain models (α , β^* , and trans conformations) with the experimental spectra reported in ref 7 for both polymorphs and the amorphous phase. The computed frequencies are scaled by 0.9748.

Table 6. Experimental and DFT-D Computed (B3LYP-D/6-31G(d,p)) Frequency Values in cm^{-1} of the Most Important Bands of α , β , and Amorphous Phase of PBT^a

expt ^{7-10,13-18}	PBT α phase		PBT β phase				expt ^{7-10,13-18}	
	1D chain B3LYP-D/6-31G (d, p)		1D all-trans chain B3LYP-D/6-31G (d, p)		1D β^* chain B3LYP-D/6-31G (d, p)			
	frequency (scaled by 0.9748) (cm^{-1})	IR intensity (km/mol)	frequency (scaled by 0.9748) (cm^{-1})	IR intensity (km/mol)	frequency (scaled by 0.9748) (cm^{-1})	IR intensity (km/mol)		
1460	1472	29	1485	1493	19	1481	22	
1455	1457	64	1470			1464	13	
1386	1388	25	1393	1394	22	1381	60	1386, 1375
1350	1336	56	960	974	98			
1323	1326	20				943	101	938
917	917	105				933	40	
811	795	27	845	835	28	836	31	
750	745	22						

^aThe computed frequencies refer to the 1D chain models (α , β^* , and trans conformations) and they are scaled by 0.9748. Computed IR intensities (km/mol) are also reported.

two bands predicted at about 1450 cm^{-1} (CH_2 bending modes). Excluding this minor detail, both calculations reproduce the same pattern: on these grounds, from now on, we will compare the experimental spectra with the computational spectra of the 1D model chains, to obtain a clearer and simpler interpretation of the structural properties of PBT polymorphs on the basis of their conformation.

In Figure 3, the IR spectra computed for the 1D model chains having respectively α , β^* and trans conformation are compared with the experimental spectra of both polymorphs and of the amorphous phase, and in Table 6 the experimental frequency values of the main marker bands are compared to the DFT-D computed values. In the Supporting Information, the sketches of the computed normal modes of vibration are reported for each one of these bands.

The frequency range which have been mostly used to investigate PBT polymorphism is the $900\text{--}1000 \text{ cm}^{-1}$ region. The band at 917 cm^{-1} (COCC torsional + CH deformation mode) has been unambiguously associated with the α phase and it has been used in the present work as a reference to determine the frequency scaling factor for all the computed spectra (see Computational Details). In addition to this band, the α form shows also a second broad band at 938 cm^{-1} : based

on the comparison with the spectrum of the amorphous phase we can verify that this band is due only to the amorphous, which is present in a non-negligible amount. This fact is indeed supported by the computed spectrum where no bands are predicted in correspondence of this peak for the α phase. In the case of the β polymorph, the experimental spectra clearly show the occurrence of a new band at 960 cm^{-1} in addition to the band at 938 cm^{-1} (the latter one demonstrating again the presence of a non-negligible amount of amorphous phase). It is now immediate to verify from the comparison with the DFT-D computed spectra that the model chain describing the occurrence of this marker band at 960 cm^{-1} is actually the trans chain (band computed at 974 cm^{-1} , CO stretching + COC bending + CH_2 deformation mode), confirming definitely that the β phase of PBT does possess chains in transplanar conformation.

It is interesting to note that the chain possessing the β^* conformation has a doublet of bands in correspondence of the 938 cm^{-1} experimental band: based on the eigenvectors sketched in the Supporting Information, we can indeed verify that these vibrations are located on the methylene units where one G torsional angle is present. On these grounds, we can assume that the 1D model chain in β^* conformation could be

considered as a representative of the several possible conformers, populated in the amorphous phase, possessing one TGT sequence somewhere on the methylene chain.

By analyzing now the 1550–1300 cm^{-1} frequency region further information is obtained. First of all, based on the DFT-D calculation, we confirm again that the doublet of bands observed at 1460/1455 cm^{-1} in the experimental spectra is associated with the α phase. In this case, the relative intensities of the two components are not predicted correctly by the calculations: in Figure 2, we have already pointed out that this is the only deficiency observed for the 1D model chain, since the spectrum computed for the α crystal reproduces very well the relative intensity of this doublet. The experimental spectra reveal that the amorphous gives two broad bands in this region: in the case of the β^* chain two peaks are indeed predicted in correspondence of these two features, thus supporting again the assumption that this model can be taken as a representative of the amorphous phase.

In the case of the β polymorph, a marker band is now observed at 1485 cm^{-1} , which is again nicely predicted by the transplanar chain model (band computed at 1493 cm^{-1} , CH_2 bending mode).

Further differences are also observed at about 1390 cm^{-1} : the α and β phase show two bands at about 1386 and 1393 cm^{-1} respectively. The α chain model and the trans chain model actually possess two bands at 1388 and 1394 cm^{-1} (CH_2 deformation modes) in very nice agreement with the experiments; in this region, the amorphous presents a broad band at about 1385–1380 cm^{-1} , predicted at 1381 cm^{-1} by the β^* model.

At last, even if no experimental spectra are available, we report in the last panel of Figure 3 the comparison of the IR spectra of the different 1D chain models in the 900–600 cm^{-1} range. In the previous literature two marker bands are here found at 811 and 750 cm^{-1} for the α phase and a band at 845 cm^{-1} for the β phase: DFT-D computed spectra show indeed the two corresponding marker bands at 795 cm^{-1} (OCO bending + CH deformation mode) and 745 cm^{-1} (CH_2 deformation mode) for the α chain and at 835 cm^{-1} (OCO bending + CH deformation mode) for the trans chain.

As a conclusion, thanks to computational vibrational spectroscopy, we have been able to demonstrate unambiguously that the β polymorph of PBT possess chains in transplanar conformation.

III.3. Simulation of the $\alpha \rightarrow \beta$ Transition. In this section, we investigate in more details the structural evolution of a PBT chain in α conformation for increasing value of the strain. This has been simulated by increasing step by step the values of the c' parameter of the chain and reoptimizing the geometry each step to monitor the changes of the conformation. The results are reported in Figure 4, showing the evolution of the torsional angles for increasing strain.

Only small changes are observed until about a strain of 14%: at this value, the τ_3 angle suddenly jumps from about 80° to about 170°, that is it evolves from the G toward the T conformation while τ_2 angle still remains stable at about 90°. If we further increase the strain, at about $\epsilon = 19\%$ also τ_2 angle shows a transition to the T conformation and the whole chain now possesses an all-trans structure.

The use of periodic boundary conditions in the calculation usually implies some difficulties and restraints for the conformational transitions; therefore, we cannot state that the transition is really a two-step evolution of the τ_2 and τ_3 angles.

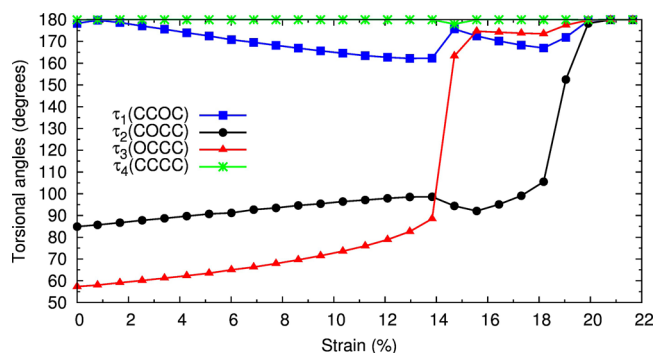


Figure 4. Evolution of the B3LYP-D/6-31G(d,p) computed torsional angles on the methylene chain (see Table 2 for the definition of the angles) for increasing values of the strain of the 1D model chain of the α phase. The strain is calculated as $(c' - c'_0) \times 100/c'_0$, where c'_0 is the optimized cell parameter of the α chain while c' is progressively increased to simulate the mechanical deformation. The numerical values of these torsional angles as a function of c' are reported in the Supporting Information.

In any case, it is clearly demonstrated again that the transition from the α to the β phase upon mechanical deformation does imply an evolution of the chain structure from the GGTG'G' to the all-trans conformation.

IV. CONCLUSIONS

Thanks to state-of-the-art computational methods, we have been able to investigate in details the crystal phase transition observed in PBT under mechanical deformation. DFT-D calculations allowed to solve unambiguously the discrepancies found in the literature about the nature of the β phase: our study reveals that this phase is characterized by an all-trans chain conformation, promoted by increasing values of the strain. This has been possible by simulating the crystal structure of the different phases of PBT and by computing their IR spectra, compared to the experimental ones: indeed the simulation of these properties is a powerful tool to support and explain the experimental data, free from any ambiguity. The results so obtained demonstrate that accurate first-principles calculations of crystalline polymers are now possible and can be applied to discuss a wide range of problems, providing answers to several open questions where experimental characterizations are not enough. Their importance is not restricted to the interpretation of the chemical/physical properties of polymers but they could be also a valuable tool in the development and characterization of innovative systems or for the design of new polymeric materials.

■ ASSOCIATED CONTENT

Supporting Information

Sketches of the main IR active modes for PBT chain (α , all-trans, β^*), table with DFT-D computed torsional angles of the methylene chain for increasing value of the c' parameter of α -PBT 1D model chain, tables with DFT-D optimized values of the cell parameters and fractional atomic coordinates obtained by full optimization of the cell of PBT α and β^* crystal, tables with DFT-D optimized values of the cell parameter and Cartesian atomic coordinates obtained by full optimization of the cell of the single polymeric chain (1D crystal) of α , all-trans, and β^* PBT chain, and tables with DFT-D computed values of frequencies (cm^{-1}) and IR intensities (km/mol) for the PBT α ,

all-trans, β^* chain, and α and β crystals. This material is available free of charge via the Internet at <http://pubs.acs.org/>.

AUTHOR INFORMATION

Corresponding Author

*(A.M.) E-mail: alberto.milani@polimi.it.

Notes

The authors declare no competing financial interest.

REFERENCES

- (1) Yokouchi, M.; Sakakibara, Y.; Chatani, Y.; Tadokoro, H.; Tanaka, T.; Yoda, K. *Macromolecules* **1976**, *9*, 266–273.
- (2) Mencik, Z. *J. Polym. Sci., Polym. Phys. Ed.* **1975**, *13*, 2173–2181.
- (3) Joly, A. M.; Nemoz, G.; Douillard, A.; Vallet, G. *Makromol. Chem.* **1975**, *176*, 479–494.
- (4) Hall, I. H.; Pass, M. G. *Polymer* **1976**, *17*, 807–816.
- (5) Stambaugh, B.; Koenig, J. L.; Lando, J. B. *J. Polym. Sci., Polym. Phys. Ed.* **1979**, *17*, 1053–1062.
- (6) Desborough, I. J.; Hall, I. H. *Polymer* **1977**, *18*, 825–830.
- (7) Stambaugh, B.; Lando, J. B.; Koenig, J. L. *J. Polym. Sci., Polym. Phys. Ed.* **1979**, *17*, 1063–1071.
- (8) Siesler, H. W. *Makromol. Chem.* **1979**, *180*, 2261–2263.
- (9) Stambaugh, B. D.; Koenig, J. L.; Lando, J. B. *J. Polym. Sci., Polym. Lett. Ed.* **1977**, *15*, 299–303.
- (10) Jakeways, R.; Smith, T.; Ward, I. M.; Wilding, M. A. *J. Polym. Sci., Polym. Lett. Ed.* **1976**, *14*, 41–46.
- (11) Jakeways, R.; Ward, I. M.; Wilding, M. A.; Hall, I. H.; Desborough, I. J.; Pass, M. G. *J. Polym. Sci., Polym. Phys. Ed.* **1975**, *13*, 799–813.
- (12) Nitzsche, S. A.; Wang, Y. K.; Hsu, S. L. *Macromolecules* **1992**, *25*, 2397–2400.
- (13) Roebuck, J.; Jakeways, R.; Ward, I. M. *Polymer* **1992**, *33*, 227–232.
- (14) Gillette, P. C.; Lando, J. B.; Koenig, J. L. *Polymer* **1985**, *26*, 235–240.
- (15) Siesler, H. W. *J. Polym. Sci., Polym. Lett. Ed.* **1979**, *17*, 453–458.
- (16) Ward, I. M.; Wilding, M. A. *Polymer* **1977**, *18*, 327–335.
- (17) Dobrovolnyarand, E.; Hsu, S.; Shih, C. *Macromolecules* **1987**, *20*, 1022–1029.
- (18) Stach, W.; Holand-Moritz, K. *J. Mol. Struct.* **1980**, *60*, 49–54.
- (19) Kawaguchi, A.; Murakami, S.; Fujiwara, M.; Nishikawa, Y. *J. Polym. Sci., Part B: Polym. Phys.* **2000**, *38*, 838–845.
- (20) Takahashi, Y.; Murakami, K.; Nishikawa, S. *J. Polym. Sci., Part B: Polym. Phys.* **2002**, *40*, 765–771.
- (21) Apostolov, A. A.; Fakirov, S.; Stamm, M.; Patil, R. D.; Mark, J. E. *Macromolecules* **2000**, *33*, 6856–6860.
- (22) Grasso, R. P.; Perry, B. C.; Koenig, J. L.; Lando, J. B. *Macromolecules* **1989**, *22*, 1267–1272.
- (23) Roche, E. J.; Stein, R. S.; Thomas, E. L. *J. Polym. Sci., Polym. Phys. Ed.* **1980**, *18*, 1145–1158.
- (24) Davidson, I. S.; Manuel, A. J.; Ward, I. M. *Polymer* **1983**, *24*, 30–36.
- (25) Torres, F. J.; Civalleri, B.; Meyer, A.; Musto, P.; Alburnia, A. R.; Rizzo, P.; Guerra, G. *J. Phys. Chem. B* **2009**, *113*, 5059–5071.
- (26) Torres, F. J.; Civalleri, B.; Pisani, C.; Musto, P.; Alburnia, A. R.; Guerra, G. *J. Phys. Chem. B* **2007**, *111*, 6327–6335.
- (27) Ferrari, A. M.; Civalleri, B.; Dovesi, R. *J. Comput. Chem.* **2010**, *31*, 1777–1784.
- (28) Civalleri, B.; Zicovich-Wilson, C. M.; Valenzano, L.; Ugliengo, P. *CrystEngComm* **2008**, *10*, 405–410.
- (29) Grimme, S. *J. Comput. Chem.* **2004**, *25*, 1463–1473.
- (30) Grimme, S. *J. Comput. Chem.* **2006**, *27*, 1787–1799.
- (31) Dovesi, R.; Orlando, R.; Civalleri, B.; Roetti, C.; Saunders, V. R.; Zicovich-Wilson, C. M. *Z. Kristallogr.* **2005**, *220*, 571–573.
- (32) Dovesi, R.; Saunders, V. R.; Roetti, C.; Orlando, R.; Zicovich-Wilson, C. M.; Pascale, F.; Civalleri, B.; Doll, K.; Harrison, N. M.; Bush, I. J.; D'Arco, P.; Llunell, M. *CRYSTAL09 User's Manual*; University of Torino: Torino, 2009.

(33) Quarti, C.; Milani, A.; Civalleri, B.; Orlando, R.; Castiglioni, C. *J. Phys. Chem. B* **2012**, *116*, 8299–8311.

(34) Galimberti, D.; Quarti, C.; Milani, A.; Brambilla, L.; Civalleri, B.; Castiglioni, C. *Vib. Spectrosc.* **2013**, *66*, 83–92.

(35) Quarti, C.; Milani, A.; Castiglioni, C. *J. Phys. Chem. B* **2013**, *117*, 706–718.

(36) Galimberti, D.; Milani, A. Submitted for publication.

(37) Becke, A. *J. Chem. Phys.* **1993**, *98*, 5648–5652.

(38) Lee, C.; Yang, W.; Parr, R. *Phys. Rev. B* **1988**, *37*, 785–789.

2.4 Crystal Field effects on the spectroscopic properties: the polyethylene test case

In this section we explored how weak interactions, such as Van der Waals forces ruling the crystal packing of polyethylene (PE), have significant effects on the IR intensities. Usually, such weak interactions were believed to produce a negligible influence on the spectra, introducing only small frequencies shifts and/or band splitting and thus justifying the use of single chain models in previous theoretical and computational approaches.

In the paper "*Modulation of the infrared absorption intensities in solid state. Role of weak intermolecular interactions in the Polyethylene crystal: a computational DFT investigation*" (D. Galimberti, A. Milani and C. Castiglioni) here reported as a draft manuscript, the IR spectrum of the Polyethylene (PE) is computed by means of different state of art quantum-chemical calculations (CRYSTAL and Gaussian codes), to investigate the effect of the crystal field on the IR intensities: Van der Waals interactions, occurring while chains are packed in the crystal, are far from being negligible and determine a remarkable variation of the IR intensities in the region of deformation modes.

On this basis we interpreted in a new prospective the IR intensity evolution with heating observed in the past by Snyder et al. [9] by means of several very accurate experiments on highly crystalline PE. The results obtained clearly demonstrated the importance of including supramolecular effects in spectra prediction through quantum-chemical investigations.

Intermolecular modulation of infrared absorption intensities in solid state. Role of weak interactions in polyethylene crystal: a computational DFT study

Daria Galimberti, Alberto Milani, Chiara Castiglioni

Dipartimento di Chimica, Materiali e Ingegneria Chimica Giulio Natta, Politecnico di Milano

Piazza Leonardo da Vinci 32 – 20133 Milano , Italy

Abstract

Density Functional Theory (DFT) calculations with periodic boundary conditions (PBC) are exploited for the study of the infrared spectrum of polyethylene. Spectral changes lead by the intermolecular packing in the orthorhombic 3-D crystal are discussed by means of a careful comparison between calculations carried out for an isolated polymer chain in the all-trans conformation, described as an ideal 1-D crystal. The results are analyzed in the framework of the “oligomer approach” through the modelling of the IR spectrum of n-alkanes of different length.

The study demonstrates that a relevant intensity modulation which especially affects CH₂ deformation transitions takes place in solid state. This finding suggests a new interpretation for the experimental evidences collected in the past by means of IR intensity measurement during thermal treatment.

1. Introduction

The study of intermolecular interactions and their role in determining the supra-molecular architecture is an evergreen topic in material science. However, the careful theoretical description of such interactions is a difficult issue, because of their intrinsic nature, often involving weak dispersion forces which require non-trivial modelling in the framework of a Quantum Chemical approach.

On the other hand, experimental data affected by the interactions occurring in the condensed phases offer unique opportunities for the understanding of the underlying physical phenomena and for the validation of the theoretical models.

The spectroscopic response in the infrared is often a sensitive probe of intermolecular interactions and experimental markers related to the presence of specific interactions can be and have been exploited for the recognition and for the characterization of supra-molecular structures [1,2]. In this framework, it is well known that strong intermolecular

interactions such as hydrogen bonds [3] determine huge changes of the infrared spectral pattern (shift of peaks frequencies, often accompanied by dramatic changes the intrinsic absorption intensities). In presence of H bonds, the analysis of the spectral features provides very effective tools for the structural diagnosis, especially when the experimental data are analyzed in conjunction with Quantum Chemical modelling [4–9]. Also the occurrence of crystalline phases and their structure can be investigated by means of infrared spectroscopy (see for instance Refs. [10–15] and bibliography herein). In this case symmetry selection rules determined by the crystal structure play a key role in the proper bands assignment and often allow to discriminate among different models of the crystal unit cell. Investigations on crystalline polymorphs, especially the field of polymer science, are based on the careful assignment of IR features [10–15].

A comprehensive interpretation of the vibrational spectra of semi-crystalline polymers is a very intriguing non-trivial topic, because in this case several different concurrent structural effects determines of the spectral pattern of the material [10–15]:

- i) the conformation of the polymer chains belonging to a crystal must fulfil the requirement of *regularity*. In other words the structure of the chain is described as a repetition along the chain axis of small translational units linked by covalent bonds. Accordingly, the single polymer chain can be modelled as an ideal 1-D crystal;
- ii) polymer chains are packed in a 3-D crystal structure, characterized by a suitable crystal cell;
- iii) according to the space group symmetry of the crystal, IR selection rules for the optical phonons at the Γ point of the first Brillouin zone rule the occurrence of IR transitions;
- iv) the unavoidable presence of the amorphous phase contributes to the IR spectrum with broad features, often superimposed to the sharp absorptions of the crystalline material; sometimes it gives rise to some specific “defect” bands.

While interpreting the infrared spectrum of a semicrystalline polymer, it is mandatory to recognize in unambiguous way the consequences of point i-iv and to clearly disentangle the different effects. On this basis, markers related to the occurrence of a regular conformation of the chains (i.e. “regularity” bands), as well as features associated to intermolecular interactions responsible of the crystal packing could be identified [10–15]. In the past, this kind of analysis was mainly based on several systematic and sophisticated experimental studies, comprehensive of the analysis of thermal evolution of the spectra and of a careful comparison with spectra of oligomers with known structure (see for instance Ref. [16–18] for the case of polyethylene and n-alkanes). Bands assignment were lead by the predictions of phonon frequencies based on empirical harmonic force fields, in the framework of space group symmetry theory. The so called “oligomer approach” [10–15] allowed to increase the set of experimental data in order to develop empirical correlations based on the direct comparison of the spectra. In this framework, the

availability of peaks frequencies of oligomers was of fundamental importance for the development of reliable empirical vibrational force fields by overlay procedures. Also defects modes ascribed to amorphous phases or structural defects inside the real crystals were modelled considering vibrational dynamics of short molecules (oligomers) in different conformations [10–14].

Several papers and reviews dealing with IR spectroscopy applied to semicrystalline polymers have appeared between 1960 – 1980 (for a complete bibliography see for instance Refs. [10–15]) and are still considered the reference for the rationalization of the vibrational behaviour of such materials. In this framework, the analysis of the infrared spectrum of polyethylene (PE) and related oligomers (linear n-alkanes) should be certainly considered a milestone and a paradigm.

Today, thanks to the growth of the computational capabilities and to the development of powerful Quantum Chemical models, algorithms and software codes, the analysis of the IR spectra can be made more and more effective by adopting suitable *first principles* theoretical modelling. In particular the implementation of the translational symmetry in Quantum Chemical codes exploiting the MO=LCAO methods and the use of the symmetry, allowed to extend the simulation of infrared and Raman spectra to rather complex molecular crystals and in particular to polymer crystals. CRYSTAL [19] code has proven to be very effective for these studies.

Unlike the previous empirical works which were mainly restricted to the prediction of vibrational frequencies, first principles calculations provide absorption intensities and Raman activities which in turns allow a direct comparison with the experimental intensity pattern. Notice that absolute intensities values, which are hardly available through solid state experiments, can be theoretically predicted.

The possibility to compute reliable vibrational spectra in solid phase open the way to a further validation of the already established correlation between spectral features and polymer structure and can help in disentangling subtle intra-molecular and inter-molecular effects which remained still obscure. Moreover, it provides tools for a deeper rationalization of these effects. In particular, while the effect of intermolecular interactions on frequencies, as for instance the occurrence *crystal splitting* of bands, can be and has been interpreted since longtime in the framework of classical vibrational dynamics, the consequence of crystal packing on absorption intensities remained so far a rather elusive matter, because of difficulties associated to absolute intensities measurement and to the intrinsic limitation of the classical approaches for the modelling of absorption intensities.

In this paper we will revisit the well established case of PE infrared spectrum, by means of Density Functional Theory (DFT) calculations with periodic boundary conditions (PBC), applied to the modelling of the structure and of the infrared spectrum of its orthorhombic crystalline phase. The study is aimed at exploring potentialities and limitation of this approach, focusing in particular on the effects of the crystal field on infrared intensities and on the performances of the CRYSTAL code [19] in this respect.

2. The IR spectrum of polyethylene

The IR spectrum of highly crystalline polyethylene samples (see Figure 1) has been experimentally investigated and rationalized in the framework of the classical vibrational dynamics by several authors [20–24]. More recently, theoretical studies on PE and its oligomers, based on quantum chemical modelling, appeared in the literature [25–27]. On these grounds the assignment of the spectral features can be considered a well established matter.

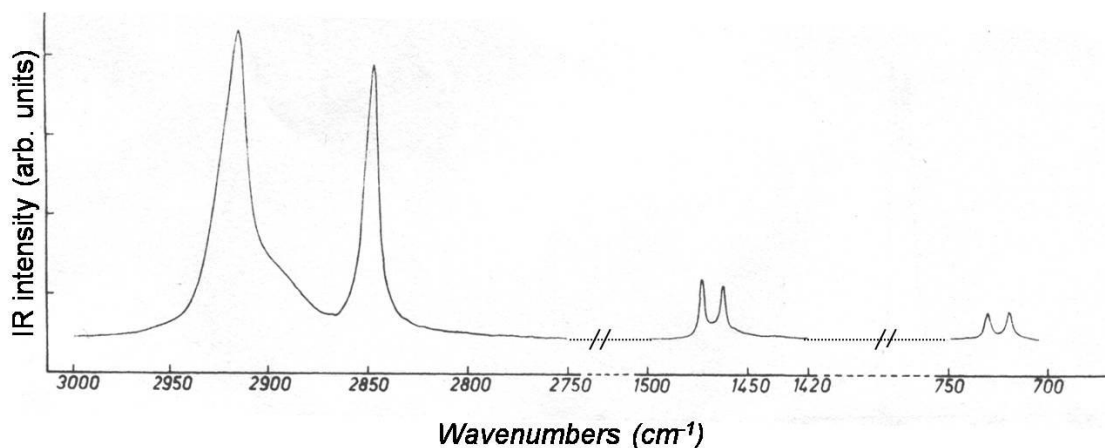


Fig. 1 Infrared spectrum of a highly crystalline PE sample (from [24])

The vibrational assignment of the IR transitions can be made firstly considering IR active phonons of a single, infinite chain in the all-trans conformation (1-D crystal), which line group is isomorphous to the D_{2h} symmetry point group, at Γ point.

Accordingly, infrared active phonons are classified and described as combination of symmetry adapted internal coordinates of the chemical unit (CH_2), as reported in Table 1. Due to the high symmetry and to the very small mixing between the high energy CH stretching vibrations with bending vibrations of PE, the IR transitions are usually described as “pure” d-, d+, δ , W, P, namely anti-symmetric and symmetric CH_2 stretching, CH_2 scissoring, wagging and rocking (the experimental frequencies are reported in Table 1). In other words, one assumes that the phonon can be safely identified with the symmetry coordinate with the major contribution in the vibrational eigenvector (see Ref. [24] for the definition of symmetry coordinates and for a detailed discussion).

The crystal packing in the 3-D crystal, described by the orthorhombic cell with two chains per unit cell, determines the doubling of the IR active phonons of B_{2u} and B_{3u} species and the symmetry coordinates of the crystal are usually described as the in phase and out-of-phase combinations of the coordinates defined for the 1-D crystal – see Table 1).

Table 1. Classification of the infrared active phonons of PE according to the 1-D crystal model (all-trans, infinite, isolated chain) and the 3-D crystal model.

Symmetry coordinate mainly involved (translational unit, single chain)	Symmetry species (1-D crystal, single chain)	Symmetry species (3D crystal)	Experimental frequency (cm ⁻¹)
d+ (out-of-phase symmetric stretching)	B _{3u}	B _{2u} , B _{3u}	2846
δ (out-of-phase scissoring)	B _{3u}	B _{2u} B _{3u}	1473 1463
W (in phase wagging)	B _{1u}	B _{1u} , A _u	-
d- (in phase antisymmetric stretching)	B _{2u}	B _{2u} , B _{3u}	2915
P (in phase rocking)	B _{2u}	B _{2u} B _{3u}	730 722

While in the stretching region the effect of the crystal packing cannot be easily recognized because of the low crystal splitting and to the complex band structure, ascribed to the occurrence of Fermi resonances [28,29], bending and rocking peaks show indeed the characteristic splitting into two IR active components, of comparable intensity.

This peculiar behavior has been taken as the signature of the orthorhombic cell, containing two different PE chains. It perfectly parallels the IR features observed for crystalline sample of odd-numbered crystalline n-alkanes, which indeed are packed according to an orthorhombic structure with two dynamically coupled chains¹. Crystal splitting shown by the orthorhombic crystals are sensitive to thermal expansion and disappear during the pre-melting phase characterized by expansion of the crystal cell and activation of collective large amplitude torsional motions of the chains [10–15,31].

Crystal splitting of rocking and scissoring bands of PE have been discussed thoroughly and models describing the vibrational coupling between neighboring chains by means of the introduction of inter-molecular force constants [30] have been proposed.

The intensity pattern of the IR spectrum of PE can be qualitatively described as follows. The CH stretching bands dominate the whole spectrum, showing absorbance values about ten times that of the deformation bands (in the following the sum of the intensities of

¹The crystal splitting is lost in the case of even-numbered n-alkanes crystal both packed according to the monoclinic cell (because of different symmetry selection rules) or triclinic cell with one only molecule per unit cell [30].

scissoring and rocking bands will be simply referred as “deformation” intensity). Even if a wagging transition is expected to occur in the IR on the basis of symmetry, its activity is so weak that it cannot be recognized in the experimental spectrum. The wide spectral region between 1400 cm^{-1} and 1300 cm^{-1} , which is completely free from fundamental transitions of the crystalline phase can show peculiar wagging marker bands ascribed to the occurrence of conformational defects, which can be characterized and quantified on this basis [10–14,31]. A rationalization of the intensity behavior of the wagging band which is silent in trans-planar polymethylene chains and shows-up in the presence of gauche defects is reported in [32].

Absorption intensities of PE have been deeply analyzed by Abbate et al. in Ref. [24], who reported integrated areas relative to the absorption bands associated to the fundamental IR transitions for solid samples of PE and for its per-deuterated derivative, both characterized by high crystallinity. For the first time in Ref. [24] a prediction of the IR absolute intensities of PE is proposed, based on experimental intensity parameters (electro-optical parameters) obtained by means of the parameterization of absolute intensities of small oligomers in gas phase [33]. The authors adopted a model of “isolated” PE chain (1-D infinite crystal) thus neglecting intermolecular electro-optical interactions.

According to the authors this lacking can be one of the reason of the unsatisfactory prediction of the intensity ratios between the CH stretching intensities and the deformation (rocking and scissoring) ones.

Beside the evidences of intermolecular interactions in the crystalline phase in terms of peaks frequencies (e.g. occurrence of doublets), Snyder et al. [34,35] showed that also infrared intensities are sensitive to the phase of the sample. In Ref. [34] very accurate experimental studies on the temperature behavior of infrared intensities of PE and odd-numbered alkanes (C17, C19, C21) are reported. As already observed by Casal et al. [36], for all the samples examined deformation intensities show a drastic drop at the solid-solid transition between the orthorhombic and the hexagonal phase; moreover a further linear intensity decrease is observed while approaching the melting. A loss of about $2/3$ of the overall intensity from the low temperature solid phase to the gas phase is reported in Ref. [34]. On the opposite, CH stretching intensities seem to be weakly sensitive to temperature changes. The observed behavior of n-alkanes and PE has been confirmed by the subsequent studies [35].

In Ref. [34] the authors discuss the possible intensity-loss mechanisms and demonstrate that nor changes of the material density, nor the refractive index variation or the occurrence of conformational disorder can quantitatively justify the observed intensity loss, which can be indeed considered as an intrinsic phenomenon. A possible interpretation has been suggested in Ref. [34] where the weakening of the deformation bands while increasing temperature is ascribed to the activation of large amplitude low frequency - “lattice-like” and torsional - modes, showing mechanical coupling with higher frequency normal modes.

The above interpretation was based on the idea that the small dispersion interactions between chains have a negligible effect on the electron density distribution and dipole

derivatives. This same hypothesis is at the basis of the determination of the setting angle of PE chain in the orthorhombic chain [37] by means the experimental measure of the intensity ratios of the two component of the rocking and scissoring doublet. The simple model proposed was based on the description of the dipole variation associated to the two phonons of the 3-D crystal as a simple vector sum of the dipole derivatives of two non-interacting chains. Notice that, according to this model, the sum of the intensities of the bands which constitute a given doublet should be exactly twice the intensity of the corresponding vibration of the single chain. Unfortunately, the experimental intensities of a single isolated all-trans chain cannot be obtained, because the all-trans regular structure occurs just in the crystal.

As shown in this study, the computational tools now available allow us to face the issue of the rationalization of the observed intensity trends with temperature from a completely new point of view, based on first principle prediction of the absolute infrared intensities of a 1-D crystal (single isolated PE chain) and of the 3-D crystal. Comparison with calculations carried out on oligomers *in vacuo* and in their crystalline phase will be also presented, in order to discuss the reliability of computed absolute intensities.

The experimental IR intensity data of PE are reported in Ref. [24] as relative values; absolute IR intensity values of crystalline n-alkanes can be taken from Ref. [38], where they were measured for low temperature (liquid Nitrogen) samples of short crystalline n-alkanes. The data, collected in Table 2, are obtained as sum of bands intensities over the whole CH stretching and over the whole deformation regions, taken from Ref. [38]. These data will be considered in the following discussion as a semi-quantitative reference to assess the quality of our predictions in terms of absolute intensities: several problems indeed occurred in the experimental determination of absolute IR intensities, due to orientation phenomena taking place in thin films. Notice, moreover, that that intensity values of n-alkanes contain also the contribution of methyl groups, so any comparison with PE should carefully take in consideration their effect.

Looking to the data of Table 2, we can realize that both in n-alkanes and in PE the deformation region shows intensity values about one order of magnitude weaker than the stretching one.

Table 2. *Experimental absolute IR intensities for crystalline n-alkanes. The data are obtained as sum of bands intensities over the whole CH stretching and deformation regions, taken from Ref. [38].*

	n-butane	n-pentane	n-hexane	n-heptane	n-octane	average (n-alkanes)	PE
$R = I^{\text{str}}/I^{\text{def}}$	7.37	6.43	6.80	7.61	6.54	6.91	9.30
I^{str}/CH (Km mol^{-1})	25	36	34	34	22	30	
I^{def}/CH (Km mol^{-1})	3.45	5.60	5.01	4.52	3.39	4.39	

From absolute stretching intensities measured on five n-alkane samples we can derive an average contribution per CH bond of 30 Km mol⁻¹, which fit very well with the very accurate gas phase values reported in the literature (average CH stretching value 28 Km mol⁻¹ per CH, see Ref. [39]).

3. Models and calculations

For geometries optimization and IR spectra predictions we adopted in this work two different methods of calculations:

- Density Functional Theory (DFT) simulations with periodic boundary conditions (PBC) have been carried out by means of CRYSTAL14 code [19], for modelling crystals of PE (1-D crystal, namely the isolated chain with PBC in the only chain axis direction and 3-D crystal) and hexane.
- Density Functional Theory (DFT) calculations by means of Gaussian09 code [40], for modelling several n-alkanes. Both molecules *in vacuo* and small clusters have been considered.

In all the cases the geometry optimization and the prediction of the IR spectra have been carried out adopting the B3LYP [41,42] hybrid exchange-correlation functional together with the 6-31G(d,p) basis set. For modelling the crystals and clusters, the B3LYP functional has been augmented with an empirical correction for dispersion interaction (B3LYP-D2) proposed by Grimme [43–45] and implemented both in CRYSTAL14 and Gaussian09.

Gaussian09 program adopt the sets of parameters proposed by Grimme [43,44] for the description of the dispersion correction, while in the case of calculations carried out with CRYSTAL code, we adopted the sets of parameters proposed by Quarti et al. [4]. These parameters have shown to give the best performance, for several polymers [6,46,47].

In the cases of calculations with PBC, full geometry optimization (cell parameters and atomic positions) of the structure of:

- the isolated infinite PE chain in its regular all-trans conformation
- clusters of PE chains
- the orthorhombic PE crystal

have been carried out by means of the CRYSTAL14 code[19].

In the case of the calculations on PE crystal while increasing the cell parameters (expanded cell) reported in Section 4.2, cell parameters have been fixed and the atomic position have been optimized. As starting guess structures for the calculations, we considered the experimentally determined crystal parameters and atomic coordinates reported by Bunn et al. [48].

In all the cases considered, the vibrational spectrum have been predicted in double harmonic approximation for the equilibrium structures, through the calculation of second derivatives of the potential energy (frequencies) and first derivative of the dipole moment (IR intensities).

In some cases (e.g. calculations on clusters and onshort alkanes), in order to remove the contribution to the spectrum of the CH₃ groups or of the chains in the external shells, we modified masses of group of atoms with fictitious masses of 5000 amu.

Different functional-basis set combinations have been tested and calculation (with and without the Grimme correction for the interactions) have been compared. For sake of conciseness, in the following discussion we will illustrate the results obtained with the method which showed the best performances. In order to allow a comparison, in Supporting Information some additional data are reported, obtained according to different choices.

It is however important to stress that the main conclusions obtained by means of the simulations here described are confirmed also adopting other computational set-up.

4. Results and discussion

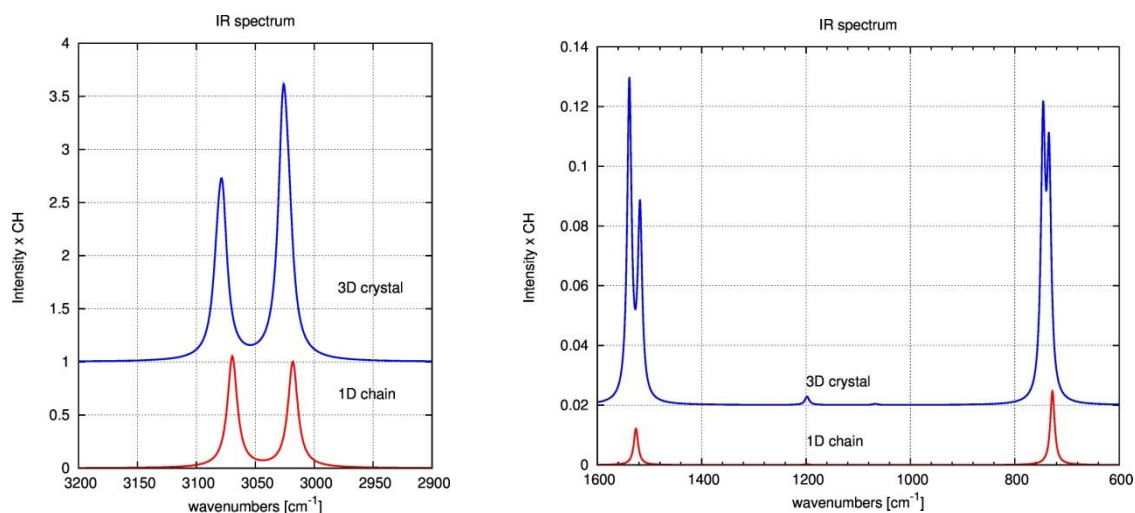
4.1 3D crystal vs 1D chain

Using the program CRYSTAL14 and applying PBC, we predicted the IR spectrum for both the whole crystal (according to the observed 3-D crystalline structure) and an isolated infinite 1-D chain characterized by a perfect trans-planar conformation.

In Figure 2 we report the plot of the computed spectrum for 3-D and 1-D crystals. In the plot, the computed intensities of each transition are normalized to the number of CH bonds in the unit cell.

The comparison of the theoretical spectrum obtained for the 3-D crystal with the experimental one (Figure 1) shows that the theoretical prediction accurately describes several relevant experimental features: (i) the general intensity pattern is reproduced (compare the calculated intensity ratio between stretching and deformation region, $R^{theo, 3D} = 14.4$ with the experimental ratio $R^{exp} = 9.3$); however, the intensity ratio between scissoring and rocking band is underestimated by the calculation by a factor of two; iii) the theoretically predicted wagging band is very weak, as suggested by the experiment; ii) the observed crystal splitting of the scissoring and rocking bands is nicely described, even if slightly overestimated in the case of the scissoring doublet by the calculation (compare the experimental splitting values of 10 cm⁻¹ and 12 cm⁻¹ [37] with the predicted values of 20 cm⁻¹ and 12 cm⁻¹ for the scissoring and rocking bands respectively). The predicted crystal splitting become 7 cm⁻¹ for the scissoring, and 2 cm⁻¹ for the rocking doublet if the calculation is carried out in absence of the Grimme correction (see Supporting Information), confirming that this correction is mandatory for a reasonable prediction of the spectral features; iv) According to the calculations also the CH stretching bands split, but the predicted splitting is very small (4 cm⁻¹ for the d- band and 5 cm⁻¹ for d+), thus justifying the fact that it has not been revealed experimentally.

Figure 2. Plot of the computed IR spectrum of PE (3-D crystal and 1-D crystal, i.e. single chain); values of IR absorption intensities, normalized to the number of CH oscillators, are reported in the Table at the bottom.



	$I^{\text{stretching}}/\text{CH}$	$I^{\text{deformation}}/\text{CH}$	$R=I^{\text{stretching}}/I^{\text{deformation}}$	$r = I^{\text{scissoring}}/I^{\text{rocking}}$
3D crystal	75	5.26	14.4	1.02
1D crystal	31.99	0.58	55.4	0.49
Experimental [24]	-	-	9.3	2.25

The 1D model obviously does not describe any crystal splitting, moreover it is immediately clear that the two models provide a very different picture also from the point of view of the intensity pattern:

- i) normalized stretching intensities and deformation intensities decrease while passing from the 3-D to the 1-D model;
- ii) the intensity ratio R between stretching and deformation intensities increases by a factor of about 4 from 3-D to 1-D model, showing that the intensity weakening of the deformation transitions is more drastic than for stretching transitions. Notice moreover that the experimental value of R ($R=9.3$) is fairly well reproduced by the calculation on 3D crystal ($R = 14.4$), but it is dramatically overestimated by the calculation for the isolated chain ($R = 55.4$). Indeed the overall intensity in the region of the deformation vibrations is 10 times smaller for the single chain compared to the 3D crystal. The comparison between the two theoretical models indicates that the CH stretching bands in the 3-D crystal are blue shifted by the crystal field. The predicted shifts are 10cm^{-1} for d-

and 5 cm^{-1} for d+ bands and this finding parallels the optimized values of CH equilibrium bond length, which are also slightly affected by the crystal field: $r_{\text{CH}}^0 = 1.098\text{ \AA}$ in the 3-D crystal, $r_{\text{CH}}^0 = 1.100\text{ \AA}$ in the isolated chain.

The above prediction seems to reflect a physical effect, on the light of the observation of thermally induced shift of the CH stretching features toward higher wave-numbers reported in Ref. [49] for PE.

Even if the spectrum predicted for the 3-D crystal is acceptable if one considers the experimental intensity ratio between the CH stretching and deformation regions, it seems to fail in the estimate of the intensity ratio of the two d+ and d- bands and in the prediction of the absolute CH stretching intensity. In addition, the calculation seems to overestimate the intensity of the lower frequency d+ band, a feature which could be partially ascribed to the fact that the CH stretching region is heavily affected by phenomena related to anharmonicity, which is proven for instance by the occurrence of Fermi resonances in this region. These effects are completely neglected by the calculation, which exploits a fully harmonic model of the intra-molecular potential. Notice however that the CH stretching intensity pattern predicted with the 1-D crystal model is very different, showing almost equal IR intensity for the d+ and d- bands.

A deeper analysis based on the comparison of computed vibrational eigenvectors shows a non-negligible mixing of the d+ and d- vibrational coordinates (symmetry coordinates of the isolated chain) in the four CH stretching phonons (B_{2u} and B_{3u} symmetry) of the 3-D crystal. This feature does not conflict with the 3-D crystal symmetry and could justify the different intensity pattern shown by the CH stretching region of the 3-D model and for the 1-D isolated chain. The discrepancies found while comparing with the experimental features could indicate that the predicted mixing is an artefact of the computation.

It is much more difficult to justify the anomalously high average $I^{\text{stretching}}/\text{CH}$ stretching intensity value predicted in the case of the 3-D crystal. In particular, the whole CH stretching IR intensity of the 3-D crystal (sum of the two stretching bands, contribution per CH bond, $I^{\text{stretching}}/\text{CH} = 75\text{ Km/mol}$) is about two times higher than the experimental determination for solid crystalline n-alkanes (average experimental determination $\langle I^{\text{stretching}}/\text{CH} \rangle = 30\text{ kmmol}^{-1}$, according to the data of Table 2). Interestingly, the prediction of $I^{\text{stretching}}/\text{CH} = 32\text{ Km/mol}$ for the 1-D isolated chain shows a better agreement with the experimental data, extrapolated from measurements on solid, crystalline n-alkanes².

In conclusion, the comparison of the computed intensity data with the experimentally available determinations suggest that the calculation on the 3-D crystal:

²It seems quite reasonable that the experimental value of $I^{\text{stretching}}/\text{CH}$ for crystalline n-alkanes could be extrapolated to the case of PE, since relevant effects while increasing the chain length (e.g. effects associated to the modulation of the electronic structure) are not expected. This is supported by the fact that linear n-alkanes of different length show similar $I^{\text{stretching}}/\text{CH}$ values.

- overestimates the CH stretching intensities, which result to be higher by a factor of about 2.
- correctly reproduces the intensity behaviour of the deformation intensities. Indeed calculations suggest that the deformation intensities are remarkably more sensitive than the CH stretching ones to the 3-D packing, as clearly demonstrated by the work of Snyder [34,35]. In his work a dramatic decrease of the scissoring and rocking intensities while approaching the pre-melting phase is indeed observed.

It is important to stress that our calculations do not take into account explicitly the effect of the temperature nor possible coupling of stretching and – thermally activated - large amplitude torsional vibrations, which is proposed in Ref. [34] as possible responsible of the intensity evolution with temperature. Our results demonstrate that the observed intrinsic change of deformation intensities should be mainly ascribed to intermolecular interactions.

Finally it is interesting to analyse the effect of Grimme correction on IR intensities. From the data reported in Table 3 we can see that in absence of Grimme correction, and therefore partially neglecting intermolecular interactions, the calculation for the 3D crystal predicts an intensity ratio of $R = 45.45$, close to the one obtained for the isolated chain. Indeed, the introduction of the Grimme correction intensifies the deformation region of factor of 4, while only slightly modifies the absorption intensity of the CH-stretching region.

Table 3. *Computed IR absorption intensities of PE 3-D crystal obtained with Grimme and without correction, and for 1-D crystal (i.e. single chain) (intensities are normalized to the number of CH oscillators in the unit cell).*

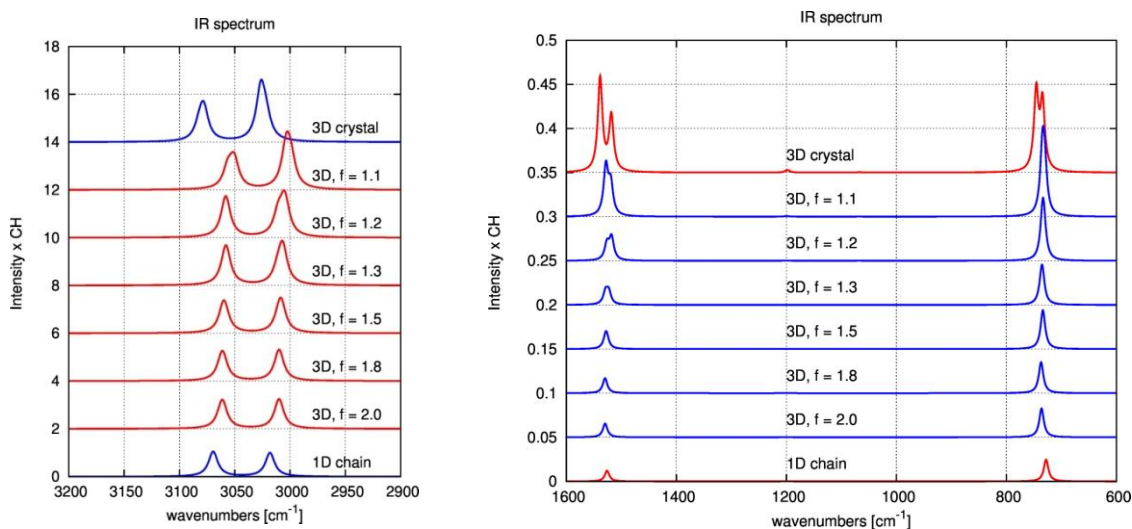
	$I^{\text{stretching}}/\text{CH}$	$I^{\text{deformation}}/\text{CH}$	$R=I^{\text{stretching}}/I^{\text{deformation}}$
3D crystal + Grimme Correction	75	5.26	14.4
1D crystal	31.99	0.58	55.4
3D crystal No-Grimme Correction	63.98	1.41	45.45

4.2 Effect of the crystal field.

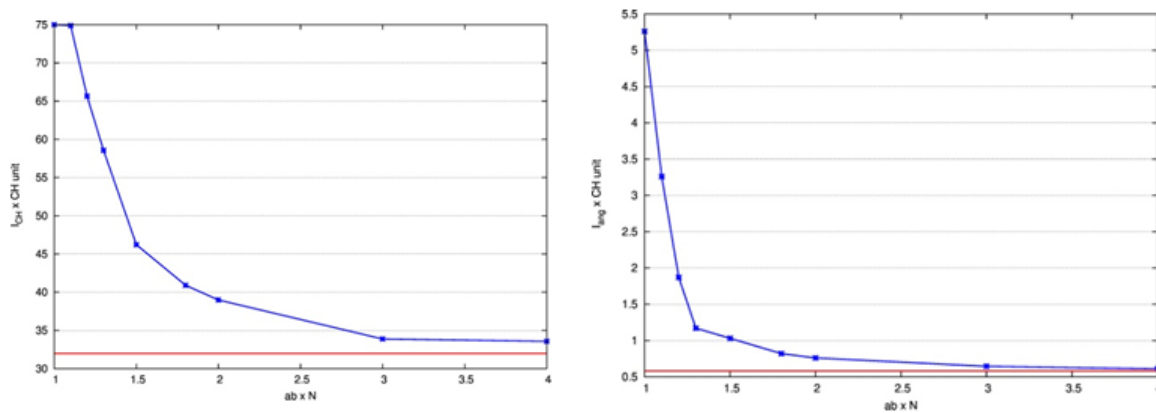
A way to prove the effect of the crystal field on absorption intensities is to follow its evolution while increasing the cell size. We started from the optimized crystal cell and expanded it in both **a** and **b** directions, orthogonal to the chain axis. The resulting computed spectra are reported in Figure 3 (from the top to the bottom) for subsequent steps during the expansion, described by the expansion factor f . For each step we fixed the values of the cell parameters and allow relaxation of the atoms positions before the calculation of the IR spectrum. Figure 3 clearly shows that the spectrum of the isolated chain is progressively recovered while the cell expands. This demonstrates that changes found while passing from the 1-D crystal to the 3-D crystal model are truly due to inter-chain effects. Since the van der Waals interactions decay in a rather short range, already at the smaller expansion of the cell the crystal field effects are remarkably depressed (notice that the crystal splitting immediately disappear). Moreover also CH stretching bands frequencies shift to values close to those of the 1-D crystal at the lower cell expansion and their intensity ratio quickly reaches the value of 1, characteristic of the 1-D case.

According to the results reported in Figure 3 we can conclude that the two calculation (for the 3-D crystal and the 1-D isolated chain) are fully consistent.

Figure 3. (a) Plot of the computed IR spectrum of PE (3-D crystal) while varying the cell volume (expansion factor in a and b directions, increasing from the top to the bottom; the factor of expansion reported refers to the equilibrium cell parameters) and computed IR spectrum of the isolated chain (1-D crystal); (b) computed absorption intensities of stretching, and deformation bands, as function of the expansion factor f ; the red lines indicate the intensity values predicted for the isolated chain; values of the computed absorption intensities, normalized to one CH oscillator, are reported in the table(c).



(a)

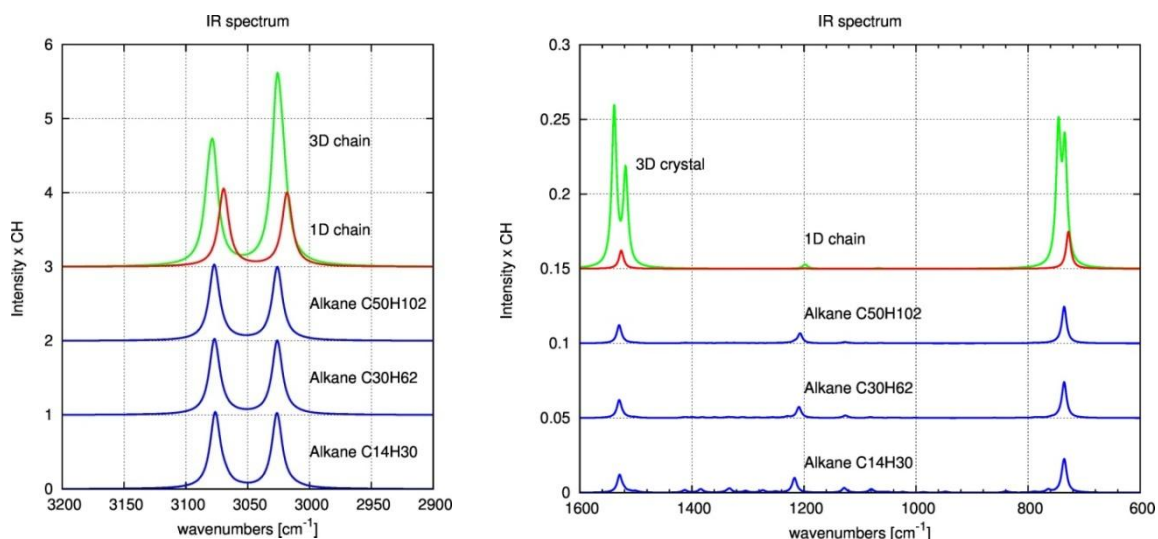


Model/expansion factor	$\Gamma^{\text{stretching}}/\text{CH}$	$\Gamma^{\text{deformation}}/\text{CH}$	$R = \Gamma^{\text{stretching}}/\Gamma^{\text{deformation}}$
3-D crystal (f = 1)	75.74	5.31	14
1.1	74.88	3.26	23
1.2	65.65	1.87	35
1.3	58.57	1.17	50
1.5	46.22	1.03	45
1.8	40.91	0.82	50
2	38.98	0.76	51
3	33.88	0.65	53
4	33.57	0.61	55
1-D crystal (f=+∞)	31.99	0.58	55

(c)

4.3 Comparison with oligomers: single chain model vs all-trans *n*-alkanes *in vacuo*

Figure 4. Comparison among the computed IR spectra of PE (single chain) and the spectra of some selected *n*-alkanes (isolated molecules, all trans conformation). In the cases of oligomers, the contributions of the methyl groups is removed adopting fictitious heavy masses for methyl hydrogen atoms (see text). At the bottom computed intensity values are reported, for the relevant spectral regions (values are normalized to the number of CH bonds in the polymethylene chains).



	$I^{\text{stretching}}/\text{CH}$	$I^{\text{deformation}}/\text{CH}$	$R=I^{\text{stretching}}/I^{\text{deformation}}$
3D crystal	75	5.26	14
1D crystal	32	0.7	55
$\text{C}_{50}\text{H}_{102}$ (weighted ends)	32	0.8	40
$\text{C}_{30}\text{H}_{62}$ (weighted ends)	32	0.9	37
$\text{C}_{14}\text{H}_{30}$ (weighted ends)	33	1.1	30

In order to discuss the relationships between absorption intensities of an all-trans infinite PE chain and those of its oligomers, *in vacuo*, we compare here the IR spectrum for the 1D crystal with the spectra predicted for several *n*-alkanes of different length in their all-

trans conformation. For a better comparison, following a computational procedure firstly proposed in Ref. [50], we decided to remove the contribution of the methyl ends by introducing fictitious masses on methyl hydrogen atoms, which allow to decouple methyl vibrations from CH₂ modes (see in Supporting Information the data obtained from calculations on chains carries “real” masses also for methyl hydrogen atoms).

From Figure 4 we can realize that even the shorter chain (C14) shows a spectral pattern similar to that of the 1-D PE crystal: the main bands peak at the same frequencies and their intensities - normalized to the number of CH bonds – are very close in value.

Minor features appear in the region below 1600cm⁻¹, where the n-alkanes spectra show a multiplicity of weak bands, absent in the case of 1D crystal. These bands corresponds to the well-known rocking, scissoring and wagging sequences, namely to normal vibrations corresponding to $q \neq 0$ phonons of the infinite chain, which are inactive in the IR for symmetry reasons in the spectrum of the 1D crystal [11–15]. As expected, sequences of bands associated to $q \neq 0$ transitions weakens when the chain length grows, approaching the infinite chain limit. The results obtained demonstrate that the IR pattern (frequencies and intensities) predicted for the infinite single chain model is fully consistent with predictions for isolated n-alkanes, without PBC, thus indicating that the oligomer approach holds also from the viewpoint of the DFT predictions.

4.4 Intermolecular effects: bundle of chains vs 3D crystal

The extent of the chain-chain interaction in the 3D packing can be investigated considering, instead of an ideally infinite assembly of chains (3-D crystal), a bundle of chains characterized by the typical packing of the orthorhombic crystal of PE. In this way it should be possible to disentangle effects on the spectrum due to short range intermolecular interactions, from possibly spurious effects related the simulation of the ideally infinite 3-D crystal with PBC in the directions orthogonal to the chain axis. Moreover, long range vs first neighbour interactions will be discussed by comparing the results obtained for bundles of different sizes. Calculations have been carried out according to the following models:

- i. *Cluster 1* : A bundle of 1-D chains where the inner chain should experience interactions like those arising from the interactions with first neighbour chains in the crystal. The model is a 1-D crystal made by a central PE chain surrounded by six chains arranged following the geometry of the 3-D orthorhombic crystal. PBC in the chain axis direction are managed in the framework of the CRYSTAL code. The masses of the atoms belonging to chains in the external shell have been arbitrarily replaced with heavy masses, in order to avoid the vibrational coupling with the central chain. In this way we aimed at describing the bare effect of intermolecular interactions among first-neighbour chains on the intensities of the vibrational modes localized on one individual chain.
- ii. *Cluster 2*: The model is similar to that described at point 1, but in this case a more sizeable cluster is considered, namely the inner chain is surrounded by two subsequent

shell of chains, the first one formed by 6 chains and the second one by 12 chains. Also in this case the geometry of the 3-D crystal is adopted and all the chains surrounding the central one carry fictitious heavy masses.

Cluster 1 model has been also applied to finite length chains ($C_{14}H_{30}$) in order to put into light possible differences while passing from an infinite bundle to a bundle of chains of finite length.

Both cluster 1 and 2 have been built starting from the optimized geometry of the 3-D crystal, and then relaxing the geometry. Only small changes in the internal coordinates have been obtained. The results are reported in Figure 5 and are quite interesting.

First of all, it is apparent that the introduction of the second shell (Cluster 2) does not modify the results obtained with Cluster 1 model, thus suggesting that the relevant interactions are confined to first neighbour chains, as expected in the case of relatively weak Van der Waals interactions.

While comparing the predictions for the polymer clusters with those for 3-D crystal and 1-D crystal of PE we can make the following observations:

- a. Rocking and scissoring splitting are not reproduced by the clusters models, because the vibrational coupling among adjacent chains is removed thanks to the introduction of “heavy masses”.
- b. The frequencies of the two main CH stretching bands in the spectra of the clusters result to be blue shifted if compared to those of the isolated chain. As already mentioned, a thermally induced shift of the CH stretching features toward higher wavenumbers has been experimentally observed [49] in the case of PE. Interestingly, this effect is present even if the peripheral chains in the two Clusters carries fictitious heavy masses, showing that the predicted blue-shift is not a mere consequence of the vibrational coupling between chains but it is induced by the crystal field, through first-neighbor interactions.
- c. The intensity ratio between d+ and d- bands in the Clusters is close to that predicted for the 1-D crystal. This confirms that the mixing of d+ and d- in the phonon eigenvectors of the 3-D crystal is the responsible of the - apparently spurious - overestimation of d+ band.
- d. IR intensity of both CH stretching and deformation regions halves from 3-D PE crystal to the case of the Clusters. Also this feature suggests the existence of some “unphysical” effect which is responsible of a general overestimation of the IR intensities while dealing with the prediction of the 3-D crystal spectrum.
- e. The cluster models allow to obtain the same intensity ratio between the stretching and the deformation regions predicted by the calculation for the 3-D crystal, in agreement with the experimental observation.
- f. On the other hand, if we directly compare the intensity data for the clusters with intensities of the isolate chain (Figure 5) we can observe that the bending region is 3-4 times stronger in the cluster case. This value is comparable with the factor 3 measured by Snyder [34] following solid-gas transition for several n-alkanes and clearly demonstrates

that short range intermolecular interactions are responsible of the observed enhancement of the bending intensities in solid phase.

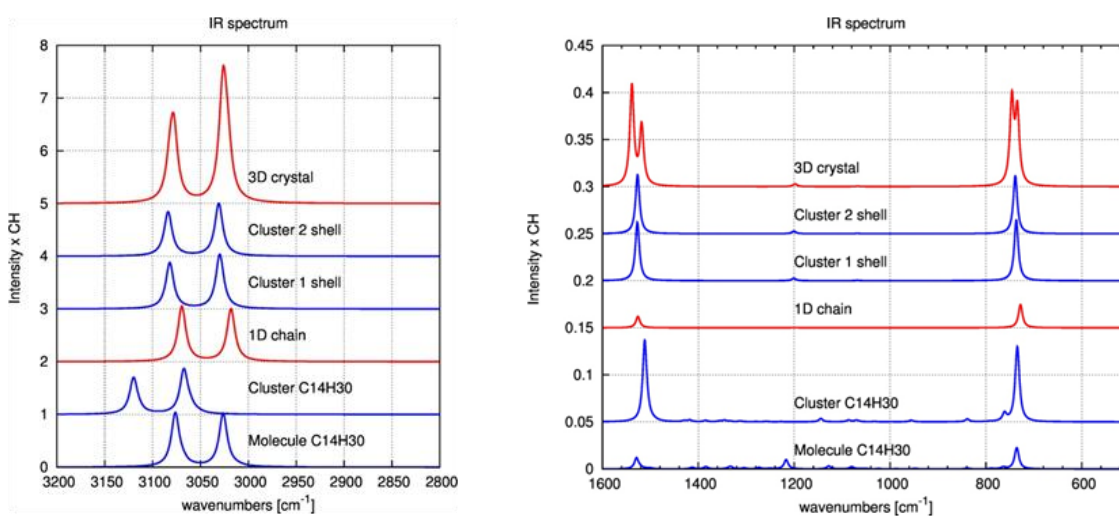
g. On the opposite, the intensity of the CH-stretching region predicted for the cluster models show negligible differences with respect to that of the isolated chain. Also this fact find a nice correspondence with the available experimental data, showing that CH stretching intensities are scarcely affected by heating.

The results obtained for the isolated C14 chain and for its cluster (Gaussian09 calculations) parallels all the finding commented above for the PE case.

In Figure 5 the average intensity values taken from calculations on the same clusters keeping “real” masses for all the chains (molecules) are also reported, showing that the observations on the intensity trends reported above still hold independently from the vibrational coupling between adjacent chains.

Figure 5. Comparison among the computed IR spectra of PE (3D crystal and 1-D single chain crystal) and the spectra of bundles of PE chains, described as 1-D crystals (see text for the description of the clusters geometries). The contributions to the spectrum of the chains surrounding the central one is removed adopting fictitious heavy masses (see text). The two spectra at the bottom of the panel are obtained for $C_{14}H_{30}$ in vacuo and for a cluster of seven $C_{14}H_{30}$ molecules. Also in this case heavy masses have been adopted in order to decouple vibrations of the methyl groups and of the peripheral chains.

The table report computed intensity values, for the relevant spectral regions (values are normalized to the number of CH bonds in the polymethylene chains). In parentheses intensity data obtained from calculations on clusters where all chains carries “real” masses. Intensity data from calculations carried out for a cluster of seven $C_{14}H_{30}$ molecules are also reported and compared with calculations on the molecule in vacuo.



	$I^{\text{stretching}}/\text{CH}$	$I^{\text{deformation}}/\text{CH}$	$R=I^{\text{stretching}}/I^{\text{deformation}}$
3D Crystal	75	5.26	14
Cluster (1-D Crystal; 2 shells)	28.74 (29.75)	1.995 (1.73)	14.40 (17.16)
Cluster (1-D Crystal; 1 shell)	29.84 (30.52)	2.04 (1.59)	14.66 (19.23)
1D Crystal (isolated chain)	32	0.58	55
Cluster of molecules ($\text{C}_{14}\text{H}_{30}$ - 1 shell, weighted ends)	26 (29.97)	3.2 (3.18)	8.13 (9.43)
$\text{C}_{14}\text{H}_{30}$ (isolated molecule; weighted ends)	33 (33.61)	1.1 (1.92)	30 (17.50)

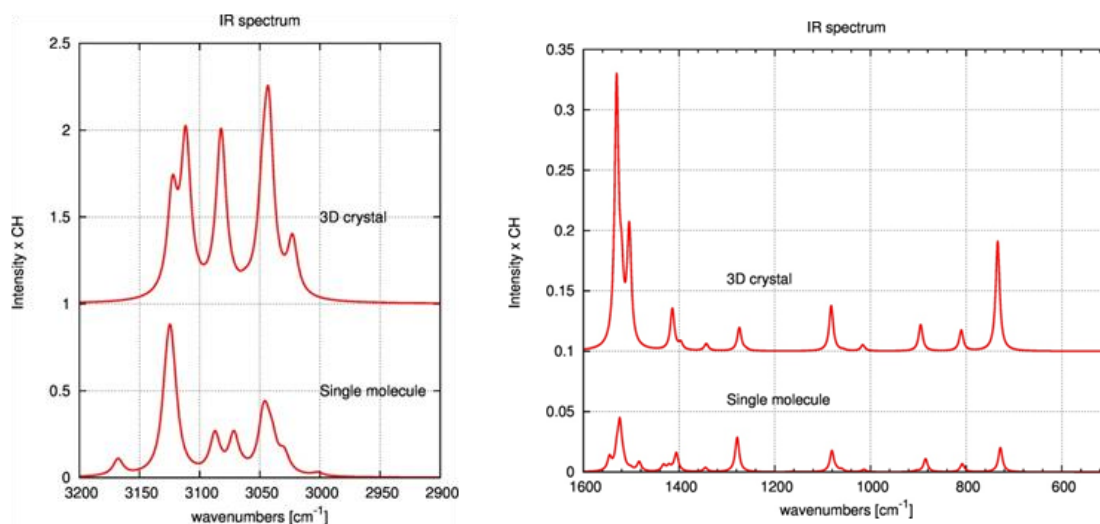
4.5 Oligomers in the crystalline phase : hexane

The phenomena induced in the IR spectrum of PE by intermolecular interactions occurring in the crystal are common to the its oligomers, as widely demonstrated by several papers where a joint analysis of the spectrum of PE and of its oligomers is presented [16–18,34–36].

In the following we will show that the trends predicted adopting different models of PE (single chain, cluster of chains and 3-D crystal) can be found also for short n-alkanes. Since the calculation of the spectrum of the 3-D crystal is computationally demanding in the case of oligomers, we decided to focus on the case of hexane.

The intensity data relevant for the discussion are reported in Figure 6, showing trends similar to those found in the case of PE. In particular the intensity of the stretching region halves from the case of the 3-D crystal to that of the isolated molecule. Moreover, the deformation intensities markedly decreases - by a factor of 4.3 - from 3-D crystal to the molecule.

Figure 6. Comparison among the computed IR spectra of hexane for the 3D crystal and for the isolated molecule, in the all-trans conformation. At the bottom computed average intensity values are reported, for the relevant spectral regions (values are normalized to the number of CH bonds); in parentheses the experimental intensity data (from Ref. [38]) are reported.



	$I^{\text{stretching}}/\text{CH}$	$I^{\text{deformation}}/\text{CH}$	$R=I^{\text{stretching}}/I^{\text{deformation}}$
3D - Crystal	65.56	9.47	6.93
Isolated molecule	34.97	3.64	11.41
Experimental	34	5.01	6.80

The comparison with the absolute absorption intensity values experimentally observed (Figure 6, table) gives a further support to the conclusions drawn for the case of PE. In particular, the predicted doubling of the CH stretching intensity value while considering the 3D crystal should be considered an artefact of the PBC calculation, while a “physical” increase of the deformation intensity is predicted in presence of intermolecular interactions. Indeed, the intensity ratio between stretching and deformation region predicted for the hexane crystal ($R=6.93$) is in very nice agreement with the experimental value ($R=6.80$).

5. Conclusions

The aim of this work was to assess the description of the IR spectra of polymers in crystalline state as obtained by means of Quantum Chemical calculations in the framework of the Density Functional Theory, carried out with CRYSTAL14 code.

The analysis has been performed according to three different models, adopted for the description of PE, namely:

- a) the all trans isolated chain, described as a 1-D Crystal;
- b) the 3-D Crystal characterized by a orthorhombic cell and two PE chains in the unit cell;
- c) two different clusters, mimicking the intermolecular environment in the crystal, without explicit application of periodic boundary condition in the **ab** plane, orthogonal to the chain axis **c**.

Moreover, several oligomers have been considered for sake of comparison, namely:

- i) isolated n-alkanes in all-trans conformation ($C_{50}H_{102}$, $C_{30}H_{62}$, $C_{14}H_{30}$), in order to assess the coherence of the oligomer approach with the description of the vibrations of an isolated polymer chain, modelled in the limit of an infinite 1-D crystal.
- ii) Cluster of $C_{14}H_{30}$ chains, in order to assess the effect of PBC in the **c** axis direction in presence of intermolecular interaction mimicking the real chain environment in the crystal.
- iii) The 3-D crystal of hexane and the isolated molecule in trans conformation in order to verify whether the conclusion drawn for the case of PE have a coherent counterpart in the case of a small n-akane.

The analysis of the results obtained has been carried out through the comparison with the available experimental data, that is:

- IR spectra of highly crystalline PE and of solid crystalline n-alkanes;
- absolute absorption intensities of n-alkanes;
- thermal evolution of the IR intensities (from low temperature solid state to gas phase in the case of n-alkanes; from low temperature solid state to the melt for PE)

The main conclusions can be summarized as follow:

1. PBC in the direction of the chain axis gives spectra fully compatible with the modelling of finite size oligomers. This fact tell us that the oligomer approach, proposed in the pioneering works dealing with the interpretation and modelling of polymer spectra, is perfectly suitable also in the light of a first principle approach.
2. Intermolecular interactions occurring while chains are packed in the crystal are far from being negligible for a good prediction of the spectra of the solid crystalline phase. Calculations carried out on 3-D PE crystal allow to predict the observed crystal splitting of rocking and scissoring bands and unveils that the effect of intermolecular interactions

determines a remarkable variation of the intrinsic deformation intensities. The phenomenon was observed in the past by Snyder [34,35]. He ascribed the intensity decrease with heating to the coupling of the rocking and scissoring vibrations to large amplitude torsional motions, thermally activated. The results obtained, through models which do not take explicitly into account thermal excitations and/or anharmonic couplings, cast new light on the role of the electro-optical intermolecular interactions related to weak dispersion interactions.

3. The absolute values of absorption intensities predicted for 3-D crystals (PE and hexane) are overestimated by a factor of about two, as shown by a careful discussion of the predictions obtained for the CH stretching region. The different computational setup exploited in this work and reported in Supporting Information give similar results and suggest that the introduction of PBC in the crystal direction characterized by Van der Waals bonds could be a very delicate issue.

References

- [1] Y. Hu, P.C. Painter, M.M. Coleman, On the infrared spectroscopic determination of self- and interassociation equilibrium constants used in the prediction of the phase behavior of hydrogen bonded polymer blends, *Macromol. Chem. Phys.* 201 (2000) 470–477. doi:10.1002/(SICI)1521-3935(20000201)201:4<470::AID-MACP470>3.0.CO;2-G.
- [2] J.S. Stephens, D.B. Chase, J.F. Rabolt, Effect of the electrospinning process on polymer crystallization chain conformation in nylon-6 and nylon-12, *Macromolecules*. 37 (2004) 877–881. doi:10.1021/ma0351569.
- [3] G. Pimentel, A. McClellan, *The Hydrogen Bond*, W. H. Freeman And Company, 1960. <http://archive.org/details/hydrogenbond031051mbp> (accessed November 23, 2015).
- [4] C. Quarti, A. Milani, B. Civalleri, R. Orlando, C. Castiglioni, Ab Initio Calculation of the Crystalline Structure and IR Spectrum of Polymers: Nylon 6 Polymorphs, *J. Phys. Chem. B*. 116 (2012) 8299–8311. doi:10.1021/jp303715v.
- [5] A. Milani, Unpolarized and Polarized Raman Spectroscopy of Nylon-6 Polymorphs: A Quantum Chemical Approach, *J. Phys. Chem. B*. 119 (2015) 3868–3874. doi:10.1021/jp5125266.
- [6] D. Galimberti, C. Quarti, A. Milani, L. Brambilla, B. Civalleri, C. Castiglioni, IR spectroscopy of crystalline polymers from ab initio calculations: Nylon 6,6, *Vib. Spectrosc.* 66 (2013) 83–92. doi:10.1016/j.vibspec.2013.02.005.
- [7] A. Milani, J. Zanetti, C. Castiglioni, E. Di Dedda, S. Radice, G. Canil, et al., Intramolecular and intermolecular OH...O and OH...F interactions in perfluoropolyethers with polar end groups: IR spectroscopy and first-principles calculations, *Eur. Polym. J.* 48 (2012) 391–403. doi:10.1016/j.eurpolymj.2011.11.022.

- [8] A. Milani, C. Castiglioni, E. Di Dedda, S. Radice, G. Canil, A. Di Meo, et al., Hydrogen bonding effects in perfluorinated polyamides: An investigation based on infrared spectroscopy and density functional theory calculations, *Polymer*. 51 (2010) 2597–2610. doi:10.1016/j.polymer.2010.04.002.
- [9] F. Muniz-Miranda, M. Pagliai, G. Cardini, R. Righini, Hydrogen bond effects in the vibrational spectra of 1,3-propanediol in acetonitrile: Ab initio and experimental study, *J. Chem. Phys.* 137 (2012) 244501. doi:10.1063/1.4770499.
- [10] S. Krimm, Infrared spectra of high polymers, in: *Fortschritte Hochpolym.-Forsch.*, Springer Berlin Heidelberg, 1960: pp. 51–172. <http://link.springer.com/chapter/10.1007/BFb0050351>
- [11] G. Zerbi, Molecular Vibrations of High Polymers, *Appl. Spectrosc. Rev.* 2 (1969) 193–261. doi:10.1080/05704926908050170.
- [12] G. Zerbi, A.J. Barnes, W.J. Orville-Thomas, Molecular Dynamics and Vibrational Spectra of Polymers, *Vib. Spectrosc. Trends.* (1977) 379–403.
- [13] G. Zerbi, Vibrational spectroscopy of very large molecules, *Adv. Infrared Raman Spectrosc.* 11 (1984) 301.
- [14] C. Castiglioni, Theory of Vibrational Spectroscopy of Polymers, in: *Handb. Vib. Spectrosc.*, John Wiley & Sons, Ltd, 2006.
- [15] P. C. Painter, M. M. Coleman, and J. L. Koenig: The Theory of Vibrational Spectroscopy and its Application to Polymeric Materials. John Wiley & Sons Ltd., New York, Chichester, Brisbane, Toronto, Singapore 1982. 530 Seiten, Preis: £ 44,50, *Berichte Bunsenges. Für Phys. Chem.* 86 (1982) 960–960. doi:10.1002/bbpc.19820861027.
- [16] R.G. Snyder, J.H. Schachtschneider, Vibrational analysis of the n-paraffins—I: Assignments of infrared bands in the spectra of C₃H₈ through n-C₁₉H₄₀, *Spectrochim. Acta.* 19 (1963) 85–116. doi:10.1016/0371-1951(63)80095-8.
- [17] J.H. Schachtschneider, R.G. Snyder, Vibrational analysis of the n-paraffins—II: Normal coordinate calculations, *Spectrochim. Acta.* 19 (1963) 117–168. doi:10.1016/0371-1951(63)80096-X.
- [18] R.G. Snyder, J.H. Schachtschneider, A valence force field for saturated hydrocarbons, *Spectrochim. Acta.* 21 (1965) 169–195. doi:10.1016/0371-1951(65)80115-1.
- [19] R. Dovesi, V.R. Saunders, C. Roetti, R. Orlando, C.M. Zicovich-Wilson, F. Pascale, et al., *CRYSTAL14 User's Manual*, University of Torino, Torino, 2014.
- [20] M. Tasumi, S. Krimm, Crystal Vibrations of Polyethylene, *J. Chem. Phys.* 46 (1967) 755–766. doi:10.1063/1.1840736.
- [21] S. Krimm, C.Y. Liang, G.B.B.M. Sutherland, Infrared Spectra of High Polymers. II. Polyethylene, *J. Chem. Phys.* 25 (1956) 549–562. doi:10.1063/1.1742963.

- [22] N. Karasawa, S. Dasgupta, W.A. Goddard, Mechanical properties and force field parameters for polyethylene crystal, *J. Phys. Chem.* 95 (1991) 2260–2272. doi:10.1021/j100159a031.
- [23] J. Barnes, B. Fanconi, Review of vibrational data and force field constants for polyethylene, *J. Phys. Chem. Ref. Data.* 7 (1978) 1309–1322. doi:10.1063/1.555586.
- [24] S. Abbate, M. Gussoni, G. Masetti, G. Zerbi, Infrared and Raman intensities of polyethylene and perdeuteropolyethylene by electro-optical parameters. Single chain, *J. Chem. Phys.* 67 (1977) 1519–1531. doi:10.1063/1.435036.
- [25] E. Koglin, R.J. Meier, Conformational dependence of Raman frequencies and intensities in alkanes and polyethylene, *Comput. Theor. Polym. Sci.* 9 (1999) 327–333. doi:10.1016/S1089-3156(99)00022-7.
- [26] R.J. Meier, Studying the length of trans conformational sequences in polyethylene using Raman spectroscopy: a computational study, *Polymer.* 43 (2002) 517–522. doi:10.1016/S0032-3861(01)00416-5.
- [27] A. Tarazona, E. Koglin, B.B. Coussens, R.J. Meier, Conformational dependence of Raman frequencies and intensities in alkanes and polyethylene, *Vib. Spectrosc.* 14 (1997) 159–170. doi:10.1016/S0924-2031(97)00013-1.
- [28] S. Abbate, G. Zerbi, S.L. Wunder, Fermi resonances and vibrational spectra of crystalline and amorphous polyethylene chains, *J. Phys. Chem.* 86 (1982) 3140–3149. doi:10.1021/j100213a017.
- [29] R.A. MacPhail, H.L. Strauss, R.G. Snyder, C.A. Elliger, Carbon-hydrogen stretching modes and the structure of n-alkyl chains. 2. Long, all-trans chains, *J. Phys. Chem.* 88 (1984) 334–341. doi:10.1021/j150647a002.
- [30] R.G. Snyder, Vibrational spectra of crystalline n-paraffins, *J. Mol. Spectrosc.* 7 (1961) 116–144. doi:10.1016/0022-2852(61)90347-2.
- [31] G. Zerbi, R. Magni, M. Gussoni, K.H. Moritz, A. Bigotto, S. Dirlikov, Molecular mechanics for phase transition and melting of n-alkanes: A spectroscopic study of molecular mobility of solid n-nonadecane, *J. Chem. Phys.* 75 (1981) 3175–3194. doi:10.1063/1.442490.
- [32] C. Castiglioni, M. Gussoni, G. Zerbi, Charge mobility in σ -bonded molecules: The infrared spectrum of polymethylene chains in the solid and liquid phases, *J. Chem. Phys.* 95 (1991) 7144–7149. doi:10.1063/1.461391.
- [33] M. Gussoni, S. Abbate, G. Zerbi, Least squares calculations of electro-optical parameters from infrared intensities of CH₄ and C₂H₆ and their deuterated derivatives, *J. Chem. Phys.* 71 (1979) 3428–3439. doi:10.1063/1.438731.
- [34] R.G. Snyder, M. Maroncelli, H.L. Strauss, V.M. Hallmark, Temperature and phase behavior of infrared intensities: the poly(methylene) chain, *J. Phys. Chem.* 90 (1986) 5623–5630. doi:10.1021/j100280a030.

- [35] H. Hagemann, R.G. Snyder, A.J. Peacock, L. Mandelkern, Quantitative infrared methods for the measurement of crystallinity and its temperature dependence: polyethylene, *Macromolecules*. 22 (1989) 3600–3606. doi:10.1021/ma00199a017.
- [36] H.L. Casal, D.G. Cameron, H.H. Mantsch, Infrared spectra of crystalline n-alkanes. Changes observed during the phase I→ phase II transition, *Can. J. Chem.* 61 (1983) 1736–1742.
- [37] S. Abbate, M. Gussoni, G. Zerbi, Infrared and Raman intensities of polyethylene and perdeuteropolyethylene: Factor group splittings, *J. Chem. Phys.* 70 (1979) 3577–3585. doi:10.1063/1.437960.
- [38] R.G. Snyder, Group Moment Interpretation of the Infrared Intensities of Crystalline n-Paraffins, *J. Chem. Phys.* 42 (1965) 1744–1763. doi:10.1063/1.1696187.
- [39] M. Gussoni, C. Castiglioni, G. Zerbi, Vibrational Intensities: Interpretation and Use for Diagnostic Purposes, in: *Handb. Vib. Spectrosc.*, John Wiley & Sons, Ltd, 2006.
- [40] M.J. Frisch, G.W. Trucks, J.R. Cheeseman, G. Scalmani, M. Caricato, H.P. Hratchian, et al., *Gaussian 09*, n.d.
- [41] A. Becke, Density-Functional Thermochemistry .3. the Role of Exact Exchange, *J. Chem. Phys.* 98 (1993) 5648–5652. doi:10.1063/1.464913.
- [42] C. Lee, W. Yang, R. Parr, Development of the Colle-Salvetti Correlation-Energy Formula into a Functional of the Electron-Density, *Phys. Rev. B.* 37 (1988) 785–789. doi:10.1103/PhysRevB.37.785.
- [43] S. Grimme, Accurate description of van der Waals complexes by density functional theory including empirical corrections, *J. Comput. Chem.* 25 (2004) 1463–1473. doi:10.1002/jcc.20078.
- [44] S. Grimme, Semiempirical GGA-type density functional constructed with a long-range dispersion correction, *J. Comput. Chem.* 27 (2006) 1787–1799. doi:10.1002/jcc.20495.
- [45] B. Civalleri, C.M. Zicovich-Wilson, L. Valenzano, P. Ugliengo, B3LYP augmented with an empirical dispersion term (B3LYP-D*) as applied to molecular crystals, *Crystengcomm*. 10 (2008) 405–410. doi:10.1039/b715018k.
- [46] D. Galimberti, A. Milani, Crystal Structure and Vibrational Spectra of Poly(trimethylene terephthalate) from Periodic Density Functional Theory Calculations, *J. Phys. Chem. B.* 118 (2014) 1954–1961. doi:10.1021/jp411560r.
- [47] A. Milani, D. Galimberti, Polymorphism of Poly(butylene terephthalate) Investigated by Means of Periodic Density Functional Theory Calculations, *Macromolecules*. 47 (2014) 1046–1052. doi:10.1021/ma402602f.
- [48] C.W. Bunn, The crystal structure of long-chain normal paraffin hydrocarbons. The “shape” of the CH₂ group, *Trans. Faraday Soc.* 35 (1939) 482–491.

- [49] I.-E. Mavrantza, D. Prentzas, V.G. Mavrantzas, C. Galiotis, Detailed atomistic molecular-dynamics simulation of the orthorhombic phase of crystalline polyethylene and alkane crystals, *J. Chem. Phys.* 115 (2001) 3937–3950. doi:10.1063/1.1386912.
- [50] N.B. da Costa, A.J.A. Aquino, M.N. Ramos, C. Castiglioni, G. Zerbi, The trans effect of lone pairs on individual X-H bonds (X = C or N). An ab initio study, *J. Mol. Struct. THEOCHEM.* 305 (1994) 19–25. doi:10.1016/0166-1280(94)80138-X.

Supporting Information

Table S1. Comparison among the computed IR spectra of PE and the spectra of some selected *n*-alkanes (isolated molecules, all trans conformation). In the cases of oligomers, the contributions of the methyl groups is removed adopting fictitious heavy masses for methyl hydrogen atoms. In parentheses intensity data obtained from calculations on chains carries “real” masses also for methyl hydrogen atoms.

	$I^{\text{stretching}}/\text{CH}$	$I^{\text{deformation}}/\text{CH}$	$R=I^{\text{stretching}}/I^{\text{deformation}}$
3D crystal	75	5.26	14
1D crystal	32	0.7	55
$\text{C}_{50}\text{H}_{102}$ (weighted ends)	32 (32)	0.8 (1.1)	40 (30)
$\text{C}_{30}\text{H}_{62}$ (weighted ends)	32 (33)	0.9 (1.3)	37 (25)
$\text{C}_{14}\text{H}_{30}$ (weighted ends)	33 (34)	1.1 (1.9)	30 (18)

Table S2 Comparison among crystal parameters and spectroscopic data of PE computed with different choice for Grimme correction, DFT functional and basis sets.

	$\Gamma^{\text{stretch}}/\text{CH}$	$\Gamma^{\text{def}}/\text{CH}$	$R=\Gamma^{\text{stretch}}/\Gamma^{\text{def}}$	$\Delta\nu_{\text{scissoring}}$ (cm^{-1})	$\Delta\nu_{\text{rocking}}$ (cm^{-1})	a (Å)	b (Å)	c (Å)
Experimental value [24]	30	4.39	9.3	10	12	4.93 4.85	7.40 7.12	2.534 2.548
B3LYP/ 6-31G(d,p) Corrected Grimme	75	5.26	14.4	20	12	4.849	7.046	2.567
No-grimme B3lyp/ 6-31G(d,p) (Re-optimized)	63.98	1.41	45.45	7.18	2.36	5.50	9.27	2.57
B3LYP/ 6-31G(d,p) Classic Grimme D2 [44]	64.64	7.72	8.38	8.36	27.9	4.45	6.48	2.55
Blyp/6-31G(d,p)	81.15	4.56	17.18	7.75	17.45	4.91	7.14	2.59
Pbe0/6-31G(d,p)	67.48	8.02	8.41	25.4	20.11	4.73	6.93	2.55
PBE/6-31G(d,p)	71.31	7.35	9.70	24.5	15.28	4.75	7.00	2.57
PBE/vtz	66.03	8.32	7.93	25.28	12.97	4.77	7.01	2.56
B3lyp/pob-tzvp	73.97	5.30	13.96	24.35	18.95	4.68	7.06	2.55

Table S3. ECCF parameters of PE

	3-D Crystal	Cluster (1shell)	Single chain
q_{H}	0.0558	0.0360	0.0195
$dq_{\text{H}}/r_{\text{CH}}$	-0.27971	-0.17194	-0.17654
r_{CH}	1.09895	1.09791	1.10018

2.5 Summary and Conclusions

In this chapter, we extended the computational investigation of crystalline polymers by using the CRYSTAL code to some new interesting cases, still lacking a quantum chemical investigations of solid state properties.

The aim was to demonstrate that state-of-the-art computational methods can provide an accurate description of the structural and vibrational properties of crystalline polymers in terms of the peculiar intra and intermolecular interactions occurring at the nanoscale.

Focusing on the structural properties, we proposed an interpretation for the polymorphic behaviour observed in even nylons by means of Density Functional Theory periodic calculations: the relative stability of the two possible α and γ phases have been investigated by analyzing in details the intramolecular and intermolecular effects taking place in these systems. We have been able to discriminate between conformational changes and effects due to intermolecular interactions by further distinguishing, in the latter case, the contribution due to hydrogen bonding and VdW interactions.

The investigation of crystalline polymers has been further expanded analyzing two aromatic polyesters: polytrimethylene terephthalate (PTT) and polybutylene terephthalate (PBT).

In these cases both structural and vibrational properties have been predicted and analyzed. The work focused on the identification of characteristic IR marker bands of the different polymorphs and on the evaluation of the effects of molecular interactions ruling the supramolecular organization of the chains and the physico-chemical behavior also at the macroscopic scale.

Full geometry optimization of the crystal structure and the calculation of the IR spectra of PTT and PBT's polymorphs have been carried out to this aim. The best setup for the simulations has been fulfilled first, since this family of polymers had been never approach before by means of periodic DFT calculations.

The results obtained for PTT demonstrated the reliability of periodic DFT calculations for the detailed investigation of structural and vibrational properties of polyesters, showing also their ability to support and complement the experimental characterization and its application in more technology-oriented environments.

As next polymer, we considered the case of PBT, that is particularly interesting since it shows a reversible transition between two different phases as a result of a mechanical deformation: this is a very interesting example of structure-properties correlations.

We were able to study the conformation and solid state structure of the two α and β polymorphs including also the simulation of the transition from the α to the β form upon mechanical stretching from a molecular prospective, that is following the evolution of the intramolecular structure of the polymer chain.

As last application of DFT-periodic calculations, we analyzed the effect of the crystal field on the IR intensities of polyethylene as a test case, demonstrating that VdW interactions, despite their weakness, can induce non-negligible changes in the infrared intensities. We thus demonstrated the importance of including in the simulation also supramolecular effects, often overlooked in quantum-chemical investigations to reduce the computational cost.

In general we can conclude that state-of-the-art DFT- periodic calculations can be a powerful tool in materials science and technology. Indeed, our work demonstrates that this kind of simulation can give a reliable description of the structural and vibrational properties of polymeric materials in connection also with properties exploited in practical applications. While, for one hand, they allow to shed light and interpret the complex intra and intermolecular phenomena taking place at the molecular level, thus being of importance for fundamental research, on the other hand they proved to be a very powerful tools to be used also in applied research and technology.

Indeed, quantum chemical calculations are finding more and more importance in the industrial environment [10] for their ability to give a detailed interpretation of the experimental data, but also for possible design purposes.

Bibliography

[1] C. Quarti, A. Milani, B. Civalleri, R. Orlando, C. Castiglioni, Ab Initio Calculation of the Crystalline Structure and IR Spectrum of Polymers: Nylon 6 Polymorphs, *J. Phys. Chem. B.* 116 (2012) 8299–8311. doi:10.1021/jp303715v.

[2] M. Yokouchi, Y. Sakakibara, Y. Chatani, H. Tadokoro, T. Tanaka, K. Yoda, Structures of Two Crystalline Forms of Poly(butylene terephthalate) and Reversible Transition between Them by Mechanical Deformation, *Macromolecules.* 9 (1976) 266–273. doi:10.1021/ma60050a018.

[3] I.H. Hall, M.G. Pass, Chain conformation of poly(tetramethylene terephthalate) and its change with strain, *Polymer.* 17 (1976) 807–816. doi:10.1016/0032-3861(76)90036-7.

[4] B.D. Stambaugh, J.L. Koenig, J.B. Lando, Infrared studies of the alpha crystal phase of poly(tetramethylene terephthalate), *J. Polym. Sci. Polym. Lett. Ed.* 15 (1977) 299–303. doi:10.1002/pol.1977.130150508.

[5] B. Stambaugh, J.L. Koenig, J.B. Lando, X-ray investigation of the structure of poly(tetramethylene terephthalate), *J. Polym. Sci. Polym. Phys. Ed.* 17 (1979) 1053–1062. doi:10.1002/pol.1979.180170613.

[6] S.A. Nitzsche, Y.K. Wang, S.L. Hsu, Application of the molecular simulation technique for clarification of the α \rightarrow β phase transformation in poly(butylene terephthalate), *Macromolecules.* 25 (1992) 2397–2400. doi:10.1021/ma00035a016.

[7] A. Kawaguchi, S. Murakami, M. Fujiwara, Y. Nishikawa, Dynamical observation of structural transition of polymers using an X-ray diffraction system with imaging plates. II. Crystalline transition of poly(butylene terephthalate), *J. Polym. Sci. Part B Polym. Phys.* 38 (2000) 838–845. doi:10.1002/(SICI)1099-0488(20000315)38:6<838::AID-POLB4>3.0.CO;2-F.

- [8] R.P. Grasso, B.C. Perry, J.L. Koenig, J.B. Lando, Structural and energetic analyses of the α to β phase transition in poly(butylene terephthalate), *Macromolecules*. 22 (1989) 1267–1272. doi:10.1021/ma00193a044.
- [9] R.G. Snyder, M. Maroncelli, H.L. Strauss, V.M. Hallmark, Temperature and phase behavior of infrared intensities: the poly(methylene) chain, *J. Phys. Chem.* 90 (1986) 5623–5630. doi:10.1021/j100280a030.
- [10] P. Deglmann, A. Schäfer, C. Lennartz, Application of quantum calculations in the chemical industry—An overview, *Int. J. Quantum Chem.* 115 (2015) 107–136. doi:10.1002/qua.24811.

Chapter 3

Investigating charge distribution and charge mobility from IR intensity parameters: new models and applications

3.0 Introduction

As highlighted in Chapter 2, IR intensities are spectroscopic observable of great interest for the analysis of intra and intermolecular interactions in complex molecular materials.

Indeed, in addition to analytical applications (e.g. quantitative determination of the concentration of molecular species), which require absolute intensities measurements, intensity data are closely related to the physicochemical materials properties at the molecular scale and so they can provide an insight on the ruling phenomena.

As an example, in our work on PBT (Section 2.3), we have shown that the analysis of the whole spectral pattern in both frequencies and intensities allow not only to identify the different stable conformations of the polymer but also to shed light on the polymorphic transition occurring under mechanical deformation.

Moreover, as clearly shown by the investigation carried out for polyethylene (Section 2.4), the modulation of the IR intensities allows to evaluate the effect of the crystal field.

The interpretation of the IR intensities can be fulfilled on the basis of different molecular parameters which give the further possibility to unfold and describe properties of the materials in terms of simple concepts, related to the charge distribution associated to given chemical bonds and to its charge mobility.

The starting point is the well known relationship between IR absorption intensity and the dipole moment of a molecular system, which in turns is the consequence of the charge distribution.

In the framework of the so-called double harmonic approximation, the absolute IR absorption intensity I_i of a band associated to the i -th normal mode Q_i can be expressed as a function of the molecular dipole moment derivatives with respect to normal mode [1,2]

$$I_i = C \left| \left(\frac{\partial \boldsymbol{\mu}}{\partial Q_i} \right)^0 \right|^2 \quad (3.1)$$

Due to the collective character of molecular vibrational modes, the mere analysis of the set of $\{(\partial \boldsymbol{\mu} / \partial Q_i)^0\}$, where i ranges over the whole set of infrared active normal modes, can hardly

bring to simple chemical concepts related to local molecular properties, e.g. describing the nature of the chemical groups (or of the atoms) in the molecules. For this reason, models and methods aimed at extracting local parameters from the set $\{(\partial\boldsymbol{\mu}/\partial Q_i)^0\}$, have been developed in the past [1–11]. In particular in the model of Electro-Optical-Parameters (EOP) [5–7], the molecular dipole is described in terms of bond dipoles $\boldsymbol{\mu} = \sum_k \boldsymbol{\mu}_k$ and the relationship between normal coordinates and internal coordinates ($\mathbf{R} = \mathbf{LQ}$) is exploited in order to obtain a set of equilibrium bond dipoles $\{\boldsymbol{\mu}_k^0\}$ and bond dipole derivatives with respect to internal displacements $\{\partial\boldsymbol{\mu}_k/\partial R_t\}$.

In a similar way, starting from the expression

$$\boldsymbol{\mu} = \sum_{\alpha} q_{\alpha} \mathbf{r}_{\alpha} \quad (3.2)$$

the Equilibrium Charges-Charge Fluxes (ECCF) [8,9] model allows to obtain equilibrium atomic charges $\{q_{\alpha}^0\}$ and charge fluxes with respect to internal parameters: $\{\partial q_{\alpha}/\partial R_t\}$.

The determination of ECCF parameters is usually done solving a set of equations in the form:

$$\left(\frac{\partial\boldsymbol{\mu}}{\partial R_t}\right)^0 = f\left(\{q_{\alpha}^0\}, \left\{\left(\frac{\partial q_{\alpha}}{\partial R_t}\right)^0\right\}\right)$$

Indeed, the set of dipole derivatives with respect to the normal coordinate Q_i , namely $(\partial\boldsymbol{\mu}/\partial Q_i)^0$, obtained from the experimental IR intensities, can be transformed into dipole derivatives with respect to the internal vibrational coordinate according to the relationship $\left(\frac{\partial\boldsymbol{\mu}}{\partial R_t}\right)^0 = \sum_i \left(\frac{\partial\boldsymbol{\mu}}{\partial Q_i}\right)^0 L_{it}^{-1}$, where \mathbf{L} is the vibrational eigenvectors matrix, obtained in the framework of Wilson GF method [12].

The development of reliable methods for the description of the molecular charge distribution and its mobility in terms of “local parameters” (i.e. point atomic charges) is a topic that has been addressed with considerable efforts since the beginning quantum chemistry. Many models have been proposed starting from the so-called Mulliken charges [13], the theory of Atoms-in-Molecules (AIM) developed by Bader[14], the Natural Population Analysis (NPA) [15,16], or charges derived from electrostatic potentials (e.g. the MK [17,18], the CHELP [19] and the CHELPG [20] models).

All these methods have however a strong limitation which makes them somewhat arbitrary: there is no experimental measurements of the atomic charges and, therefore, it is not possible to relate these charges to experimentally measurable quantities, or at least to validate them directly and unambiguously.

From this it is possible to see the significant advantage of a picture of the molecular charge distribution derived from IR intensities: indeed it provides a straightforward description of the charge distribution in molecules which directly comes from measurable properties (IR intensities).

Electro-Optical-Parameters (EOP) [5–7] and the Equilibrium Charges-Charge Fluxes (ECCF) [8,9] derived from observed absolute infrared intensities have a theoretical counterpart. They can be obtained from the computed Atomic Polar Tensors (APT), namely the Cartesian first

derivatives of the dipole moment, after suitable parameterization; a model which allows to extract “IR charges” in a straightforward way from computed APT tensors of planar molecules has been recently proposed [21,21,22].

Atomic charges and charge fluxes have been obtained from computed APTs also in the framework of: Charge-Charge Flux-Overlap (CCFO) [10,11], CCFOModified [23–25] and Charge-Charge Flux-Dipole Flux (CCDFD) [26–29] models. In addition, Generalized Atomic Polar Tensor (GAPT) charges have been proposed [30].

The success of ECCF model, is due to the fact that it has the advantage of providing a description of the charge distribution of the molecule either from the point of view of point (static) atomic charges and their mobility (i.e. charge fluxes).

ECCF are valuable parameters for the description and rationalization of several intra and intermolecular effects, such as inductive effects, charge backdonation, hyperconjugation; moreover they allows to identify atoms able to form hydrogen bonds or responsible for strong electrostatic interaction [31–34].

However some issues limited their use in the past. First, their calculation from experimental absolute intensity requires an accurate knowledge of the vibrational force field of the molecule (\mathbf{L} matrix).

Second, from the IR experimental intensity we are unable to obtain the sign of the $(\partial\boldsymbol{\mu}/\partial Q_i)^0$ (see Eq. (3.1)); in this regard in the past various methods and models have been proposed to solve the “sign” issue [24,35].

Another problem arising from the use of experimental intensity is the overlap of different bands of the spectrum makes very complex the measurements of the absolute intensity even for very simple molecules, implying inaccuracies in the determination of $(\partial\boldsymbol{\mu}/\partial Q_i)^0$ values.

The advent of very accurate quantum-chemical calculations have allowed to overcome these problems.

Recently, It has been demonstrate [36] that current state-of-the-art ab-initio/Density functional theory (DFT) calculations allow to compute absolute IR intensities with an high accuracy and in very good agreement with available experimental data.

The absolute IR absorption intensity I_i of a band associated to the i -th normal mode Q_i is calculated starting from the computed molecular dipole moment derivatives with respect to the Cartesian displacements (ξ_k) of the atoms (Atomic Polar Tensor), which are automatically calculated when computing the IR spectra by means of ab-initio/DFT models [1,2]:

$$I_i = C \left| \left(\frac{\partial \boldsymbol{\mu}}{\partial Q_i} \right)^0 \right|^2 = \left| \sum_k \left(\frac{\partial \boldsymbol{\mu}}{\partial \xi_k} \right)^0 L_{ki} \right|^2 \quad (3.3)$$

In Eq. (3.3) \mathbf{L} is the transformation matrix from Cartesian to normal coordinates (obtained as output of the calculations) and C is a constant depending on the adopted units.

The $3N$ values $\left(\frac{\partial \boldsymbol{\mu}}{\partial \xi_k} \right)^0$ (N number of atoms in the given molecules) are usually collected in 3×3 matrices referred to each individual atom β , such that the generic element of the ATP of β can be written as:

$$P_{uv}^{\beta} = \left(\frac{\partial \mu_u}{\partial v_{\beta}} \right)^0 \quad (3.4)$$

In P_{uv}^{β} , μ_u is the x, y or z component of the molecular dipole moment, while v_{β} is a Cartesian displacement of β atom, namely $v_{\beta} = x_{\beta}, y_{\beta}$ or z_{β} , upon which the derivative of the dipole moment is carried out.

Substituting Eq. (3.2) in Eq. (3.4) we get

$$\mathbf{P}^{\beta} = q_{\beta}^0 \cdot \mathbf{I} + \tilde{\mathbf{x}}^0 \cdot \left(\frac{\partial \mathbf{q}}{\partial \xi} \right)_{\beta}^0 \quad (3.5)$$

where \mathbf{I} is the 3x3 identity matrix, $\tilde{\mathbf{x}}^0$ is the 3xN matrix that collects, along its columns, the equilibrium Cartesian coordinates of each atom, while $\left(\frac{\partial \mathbf{q}}{\partial \xi} \right)_{\beta}^0$ is the Nx3N matrix of the Cartesian charge fluxes, restricted in Eq. (3.5) to the derivatives relative to Cartesian displacements of the β atom (Nx3 matrix).

Then the general element P_{uv}^{β} of the ATP tensor is a function both of the equilibrium atomic charge q_{β}^0 and of charge fluxes which, in principle, should be obtained by solving the system of equations described by Eq. (3.5) and considering the whole set of 9xN components of the APT of the N atoms in the molecule. Unfortunately, the number of unknowns is usually greater than the number of equations obtained.

However, in the special case of a planar molecule, it is always possible to obtain from the ATPs a unique set of equilibrium atomic charges. Indeed, by choosing a suitable reference system with an axis (z) orthogonal to the plane of the molecule, it is possible to extract the equilibrium atomic charge directly from the zz diagonal elements of \mathbf{P}^{β} according to the relationship:

$$P_{zz}^{\beta} = \left(\frac{\partial \mu_z}{\partial z_{\beta}} \right)^0 = q_{\beta}^0$$

It has been demonstrated both in the past [25], but also in recent works [30,36] that the IR charges defined according the ECCF model are in good agreement with the charges computed according to other common schemes, such as electrostatic charges (MK [17,18], CHELP [19] or CHELPG [20]) or Hirshfeld [37] charges.

Furthermore, it has been shown also that the description of the molecular charge distribution so obtained is consistent with many intramolecular phenomena [21,36] and several papers revisited the applications of these models from a computational perspective [21,22,26–29,36]. However, these studies focused mainly on the analysis of static equilibrium charges, neglecting charge fluxes (CF), even if it has been demonstrated that they can be important actors in the description of the charge distribution of a molecular system and related phenomena [31,35]. Only recently, a renewed attention has been directed towards the investigation of CF parameters [22,32–34,36,38,39].

The minor interest in charge fluxes is justified by the fact that, also in the case of planar molecules, the set of CF determined according to Eq. (3.5) is not unique. Even if it is possible

to define unambiguously the static charges, however for CF, the number of unknowns exceeds the number of independent equations, so that the ECCF set can be determined only if some unknowns are arbitrary neglected.

In the past the analysis of the results coming by the ECCF parameterization was often restricted to the set of atomic equilibrium charges $\{q_\alpha^0\}$ and to the so called “principal charge flux” $\partial q_\alpha / \partial r_{x\alpha}$, namely to the charge flux on the atom α , induced by the stretching of the bond (X- α) to which the atom α belong. Only very few papers suggested a physical meaning for non principal charge fluxes (i.e. stretching fluxes induced on atoms not directly involved in the bond which stretches - $\partial q_\alpha / \partial r'$ - or bending charge fluxes - $\partial q_\alpha / \partial \varphi$) [40–42].

In this context and starting from these last works, our work tried to overcome the different approximated approaches, to propose a new method to deal with charge fluxes parameters.

3.1 Deriving the charge fluxes from the second derivatives of the molecular dipole

As described in detail in our paper “*Charge mobility in molecules: Charge fluxes from second derivatives of the molecular dipole*” (D. Galimberti, A. Milani, and C. Castiglioni *J. Chem. Phys.* 138, 164115 (2013), that can be found after this discussion), to which we refer the reader for a complete discussion, it is possible to propose a model which allows to obtain the whole set of ECCF, from computed APT and their computed derivatives.

The model, which is based on the equations developed by Dinur[43,44], provides an analytical method for the determination of ECCF of planar molecules. The method requires to calculate second derivatives of the molecular dipole moment. The use of second derivatives allows to obtain all the charge fluxes without introducing any further approximation in addition to the hypothesis that the molecular dipole is described in terms of localized point atomic charges.

By this way it is no longer necessary to adopt approximations, usually consisting in neglecting charge fluxes relative to atoms distant from the one displaced (i.e. non-principal fluxes).

Based on density functional theory calculations, carried out for several small benchmark molecules, we implemented the new set of equations and we evaluated the complete set of charge fluxes for each molecule.

The data so obtained, demonstrate that non principal charge fluxes are not always negligible and their values are sometimes comparable to those of principal charge fluxes. Both principal and non-principal charge fluxes are found to play an important role for the interpretation of the spectral behaviour and both can be of fundamental importance to rationalize those phenomena which could affect the molecular structure and the intermolecular interactions with the environment (see for example the H-bond case, in Section 3.2).

This model, despite its potentiality, still shows some limitations. In the case of large molecules, the computational time required can restrict its applicability: indeed for a molecule of N atoms the method requires the analytical calculation of $6N$ APTs in order to obtain the second derivatives. Moreover, the model validity is limited to the case of planar systems only.

For the general case of non-planar molecules IR atomic charges calculation, local planes can be suitably selected for an approximate calculation of the atomic charges[22,36].

In this ground, in order to evaluate a generalization of the model to the prediction of the whole set of ECCF in complex and non-planar molecules, we investigated the degree of localization of charge fluxes, to verify the arbitrariness of the local approximation.

Our results show that neglecting the contribution from all the non-principal fluxes in the APT partitioning often gives a large overestimation of the principal charge flux value; on the other hand, it is interesting to notice that the trend obtained in local approximation is similar to the one shown by exact charge fluxes. This explains why the approximated models proposed in the past provided in many cases a good interpretation of the remarkable differences observed in IR intensities while considering different sets of molecules.

While often non-principal fluxes are far from being negligible, the physical intuition suggests that charge fluxes should be anyway characterized by some localization: to support this expectation we compare principal and non-principal stretching fluxes for polyenes of

increasing length. Both for butadiene and hexatriene, atoms four or more bonds away from the a H(1) under investigation, show negligible fluxes induced by CH stretching of the bond (1-2), thus confirming the quite local nature of fluxes even in the presence of an extended electrons conjugation (and thus of mobile electron charge). On this basis, it is reasonable to suppose that in molecules in which relevant charge delocalisation phenomena are absent, the local nature of the fluxes is even more marked. This partial localization pave the way to the possibility to extend the model for the calculation of approximated charge fluxes also in non planar systems.

Charge mobility in molecules: Charge fluxes from second derivatives of the molecular dipole

Daria Galimberti, Alberto Milani,^{a)} and Chiara Castiglioni

Dipartimento di Chimica, Materiali e Ingegneria Chimica 'Giulio Natta', Politecnico di Milano, Piazza Leonardo da Vinci 32, 20133 Milano, Italy

(Received 7 March 2013; accepted 3 April 2013; published online 25 April 2013)

On the basis of the analytical model previously suggested by Dinur, we discuss here a method for the calculation of vibrational charge fluxes in planar molecules, obtained as numerical second derivatives of the molecular dipole moment. This model is consistent with the partitioning of the atomic polar tensors into atomic charge and charge fluxes according to the Equilibrium Charges-Charge Fluxes model and it is directly related to experimentally measurable quantities such as IR intensities. On the basis of density functional theory calculations carried out for several small benchmark molecules, the complete set of charge fluxes is calculated for each molecule and compared with the approximated flux parameters previously derived and reported in the past literature. The degree of localization of charge fluxes is investigated and discussed; in addition, some approximations are analyzed in order to verify the applicability of the method to large and/or non-planar molecules, aimed at obtaining a description of the electron charge mobility in different molecular environments. © 2013 AIP Publishing LLC. [<http://dx.doi.org/10.1063/1.4802009>]

I. INTRODUCTION

The development of reliable methods for the description of the molecular charge distribution and its mobility in terms of “local parameters” (i.e., point atomic charges) is of considerable importance not only in theoretical and computational chemistry, but also in other fields such as molecular biology, molecular physics, and materials science.

Effects of polarization of the electronic cloud, charge transfer between chemical groups, localization of charge excess on specific molecular sites have indeed direct effects on intramolecular and intermolecular interactions determining chemical-physical properties of the molecule and also affecting their supra-molecular arrangement at the nanoscale. Furthermore, a correct determination of a set of atomic charges is one of the fundamental ingredients for the construction of force fields used in molecular mechanics and molecular dynamics,¹ due to their importance in affecting the final properties also on a much larger scale.

Considering in particular the determination of atomic charges, many methods have been developed and implemented since the birth of quantum chemistry (for a general discussion and comparison among them see Refs. 2 and 3) and they are widely used in all the fields of molecular sciences. In several pioneering works dealing with the parametrization and interpretation of IR intensities,^{4–8} some models have been proposed to extract, from the measured absolute absorption intensities, local charge parameters (Atomic Polar Tensor (APTs),⁵ Electro-Optical-Parameters (EOP),⁶ Equilibrium Charges-Charge Fluxes (ECCF)⁷). Moreover, from computed APTs, parameters have been derived according to

Charge-Charge Flux-Overlap (CCFO)⁸ and CCFOM^{9,10} models, Charge-Charge Flux-Dipole Flux (CCFDF) model^{11,12} and Generalized Atomic Polar tensor (GAPT) charges,¹³ and IR charges^{3,14–16} have been extracted, providing a straightforward description of the charge distribution in molecules which has also the advantage of being related to a measurable properties (IR intensities). Considering in particular ECCF model, both intramolecular and intermolecular effects, such as inductive effects, charge backdonation, hyperconjugation, occurrence of atoms able to form hydrogen bonds or responsible for strong electrostatic interaction, were rationalized in the past in terms of charge and charge flux parameters.^{17–23}

Due to their local character, APTs found a wide application in the past, not only for the parametrization of IR intensities and the determination of related charge parameters²⁴ but also for studies in a broader context. Indeed, they have been used in the theoretical investigation of intermolecular forces based on polarization and polarizability properties of molecules or in the investigation of nuclear electric shielding tensors.^{25–27}

Recently, due to the high accuracy of current state-of-the-art *ab initio*/density functional theory (DFT) calculations, which allow to easily compute APTs, several papers revisited the applications of the models mentioned above from a computational perspective, including both their application^{11,12,14–16} and implementation.³ However, till now these studies focused mainly on the analysis of equilibrium charges, even if also charge fluxes (CF) are important actors in the description of the charge distribution of a molecular system and related phenomena, as shown in the past literature.^{17,18} Only recently, a renewed attention has been directed toward the investigation of CF parameters^{14,15,23,28} and there is still room for wide computational and theoretical investigations.

^{a)} Author to whom correspondence should be addressed. Electronic mail: alberto.milani@polimi.it

In these grounds and following the previous model proposed by Dinur,²⁵ we present and discuss here a method to extract the complete set of charge fluxes for planar molecules through the evaluation of appropriate derivatives of APT (i.e., second derivatives of the dipole) obtained by means of DFT calculations. The model is then applied to different molecules, focusing also on the relative importance of principal and non-principal charge fluxes. From this analysis, it turns out that CF are not so localized, as assumed in the past and further new insights on their behavior are obtained. The results here presented pave the way for a further step, consisting in the generalization of the method also to the case of non-planar molecules.

II. ANALYTICAL MODEL

The absolute IR absorption intensity I_i of a band associated to the i th normal mode Q_i can be expressed as a function of the molecular dipole moment derivatives with respect to the Cartesian displacements of the atoms, calculated at the equilibrium geometry:⁴

$$I_i = C \left| \left(\frac{\partial \boldsymbol{\mu}}{\partial Q_i} \right)^0 \right|^2 = C \left| \sum_k \left(\frac{\partial \boldsymbol{\mu}}{\partial \xi_k} \right)^0 L_{ki} \right|^2. \quad (1)$$

In Eq. (1) \mathbf{L} is the transformation matrix from Cartesian to normal coordinates, C is a constant depending on the adopted units, and ξ_k is the k th component of the $\boldsymbol{\xi}$ vector which collects the $3N$ Cartesian coordinates of the N atoms belonging to the given molecules.

The $3N$ values $(\partial \boldsymbol{\mu} / \partial \xi_k)^0$ are usually collected in 3×3 matrices, called APTs, related to the Cartesian displacement of an individual atom β . The general element of the APT of the atom β is usually written as

$$P_{uv}^\beta = \left(\frac{\partial \mu_u}{\partial v_\beta} \right)^0, \quad (2)$$

where μ_u is the x , y , or z component of the molecular dipole moment, while v_β is a Cartesian displacement of β atom, namely $v_\beta = x_\beta, y_\beta, \text{ or } z_\beta$, upon which the derivative of the dipole moment is carried out. All the derivatives are evaluated at the equilibrium geometry ($\boldsymbol{\xi} = 0$) of the molecule.

The relationship between APTs and charges and charge fluxes, according to the ECCF model⁷ has been explored in the past^{9,10,14–18} and it is here only briefly summarized. The assumptions behind ECCF model is that the molecular dipole moment can be expressed as a sum of atomic contributions, in particular of localized atomic charges.

$$\boldsymbol{\mu} = \sum_\alpha q_\alpha \cdot \mathbf{r}_\alpha, \quad (3)$$

where \mathbf{r}_α is the position vector of the α atom.

Substituting Eq. (3) in Eq. (2) we get

$$\mathbf{P}^\beta = q_\beta^0 \mathbf{I} + \bar{\mathbf{x}}^0 \left(\frac{\partial q}{\partial \boldsymbol{\xi}} \right)_\beta^0, \quad (4)$$

where \mathbf{I} is the 3×3 identity matrix, $\bar{\mathbf{x}}^0$ is the $3 \times N$ matrix that collects, along its columns, the equilibrium Cartesian coordinates of each atom, while $(\partial q / \partial \boldsymbol{\xi})^0$ is the $N \times 3N$ matrix of

the Cartesian charge fluxes, restricted in Eq. (4) to the derivatives relative to Cartesian displacements of the β atom ($N \times 3$ matrix). Then the general element P_{uv}^β of the APT tensor is a function both of the equilibrium atomic charge q_β^0 (EC) and of CF and a set of ECCF can be obtained solving the system of equations described by Eq. (4), considering the whole set of $9 \times N$ components of the APT of the N atoms in the molecule. Unfortunately, in general, the number of unknowns exceeds the number of independent equations in the system, so that the ECCF set can be determined from Eq. (4) only if some unknowns are set equal to 0, or some further relationships among different ECCF are introduced. In particular, “local approximations” are often adopted, where some fluxes relative to atoms distant from the one displaced (i.e., non-principal fluxes) are considered negligible.

For this reason the set of ECCF determined according to the relationships set by Eq. (4) is not unique. However, in the case of a planar molecule it is always possible to obtain from APTs a unique set of equilibrium atomic charges. Indeed, by choosing the suitable reference system with an axis (z) orthogonal to the plane of the molecule, it is possible to extract the equilibrium atomic charge directly from the zz diagonal elements of its APT according to the relationship:

$$P_{zz}^\alpha = \left(\frac{\partial \mu_z}{\partial z_\alpha} \right)^0 = q_\alpha^0. \quad (5)$$

In Eq. (5), the derivative is evaluated at the equilibrium geometry but the relationship can be extended to any arrangement of the nuclei, also outside their equilibrium positions. Accordingly, P_{zz}^α can be regarded as a function of the whole set of Cartesian atomic displacements and it can be further derived. In particular, according to Dinur,²⁵ deriving with respect to a given Cartesian coordinate ξ_k , we obtain

$$\left(\frac{\partial q_\alpha}{\partial \xi_k} \right)^0 = \left(\frac{\partial^2 \mu_z}{\partial z_\alpha \partial \xi_k} \right)^0 = \left(\frac{\partial P_{zz}^\alpha}{\partial \xi_k} \right)^0. \quad (6)$$

Equation (6), applied to the N P_{zz}^α component (considering all the derivatives with respect to each displacement ξ_k), allows to obtain the whole set of $(\partial q / \partial \boldsymbol{\xi})^0$. In the following we adopt a shortened notation by omitting the apex “0” for quantities which are evaluated at equilibrium geometry.

By standard transformations between Cartesian coordinates and internal coordinates, it is also possible to calculate:

$$\frac{\partial q}{\partial \mathbf{R}} = \frac{\partial q}{\partial \boldsymbol{\xi}} \cdot \mathbf{A} \quad (7)$$

and vice versa:

$$\frac{\partial q}{\partial \boldsymbol{\xi}} = \frac{\partial q}{\partial \mathbf{R}} \cdot \mathbf{B}, \quad (8)$$

where the \mathbf{B} matrix defines the linear transformation from Cartesian displacements to internal $\mathbf{R} = \mathbf{B}\boldsymbol{\xi}$ coordinates according to the Wilson, Decius, and Cross definitions²⁹ and \mathbf{A} is the generalized inverse of the \mathbf{B} matrix.

Therefore, from the second derivatives of the molecular dipole moment (first derivatives of atomic polar tensor), it is possible to obtain the *internal* charge fluxes $\partial q / \partial \mathbf{R}$, namely, the flux parameters defined in the ECCF model. Compared to

parametrization techniques simply based on the expressions of the first derivatives of the dipole moment (Eq. (4)) widely used in the past, the calculation of the second derivatives allows to obtain the *whole set* of charge fluxes, without introducing any further approximations in addition to the hypothesis of Eq. (3).

In this regard and in order to better appreciate the potentiality of the method here proposed, it is worthwhile to recall that the impossibility to determine a unique and reliable set of charge fluxes through Eq. (4) strongly damped in the past the efforts to deeply analyze and correlate these parameters. The same reasons made uncertain the use of CF for the study and rationalization of molecular properties. Often the analysis of the results coming by the ECCF parametrization was restricted to the set of atomic equilibrium charges $\{q^\circ_\alpha\}$ and to the so called “principal charge flux” $\partial q_\alpha/\partial r_{X\alpha}$, namely, to the charge flux on the atom α , induced by the stretching of the bond ($X-\alpha$) to which the atom α belongs. Only very few papers guessed a physical meaning of non-principal charge fluxes (i.e., stretching fluxes induced on atoms not directly involved in the bond which stretches, namely, $\partial q_\alpha/\partial r'$ or bending charge fluxes, $\partial q_\alpha/\partial \varphi$).^{20,21}

On the other hand, it is pleasant to notice that the model described by Eq. (6) can provide principal charge fluxes in a very straightforward way. Indeed, in order to predict the principal stretching fluxes generated on a terminal atom (e.g., H atoms of a CH bond), it is not necessary to compute the whole set of second derivatives of the dipole moment: in fact, if a reference system is chosen such that the x-axis is parallel to the CH bond, we obtain

$$\frac{\partial P_{zz}^H}{\partial x_H} = \frac{\partial q_H}{\partial x_H} = \sum_k \frac{\partial q_H}{\partial R_k} \frac{\partial R_k}{\partial x_H} = \frac{\partial q_H}{\partial r_{CH}} \frac{\partial r_{CH}}{\partial x_H} = \frac{\partial q_H}{\partial r_{CH}}. \quad (9)$$

This equation holds since $\partial R_k/\partial x_H \neq 0$ only if $R_k = r_{CH}$.

In other words, the principal stretching fluxes affecting a terminal atom can be obtained simply displacing the terminal atom along the bond, thus reducing the number of derivatives to be calculated analytically from 6N to 2 (see Sec. III).

III. COMPUTATIONAL DETAILS

In a previous paper,¹⁴ we investigated the reliability of different combinations of DFT functional/basis set for the best prediction of IR intensities and hence of APT components. As a result, we found that PBE0 functional³⁰ in conjunction with aug-cc-pVTZ basis set was the best combination (among those investigated); on this basis we adopt this combination also in this work for the calculation of the APT components to be used in the model described in Sec. II.

For all the molecules presented here, we carried out geometry optimization and IR intensity calculations by means of the GAUSSIAN 09 code.³¹ Based on the APTs so obtained (first derivatives of the dipole moment), second derivatives of the dipole moments have been calculated numerically to obtain the terms reported in Eq. (6).

The calculation of the second derivatives, has been carried out for each $\partial P_{zz}^\alpha/\partial \xi_k$ according to the following procedure:

- (1) Two new input geometries have been generated displacing ξ_k of $+0.001 \text{ \AA}$ and -0.001 \AA from the equilibrium geometry.
- (2) An IR intensity calculation is carried out for these new inputs to obtain the APTs in the displaced geometries. On this basis we calculated numerically the first derivatives of P_{zz} , e.g., the second derivatives of the z component of the dipole moment according to the following formula:

$$\left(\frac{\partial P_{zz}}{\partial \xi_k}\right)^0 = \frac{P_{zz}(\xi_k^0 + \Delta h) - P_{zz}(\xi_k^0 - \Delta h)}{2 \cdot \Delta h}.$$

IV. RESULTS AND DISCUSSION

A. Charge and charge fluxes

It has been demonstrated both in the past¹⁰ and also in recent works^{3,14} that the IR charges defined according the ECCF model are in good agreement with the ones computed according to other common schemes, such as electrostatic (MK (Merz-Kollman),³² CHELP,³³ or CHELPG³⁴) or Hirshfeld³⁵ charges. Furthermore, it has been shown also that the picture of the molecular charge distribution so obtained is consistent with many intramolecular phenomena.^{3,14} In addition, it is important to stress that for planar molecules the definition of charge given in Eq. (5) is independent from the introduction of multipoles of higher order or from a particular partitioning of the molecules in terms of “sites” carrying point charges.^{25,26}

We discuss here the soundness of the definition of charge fluxes as first derivatives of APTs (Eqs. (6) and (7)), checking the compatibility of the set of charge fluxes obtained according to the method presented in Sec. II with some simple physical requirements.

First, we tested the charge neutrality condition for neutral molecules. This requirement implies:

$$\sum_\alpha \frac{\partial q_\alpha}{\partial \xi_k} = 0, \quad \forall k \quad (10)$$

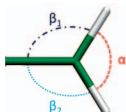
or equivalently:

$$\sum_\alpha \frac{\partial q_\alpha}{\partial R_k} = 0, \quad \forall k. \quad (11)$$

We checked both conditions for a wide set of molecules and we found that the molecular neutrality is always well reproduced (errors are always lower than 0.002 e) (see data reported in the supplementary material³⁶). For example, for ethylene we found a maximum deviation from neutrality of 0.001 e (Table I), while for formaldehyde the conditions (Eqs. (10) and (11)) are satisfied beyond the fourth decimal place. Accordingly, errors related to deviation from neutrality are of the same order of magnitude of the numerical errors in our calculation of second derivatives of the dipole.

As a second check we verified that the charges and charge fluxes obtained are actually able to describe the molecular dipole moment and its derivatives. In particular, for a wide set of molecules, we tested if the APTs “reconstructed” according to Eq. (4), using charges and charge fluxes computed

TABLE I. Stretching $\partial q_\alpha/\partial r$ and bending ($\partial q_\alpha/\partial \bar{\alpha}$ and $\partial q_\alpha/\partial \bar{\beta}$) charge fluxes obtained through Eqs. (6) and (7) for C_2H_4 , CH_2O , C_2H_2 , HCN. For comparison, we also report the values (*past*) predicted in the past from APTs parametrization, by models neglecting some non-principal fluxes (see text).²⁰



$$\bar{\alpha} = \frac{1}{\sqrt{6}}(2\alpha - \beta_1 - \beta_2)$$

$$\bar{\beta} = \frac{1}{\sqrt{2}}(\beta_1 - \beta_2)$$

C₂H₄			r_{CH}	$\bar{\beta}$	$\bar{\beta}$	$\bar{\alpha}$	$\bar{\alpha}$	
	r_{CC}	$r_{\text{CH}(13)}$	<i>past</i>		<i>past</i>		<i>past</i>	
C(1)	-0.0615	0.0355	0.233	0.0000		-0.0316		
C(2)	-0.0615	0.0188	0.000	0.0000		-0.0261		
H(3)	0.0310	-0.1016	-0.220	0.0433	0.050	0.0284	0.052	
H(4)	0.0310	0.0132	-0.013	-0.0433	-0.050	0.0284	0.052	
H(5)	0.0310	0.0619	0.000	-0.0167	0.000	0.0003	0.000	
H(6)	0.0310	-0.0276	0.000	0.0167	0.000	0.0003	0.000	
$\sum_{\alpha} \partial q_{\alpha}/\partial R_i$	0.0010	0.0003		0.0000		-0.0004		
CH₂O			r_{CO}	r_{CH}	$\bar{\beta}$	$\bar{\alpha}$	$\bar{\alpha}$	
	r_{CO}	<i>past</i>	$r_{\text{CH}(23)}$	<i>past</i>	$\bar{\beta}$	<i>past</i>	<i>past</i>	
O(1)	-0.3015	-0.387	0.1398	0.000	0.0000	0.000	-0.0070	0.000
C(2)	-0.1880	0.387	-0.0831	0.357	0.0000	0.100	-0.0479	-0.098
H(3)	0.2447	0.000	-0.1751	-0.316	0.0561	0.050	0.0274	0.049
H(4)	0.2447	0.000	0.1185	-0.041	-0.0561	-0.050	0.0274	0.049
$\sum_{\alpha} \partial q_{\alpha}/\partial R_i$	0.0000		0.0000		0.0000		0.0000	
HCN		r_{CN}	r_{CH}	r_{CH}	r_{CH}			
	r_{CN}	<i>past</i>		<i>past</i>				
C(1)	-0.5562		-0.0905					
N(2)	0.4163	0.419	0.0455					
H(3)	0.1402		0.0455	-0.010				
$\sum_{\alpha} \partial q_{\alpha}/\partial R_i$	0.0003		0.0005					
HCCH		r_{CC}	$r_{\text{CH}(13)}$					
C(1)		-0.0560	-0.0230					
C(2)		-0.0560	-0.0200					
H(3)		0.0560	0.0200					
H(4)		0.0560	0.0230					
$\sum_{\alpha} \partial q_{\alpha}/\partial R_i$		0.0000	0.0000					

from Eqs. (5) and (7), namely:

$$\mathbf{P}^{\beta} = q_{\beta}^0 \mathbf{I} + \bar{\mathbf{x}}^0 \left(\frac{\partial q}{\partial \mathbf{R}} \right) \mathbf{B}^{\beta} \quad (12)$$

coincide with those provided directly by DFT calculations (APTs are indeed analytically computed in a standard IR spectrum calculation). In the worst cases the numerical differences found affect the third decimal place (see data reported in the supplementary material³⁶ for some cases). However, in many cases, there are no differences until the fourth decimal place. On the other hand, the IR intensities calculated using APTs reconstructed according to Eq. (12), show always differences lower than 1 km/mol from those directly predicted by DFT calculations: for example, for formaldehyde a maximum deviation from the predicted value of 0.63% is found (see Table II).

Charges and charge fluxes calculated according to the model presented here are hence able to correctly reproduce experimentally measurable quantities such as the intensity IR.

Equations (5) and (6) are, therefore, a powerful tool for the study of the distribution of molecular charge and its mobility in the case of planar molecules.

B. Localization of charge fluxes

The model described and adopted above allows to derive, in the case of planar molecules, the whole set of charges

TABLE II. IR intensity of formaldehyde predicted from DFT calculations and from the APTs reconstructed by means of Eq. (12).

Frequencies (cm ⁻¹)	IR Intensities from GAUSSIAN 09 (km/mol)	Reconstructed IR intensities (km/mol)	% error (absolute value)
1202	6.14	6.14	0
1263	11.56	11.55	0.09
1528	11.08	11.01	0.63
1846	114.33	114.39	0.05
2903	70.78	70.85	0.10
2962	111.64	111.51	0.12

and charge fluxes, from the second derivatives of the dipole moment. However, in the case of large molecules, the computational time requested can restrict its applicability: indeed for a molecule of N atoms the method requires the analytical calculation of $6N$ APTs in order to obtain the second derivatives. Furthermore, many molecules of interest are partially or totally non-planar. In the latter case Eq. (5) contains additional charge flux terms and Eq. (6) does not hold any more. To handle such cases we are thus forced to introduce some approximations, e.g., we have to neglect some flux contributions, assuming that their values are small.

In the case of IR atomic charges calculation, local planes can be suitably selected³⁷ allowing to use Eq. (5) for an approximate estimate of the charge.^{3,14,15} The same technique can be used also for the definition of approximated charge fluxes from second derivatives of dipole according to Eq. (6), provided that the z axis is oriented normal to the local plane.

In order to verify the degree of arbitrariness of these approximations, we will analyze the behavior of the whole set of the *exact* charge fluxes, computed for several small planar molecules according to Eqs. (6) and (7). In particular, we will focus on the relative importance of the non-principal fluxes with respect to the principal ones. In Table I we reported the values for the fluxes obtained for some significant cases and we compared them with those reported in the literature as obtained by models that neglected some non-principal fluxes.

The results obtained suggest that the non-principal fluxes are not always negligible, even if they involve atoms relatively distant from the ones which are displaced. A remarkable example is given by the flux parameters related to C=O stretching of formaldehyde: if we assume $\partial q_H/\partial r_{CO} = 0$, we found, due to charge neutrality, a large charge flux on C, namely, $\frac{\partial q_C}{\partial r_{CO}} = 0.387 e/A$. Instead, if we use Eqs. (6) and (7) in order to obtain the whole set of fluxes, we found that fluxes on the two hydrogen atoms are far from being negligible ($\partial q_H/\partial r_{CO} = 0.245 e/A$) and this leads to a smaller and negative flux on C. Likewise, in the case of the CH stretching, if we assume, as it was done in the past, a flux equal to zero on the oxygen atom, we get a quite strong flux on the C atom ($\partial q_C/\partial r_{CH} = 0.357 e/A$). Instead, fluxes obtained through second dipole derivatives indicate that carbon is affected by a relatively weak flux ($\partial q_C/\partial r_{CH} = -0.083 e/A$), while a stronger one takes place on oxygen ($\partial q_O/\partial r_{CH} = -0.140 e/A$). Also the non-principal flux on the adjacent H atom (H(4) in Fig. 1) is stronger ($\partial q_H/\partial r'_{CH} = 0.119 e/A$) than that on carbon. So the C atom seems to act as a bridge

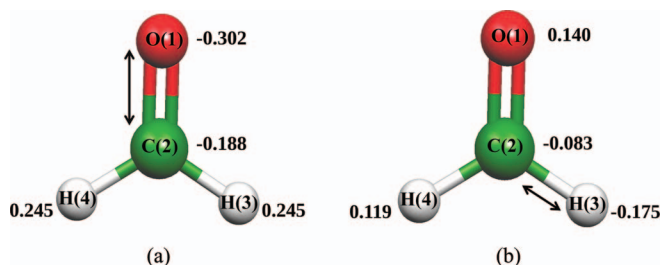


FIG. 1. Principal and non-principal charge fluxes calculated with Eqs. (6) and (7) for CH_2O : (a) CO and (b) CH (2–3) stretching fluxes.

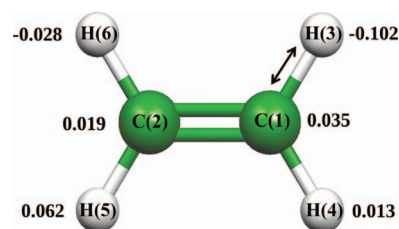


FIG. 2. CH (1–3) stretching fluxes for the ethylene.

across which the charge from “non-bonded” atoms flows toward the displaced atom (H(3)) (Figure 1).

If we now consider the case of ethylene, looking in particular to the fluxes due to the CH stretching (stretching of the CH(1–3) bond in Figure 2) we can see that, according to our model, both *cis* and *trans* H atoms on the opposite side of the molecule are affected by charge rearrangement during this displacement. On the opposite, the “old” approximation postulated a null flux for this two H atom and overestimated by an order of magnitude the CH stretching flux of the C(1) atom.

According to fluxes parameters calculated from second derivatives, we can conclude that also in ethylene the two carbon atoms act as a bridge across which charge flows from one moiety to the other of the molecule.

Also ethylene derivatives with one or more H atoms substituted with F, Cl, or Br, show the same behavior (see data reported in the supplementary material³⁶).

We now focus on principal CH stretching fluxes comparing the values obtained for several planar molecules (C_2H_4 and its halogenated derivatives, some polyenes, C_2H_2 , C_4H_2 , HCN, CH_2O , and its halogenated derivatives, HCOOH and its halogenated derivatives).

In Figure 3 the fluxes calculated using Eq. (9) are compared to those obtained from Eq. (4) totally neglecting non-principal fluxes, according to a procedure often adopted in the past, and referred as “0 order approximation.” (In the 0 order approximation the principal charge flux can be straightforwardly derived according to the relationship:

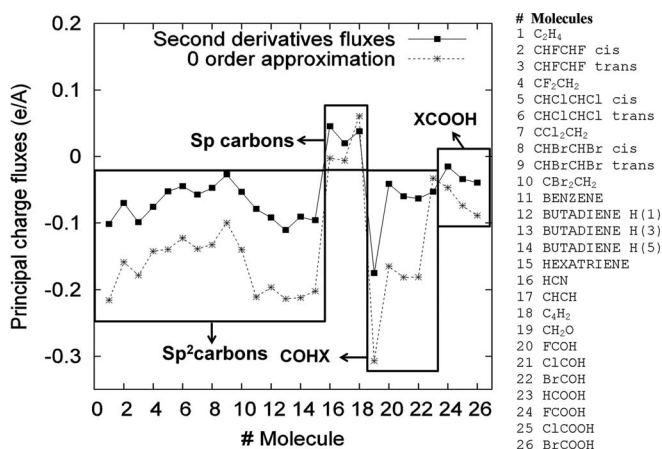


FIG. 3. CH stretching principal fluxes on H belonging to many different molecules. Comparison between fluxes obtained from the second derivatives of the molecular dipole (Eq. (9)) and those calculated from APTs completely neglecting the non-principal charge fluxes (0 order approximation, see text).

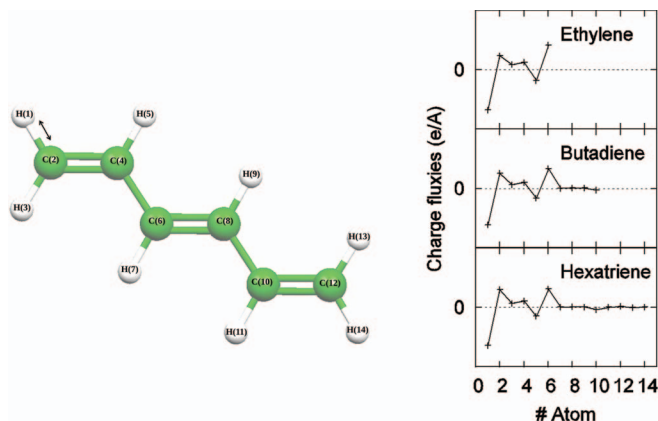


FIG. 4. CH (1–2) stretching fluxes for ethylene, butadiene, and hexatriene. Atoms are numbered by increasing distance (number of bonds in between) from H(1).

$\partial q_H / \partial r_{CH} = \mathbf{1} / r_{CH} \cdot (P_{xx}^H - P_{zz}^H)$ which holds when the x axis is directed along the bond and z axis is orthogonal to the molecular plane.)

The results obtained show again that neglecting the contribution from all the non-principal fluxes in the APT partitioning often gives a large overestimation of the $\partial q_H / \partial r_{CH}$ value; on the other hand, it is interesting to notice that trends obtained considering the 0-order approximated $\partial q_H / \partial r_{CH}$ parallel those shown by fluxes obtained from Eq. (9). This explains why the approximated models proposed in the past provided in many cases a good interpretation of the remarkable differences observed in IR intensities while considering series of different molecules.

While often non-principal fluxes are far from being negligible, the physical intuition suggests that charge fluxes should be anyway characterized by some localization: to support this expectation we compare principal and non-principal stretching fluxes for polyenes of increasing length (Figure 4).

Both for butadiene and hexatriene, atoms four or more bonds away from H(1), show negligible fluxes induced by CH stretching of the bond (1–2), thus confirming the quite local nature of fluxes even in the presence of an extended π electrons conjugation (and thus of mobile electron charge). On this basis, it is reasonable to suppose that in molecules in which relevant charge delocalization phenomena are absent, the local nature of the fluxes is even more marked.

C. Local approximations

Since we have verified that charge fluxes show some localization, we tried to assess the threshold distance from an atom β such that non-principal fluxes $\partial q^\alpha / \partial R_t$ due to its displacements does not contribute significantly to \mathbf{P}^β and can be thus neglected. In particular we have tested different approximations to evaluate their ability to correctly reproduce the APTs and IR intensities. Two strategies have been adopted:

A. By means of Eqs. (6) and (7) we determined the matrix $\partial q / \partial \mathbf{R}$. For each atom β of the molecule whose APT has to be predicted, we built a new charge fluxes matrix $[\partial q / \partial \mathbf{R}]_{app,\beta}$ such that its elements $(\partial q^\alpha / \partial R_t)_{app,\beta}$ are defined according to the following equations:

$$(\partial q^\alpha / \partial R_t)_{app,\beta} = (\partial q^\alpha / \partial R_t) \text{ if the distance between } \beta \text{ and } \alpha \text{ atoms is less than or equal to } n \text{ bonds}$$

$$(\partial q^\alpha / \partial R_t)_{app,\beta} = 0 \text{ if the distance between } \beta \text{ and } \alpha \text{ atoms is more than } n \text{ bonds}$$

From Eq. (12) we obtain

$$\mathbf{P}_{app}^\beta = q_\beta^0 \mathbf{I} + \tilde{\mathbf{x}}_0 \cdot \left[\frac{\partial q}{\partial \mathbf{R}} \right]_{app,\beta} \cdot \mathbf{B}^\beta. \quad (13)$$

B. For each atom β , we determine the matrix $[\partial q / \partial \mathbf{R}]_{app,\beta}$ through Eq. (7), starting from an approximated Cartesian charge fluxes matrix $[dq/d\xi]_{app,\beta}$ defined in the following way:

$$(\partial q^\alpha / \partial \xi_k)_{app,\beta} = (\partial q^\alpha / \partial \xi_k) \text{ if } \xi_k \text{ is a Cartesian displacement relative to a } \gamma \text{ atom such that the distance between } \gamma \text{ and } \beta \text{ atoms is less than or equal to } n \text{ bonds}$$

$$(\partial q^\alpha / \partial \xi_k)_{app,\beta} = 0 \text{ if } \xi_k \text{ is a Cartesian displacement relative to a } \gamma \text{ atom such that the distance between } \gamma \text{ and } \beta \text{ atom is more than } n \text{ bonds.}$$

This second procedure may be of practical interest for the determination of approximated $\partial q^\alpha / \partial R_t$ of large molecules for which only charge fluxes relative to specific chemical groups are of interest.

Also in this case each \mathbf{P}_{app}^β is reconstructed according to Eq. (13).

In both cases, we estimated the approximated IR intensity from the obtained \mathbf{P}_{app}^β using Eq. (1).

Our calculations indicate that the two ways give substantially equivalent results if we take the same threshold value n (e.g., if we assume the same “electro-optical” interaction distance). For this reason we will refer in the following to the only results achieved following strategy B.

The values obtained show that neglecting all fluxes involving atoms four or more bonds away from the given atom does not introduce significant errors in the prediction of APTs and IR intensity, even in cases where there is a strong

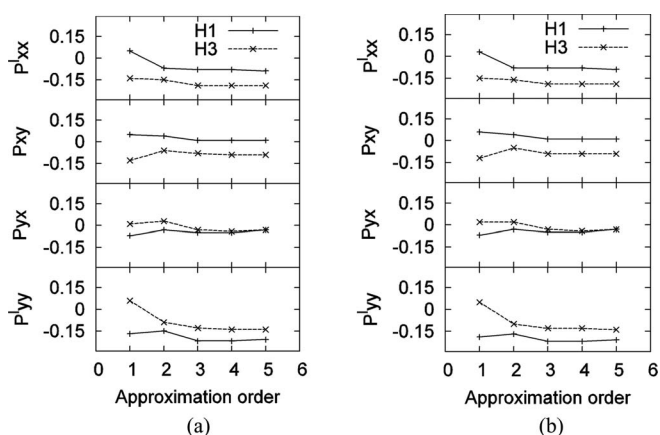


FIG. 5. APTs elements for H(1) and H(3) of butadiene, reconstructed using Eq. (12), with decreasing degree of approximation: namely, method A (panel (a)) and method B (panel (b)) with $n = 1, 2, 3$, or 4 bonds from the β atom. The last value reported in the plot corresponds to the true value of the APT element directly obtained by DFT calculations. The charge contribution has been subtracted in the diagonal values reported ($P'_{ii} = P_{ii} - q^0$).

TABLE III. Comparison between IR intensities of butadiene directly obtained by DFT calculations and those obtained by the approximated APT (method B) with $n = 1, 2, 3,$ or 4 bonds from the β atom. The IR active modes absent in the list, show negligible intensity in any approximations. Values relative to out of plane modes are written in boldface. The vertical lines allows to identify the approximation step where the difference between the *true* (from GAUSSIAN 09 output) and the approximated IR intensity become less than 1 km/mol (for modes with low intensity) and 5 km/mol (for mode with high intensity).

Modes	Frequency (cm^{-1})	1 order approximation	2 order approximation	3 order approximation	4 order approximation	DFT computed
7	174	1	1	1	1	1
8	292	1	2	4	4	3
10	540	13	13	13	13	13
14	947	85	85	85	85	85
15	995	30	3	0	1	2
17	1058	35	35	35	35	35
20	1313	8	7	2	2	2
21	1412	100	7	7	8	6
23	1665	59	16	26	25	23
26	3150	15	3	11	14	15
28	3158	17	5	9	8	8
30	3243	2	0	18	19	17

conjugation, e.g., butadiene (Figure 5). However, more local approximations may generate errors which exceed the 100%. For example, considering the stretching of a vinyl CH bond of butadiene, the whole $\text{CH}_2\text{-CH-}$ fragment is affected by relevant charge fluxes. The comparison between the IR intensities predicted by DFT calculations with those obtained by the approximated polar tensors P_{app}^β (Table III), shows that, as expected, errors affect only the IR transitions associated to modes of vibration occurring in the molecular plane; for symmetry reasons out of plane displacements do not involve charge fluxes, consistently with the definition of charge as the first derivative of the dipole moment in the out-of-plane direction (see Eq. (5)). On the contrary, in-plane modes can be affected by large charge fluxes, because of the presence of conjugated double bonds, carrying highly polarizable charge density.

V. CONCLUSIONS

The characterization of the molecular charge distribution in terms of static and dynamical parameters, such as atomic charges and charge fluxes, provides a nice tool for analyzing both qualitatively and quantitatively peculiar intramolecular and intermolecular phenomena ruling the chemical-physical properties of different molecular systems. In this paper, we developed and applied an analytical model to calculate the charge flux parameters in planar molecules, complementing other models previously proposed and focused only on atomic charges. The results proved to be interesting and reliable thus paving the way for further possible investigations: from one side, there is room for the generalization of the model to complex and non-planar molecules, including the development of computational tools for an automatic procedure for the determination of charge fluxes. On the other side, the possibility to calculate both principal and non-principal fluxes has an important application for the detailed investigation of intramolecular and intermolecular interaction, possibly focusing in particular on specific interactions such as hydrogen

bonding. On this subject some papers are recently appeared in the literature^{15,23,28} where charge flux parameters are analyzed to obtain insight on this intriguing phenomenon. In addition, the close relationship between charges, charge fluxes, and IR intensities further enhances their importance and their field of applicability, which extends not only to computational chemistry but also to computational/experimental vibrational spectroscopy and to the spectroscopic characterization of complex molecular materials or systems.

¹M. P. Allen and T. J. Tildesley, *Computer Simulation of Liquids* (Clarendon Press, Oxford, 1987).

²C. F. Guerra, J. W. Handgraaf, E. J. Baerends, and F. M. Bickelhaupt, *J. Comput. Chem.* **25**, 189 (2004); F. De Proft, J. M. L. Martin, and P. Geerling, *Chem. Phys. Lett.* **250**, 393 (1996); F. Martin and H. Zipse, *J. Comput. Chem.* **26**, 97 (2005); H. Hu and W. Yang, *J. Chem. Theory Comput.* **3**, 1004 (2007); F. De Proft, C. Van Alsenoy, A. Peeters, W. Langenaeker, and P. Geerlings, *J. Comput. Chem.* **23**, 1198 (2002); E. Sigfridsson and U. Ryde, *ibid.* **19**, 377 (1998); F. De Proft, P. Geerlings, and J. M. L. Martin, in *Recent Developments and Applications of Modern Density Functional Theory*, edited by J. M. Seminario (Elsevier Science B.V., Amsterdam, 1996).

³A. Milani, M. Tommasini, and C. Castiglioni, *Theor. Chem. Acc.* **131**, 1139 (2012).

⁴L. M. Sverdlov, M. A. Kovner, and E. P. Krainov, *Vibrational Intensities of Polyatomic Molecules* (Wiley, New York, 1972); J. Overend, "Quantitative intensity studies and dipole moment derivatives," in *Infrared Spectroscopy and Molecular Structure*, edited by M. Davies (Elsevier, Amsterdam, 1963), p. 345; W. B. Person, in *Vibrational Intensities in Infrared and Raman Spectroscopy*, edited by G. Zerbi (Elsevier Scientific Publishing Company, Amsterdam, 1982).

⁵J. F. Biarge, J. Herranz, and J. Morcillo, *Ann. R. Soc. Espan. Fis. Quim. (Madrid)* **A57**, 81 (1961); W. B. Person and J. B. Newton, *J. Chem. Phys.* **61**, 1040 (1974).

⁶L. A. Gribov, *Intensity Theory for Infrared Spectra of Polyatomic Molecules* (Consultant's Bureau, New York, 1964); M. Gussoni and S. Abbate, *J. Chem. Phys.* **65**, 3439 (1976); M. Gussoni, *Prik. Spectroscop.* **XLII**, 265 (1985).

⁷J. C. Decius, *J. Mol. Spectrosc.* **57**, 348 (1975); A. J. van Straten and W. M. A. Smit, *ibid.* **62**, 297 (1976).

⁸W. T. King and G. B. Mast, *J. Phys. Chem.* **80**, 2521 (1976); W. T. King, G. B. Mast, and P. P. Blanchette, *J. Chem. Phys.* **56**, 4440 (1972).

⁹M. Gussoni, M. N. Ramos, C. Castiglioni, and G. Zerbi, *Chem. Phys. Lett.* **142**, 515 (1987); M. Gussoni, C. Castiglioni, M. N. Ramos, M. Rui, and G. Zerbi, *J. Mol. Struct.* **224**, 445 (1990).

- ¹⁰M. N. Ramos, M. Gussoni, C. Castiglioni, and G. Zerbi, *Chem. Phys. Lett.* **151**, 397 (1988).
- ¹¹R. L. A. Haiduke and R. E. Bruns, *J. Phys. Chem. A* **109**, 2680 (2005).
- ¹²J. V. Da Silva, R. L. A. Haiduke, and R. E. Bruns, *J. Phys. Chem. A* **110**, 4839 (2006); J. V. Da Silva, S. H. D. M. Faria, R. L. A. Haiduke, and R. E. Bruns, *ibid.* **111**, 515 (2007); S. H. D. M. Faria, J. V. Da Silva, R. L. A. Haiduke, L. N. Vidal, P. A. M. Vazquez, and R. E. Bruns, *ibid.* **111**, 7870 (2007).
- ¹³J. Cioslowski, *J. Am. Chem. Soc.* **111**, 8333 (1989).
- ¹⁴A. Milani and C. Castiglioni, *J. Phys. Chem. A* **114**, 624 (2010).
- ¹⁵A. Milani, D. Galimberti, C. Castiglioni, and G. Zerbi, *J. Mol. Struct.* **976**, 342 (2010).
- ¹⁶A. Milani and C. Castiglioni, *J. Mol. Struct.: THEOCHEM* **955**, 158 (2010).
- ¹⁷M. Gussoni, C. Castiglioni, and G. Zerbi, *J. Phys. Chem.* **88**, 600 (1984).
- ¹⁸M. Gussoni, C. Castiglioni, and G. Zerbi, *Handbook of Vibrational Spectroscopy*, edited by J. Chalmers and P. Griffiths (John Wiley & Sons, Chichester, UK, 2001), Vol. 3, p. 2040.
- ¹⁹N. B. Da Costa, A. J. A. Aquino, M. N. Ramos, C. Castiglioni, and G. Zerbi, *J. Mol. Struct.: THEOCHEM* **305**, 19 (1994); C. Castiglioni, M. Gussoni, and G. Zerbi, *J. Mol. Struct.* **198**, 475 (1989); **141**, 341 (1986); P. Jona, M. Gussoni, and G. Zerbi, *J. Phys. Chem.* **85**, 2210 (1981).
- ²⁰C. Castiglioni, M. Gussoni, and G. Zerbi, *J. Chem. Phys.* **82**, 3534 (1985).
- ²¹M. Gussoni, C. Castiglioni, M. Miragoli, G. Lugli, and G. Zerbi, *Spectrochim. Acta, Part A* **41**, 371 (1985); C. Castiglioni, M. Gussoni, and G. Zerbi, *Solid State Commun.* **56**, 863 (1985).
- ²²M. Gussoni, C. Castiglioni, and G. Zerbi, *J. Chem. Phys.* **80**, 1377 (1984); *Chem. Phys. Lett.* **99**, 101 (1983); C. Castiglioni, M. Gussoni, and G. Zerbi, *J. Chem. Phys.* **80**, 3916 (1984).
- ²³R. C. M. U. Araujo, J. B. P. Da Silva, and M. N. Ramos, *Spectrochim. Acta, Part A* **51**, 821 (1995); V. H. Rusu, J. B. P. Da Silva, and M. N. Ramos, *Vib. Spectrosc.* **46**, 52 (2008); K. C. Lopes, F. S. Pereira, R. C. M. U. De Araújo, and M. N. Ramos, *J. Mol. Struct.* **565–566**, 417 (2001); M. N. Ramos, K. C. Lopes, W. L. V. Silva, A. M. Tavares, F. A. Castriani, S. A. Do Monte, E. Ventura, and R. C. M. U. Araujo, *Spectrochim. Acta, Part A* **63**, 383 (2006).
- ²⁴W. B. Person and G. Zerbi, *Vibrational Intensities in Infrared and Raman Spectroscopy* (Elsevier Scientific Pub. Co., Amsterdam, 1982).
- ²⁵U. Dinur, *J. Phys. Chem.* **95**, 6201 (1991); *Chem. Phys. Lett.* **166**, 211 (1990).
- ²⁶U. Dinur and A. T. Hagler, *J. Chem. Phys.* **91**, 2949 (1989).
- ²⁷Y. Q. Liang and K. L. C. Hunt, *J. Chem. Phys.* **98**, 4626 (1993); K. L. C. Hunt and Y. Q. Liang, *ibid.* **95**, 2549 (1991); K. L. C. Hunt, *ibid.* **90**, 4909 (1989); P. Lazzaretti and R. Zanasi, *ibid.* **83**, 1218 (1985); P. Lazzaretti and R. Zanasi, *Chem. Phys. Lett.* **112**, 103 (1984); P. W. Fowler and A. D. Buckingham, *Chem. Phys.* **98**, 167 (1985); P. Lazzaretti, M. C. Caputo, and M. B. Ferraro, *ibid.* **246**, 75 (1999).
- ²⁸H. Torii, *J. Phys. Chem. B* **114**, 13403 (2010); *J. Chem. Phys.* **133**, 034504 (2010); *J. Phys. Chem. Lett.* **3**, 112 (2012).
- ²⁹E. B. Wilson, J. C. Decius, and P. C. Cross, *Molecular Vibrations* (McGraw Hill, New York, 1955).
- ³⁰C. Adamo and V. Barone, *J. Chem. Phys.* **110**, 6158 (1999).
- ³¹M. J. Frisch, G. W. Trucks, H. B. Schlegel *et al.*, GAUSSIAN 09, Revision A.1, Gaussian, Inc., Wallingford, CT, 2009.
- ³²B. H. Besler, K. M. Merz, Jr., and P. A. Kollman, *J. Comput. Chem.* **11**, 431 (1990); U. C. Singh and P. A. Kollman, *J. Comput. Chem.* **5**, 129 (1984).
- ³³L. E. Chirlian and M. M. Francl, *J. Comput. Chem.* **8**, 894 (1987).
- ³⁴C. M. Breneman and K. B. Wiberg, *J. Comput. Chem.* **11**, 361 (1990).
- ³⁵F. L. Hirshfeld, *Theor. Chem. Acc.* **44**, 129 (1977).
- ³⁶See supplementary material at <http://dx.doi.org/10.1063/1.4802009> for table with stretching and bending charge fluxes, tables with the comparison between computed APTs and “reconstructed” ones, table with CH stretching principal fluxes on H belonging to many different molecules obtained with different approximations, table with CH stretching fluxes for ethylene, butadiene, and hexatriene.
- ³⁷The definition of the “local plane” is not always straightforward: in Refs. **14** and **15** several non-trivial cases are discussed and guidelines for a suitable choice of a local plane are proposed. Moreover, in Ref. **3** a method useful to correct atomic charges obtained from APTs of non-planar molecules, after a (quite arbitrary) definition of the “local plane” is proposed.

3.2 Extension of the model to interacting molecules: hydrogen-bonding interactions

It is well known that one of the characteristic phenomena associated to the formation of hydrogen bond is a considerable intensification of the X-H stretching band in the IR spectrum [45] which takes place concurrently with a very large frequency red-shift, often reaching $\Delta\nu$ values of different hundreds of cm^{-1} .

In the past, many authors [26–29,32–34,38,39] rationalized this intensity modulation as consequence of strong charge fluxes taking place in the dimer, but not present for the isolated molecule. In particular, due to the lack of a method to compute the whole set of charge flux parameters in the framework of ECCF model, the whole charge flux was conventionally described by the principal stretching charge flux $\frac{dq_H}{dr_{XH}}$ namely it was ascribed to a fluctuation of the atomic charge of the only hydrogen atom involved in the H-bond, due to the only stretching of the covalent X-H bond.

On the other hand, in Section (3.1) and in our paper “*Infrared intensities and charge mobility in hydrogen bonded complexes*” (D. Galimberti, A. Milani, and C. Castiglioni *J. Chem. Phys.* 139, 074304 (2013) that can be found after this discussion), we have demonstrated that *non principal* charge fluxes can play an important role in the description of the charge distribution and its mobility.

Moreover, evidences of the non-local character of charge fluxes in H-bonded complexes had been provided also by Torii [46,47], who showed that the charge density fluctuation associated with the OH stretching in a water dimer (namely $\delta\rho^{el}(\mathbf{r})/\partial Q_{OH}$ where Q_{OH} is the OH- stretching normal mode of the dimer), has a delocalized character.

In our work we compute the whole set of ECCF parameters for set of different kind of small H-bonded complexes to evaluate the relative importance of the principal and non-principal charge fluxes. To this aim linear, T-shape and bi-dentated dimers have been considered (see the paper for more details). In order to verify the reliability of the model for larger systems, we also consider the guanine-cytosine pair as a test case.

The computed values show that the H-bond formation involves a redistribution of charge density in the dimer with respect to the isolated fragments; in particular a net transfer of electron charge from the acceptor to the donor molecule. In most of the cases, the equilibrium charges showing a non-negligible perturbation after dimer formation are those of the atoms belonging to the -XH...Y fragment.

However, the changes of the equilibrium charges after the formation of the dimer are too small to justify the huge intensity increase of X-H stretching band upon H-bonding. It is then evident that a remarkable contribution due to charge fluxes between the two molecules needs to be taken into account.

The predicted values for the charge fluxes (both principal and non-principal) shows that the H-bond formation increases the charge mobility during the vibrational modes. Indeed, during the Q_{XH} mode, there is a further negative charge flux from the acceptor to the donor when r_{XH} stretches. These fluxes are in general large and add up to the contribution arising from

the static charge - transferred already at equilibrium - making the donor even more negatively charged.

The contribution of the charge fluxes to the dipole moment change fully account for the huge IR intensity observed for X-H stretching modes in the H-bonded complexes: we indeed found an excellent correlation between the calculated absolute intensity of the mode Q_{XH} and the contribution arising from the computed fluxes. This correlation seems only weakly affected by the kind of donor-acceptor pair or of the type of H-bond considered.

Also in this case, our data shows that the charge flux are not localized and non principal charge flux play an important role. Indeed, the flux term relative to hydrogen is small in most of the cases, so that dq_H/dQ_{XH} provides only a small contribution to the global charge flux on the donor, in contrast to the past model. In this case the H atoms seems to act only as a "bridge" for the charge flux during the vibration.

It is interesting to observe that the normal mode analysis has showed that, regardless of the type of H-bond, the normal mode Q_{XH} is never a pure r_{XH} stretching in the complex, but always involves a combination of the stretching of the XH bond and of the hydrogen bond H...Y , which is kinetically coupled to it. The normal mode Q_{XH} can be always described as an oscillation of the hydrogen atom between the donor and the acceptor.

Infrared intensities and charge mobility in hydrogen bonded complexes

Daria Galimberti, Alberto Milani,^{a)} and Chiara Castiglioni

Dipartimento di Chimica, Materiali e Ingegneria Chimica "Giulio Natta," Politecnico di Milano, Piazza Leonardo da Vinci 32, 20133 Milano, Italy

(Received 2 July 2013; accepted 31 July 2013; published online 20 August 2013)

The analytical model for the study of charge mobility in the molecules presented by Galimberti *et al.* [J. Chem. Phys. **138**, 164115 (2013)] is applied to hydrogen bonded planar dimers. Atomic charges and charge fluxes are obtained from density functional theory computed atomic polar tensors and related first derivatives, thus providing an interpretation of the IR intensity enhancement of the X–H stretching band observed upon aggregation. Our results show that both principal and non-principal charge fluxes have an important role for the rationalization of the spectral behavior; moreover, they demonstrate that the modulation of the charge distribution during vibrational motions of the –XH···Y– fragment is not localized exclusively on the atoms directly involved in hydrogen bonding. With these premises we made some correlations between IR intensities, interaction energies, and charge fluxes. The model was tested on small dimers and subsequently to the bigger one cytosine-guanine. Thus, the model can be applied to complex systems. © 2013 AIP Publishing LLC. [<http://dx.doi.org/10.1063/1.4818416>]

I. INTRODUCTION

The knowledge of the molecular charge distribution is particularly important in chemical physics, materials science, and molecular biology, since it has direct effects on the intra- and inter-molecular interactions which determine the properties of the molecule and its arrangement at the nanoscale. Phenomena such as polarization of the electronic cloud, charge transfer between chemical groups, localization of excess of electronic charge on specific molecular sites are indeed crucial in molecular interactions.

Furthermore, the development of suitable models for the calculations of atomic charges and charge fluxes (e.g., induced by atoms displacements) is important in computational chemistry and these are one of the fundamental ingredients for the construction of force fields that are used in molecular mechanics and molecular dynamics simulations.¹ To this aim, many methods have been proposed and implemented^{2,3} and are now widely used. Some models allow to extract local charge parameters from the measured absolute absorption intensities,^{4–11} among them the Equilibrium Charges Charge Fluxes (ECCF) model⁷ proved to be particularly effective in the interpretation of both intra and inter-molecular effects (e.g., inductive effects, charge backdonation, hyperconjugation, formation of hydrogen bonds, or strong electrostatic interactions^{12–18}). ECCF parameters can be calculated following two different ways. The set of the dipole derivatives with respect to normal coordinates Q_i , namely, the parameters $\left(\frac{\partial \mu}{\partial Q_i}\right)^0$, obtained from experimental IR intensities can be transformed into dipole derivatives with respect to the internal vibrational coordinates according to the relationship $\left(\frac{\partial \mu}{\partial R_i}\right)^0 = \sum_i \left(\frac{\partial \mu}{\partial Q_i}\right)^0 L_{it}^{-1}$, where L is the vibrational

eigenvectors matrix. From algebraic expressions in the form $\left(\frac{\partial \mu}{\partial R_i}\right)^0 = f\left(\{q_\alpha^0\}, \left\{\left(\frac{\partial q_\alpha}{\partial R_i}\right)^0\right\}\right)$ an ECCF set can be derived.

In a similar way, ECCF can be obtained by the suitable algebraic expressions of the Atomic Polar Tensors (APT) (see Sec. II). The last approach is preferred when ECCF are calculated on a fully theoretical ground: indeed APTs are now easily computed by standard codes since they are required for the computation of IR intensity. Thanks to the high accuracy of current state-of-the-art *ab initio*/Density Functional Theory (DFT) calculations, several papers revisited the applications of these models from a computational perspective, including both their application^{9–11,19,20} and implementation.³ Many studies focused mainly on the analysis of equilibrium charges while only in recent papers also charge fluxes have been analyzed.^{9,10,18,21,22} In a very recent paper,²³ we presented an analytical method to extract the whole set of charge fluxes through the evaluation of second derivatives of the dipole (i.e., APTs derivatives); the method has been applied with success to different planar molecules, shedding light on some peculiar properties of charge flux parameters.

The objective of this paper is to extend our methodology previously developed to hydrogen-bonded complexes for interpreting intermolecular associations.

II. MODELS AND THEORY

A. The analytical model

The results here reported are obtained by applying the analytical model presented in a previous paper²³ to which we refer for a detailed description; in the following we recall just the main points.

Atomic charges and charge fluxes are extracted in the framework of the ECCF model on the basis of molecular dipole moment derivatives with respect to Cartesian

^{a)} Author to whom correspondence should be addressed. Electronic mail: alberto.milani@polimi.it

displacements $\left(\frac{\partial \mu}{\partial \xi_k}\right)^0$ where ξ_k is the k th component of the ξ vector which collects the $3N$ Cartesian coordinates of the N atoms belonging to the given molecules. These derivatives are usually collected in 3×3 matrices called APTs whose components can be written, for an individual atom β , as $P_{uv}^\beta = \left(\frac{\partial \mu_u}{\partial v_\beta}\right)^0$, where μ_u represents the x , y , or z component of the molecular dipole moment, while v_β is a Cartesian displacement of the β atom ($v_\beta = x_\beta, y_\beta, \text{ or } z_\beta$) upon which the derivative of the dipole moment is carried out. All these derivatives are evaluated at the equilibrium geometry ($\mathbf{v} = \mathbf{0}$) of the molecule. APTs are related to the absolute IR absorption intensities, thus providing a relationship between APTs and experimentally measurable quantities.

The relationship between APTs, charges, and charge fluxes is based on the assumption

$$\boldsymbol{\mu} = \sum_{\alpha} q_{\alpha} \cdot \mathbf{r}_{\alpha}, \quad (1)$$

where \mathbf{r}_{α} is the position vector of the α atom.

If the molecular dipole which appears in the definition of APT is written according to Eq. (1), it is possible to express each APT component as a function of atomic charges and charge fluxes, thus providing a set of equations from which ECCF parameters can be derived. Unfortunately, the number of unknowns, namely, the whole set of charges and charge fluxes, exceeds the number of independent equations so obtained.

However, following the model firstly introduced by Dinur²⁴ and according to the procedure illustrated in Ref. 23, we showed that, in the case of a planar molecule, it is possible to determine the whole set of ECCF. By choosing a suitable reference system with an axis (z) orthogonal to the plane of the molecule one obtains the following expressions:

$$P_{zz}^{\alpha} = \left(\frac{\partial \mu_z}{\partial z_{\alpha}}\right)^0 = q_{\alpha}^0, \quad (2)$$

$$\left(\frac{\partial q_{\alpha}}{\partial \xi_k}\right)^0 = \left(\frac{\partial^2 \mu_z}{\partial z_{\alpha} \partial \xi_k}\right)^0 = \left(\frac{\partial P_{zz}^{\alpha}}{\partial \xi_k}\right)^0. \quad (3)$$

If Eq. (3) is applied to each P_{zz}^{α} component ($\alpha = 1, \dots, N$) and the derivatives with respect to each Cartesian displacement ξ_k ($k = 1, \dots, 3N$) are calculated, the $(N \times 3N)$ matrix $(\partial q / \partial \xi)^0$ is obtained. By standard transformations between Cartesian coordinates, internal coordinates, and normal coordinates, it is also possible to obtain

$$\frac{\partial q}{\partial \mathbf{R}} = \frac{\partial q}{\partial \xi} \cdot \mathbf{A} \quad (4)$$

and

$$\frac{\partial q}{\partial \mathbf{Q}} = \frac{\partial q}{\partial \xi} \cdot \mathbf{L}, \quad (5)$$

where the L matrix defines the linear transformation from Cartesian displacements to normal coordinates ($\mathbf{x} = \mathbf{L} \mathbf{Q}$). Notice that in Eqs. (4) and (5) and in all the subsequent expressions we adopted a shortened notation by omitting the apex "0" for quantities evaluated at equilibrium geometry.

Therefore, from the second derivatives of the molecular dipole moment (first derivatives of atomic polar tensors), we can derive the whole matrices of the fluxes: $\partial q / \partial \mathbf{R}$ and $\partial q / \partial \mathbf{Q}$.

B. Computational details

We will apply the model described above to compute the ECCF parameters, and in particular, the XH stretching charge fluxes of dimers possessing one or more intermolecular H-bonds. In the following the molecular fragment involved in the hydrogen bridge will be indicated as $\text{-XH} \cdots \text{Y}$, where X is the atom of the donor molecule directly linked to H and Y is the acceptor atom or bond.

Firstly, we will investigate small dimers, while in the last section we will focus on the cytosine-guanine dimer as a test case for guessing the extension of the model to larger and significant intermolecular complexes.

The dimers under study will be classified into three groups according to the hydrogen bond geometry:

- *Linear*: the dimer has only one H-bond, linking the hydrogen atom and the acceptor atom Y, thus, determining a linear arrangement of the two molecules (see, for example, Figures 3(a) and 3(b)). The following dimers have been studied: $\text{HCN} \cdots \text{HCN}$, $\text{HCN} \cdots \text{HC}_3\text{N}$, $\text{HC}_3\text{N} \cdots \text{HCN}$, $\text{HCN} \cdots \text{HCl}$, $\text{HCN} \cdots \text{HF}$, $\text{H}_2\text{O} \cdots \text{HCN}$, $\text{H}_2\text{O} \cdots \text{HC}_3\text{N}$, $\text{HC}_3\text{N} \cdots \text{HC}_3\text{N}$, $\text{HC}_3\text{N} \cdots \text{HF}$, $\text{HC}_3\text{N} \cdots \text{HCl}$, $\text{HCN} \cdots \text{H}_2\text{O}$, $\text{HC}_3\text{N} \cdots \text{H}_2\text{O}$.
- *T-shape*: the dimer has only one H-bond, located between a hydrogen and an acceptor triple bond (Y = CC) (see, for example, Figure 3(c)). The following cases have been considered: $\text{CHCH} \cdots \text{HF}$, $\text{CHCH} \cdots \text{HCl}$, $\text{CHCH} \cdots \text{HCN}$, $\text{CHCH} \cdots \text{HC}_3\text{N}$.
- *Bidentate*: the dimer possesses two linear H-bonds. In all the cases examined in this work ($\text{HCOOH} \cdots \text{HCOOH}$, $\text{FCOOH} \cdots \text{FCOOH}$, $\text{ClCOOH} \cdots \text{ClCOOH}$, $\text{BrCOOH} \cdots \text{BrCOOH}$) the two monomers are the same (see, for example, Figure 3(d)).

According to previous papers,^{9,11,23} reliable results for the calculation of APT can be obtained by means of DFT calculations using PBE0/aug-cc-pVTZ combination of functional/basis set and we adopted this combination also in this work. In the case of the cytosine-guanine dimer, due to the larger size of the complex, we reduced the basis set level to 6-311++G(d,p): indeed, in Ref. 9, we demonstrated also that PBE0/6-311++G(d,p) calculations give a good description of IR intensities and it is the best choice for large systems while maintaining an acceptable computational cost. In addition, we carried out further calculations on both isolated molecules and small dimers to verify that charge fluxes previously computed at higher level are well reproduced with this basis set.

For all the systems here investigated, we carried out geometry optimization and IR intensity calculations by means of the GAUSSIAN09 code.²⁵

Based on the APTs so predicted (first derivatives of the dipole moment), second derivatives of the dipole moments

have been carried out numerically (with a displacement from the equilibrium geometry of +0.001 Å) to obtain the quantities reported in Eq. (3).

For a reliable evaluation of the interaction energy, we adopted the counterpoise (CP)²⁶ correction for the Basis Set Superposition Error (BSSE) during the whole geometry optimization.

Through Eqs. (2) and (3) we calculate the whole set of ECCF parameters for the dimers listed above. We tested the charge neutrality for the globally neutral systems and we found that this requirement is always fulfilled. As a second check we verified that the charges and charge fluxes obtained are actually able to reproduce the computed molecular dipole moment and its first derivatives according to

$$\mathbf{P}^\beta = q_\beta^0 \mathbf{I} + \bar{\mathbf{x}}^0 \begin{pmatrix} \frac{\partial q}{\partial \xi} \\ \beta \end{pmatrix} \quad (6)$$

In particular, we verified that the APTs “reconstructed” setting in Eq. (6) charges and charge fluxes computed from Eqs. (2) and (3) coincide with those provided directly by DFT calculations (see Ref. 23 for details).

III. RESULTS AND DISCUSSION

A. Normal modes analysis

In this work we will focus mainly on charge fluxes associated with the XH stretching modes and, in particular, on their modulation by the occurrence of a hydrogen bond. Indeed it is well known that one of the characteristic phenomena associated to the formation of a hydrogen bond is a remarkable intensification of the X–H stretching band in the IR spectrum²⁷ which takes place concurrently with a very large downward shift of the frequency (often reaching $\Delta\nu$ values of about 200 cm^{-1}).

In the past, many authors^{18,22} suggested to ascribe the observed intensity increase to strong charge fluxes occurring in the dimer but not present in the isolated molecule. In particular, because of the lack of a method to compute the whole set of charge flux parameters, the whole charge flux was conventionally described by the so called *principal* stretching charge flux $dq_{\text{H}}/dr_{\text{XH}}$, namely, it was ascribed to a remarkable fluctuation of the atomic charge of the hydrogen atom, associated to the stretching of the XH bond, described by the internal coordinate r_{XH} , i.e.:

$$I_{\text{XH}} \propto \left| q_{\text{H}} + \frac{dq_{\text{H}}}{dr_{\text{XH}}} \cdot r_{\text{XH}} \right|^2 \quad (7)$$

In a previous paper²³ we have demonstrated that, also in the case of isolated molecules, *non-principal* charge fluxes are not negligible, but their values are often comparable to those of principal charge fluxes. Another evidence of the non-local character of charge fluxes in H-bonded complexes has been provided by Torii,²² who showed that the charge density fluctuation associated with the OH stretching in a water dimer, namely, $\partial\delta\rho^{\text{el}}(r)/\partial Q_{\text{OH}}$, where Q_{OH} is the OH-stretching normal mode of the dimer, has a delocalized character.

For the above reasons, we decided to exploit our model in order to go beyond the approximation described by Eq. (7),

aiming at a more exhaustive description of the phenomena involved.

As a first step, we carefully analyze the dynamics of the X–H stretching normal mode in a H bonded dimer in comparison with the corresponding mode of the isolated donor molecule.

In the following discussion the mode associated to the XH stretching band of the spectrum will be referred as Q_{XH} both in the case of the dimer and for the isolated molecule. It is well-known that in the latter case the normal mode Q_{XH} is localized and corresponds substantially to the stretching of the r_{XH} internal coordinate; this picture does not hold any more when the H atom belonging to the XH bond is involved in a H-bond, thus making Eq. (7) a too rough assumption also from the view point of the normal mode description.

This can be easily verified considering explicitly all the coordinates involved. While describing the vibrational dynamics of a complex, the H-bond $\text{Y} \cdots \text{H}$ is treated as a “true” intra-molecular bond of the super-molecule, i.e., of the dimer; accordingly, new internal coordinates, as, for instance, $\text{Y} \cdots \text{H}$ stretching and bendings relative to the fragment $\text{Y} \cdots \text{HX}$ are defined following to Wilson, Decius, and Cross model.²⁸ In this frame it is possible to analyze the vibrational eigenvector $\mathbf{L}(Q_{\text{XH}})$ associated to Q_{XH} in terms of the individual weights relative to the internal coordinates of the super-molecule: in particular, its t -th component, $L_t(Q_{\text{XH}}) = dR_t/dQ_{\text{XH}}$, describes the contribution of the R_t vibrational displacement during the mode Q_{XH} .

In Table I we report the main eigenvectors components in the case of linear, T-shape H-bonds and bidentate dimers. These values show that, regardless of the type of H-bond, the normal mode Q_{XH} is never a pure r_{XH} stretching in the complex, but always involves a combination of the stretching of the XH bond and of the hydrogen bond $\text{H} \cdots \text{Y}$, which is kinetically coupled to it.

For example, in the case of $\text{HCN} \cdots \text{HCN}$, during the positive phase of Q_{CH} , r_{CH} lengthens ($dr_{\text{CH}}/dQ_{\text{CH}} = 1.015 \text{ amu}^{-1/2}$) and $r_{\text{H} \cdots \text{Y}} = r_{\text{H} \cdots \text{N}}$ simultaneously shortens of nearly the same amount ($dr_{\text{H} \cdots \text{N}}/dQ_{\text{CH}} = -0.896 \text{ amu}^{-1/2}$).

In some cases we also found non-negligible contributions from the stretching of other RH bonds belonging either to the donor or to the acceptor monomer (see, for example, the contribution of the CH stretching in HCOOH) or from bending coordinates. However, the Q_{XH} mode can be always described as an oscillation of the hydrogen atom between the donor and the acceptor, while the centers of mass of the two molecules practically do not move. This is more evident if we analyze the eigenvectors in Cartesian coordinates (see examples in Table II). For example, for $\text{HC}_3\text{N} \cdots \text{HCl}$, the hydrogen involved in the H-bond is the only one showing a non-negligible value of dx_k/dQ_{CH} (-0.98), while all other atoms are at rest.

The predicted eigenvectors are consistent with the definition of the H-bond reported by Gilli²⁹: the same proton (the hydrogen) is regarded as the central atom between two bonds each one involving a different acceptor atom (i.e. X and Y), carrying an electron pair. While at the equilibrium molecular geometry X–H is shorter than $\text{H} \cdots \text{Y}$, during the HX stretching mode both X–H and $\text{H} \cdots \text{Y}$ distances are modulated along

TABLE I. Main components of the eigenvectors $L_i(Q_{XH}) = dR_i/dQ_{XH}$. For complexes with more than one H atom dr'_{RH}/dQ_{XH} is the eigenvector component relative to the stretching of the RH' bond (H' is the hydrogen atom not involved in the H-bond). For T-shape dimers the H bond stretching is described by the internal stretching coordinate ($r_{H...C}$) between H and one of the two carbon atoms forming the triple CC bond. For bidentate dimers the O–H stretching mode is the out of phase combination of the two OH stretching. Labels “Symm” and “Asymm” refer to the in phase and out-of-phase OH stretchings of a donor H₂O molecule, or to the in-phase /out of phase CH/OH stretchings of the complexes involving HCOOH.

	Acceptor donor	dr_{XH}/dQ_{XH} (amu ^{-1/2})	$dr_{Y...H}/dQ_{XH}$ (amu ^{-1/2})	dr'_{RH}/dQ_{XH} (amu ^{-1/2})
Linear	HCN···HCN	1.015	-0.896	
	HCN···HC ₃ N	1.022	-0.911	
	HC ₃ N···HCN	1.016	-0.898	
	HCN···HCl	1.010	-0.984	
	HCN···HF	1.022	-0.971	
	H ₂ O···HCN	1.014	-0.895	
	H ₂ O···HC ₃ N	1.022	-0.912	
	HC ₃ N···HC ₃ N	1.023	-0.914	
	HC ₃ N···HF	1.022	-0.970	
	HC ₃ N···HCl	1.010	-0.984	
	HCN···H ₂ O(Asymm)	0.355	-0.317	-0.968
	HC ₃ N···H ₂ O(Asymm)	0.358	-0.320	-0.968
	HCN···H ₂ O(Symm)	0.963	-0.914	0.338
HC ₃ N···H ₂ O(Symm)	0.962	-0.913	0.341	
T-shape	CHCH···HF	1.022	-0.932	
	CHCH···HCl	1.010	-0.950	
	CHCH···HCN	1.017	-0.876	
	CHCH···HC ₃ N	1.024	-0.892	
Bidentate	HCOOH···HCOOH (ASymm)	0.584	-0.547	-0.435
	HCOOH···HCOOH (Symm)	0.430	-0.404	0.590
	FCOOH···FCOOH	0.724	-0.676	
	ClCOOH···ClCOOH	0.725	-0.678	
	BrCOOH···BrCOOH	0.725	-0.677	

the trajectory which describes the transition between the two following structures:

$(R-X-H) \cdots Y$ and $(R-X)^{-1} \cdots (H-Y)^{+1}$. The assumption that Q_{XH} coincides with the internal coordinate r_{XH} is, therefore, erroneous: to explain the intensification of the X–H stretching mode we need to consider charge fluxes of the normal mode dq_a/dQ_{XH} rather than fluxes related to the only XH stretching coordinate, dq_a/dr_{XH} .

It is interesting to note that the r_{XH} stretching weight in the Q_{XH} eigenvectors of the dimer and of the isolated donor molecule are similar; hence, it will be acceptable to make a comparison between the charge fluxes associated to the internal stretching coordinate r_{XH} in the two cases, while discussing its role in determining the intensity of the band associated to Q_{XH} .

B. Charges and charge fluxes

We first focus on the equilibrium atomic charges calculated by means of Eq. (2) (IR charges) and whose reliability has been already demonstrated in previous papers^{3,9,30} also in connection with H-bond properties.¹³

As expected, the computed values show that the H-bond formation involves a redistribution of charge density in the dimer with respect to the isolated fragments. For instance, in

the case of the hydrogen atom involved in the H-bond q_H is less positive than in the isolated molecule (see Table III).

In most of the cases the equilibrium charges showing a non-negligible perturbation after dimer formation are those of atoms belonging to the $-XH \cdots Y$ fragment: for example, in the case of ClCOOH···ClCOOH dimer, both the chlorine and the carbon atoms show variations lower than $0.01e$ due to the formation of the H-bond (Figure 1(a)). Similarly, in CHCH···HCN, the H atoms of acetylene show a variation of their equilibrium charge of $0.003e$ (Figure 1(b)).

If we now consider the total charge of each monomer in the dimer, we find a net transfer of electron charge from the acceptor to the donor molecule (see Table IV). This is in agreement with the results reported by other authors^{22,30} and it is also consistent with NBO (Natural Bond Orbital) analysis,³¹ showing that the formation of the H-bond is accompanied by electron charge transfer from the lone pair of the acceptor atom (Y) to the σ^* antibonding orbital of the XH bond of the donor.

A peculiar case is represented by bidentate dimers: each molecule acts both as acceptor and donor and, due to the symmetric structure of the complex, there is obviously no net charge transfer from one molecule to the other.

On the other hand the small changes of the equilibrium charges after the formation of the dimer cannot justify the

TABLE II. Cartesian components of the eigenvectors $L_k^{\xi}(Q_{XH}) = d\xi_k/dQ_{XH}$ for the normal mode Q_{XH} . The left hand side molecule of the dimer is always the one playing the role of proton acceptor (A), while the right hand side one is the donor (D). For linear complexes, the x-axis lies along the hydrogen bond and is oriented from A to D; for T-shape complexes the y axis is orthogonal to the acceptor CC bond.

HCN...HCN		dx_k/dQ_{XH} Isolated ($\text{amu}^{-1/2}$)	dx_k/dQ_{XH} Dimer ($\text{amu}^{-1/2}$)	
A	H		-0.03956	
	C		0.00371	
	N		-0.00064	
D	H	-0.90645	-0.89677	
	C	0.11424	0.11851	
	N	-0.03273	-0.03678	
HC ₃ N...HCl		dx_k/dQ_{XH} isolated ($\text{amu}^{-1/2}$)	dx_k/dQ_{XH} dimer ($\text{amu}^{-1/2}$)	
A	H		-0.00319	
	C		0.00025	
	C		-0.00005	
	C		-0.00375	
	N		0.00203	
D	H	-0.98216	-0.98156	
	Cl	0.02792	0.02840	
HCCH HCN		dy_k/dQ_{XH} isolated ($\text{amu}^{-1/2}$)	dy_k/dQ_{XH} dimer ($\text{amu}^{-1/2}$)	dx_k/dQ_{XH} dimer ($\text{amu}^{-1/2}$)
A	C		-0.00017	0.00127
	C		-0.00017	-0.00127
	H		0.00019	-0.00303
	H		0.00019	0.00303
D	H	-0.90645	-0.90008	0.00000
	C	0.11424	0.11740	0.00000
	N	-0.03273	-0.03563	0.00000

huge intensity increase of the X–H stretching band; it will be proven in the following that the remarkable contribution due to charge fluxes between the two molecules needs to be taken into account. Indeed, during the Q_{XH} mode of the complex there is a further negative charge flux from the acceptor

to the donor molecule during the positive phase of the mode (i.e., when r_{XH} elongates), as also seen by the Torii analysis²² in the case of H₂O complexes (see Table IV, where charge fluxes values for the dimers are reported, as calculated by means of Eqs. (3)–(5)). These fluxes are, in general, large

TABLE III. IR charges (units of e) of the hydrogen involved in the H-bond in the case of the dimer and for the isolated molecule (PBE0/aug-cc-pVTZ calculations).

	Acceptor	donor	q_H isolated (e)	q_H dimer (e)	$q_H^{dimer} - q_H^{iso}$ (e)
Linear	HCN...HCN		0.258	0.226	-0.032
	HC ₃ N...HCN		0.258	0.224	-0.034
	HCN...HCl		0.185	0.146	-0.039
	HCN...HF		0.409	0.318	-0.091
	HC ₃ N...HC ₃ N		0.205	0.174	-0.031
	HCN...HC ₃ N		0.205	0.176	-0.029
	HC ₃ N...HF		0.409	0.314	-0.095
	HC ₃ N...HCl		0.185	0.145	-0.040
	H ₂ O...HCN		0.258	0.228	-0.030
	H ₂ O...HC ₃ N		0.205	0.177	-0.028
	HCN...H ₂ O		0.330	0.274	-0.056
	HC ₃ N...H ₂ O		0.330	0.271	-0.059
	T-shape	CHCH...HF		0.409	0.288
CHCH...HCl			0.185	0.125	-0.060
CHCH...HCN			0.258	0.214	-0.044
CHCH...HC ₃ N			0.205	0.165	-0.040
Bidentate	HCOOH...HCOOH		0.336	0.272	-0.064
	FCOOH...FCOOH		0.344	0.267	-0.077
	ClCOOH...ClCOOH		0.345	0.272	-0.073
	BrCOOH...BrCOOH		0.345	0.273	-0.072

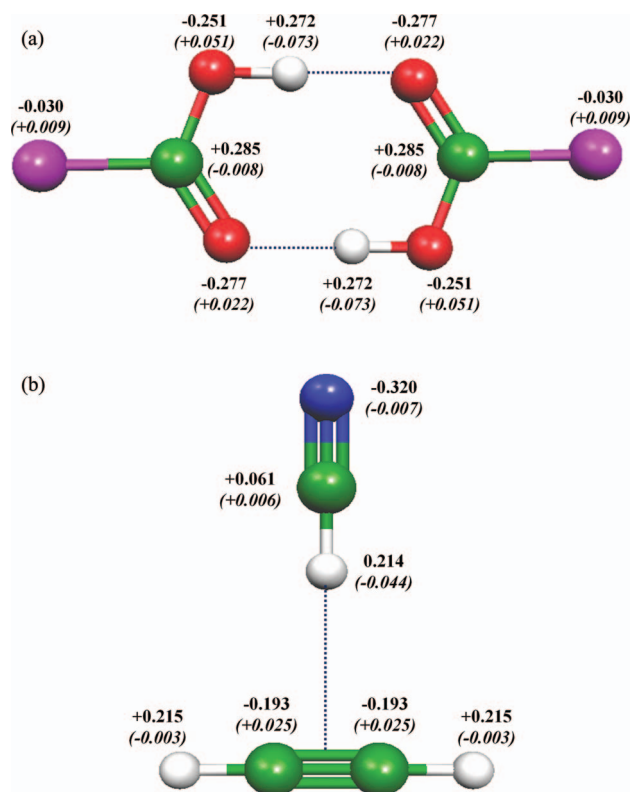


FIG. 1. IR charges (in units of e) for (a) $\text{ClCOOH}\cdots\text{ClCOOH}$, (b) $\text{CHCH}\cdots\text{HCN}$ (PBE0/aug-cc-pVTZ calculations). In brackets we reported the difference between equilibrium charges of the dimer and of the isolated molecule ($q_a^{\text{dimer}} - q_a^{\text{iso}}$).

and add up to the contribution arising from the displacement of the static charges, making the donor even more negatively charged. This should be expected simply considering the two ideal structures mentioned above, namely, a dimer characterized by two weakly bonded neutral monomers and a charge transfer structure where a proton is transferred from the donor to the acceptor. Indeed, the acceptor results to be more positively charged as the X–H bond stretches and H \cdots Y bond simultaneously shrinks, i.e., during Q_{XH} . The total flux assumes higher values in those cases where the donor molecule contains halogen atoms (e.g., F and Cl) and ranges between 0.1 and 0.5 eA^{-1} . The contribution of the charge fluxes to the dipole moment derivative fully account for the huge IR intensity observed for X–H stretching modes in the H-bonded complexes: we indeed find an excellent correlation between the calculated absolute intensity of the mode Q_{XH} and the contribution from the computed fluxes, which can be estimated according to the expression

$$I^{\text{Fluxes}} \div \left(\sum x_a \frac{dq_a}{dQ_{\text{XH}}} \right)^2, \quad (8)$$

where the x axis is oriented along the H-bond, see Figure 2. This correlation seems to be weakly affected by the kind of acceptor-donor pair or by the type of H-bond considered. Indeed, there are no marked differences between linear bonds, T-shape, and bidentate complexes in this respect.

Our results demonstrate that the charge flux contribution during XH stretching is dominant in determining the IR

TABLE IV. Total charge of the donor molecule, total charge flux on the donor molecule during the positive phase of the Q_{XH} mode ($\partial r_{\text{XH}}/\partial Q_{\text{XH}} > 0$), IR intensity of the Q_{XH} band, and interaction energy of the dimer (corrected for the BSSE error by means of the CP procedure). Values are obtained by means of DFT PBE0/aug-cc-pVTZ calculations. The labels “Symm” and “Asymm” refer to the in phase and out-of-phase OH stretchings in the H_2O molecule acting as donor or to the in-phase or out of phase CH/OH stretchings of the complexes involving HCOOH.

	Acceptor donor	q_{tot} donor (e)	$dq_{\text{tot}}/dQ_{\text{XH}}$ donor ($e/\text{A} \cdot \text{amu}^{1/2}$)	IR intensity (km/mol)	Interaction energy (BSSE corr) (kJ/mol)
Linear	$\text{HCN}\cdots\text{HCN}$	−0.051	−0.108	380	−19.138
	$\text{HC}_3\text{N}\cdots\text{HCN}$	−0.053	−0.110	495	−19.104
	$\text{HCN}\cdots\text{HCl}$	−0.080	−0.191	737	−19.054
	$\text{HCN}\cdots\text{HF}$	−0.099	−0.270	1024	−32.250
	$\text{HC}_3\text{N}\cdots\text{HC}_3\text{N}$	−0.049	−0.102	567	−17.050
	$\text{HCN}\cdots\text{HC}_3\text{N}$	−0.049	−0.101	452	−17.058
	$\text{HC}_3\text{N}\cdots\text{HF}$	−0.100	−0.271	1461	−31.924
	$\text{HC}_3\text{N}\cdots\text{HCl}$	−0.080	−0.192	1008	−18.749
	$\text{H}_2\text{O}\cdots\text{HCN}$	−0.053	−0.117	370	−21.422
	$\text{H}_2\text{O}\cdots\text{HC}_3\text{N}$	−0.050	−0.106	435	−18.920
	$\text{HCN}\cdots\text{H}_2\text{O}$ (Asymm)	−0.058	−0.044	116	−15.619
	$\text{HCN}\cdots\text{H}_2\text{O}$ (Symm)	−0.058	−0.126	263	−15.619
	$\text{HC}_3\text{N}\cdots\text{H}_2\text{O}$ (Asymm)	−0.058	−0.045	148	−15.318
	$\text{HC}_3\text{N}\cdots\text{H}_2\text{O}$ (Symm)	−0.058	−0.125	363	−15.318
T-shape	$\text{CHCH}\cdots\text{HF}$	−0.092	−0.247	747	−20.121
	$\text{CHCH}\cdots\text{HCl}$	−0.068	−0.182	538	−11.824
	$\text{CHCH}\cdots\text{HCN}$	−0.044	−0.096	263	−9.527
	$\text{CHCH}\cdots\text{HC}_3\text{N}$	−0.039	−0.085	305	−8.213
Bidentate	$\text{HCOOH}\cdots\text{HCOOH}$ (Asymm)	0.000	−0.370	1426	−69.517
	$\text{HCOOH}\cdots\text{HCOOH}$ (Symm)	0.000	−0.306	1643	−69.517
	$\text{FCOOH}\cdots\text{FCOOH}$	0.000	−0.480	3029	−74.161
	$\text{ClCOOH}\cdots\text{ClCOOH}$	0.000	−0.456	4094	−65.772
	$\text{BrCOOH}\cdots\text{BrCOOH}$	0.000	−0.445	4606	−63.124

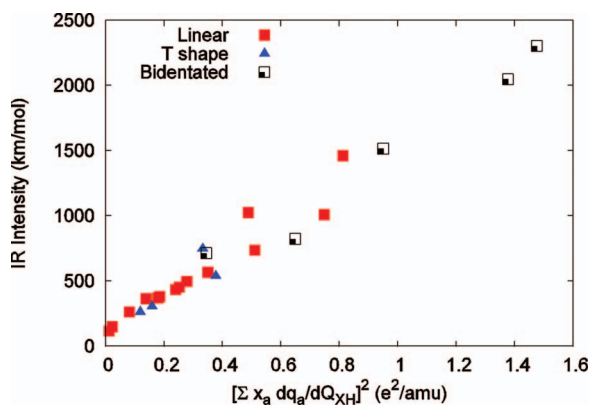


FIG. 2. Correlation between charge flux contributions (calculated according to Eq. (8), units of e^2/amu) and the IR intensity of Q_{XH} stretching mode (in units of km/mol). All the parameters are computed by means of DFT PBE0/au-cc-pVTZ calculations. The x-axis is oriented along the hydrogen bond. In the case of bidentate dimers the contribution for only one H-bond has been considered in the plot.

intensity behavior of Q_{XH} upon hydrogen bonding, as already argued in the past by some authors.^{18,22}

It is interesting to note that the total intermolecular flux during the Q_{XH} mode in the case of symmetric bidentate dimers is not vanishing but it is quite large due to the strong H-bond, contrary to the net transferred charge at the equilibrium, which is zero for symmetry reasons. This behaviour is due to the vibrational dynamics of these systems: indeed, even if each molecule of the dimer is acting both as acceptor and donor, the IR active normal mode is given by the antisymmetric combination of the two OH stretchings (see, for instance, Figure 3(d)). For this reason the individual charge fluxes associated to the out of phase displacements of the two H atoms involved in the two H bridges add up to give a large total flux value.

Finally, it should be noted that in the case of T-shape dimers, the charge transfer (both in terms of equilibrium charges and charge fluxes) is slightly lower than for other dimers sharing the same donor. The differences, are however moderate: in fact, interaction energies and IR intensity are of the same order of magnitude as in the case of linear dimers with the same donor.

We will now focus on the hydrogen atom involved in the H-bond. As already mentioned, in the past many authors ignored all non-principal fluxes and attributed the whole charge flux to the hydrogen atom, according to Eq. (7); moreover, charge fluxes due to the stretching of the H bond (namely, to $r_{\text{Y...H}}$), which is heavily involved in the Q_{XH} normal mode of the complex, was completely neglected. The data reported in Table V clearly show another trend.

The flux term relative to hydrogen is generally negative indicating a reinforcement of the negative charge injection from the acceptor, already demonstrated by the equilibrium charges of the dimer. On the other hand values of fluxes on H are anyway small in most cases, so that $dq_{\text{H}}/dQ_{\text{XH}}$ concur with a small contribution to the global charge flux on the donor. In bidentate dimers the flux of H is less than one tenth of the total.

This feature can be better rationalized in terms of fluxes with internal coordinates displacements. From the eigenvec-

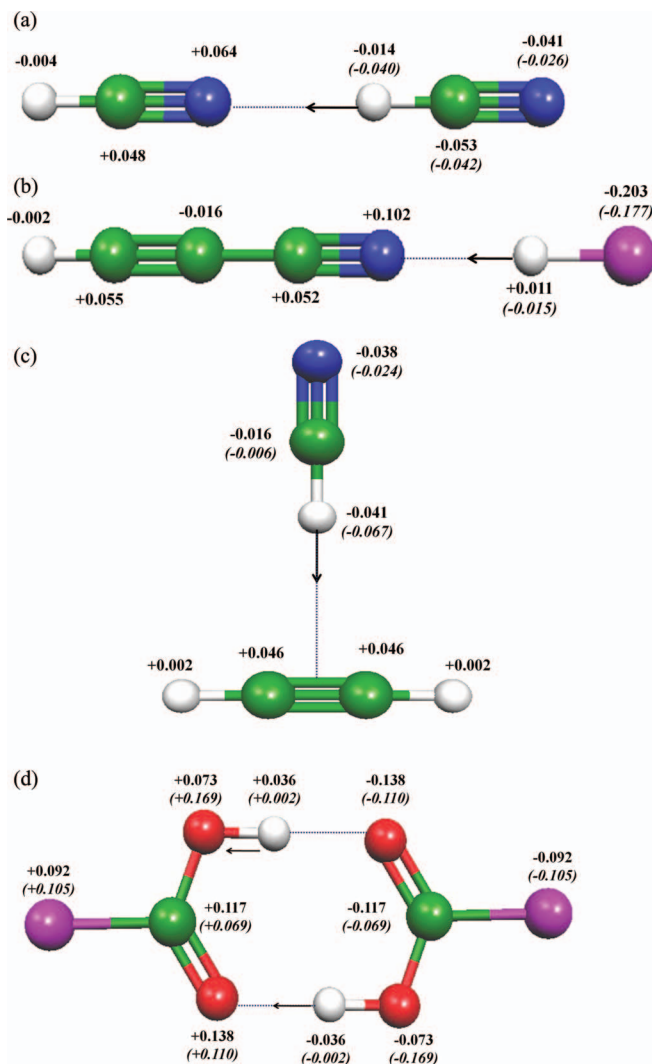


FIG. 3. Charge fluxes ($e/\text{\AA} \cdot \text{amu}^{1/2}$) for the Q_{XH} mode (a) $\text{HCN} \cdots \text{HCN}$, (b) $\text{HC}_3\text{N} \cdots \text{HCl}$, (c) $\text{CHCH} \cdots \text{HCN}$, (d) $\text{CICOOH} \cdots \text{CICOOH}$. In parentheses the difference between charge fluxes in the dimer and in the isolated molecule are reported (PBE0/au-cc-pVTZ calculations).

tors analysis we found that Q_{XH} is approximately the combinations of r_{XH} and $r_{\text{Y...H}}$ stretching, with opposite sign and weight ≈ 1 (see Table I). So we can approximate $dq_{\text{H}}/dQ_{\text{XH}}$ as

$$\frac{dq_{\text{H}}}{dQ_{\text{XH}}} \approx \frac{dq_{\text{H}}}{dr_{\text{XH}}} - \frac{dq_{\text{H}}}{dr_{\text{Y...H}}}.$$

Since in most cases, $dq_{\text{H}}/dr_{\text{XH}}$ and $dq_{\text{H}}/dr_{\text{Y...H}}$ show the same sign and are similar in magnitude (or are both small), $dq_{\text{H}}/dQ_{\text{XH}}$ is small (Table VI).

On the other side, charge fluxes ($dq_{\alpha}/dr_{\text{XH}}$ and $dq_{\alpha}/dr_{\text{Y...H}}$) relative to the two electron-rich atoms ($\alpha = \text{X}$ or Y) between which the hydrogen oscillates, often show opposite sign. As an example, in the case of $\text{HCN} \cdots \text{HCN}$, the fluxes on N of the acceptor molecule are $dq_{\text{N}}/dr_{\text{XH}} = 0.068 e/\text{\AA}$ and $dq_{\text{N}}/dr_{\text{Y...H}} = -0.045 e/\text{\AA}$, while on C of the donor $dq_{\text{C}}/dr_{\text{XH}} = -0.135 e/\text{\AA}$ and $dq_{\text{C}}/dr_{\text{Y...H}} = 0.012 e/\text{\AA}$. The two flux terms in these case sum up during the Q_{XH} oscillation, giving rise to the strong global flux characteristic of the Q_{XH} normal mode.

TABLE V. dq_H/dQ_{XH} values for the isolated donor molecule and for the donor molecule in the dimer; the global flux on the donor (dq_{tot}/dQ_{XH}) is also reported for sake of comparison. In bidentate dimers, we conventionally chose as “donor” the monomer characterized by a contribution $\partial r_{XH}/\partial Q_{XH} > 0$ in the Q_{XH} eigenvector (right molecule in Figure 3(d)), consistently with the other cases.

	DIMER acceptor donor	dq_H/dQ_{XH} isolated (e/A · amu ^{1/2})	dq_H/dQ_{XH} dimer (e/A · amu ^{1/2})	$\Delta(dq_H/dQ_{XH})$ (e/A · amu ^{1/2})	dq_{tot}/dQ_{XH} donor (e/A · amu ^{1/2})
Linear	HCN···HCN	0.026	-0.014	-0.040	-0.108
	HC ₃ N···HCN	0.026	-0.016	-0.042	-0.110
	HCN···HCl	0.025	0.011	-0.014	-0.191
	HCN···HF	-0.081	-0.143	-0.062	-0.270
	HC ₃ N···HC ₃ N	0.072	0.041	-0.031	-0.102
	HCN···HC ₃ N	0.072	0.042	-0.030	-0.101
	HC ₃ N···HF	-0.081	-0.144	-0.063	-0.271
	HC ₃ N···HCl	0.025	0.011	-0.014	-0.192
	H ₂ O···HCN	0.026	-0.010	-0.036	-0.117
	H ₂ O···HC ₃ N	0.072	0.049	-0.023	-0.106
	HCN···H ₂ O(Asymm)	-0.026	-0.003	0.023	-0.044
	HCN···H ₂ O(Symm)	-0.060	-0.191	-0.131	-0.126
	HC ₃ N···H ₂ O(Asymm)	-0.026	-0.004	0.022	-0.045
	HC ₃ N···H ₂ O(Symm)	-0.060	-0.190	-0.130	-0.125
T-shape	CHCH···HF	-0.081	-0.184	-0.103	-0.247
	CHCH···HCl	0.025	-0.031	-0.056	-0.182
	CHCH···HCN	0.026	-0.041	-0.067	-0.096
	CHCH···HC ₃ N	0.072	0.016	-0.056	-0.085
Bidented	HCOOH···HCOOH(Asymm)	-0.054	-0.045	0.009	-0.370
	HCOOH···HCOOH(Symm)	-0.054	-0.015	0.039	-0.306
	FCOOH···FCOOH	-0.015	-0.025	-0.010	-0.480
	ClCOOH···ClCOOH	-0.034	-0.036	-0.002	-0.456
	BrCOOH···BrCOOH	-0.039	-0.037	-0.001	-0.445

We can conclude that in most cases the hydrogen atom involved in the H-bond behaves simply as a bridge through which the electron charge flows between the two molecules, regardless of the nature of the H-bond. For example, in the case of HCN···HCN, the flux on H is

-0.014 e/(A · amu^{1/2}), while that on C and N (both in the acceptor and in the donor) exceed 0.040 e/(A · amu^{1/2}) in absolute value (Figure 3(a)). In the case of HC₃N···HCl, the flux on Cl is one order of magnitude larger than that of H (Figure 3(b)).

TABLE VI. Charge fluxes on the donor hydrogen atom: XH stretching flux (dq_H/dr_{XH}) of the isolated donor molecule and of the dimer; flux relative to the stretching of the hydrogen bond ($dq_H/dr_{Y...H}$).

	Acceptor donor	dq_H/dr_{XH} isolated (e/A)	dq_H/dr_{XH} dimer (e/A)	$dq_H/dr_{Y...H}$ dimer (e/A)
Linear	HCN···HCN	0.046	0.037	0.034
	HC ₃ N···HCN	0.046	0.036	0.035
	HCN···HCl	0.025	0.049	0.039
	HCN···HF	-0.080	-0.048	0.098
	HC ₃ N···HC ₃ N	0.075	0.074	0.034
	HCN···HC ₃ N	0.075	0.074	0.033
	HC ₃ N···HF	-0.080	-0.046	0.100
	HC ₃ N···HCl	0.025	0.049	0.040
	H ₂ O···HCN	0.046	0.036	0.029
	H ₂ O···HC ₃ N	0.075	0.074	0.027
	HCN···H ₂ O	-0.188	-0.118	0.062
	HC ₃ N···H ₂ O	-0.188	-0.116	0.064
T-shape	CHCH···HF	-0.080	-0.078	0.094
	CHCH···HCl	0.025	0.020	0.046
	CHCH···HCN	0.046	0.015	0.036
	CHCH···HC ₃ N	0.075	0.051	0.033
Symmetric	HCOOH···HCOOH	-0.053	-0.012	0.055
	FCOOH···FCOOH	-0.015	0.016	0.064
	ClCOOH···ClCOOH	-0.034	-0.001	0.057
	BrCOOH···BrCOOH	-0.039	-0.005	0.055

TABLE VII. Charges and charge fluxes on hydrogen atoms not involved in the H-bond (boldface in the table). The net flux (dq_{tot}/dQ_{RH}) is referred to the acceptor (for the neutrality condition the global flux on the donor has the same absolute value of the acceptor one, but opposite sign).

	Acceptor donor	q_H isolated (e)	q_H dimer (e)	dq_H/dr_{RH} isolated (e/A)	dq_H/dr_{RH} dimer (e/A)	dq_{tot}/dQ_{RH} (e/A · amu ^{1/2})
Linear	HCN ··· HCN	0.258	0.252	0.046	0.071	0.002
	HC₃N ··· HCN	0.205	0.204	0.075	0.088	0.002
	HCN ··· HCl	0.258	0.248	0.046	0.074	0.000
	HCN ··· HF	0.258	0.250	0.046	0.082	0.000
	H₂O ··· HCN	0.330	0.335	-0.188	-0.144	0.004
	HCN ··· H₂O	0.258	0.251	0.046	0.066	0.000
	HCN ··· HC₃N	0.258	0.251	0.046	0.069	0.002
	HC₃N ··· HC₃N	0.205	0.204	0.075	0.087	0.002
	HC₃N ··· HF	0.205	0.204	0.075	0.091	0.002
	HC₃N ··· HCl	0.205	0.204	0.075	0.087	0.002
T-shape	CHCH ··· HF	0.218	0.219	0.020	0.047	0.006
	CHCH ··· HCl	0.218	0.213	0.020	0.041	0.007
	CHCH ··· HCN	0.218	0.215	0.020	0.036	0.004
	CHCH ··· HC₃N	0.218	0.213	0.020	0.035	0.004

Charge fluxes during the normal mode Q_{XH} show that the perturbation induced by the H-bond is less localized than what is shown by equilibrium charges. If we consider again the case of $\text{ClCOOH} \cdots \text{ClCOOH}$, we can verify that variations of the “static” charge on C and Cl are small, while dq_a/dQ_{XH} fluxes are large, showing variations reaching the 100% of their values in the isolated molecule (see Figures 2(a) and 3(d)).

In conclusion, we can state that the large charge fluxes responsible for the increase of the IR intensity of XH stretching band cannot be simply ascribed to the fluctuation of the charge localized on the hydrogen atom: this conclusion highlights again the importance of a method for the calculation of the whole set of ECCF parameters.

On the other hand, not all the normal modes of the dimers are affected by H-bond: for instance, the RH stretching of a RH bond not involved in the hydrogen bridge determines localized charge fluxes in most cases, both considering the isolated molecule and the complex. Indeed it is ineffective in determining net inter-molecular charge flux because of the vanishingly small values of the non-principal fluxes on the partner molecule. Furthermore, the formation of the H-bond only leads to a small variation of the principal charge flux

on the hydrogen atoms not involved in the H-bond. dq_H/dr_{RH} shows indeed a modulation not exceeding 0.02 e/A in all cases examined (see Table VII).

C. A test case: The cytosine-guanine dimer

In order to extend and to verify the reliability of the previous model for the study of larger systems we investigated the guanine-cytosine pair as a test case. This dimer has been selected due to the planar geometry of the complex, required for the applications of Eqs. (2) and (3).²³

This dimer adopts the planar Watson-Crick configuration with three H-bonds (see Figure 4). In agreement with previous works, based both on experimental³² and computational³³ evidences, we obtained a good description of the IR spectra. We calculated charges and charge fluxes by means of Eqs. (2), (3), and (5) for the dimer and for the isolated molecule of cytosine. In the case of guanine equilibrium charges for the isolated molecule are not reported: indeed the molecule does not possess a planar geometry when isolated, and the model for the calculation of ECCF does not apply

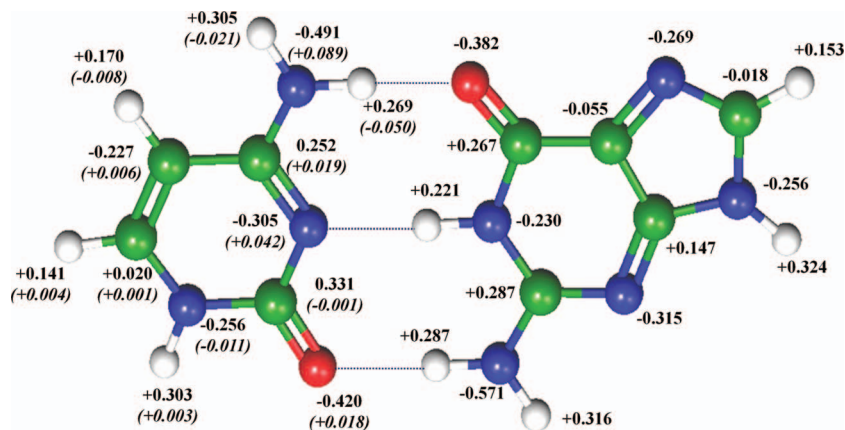


FIG. 4. Equilibrium IR charges (in units of e) of the cytosine-guanine dimer (PBE0/6-311++G(d,p)). In the case of cytosine we reported in parentheses the differences with respect to equilibrium charges of the isolated molecule.

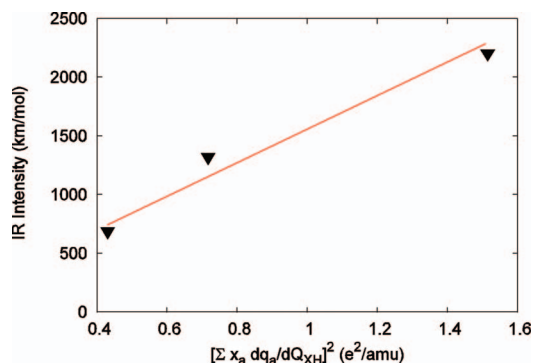


FIG. 5. Correlation between the IR intensity of NH stretching bands and the flux contributions for the three Q_{XH} modes of the cytosine-guanine dimer, evaluated according to Eq. (8) (units of e^2/amu , PBE0/6-311++G(d,p) calculations). The x-axis is oriented along the hydrogen bond. The fitting line obtained for the small dimers analyzed (data shown in Figure 2) is reported.

exactly in this case, while a suitable approximated method for the derivation of charge fluxes has not been developed yet.

Cytosine behaves as an acceptor for two of the three H-bonds, while in the third it plays the role of the donor (Figure 4). We, therefore, expect that the cytosine has a predominant character of acceptor and, according to the previous analysis, it is expected to carry a net positive charge, while guanine, having the nature of the donor, should be negatively charged. Our results show that after the formation of the H-bond cytosine actually takes a net charge of $+0.093e$.

Also in this case, the formation of H-bond leads to significant changes in the charge distribution only for the atoms directly involved or close to the H-bond. Again, the donor hydrogen of cytosine becomes less positive in the dimer, while the acceptor atoms (N and O) give electronic charge to the donor.

If we analyze the three modes of vibration associated with the H-bond (Figure 6), we can realize that each of them is the combination of one or more stretchings of the NH bonds involved in the hydrogen bridges, with small contributions from the stretching of the NH bonds of the NH_2 groups not directly involved in intermolecular bonds.

Despite the greater complexity of these normal modes, also in this case the eigenvectors analysis shows that the Q_{XH} mode is related to the oscillation of the hydrogen atoms between the donor and the acceptor while the centers of mass of the two molecules remain practically fixed.

Also the charge fluxes analysis confirms what has been previously stated:

The three NH stretching normal modes follow the nice correlation between the IR intensity and the fluxes contribution (Eq. (8)), already found for small dimers (Figure 5).

Mode A, at 3404 cm^{-1} , is mainly due to the stretching of the N(26)–H(28) bond ($\partial r_{26-28}/\partial Q_A = 0.998\text{ amu}^{-1/2}$) and to the corresponding out-of-phase stretching of the intermolecular bond O(10)··H(28) ($\partial r_{10-28}/\partial Q_A = -0.931\text{ amu}^{-1/2}$). Considering this bond, the guanine behaves as a donor and receives a net negative flux of $-0.200\text{ e}/(\text{A} \cdot \text{amu}^{1/2})$. The fluxes are not localized: indeed some of the ring atoms of cytosine show non-negligible fluxes due to the A normal mode. The flux on C(6) is, for example, $0.022\text{ e}/(\text{A} \cdot \text{amu}^{1/2})$ and

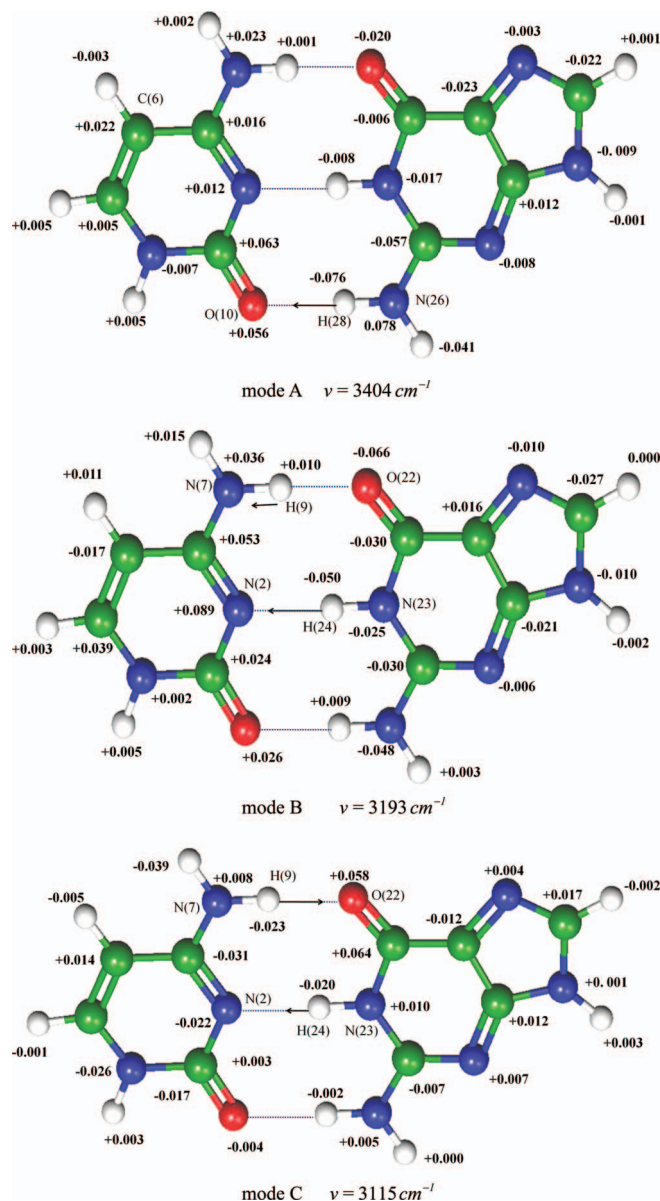


FIG. 6. Charge fluxes (in units of $e/\text{A} \cdot \text{amu}^{1/2}$) for the three Q_{XH} modes of the cytosine-guanine dimer (PBE0/6-311++G(d,p)).

it is due to a mode which is absent in the isolated molecule (the NH which stretches belong to guanine). Furthermore, we want to stress that also in this case the net flux (dq_H/dQ_{XH}) on H(28), which is indeed the only atom strongly involved in mode A, is only a partial contribution of the total flux on the donor.

Mode B, found at 3193 cm^{-1} , is given mainly by the stretching of the bond N(23)–H(24) ($\partial r_{23-24}/\partial Q_B = 0.958\text{ amu}^{-1/2}$ and $\partial r_{2-24}/\partial Q_B = -0.884\text{ amu}^{-1/2}$), but it contains a non-negligible contribution of N(7)–H(9) stretching ($\partial r_{7-9}/\partial Q_B = -0.356\text{ amu}^{-1/2}$ and $\partial r_{9-22}/\partial Q_B = 0.331\text{ amu}^{-1/2}$). Both molecules act then as acceptor and donor. Since the two components are in phase opposition, as for bidentate dimers, the two flux contributions add up together, originating a large total flux of $-0.295\text{ e}/(\text{A} \cdot \text{amu}^{1/2})$ on guanine. Indeed, also for this mode we find an electron flux from the donor to the acceptor fragment, upon elongation of the XH bond.

The mode C, which falls at 3115 cm^{-1} , is a combination of the N(7)–H(9) and N(23)–H(24) stretching as in the previous case, although now the contribution due to the stretching of N(7)–H(9) is dominant. Thus, considering the H bond mainly involved in the normal mode, the cytosine molecule plays the role of the donor. For this mode the two stretchings are in phase, the two flux contributions have opposite sign and partially cancel each other. The global flux on the donor, is therefore of small magnitude ($0.138\text{ e/A} \cdot \text{amu}^{1/2}$). It is interesting to observe that for this the normal mode the donor character is dominant for cytosine ($\partial r_{7-9}/\partial Q_C = 0.954\text{ amu}^{-1/2}$ while $\partial r_{23-24}/\partial Q_C = 0.363\text{ amu}^{-1/2}$), and the flux of electrons proceeds from guanine to cytosine.

IV. CONCLUSIONS

Our results show that atomic charge and charge fluxes obtained by means of the ECCF model and DFT calculated APTs can provide a rationalization of hydrogen bonding effects in terms of molecular charge distribution and its mobility. Furthermore, a detailed interpretation of IR intensity behavior can be obtained and it can be related to atomic parameters.

It has been proven that not only atomic charges at the equilibrium but also charge fluxes during vibrational motions are very important for the investigation of the physico-chemical properties of molecular systems and in some cases, such that of hydrogen bonded dimers, the latter are even more important. The application here presented demonstrates that both analytical models and current state-of-the-art computational methods have reached a suitable accuracy. This will allow us to extend this analysis to larger systems such as molecular materials and biological molecules. In this way we will be able to understand some phenomena which could affect their structure; at the same time it will be possible to better describe molecules interaction with the environment. The model here applied is still limited to the case of planar systems; however, similarly to the case of atomic charges,³ we believe that it would be possible to extend the model for the calculation of approximated charge fluxes also in non-planar systems. The development of such a general theory would be beneficial not only for spectroscopy experts as a tool for the rationalization of the IR intensity behavior, but also for many other applications of interest in the field of computational and experimental chemical physics.

¹M. P. Allen and T. J. Tildesley, *Computer Simulation of Liquids* (Clarendon Press, Oxford, 1987).

²C. F. Guerra, J. W. Handgraaf, E. J. Baerends, and F. M. Bickelhaupt, *J. Comput. Chem.* **25**, 189 (2004); F. De Proft, J. M. L. Martin and P. Geerling, *Chem. Phys. Lett.* **250**, 393 (1996); F. Martin and H. Zipse, *J. Comput. Chem.* **26**, 97 (2005); H. Hu and W. Yang, *J. Chem. Theory Comput.* **3**, 1004 (2007); F. De Proft, C. Van Alsenoy, A. Peeters, W. Langenaeker and P. Geerlings, *J. Comput. Chem.* **23**, 1198 (2002); E. Sigfridsson and U. Ryde, *ibid.* **19**, 377 (1998); F. De Proft, P. Geerlings, and J. M. L. Martin, in *Recent Developments and Applications of Modern Density Functional Theory*, edited by J. M. Seminario (Elsevier Science B.V., Amsterdam 1996).

³A. Milani, M. Tommasini, and C. Castiglioni, *Theor. Chem. Acc.* **131**, 1139 (2012).

⁴L. M. Sverdlov, M. A. Kovner, and E. P. Krainov, *Vibrational Intensities of Polyatomic Molecules* (Wiley, New York, 1972); J. Overend, "Quantitative intensity studies and dipole moment derivatives," in *Infrared Spectroscopy and Molecular Structure*, edited by M. Davies (Elsevier, Amsterdam, 1963), p. 345; W. B. Person *Vibrational Intensities in Infrared and Raman Spectroscopy*, edited by G. Zerbi (Elsevier Scientific publishing company, Amsterdam, 1982).

⁵J. F. Biarge, J. Herranz, and J. Morcillo, *Ann. R. Soc. Espan. Fis. Quim.* **A57**, 81 (1961); W. B. Person and J. B. Newton, *J. Chem. Phys.* **61**, 1040 (1974).

⁶L. A. Gribov, *Intensity Theory for Infrared Spectra of Polyatomic Molecules* (Consultant's Bureau, New York, 1964); M. Gussoni and S. Abbate, *J. Chem. Phys.* **65**, 3439 (1976); M. Gussoni, *Prik. Spectrosc.* **XLII**, 265 (1985).

⁷J. C. Decius, *J. Mol. Spectrosc.* **57**, 348 (1975); A. J. van Straten and W. M. A. Smit, *J. Mol. Spectrosc.* **62**, 297 (1976).

⁸W. T. King and G. B. Mast, *J. Phys. Chem.* **80**, 2521 (1976); W. T. King, G. B. Mast, and P. P. Blanchette, *J. Chem. Phys.* **56**, 4440 (1972).

⁹A. Milani and C. Castiglioni, *J. Phys. Chem. A* **114**, 624 (2010).

¹⁰A. Milani, D. Galimberti, C. Castiglioni, and G. Zerbi, *J. Mol. Struct.* **976**, 342 (2010).

¹¹A. Milani and C. Castiglioni, *J. Mol. Struct.:THEOCHEM* **955**, 158 (2010).

¹²M. Gussoni, C. Castiglioni, and G. Zerbi, *J. Phys. Chem.* **88**, 600 (1984).

¹³M. Gussoni, C. Castiglioni, and G. Zerbi, *Handbook of Vibrational Spectroscopy*, edited by J. Chalmers and P. Griffiths (John Wiley and Sons, Chichester, UK, 2001), Vol. 3, p. 2040.

¹⁴N. B. Da Costa, A. J. A. Aquino, M. N. Ramos, C. Castiglioni, and G. Zerbi, *J. Mol. Struct.:THEOCHEM* **305**, 19 (1994); C. Castiglioni, M. Gussoni, and G. Zerbi, *J. Mol. Struct.* **198**, 475 (1989); **141**, 341 (1986); P. Jona, M. Gussoni, and G. Zerbi, *J. Phys. Chem.* **85**, 2210 (1981).

¹⁵C. Castiglioni, M. Gussoni, and G. Zerbi, *J. Chem. Phys.* **82**, 3534 (1985).

¹⁶M. Gussoni, C. Castiglioni, M. Miragoli, G. Lugli, and G. Zerbi, *Spectrochim. Acta: A-M* **41**, 371 (1985); C. Castiglioni, M. Gussoni, and G. Zerbi, *Solid State Commun.* **56**, 863 (1985).

¹⁷M. Gussoni, C. Castiglioni, and G. Zerbi, *J. Chem. Phys.* **80**, 1377 (1984); *Chem. Phys. Lett.* **99**, 101 (1983); C. Castiglioni, M. Gussoni, and G. Zerbi, *J. Chem. Phys.* **80**, 3916 (1984).

¹⁸R. C. M. U. Araujo, J. B. P. Da Silva, and M. N. Ramos, *Spectrochim. Acta A* **51**, 821 (1995); V. H. Rusu, J. B. P. Da Silva, and M. N. Ramos, *Vib. Spectrosc.* **46**, 52 (2008); K. C. Lopes, F. S. Pereira, R. C. M. U. De Araujo, and M. N. Ramos, *J. Mol. Struct.* **565–566**, 417 (2001); M. N. Ramos, K. C. Lopes, W. L. V. Silva, A. M. Tavares, F. A. Castriani, S. A. Do Monte, E. Ventura, and R. C. M. U. Araujo, *Spectrochim. Acta A* **63**, 383 (2006).

¹⁹R. L. A. Haiduke and R. E. Bruns, *J. Phys. Chem. A* **109**, 2680 (2005).

²⁰J. V. Da Silva, R. L. A. Haiduke, and R. E. Bruns, *J. Phys. Chem. A* **110**, 4839 (2006); J. V. Da Silva, S. H. D. M. Faria, R. L. A. Haiduke, and R. E. Bruns, *ibid.* **111**, 515 (2007); S. H. D. M. Faria, J. V. Da Silva, R. L. A. Haiduke, L. N. Vidal, P. A. M. Vazquez, and R. E. Bruns, *ibid.* **111**, 7870 (2007).

²¹H. Torii, *J. Chem. Phys.* **133**, 034504 (2010); *J. Phys. Chem. Lett.* **3**, 112 (2012).

²²H. Torii, *J. Phys. Chem. B* **114**, 13403 (2010); *J. Phys. Chem. A* **117**, 2044 (2013).

²³D. Galimberti, A. Milani, and C. Castiglioni, *J. Chem. Phys.* **138**, 164115 (2013).

²⁴U. Dinur, *J. Phys. Chem.* **95**, 6201 (1991); *Chem. Phys. Lett.* **166**, 211 (1990); U. Dinur and A. T. Hagler, *J. Chem. Phys.* **91**, 2949 (1989).

²⁵M. J. Frisch, G. W. Trucks, H. B. Schlegel *et al.*, GAUSSIAN 09, Revision A.1, Gaussian, Inc., Wallingford, CT, 2009.

²⁶S. F. Boys and F. Bernardi, *Mol. Phys.* **19**, 553 (1970); S. Simon, M. Duran, and J. J. Dannenberg, *J. Chem. Phys.* **105**, 11024 (1996).

²⁷G. C. Pimentel and A. L. McClellan, *The Hydrogen Bond* (W.H. Freeman, San Francisco, 1960).

²⁸E. B. Wilson, J. C. Decius, and P. C. Cross, *Molecular Vibrations* (McGraw Hill, New York, 1955).

²⁹P. Gilli and G. Gilli, *J. Mol. Struct.* **972**, 2 (2010).

³⁰R. W. Gora, S. J. Grabowski, and J. Leszczynski, *J. Phys. Chem. A* **109**, 6397 (2005); G. Baranovic, N. Biliskov, and D. Vojta, *ibid.* **116**, 8397 (2012).

³¹A. E. Reed, L. A. Curtiss, and F. Weinhold, *Chem. Rev.* **88**, 899 (1988); A. E. Reed, R. B. Weinstock, and F. Weinhold, *J. Chem. Phys.* **83**, 735 (1985).

³²M. Yang, L. Szyc, K. Rottger, H. Fidler, E. T. J. Nibbering, T. Elsaesser, and F. Temps, *J. Phys. Chem. B* **115**, 5484 (2011).

³³R. Santamaria, E. Charro, A. Zacarias, and M. Castro, *J. Comput. Chem.* **20**, 511 (1999).

3.3 Summary and Conclusions

The IR intensities parameters have shown to be powerful tools in the interpretation of both intra and inter-molecular effects. In particular they allowed to describe the molecular charge distribution in terms of static and dynamical parameters, such as atomic charges and charge fluxes, that have the important advantage of being directly related to experimentally measurable quantities.

While many previous investigations focused mainly on the analysis of equilibrium charges, we revisited the model proposed by Dinur [43,44], to develop and implement a method for the calculation of a complete and unique set of charge and charge fluxes parameter for planar molecules.

The consistency of our model with the partitioning of the atomic polar tensors into atomic charge and charge fluxes have been proved.

Regarding this, it is important to remember how the DFT calculated APTs can be used to predict the IR intensities both in the standard *static* approach where the vibrational spectrum is calculated in double harmonic approximation for equilibrium structures, but also in the *dynamic* approach, based on First-Principle Molecular Dynamics (FPMD) simulations. Indeed, as we will illustrate in Section 4.2, it is possible to evaluate the IR spectrum from the correlation functions of the APTs, derived from the trajectory of the molecules in their phase space.

We tested the validity of the model for several small benchmark molecules, proving its reliability. We also demonstrate that the parameters derived from the APTs can provide a rationalization of the intermolecular behaviour, in terms of molecular charge distribution and its mobility. In particular, in the case of the H-bond, a detailed interpretation of the enhancement of the X–H stretching band observed upon aggregation have been obtained.

In general our model shows that not only static atomic charges but also charge fluxes during vibrational motions are very important for the investigation of the physicochemical properties of molecular systems and in some cases, such that of hydrogen bonded dimers, the latter are even more important.

Moreover, both principal and non-principal charge fluxes have an important role for the rationalization of the spectral behaviour; we demonstrate that for example in the case of the H-bond, the modulation of the charge distribution during vibrational motions of the $-XH \cdots Y-$ fragment is not localized exclusively on the atoms directly involved in hydrogen bonding. From this it is possible to see how a model that allowed to calculate the whole set of both principal and non-principal fluxes has important application for the detailed investigation of intramolecular and intermolecular interaction.

Despite the potentiality, the model here applied has a strong limitation: its validity is limited to the case of planar systems and many molecules of interest are partially or totally non-planar. However, similarly to the case of atomic charges, we believe that it would be possible to extend the model for the calculation of approximated charge fluxes also in non-planar systems.

Actually, while often non-principal fluxes are far from being negligible, we demonstrate a partial character of localization, paving the way to the possibility to extend the model for the calculation of approximated charge fluxes in non planar systems.

This will allow to extend this analysis to larger systems such as molecular materials and biological molecules. In this way we will be able to understand some phenomena which could affect their structure; at the same time it will be possible to better describe molecular interaction with the environment.

Bibliography

- [1] W.B. Person, G. Zerbi, *Vibrational intensities in infrared and Raman spectroscopy*, Elsevier Science Ltd, 1982.
- [2] L.M. Sverdlov, M.A. Kovner, E.P. Krainov, *Vibrational Intensities of Polyatomic Molecules*, Wiley, New York, 1972.
- [3] W.B. Person, J.H. Newton, Dipole moment derivatives and infrared intensities. I. Polar tensors, *J. Chem. Phys.* 61 (1974) 1040–1049. doi:10.1063/1.1681972.
- [4] J.F. Biarge, J. MORCILLO, J. HERRANZ, ON INTERPRETATION OF INFRARED INTENSITIES IN GASES, in: *An. REAL Soc. ESPANOLA Fis. QUIMICA*, 1961: p. 81.
- [5] L.A. Gribov, *Intensity theory for infrared spectra of polyatomic molecules*, Consultants Bureau, 1964.
- [6] M. Gussoni, S. Abbate, Infrared absorption intensities: Transferability of electro-optical parameters, *J. Chem. Phys.* 65 (1976) 3439–3445. doi:10.1063/1.433597.
- [7] M. Gussoni, *Prik Spectrosk XLII*. (1985) 265.
- [8] J.C. Decius, An effective atomic charge model for infrared intensities, *J. Mol. Spectrosc.* 57 (1975) 348–362. doi:10.1016/0022-2852(75)90296-9.
- [9] A.J. van Straten, W.M.A. Smit, Bond charge parameters from integrated infrared intensities, *J. Mol. Spectrosc.* 62 (1976) 297–312. doi:10.1016/0022-2852(76)90271-X.
- [10] W.T. King, G.B. Mast, Infrared intensities, polar tensors, and atomic population densities in molecules, *J. Phys. Chem.* 80 (1976) 2521–2525. doi:10.1021/j100563a018.
- [11] W.T. King, G.B. Mast, P.P. Blanchette, Infrared Intensity Sum Rule and Effective Charges, *J. Chem. Phys.* 56 (1972) 4440–4446. doi:10.1063/1.1677887.

- [12] J.E.B. Wilson, J.C. Decius, P.C. Cross, *Molecular Vibrations: The Theory of Infrared and Raman Vibrational Spectra*, New edition edition, Dover Publications, New York, 1980.
- [13] R.S. Mulliken, Electronic Population Analysis on LCAO–MO Molecular Wave Functions. I, *J. Chem. Phys.* 23 (1955) 1833–1840. doi:10.1063/1.1740588.
- [14] R.F.W. Bader, *A quantum theory of molecular structure and its applications*, *Chem. Rev.* 91 (1991) 893–928. doi:10.1021/cr00005a013.
- [15] A.E. Reed, R.B. Weinstock, F. Weinhold, Natural population analysis, *J. Chem. Phys.* 83 (1985) 735–746. doi:10.1063/1.449486.
- [16] A.E. Reed, L.A. Curtiss, F. Weinhold, Intermolecular interactions from a natural bond orbital, donor-acceptor viewpoint, *Chem. Rev.* 88 (1988) 899–926. doi:10.1021/cr00088a005.
- [17] B. Besler, K. Merz, P. Kollman, Atomic Charges Derived from Semiempirical Methods, *J. Comput. Chem.* 11 (1990) 431–439. doi:10.1002/jcc.540110404.
- [18] U.C. Singh, P.A. Kollman, An approach to computing electrostatic charges for molecules, *J. Comput. Chem.* 5 (1984) 129–145. doi:10.1002/jcc.540050204.
- [19] L. Chirlian, M. Francl, Atomic Charges Derived from Electrostatic Potentials - a Detailed Study, *J. Comput. Chem.* 8 (1987) 894–905. doi:10.1002/jcc.540080616.
- [20] C. Breneman, K. Wiberg, Determining Atom-Centered Monopoles from Molecular Electrostatic Potentials - the Need for High Sampling Density in Formamide Conformational-Analysis, *J. Comput. Chem.* 11 (1990) 361–373. doi:10.1002/jcc.540110311.
- [21] A. Milani, M. Tommasini, C. Castiglioni, Atomic charges from IR intensity parameters: theory, implementation and application, *Theor. Chem. Acc.* 131 (2012). doi:10.1007/s00214-012-1139-5.
- [22] A. Milani, D. Galimberti, C. Castiglioni, G. Zerbi, Molecular charge distribution and charge fluxes from Atomic Polar Tensors: The case of OH bonds, *J. Mol. Struct.* 976 (2010) 342–349. doi:10.1016/j.molstruc.2010.03.031.
- [23] M. Gussoni, M. Ramos, C. Castiglioni, G. Zerbi, Abinitio Counterpart of Infrared Atomic Charges, *Chem. Phys. Lett.* 142 (1987) 515–518. doi:10.1016/0009-2614(87)80654-1.
- [24] M. Gussoni, C. Castiglioni, M.N. Ramos, M. Rui, G. Zerbi, Infrared intensities: from intensity parameters to an overall understanding of the spectrum, *J. Mol. Struct.* 224 (1990) 445–470. doi:10.1016/0022-2860(90)87033-T.
- [25] M. Ramos, M. Gussoni, C. Castiglioni, G. Zerbi, Abinitio Counterpart of Infrared Atomic Charges - Comparison with Charges Obtained from Electrostatic Potentials, *Chem. Phys. Lett.* 151 (1988) 397–402. doi:10.1016/0009-2614(88)85156-X.

- [26] R.L.A. Haiduke, R.E. Bruns, An atomic charge-charge flux-dipole flux atom-in-molecule decomposition for molecular dipole-moment derivatives and infrared fundamental intensities, *J. Phys. Chem. A*. 109 (2005) 2680–2688. doi:10.1021/jp045357u.
- [27] J.V. da Silva, R.L.A. Haiduke, R.E. Bruns, QTAIM charge-charge flux-dipole flux models for the infrared fundamental intensities of the fluorochloromethanes, *J. Phys. Chem. A*. 110 (2006) 4839–4845. doi:10.1021/jp060553h.
- [28] J.V. da Silva, S.H.D.M. Faria, R.L.A. Haiduke, R.E. Bruns, QTAIM charge-charge flux-dipole flux models for the infrared fundamental intensities of difluoro- and dichloroethylenes, *J. Phys. Chem. A*. 111 (2007) 515–520. doi:10.1021/jp065422v.
- [29] S.H.D.M. Faria, J.V. da Silva, R.L.A. Haiduke, L.N. Vidal, P.A.M. Vazquez, R.E. Bruns, Quantum theory of atoms in molecules charge-charge flux-dipole flux models for the infrared intensities of X₂CY (X = H, F, Cl; Y = O, S) molecules, *J. Phys. Chem. A*. 111 (2007) 7870–7875. doi:10.1021/jp072763f.
- [30] J. Cioslowski, A New Population Analysis Based on Atomic Polar Tensors, *J. Am. Chem. Soc.* 111 (1989) 8333–8336. doi:10.1021/ja00204a001.
- [31] M. Gussoni, C. Castiglioni, G. Zerbi, Physical meaning of electrooptical parameters derived from infrared intensities, *J. Phys. Chem.* 88 (1984) 600–604. doi:10.1021/j150647a053.
- [32] V.H. Rusu, J.B.P. da Silva, M.N. Ramos, Influence of the F-H center dot center dot center dot N hydrogen bond on the C-H isolated stretching in aromatic azines, *Vib. Spectrosc.* 46 (2008) 52–56. doi:10.1016/j.vibspec.2007.09.002.
- [33] K.C. Lopes, F.S. Pereira, R. de Araujo, M.N. Ramos, An ab initio study of the structural and vibrational properties of the C₃H₆-HCN, C₂H₄-HCN and C₂H₂-HCN hydrogen-bonded complexes, *J. Mol. Struct.* 565 (2001) 417–420. doi:10.1016/S0022-2860(00)00932-7.
- [34] M.N. Ramos, K.C. Lopes, W.L.V. Silva, A.M. Tavares, F.A. Castriani, S.A. do Monte, et al., An ab initio study of the C₂H₂-HF, C₂H(CH₃)-HF and C-2(CH₃)₂-HF hydrogen-bonded complexes, *Spectrochim. Acta Part -Mol. Biomol. Spectrosc.* 63 (2006) 383–390. doi:10.1016/j.saa.2005.05.024.
- [35] C. Castiglioni, M. Gussoni, G. Zerbi, *Handbook of Vibrational Spectroscopy*, edited by J. Chalmers and P. Griffiths, John Wiley and Sons, Chichester, UK, 2001.
- [36] A. Milani, C. Castiglioni, Modeling of Molecular Charge Distribution on the Basis of Experimental Infrared Intensities and First-Principles Calculations: The Case of CH Bonds, *J. Phys. Chem. A*. 114 (2010) 624–632. doi:10.1021/jp908146d.

- [37] F.L. Hirshfeld, Bonded-atom fragments for describing molecular charge densities, *Theor. Chim. Acta.* 44 (1977) 129–138. doi:10.1007/BF00549096.
- [38] H. Torii, Intermolecular charge flux as the origin of infrared intensity enhancement upon halogen-bond formation of the peptide group, *J. Chem. Phys.* 133 (2010) 034504. doi:10.1063/1.3456183.
- [39] H. Torii, Mechanism of the Secondary Structure Dependence of the Infrared Intensity of the Amide II Mode of Peptide Chains, *J. Phys. Chem. Lett.* 3 (2012) 112–116. doi:10.1021/jz201540r.
- [40] C. Castiglioni, M. Gussoni, Intramolecular Electrical and Dynamical Interactions in Formaldehyde - a Discussion Based on Infrared Intensity Data, *J. Chem. Phys.* 82 (1985) 3534–3542. doi:10.1063/1.448932.
- [41] M. Gussoni, C. Castiglioni, M. Miragoli, G. Lugli, G. Zerbi, Derivation of Charge-Distribution from Infrared Intensities - the Case, *Spectrochim. Acta Part -Mol. Biomol. Spectrosc.* 41 (1985) 371–380. doi:10.1016/0584-8539(85)80118-5.
- [42] C. Castiglioni, G. Zerbi, M. Gussoni, Peierls Distortion in Trans Polyacetylene - Evidence from Infrared Intensities, *Solid State Commun.* 56 (1985) 863–866. doi:10.1016/0038-1098(85)90421-1.
- [43] U. Dinur, On the Interpretation of Infrared Intensities in Planar Molecular-Systems, *Chem. Phys. Lett.* 166 (1990) 211–216. doi:10.1016/0009-2614(90)87277-X.
- [44] U. Dinur, Charge Flux and Electrostatic Forces in Planar Molecules, *J. Phys. Chem.* 95 (1991) 6201–6211. doi:10.1021/j100169a030.
- [45] G. Pimentel, A. McClellan, *The Hydrogen Bond*, W. H. Freeman And Company, 1960. <http://archive.org/details/hydrogenbond031051mbp> (accessed November 23, 2015).
- [46] H. Torii, Intra- and Intermolecular Charge Fluxes Induced by the OH Stretching Mode of Water and Their Effects on the Infrared Intensities and Intermolecular Vibrational Coupling, *J. Phys. Chem. B.* 114 (2010) 13403–13409. doi:10.1021/jp106952q.
- [47] H. Torii, Extended Nature of the Molecular Dipole of Hydrogen-Bonded Water, *J. Phys. Chem. A.* 117 (2013) 2044–2051. doi:10.1021/jp4013015.

Chapter 4

First-Principles molecular dynamics simulations for the prediction of the structure and vibrational spectra of complex systems

4.0 Introduction

In previous chapters we showed that quantum-chemical calculations can provide important information about the molecular structure in terms of intra and intermolecular interactions, and how these molecular effects can drastically influence also the macroscopic properties of the system. By focusing on vibrational spectroscopy in particular, we demonstrated the importance of these techniques to support the interpretation of the experimental measurements and to rationalize the physical effects taking place.

So far, the prediction of IR vibrational spectra has been carried out according to the usual approach, where, after geometry optimizations, the spectra are computed in double harmonic approximation. We will conventionally refer to this approach as to *static* approach.

Despite its reliability and accuracy, this procedure suffers however some intrinsic limitations:

1) Simulation for an individual equilibrium structure at once

When more than one minimum of the potential energy surface exists (e.g. conformational flexible systems ...), all the minimum geometries of the system need to be taken into account, or at least those showing non-negligible population at a chosen temperature. Indeed the final spectrum must include the contribution of all the relevant structures to be compared with the experimental one.

While increasing the dimension of the system under study, and moving from an ordered phase (i.e. crystals) to a disordered phase (i.e. amorphous, liquid, gas phase) the exploration of such a multi-dimensional potential energy surface becomes an expensive and complex task, and rapidly becomes unfeasible. Moreover, the simulation of the real spectrum requires that a huge number of spectra (one for each stable structure) is calculated and averaged properly. In the case of large flexible molecules, when explicitly introducing solvent molecules or for large supermolecular systems, these can be critical issues.

2) Non-trivial description of environmental effects

No information about the external variables (temperature, pressure, external forces) is present in *static* calculations. They must be introduced with *ad hoc* procedures (e.g. the PCM [1] for the description of solvent effects) or by means of specific models which cannot straightforwardly and automatically be extended to other cases.

3) Band shape

The spectrum profile is obtained from the computed IR intensities (i.e. from the set of $|\partial\boldsymbol{\mu}/\partial Q_i|^2$ values), by assuming that each absorption band is characterized by a Lorentzian shape with fixed band width. The band widths are arbitrarily selected to obtain a good fit of the experimental features and cannot describe at all the inhomogeneous broadening phenomena which affects the experimental results.

In recent years, an alternative method has been exploited for the prediction of the vibrational spectra in the framework of first order perturbation theory. According to this formalism, the IR intensity $I(\omega)$ can be written as [2,3]:

$$I(\omega) \propto \int dt e^{i\omega t} \langle \boldsymbol{\mu}(t) \boldsymbol{\mu}(0) \rangle \quad (4.1)$$

where $\boldsymbol{\mu}(t)$ is the instantaneous dipole moment of the system at the time t .

The correlation function of the dipole moment $\langle \partial\boldsymbol{\mu}(t) \partial\boldsymbol{\mu}(0) \rangle$ can be easily evaluated from a molecular dynamic simulation, where external parameters, such as temperature, pressure, stresses, can be straightforwardly included in the calculations, by using standard algorithms and well-assessed methods (e.g. thermostat, barostat...).

Moreover, during suitably long trajectories, the system is free to explore all the accessible points on the potential energy surface. Therefore the different intramolecular (i. e. molecular conformations) and intermolecular configurations (e.g. clusters formation) can be automatically sampled and give their contribution to the total dipole correlation function and hence to the IR spectrum. No arbitrary models for the determination of band shapes are required, since Eq. (4.1) already provides the whole spectrum profile automatically predicting the inhomogeneous broadening of the bands.

Due to the need of a very accurate description of the vibrational force field (second derivatives of the molecular potential) and of the dipole moment, classical molecular dynamics simulations cannot guarantee the accuracy required for the description of the vibrational properties and quantum chemical calculations are mandatory to this aim. On the other hand, full quantum dynamics is not yet affordable for systems of more than a couple of atoms due to the huge computational cost required.

A good compromise between computation cost and accuracy are First Principles MD (FPMD) simulations: in this case the nuclei are moving following the Newton classical equations of motion, but the forces are evaluated at each time step by solving the electronic problem in Born-Oppenheimer approximation (BOMD). The solution of the electronic problem is usually carried out in the framework of DFT and opens the possibility to give an accurate evaluation of the vibrational force field while keeping all the advantages of a *dynamic*

approach capable to describe in a realistic way the trajectory of the molecules in a given time interval and in a given environment.

In this perspective, the CP2K code is very powerful and its capabilities have been widely demonstrated [4] in the last years.

Indeed, First Principles MD (FPMD) simulations recently appeared as an intriguing alternative to standard *static* calculations for the prediction of the vibrational properties of molecular systems [5–8]. In this context, however, applications are still limited and their extensions to many different fields of molecular and materials science are lacking.

In the next chapter we will explore the advantages and limitations of this technique (called here *dynamic*), in the two cases of a flexible halogenated molecule in condensed phase (Section 4.1) and for crystalline polyethylene (Section 4.3).

The computational setups protocols and procedures for a reliable prediction of the spectra will be investigated in details and we will also propose a method to overcome some of the limitations found for this approach (Section 4.2).

4.1 *Static vs dynamic* DFT prediction of IR spectra of flexible molecules in condensed phase: the (ClCF₂CF(CF₃)OCF₂CH₃) molecule as a test case

To discuss the advantage and the limitations of the *static* and *dynamic* approaches for prediction of the IR spectrum of condensed phase systems, we carried out a computational investigation on the (ClCF₂CF(CF₃)OCF₂CH₃) molecule, named N1. The computed spectra were compared to the experimental gas phase and liquid phase spectra of the system, registered by researchers of Solvay Specialty Polymers.

N1 molecule is a partially halogenated ether with a quite flexible structure that, at room temperature, explores a large portion of the potential surface, implying the co-existence of different conformers which contribute to the vibrational spectra. This behaviour makes N1 an ideal test case to investigate the reliability and the potentialities of MD-based computational techniques in vibrational spectroscopy.

On one hand, a *static* approach, based on usual DFT computations allows to identify the several stable conformers of N1 (through simulations *in vacuo*) and to calculate its IR response at finite temperatures as a sum of the contributions of the different conformers, weighted according to the Boltzmann distribution. The availability of the Raman spectrum at room temperature, allowed a further validation of this approach.

On the other hand, in the case of the *dynamic* approach the simulations have been carried out by means of the CP2K code on the condensed phase system using different kinds of equilibrations (NVT or NpT), and on the isolate molecule.

As illustrated in the paper “*Static vs dynamic DFT prediction of IR spectra of flexible molecules in condensed phase: the (ClCF₂CF(CF₃)OCF₂CH₃) molecule as a test case*” (D. Galimberti, A. Milani, M.P. Gaigeot, S. Radice, C. Tonelli, R. Picozzi, C. Castiglioni) here reported as a draft manuscript, FPMD simulations shows to be a promising technique in the study of the spectroscopic response of flexible molecules in condensed phases, even if they show a few limitations together with their interesting potentialities.

In the following draft, *static* and *dynamic* approaches are discussed in details in order to understand their limits of applications and the possible role that FPMD could play in the next future in the field of polymer's science and characterization.

Static vs dynamic DFT prediction of IR spectra of flexible molecules in condensed phase: the (ClCF₂CF(CF₃)OCF₂CH₃) molecule as a test case

Daria Galimberti*^a, Alberto Milani^a, Marie-Pierre Gaigeot^b, Stefano Radice^c, Claudio Tonelli^c,
Rosaldo Picozzi^c, Chiara Castiglioni^a

^a *Politecnico di Milano – Dip. Chimica, Materiali, Ing. Chimica “G. Natta”*

P.zza Leonardo da Vinci 32 – 20133 Milan, Italy

^b LAMBE CNRS UMR8587, Université d'Evry val d'Essonne, Boulevard F. Mitterrand, BatMaupertuis,
91025 Evry, France

^c Solvay Specialty Polymers RD&T Center, Viale Lombardia 20 20021 Bollate (MI) Italy

Abstract

First-principles molecular dynamics (FPMD) calculations in the framework of Density Functional Theory (DFT) are carried out for the prediction of the infrared spectrum of the fluorinated molecule ClCF₂CF(CF₃)OCF₂CH₃. This molecule is characterized by a flexible structure, allowing the co-existence of several stable conformers, showing different equilibrium values of the torsional angles.

The performances of the *dynamic* approach – by means of FPMD simulations - are critically assessed through the comparison with experimental spectra. Moreover, the advantages and limitations of FPMD results are discussed with respect to the *static* approach, based on the overlay of the DFT predicted spectroscopic response of each individual stable conformer, obtained through vibrational normal modes from harmonic intramolecular potential energy. FPMD approach showed good potentialities, especially for the calculation of the spectra of the liquid phase. In this case, intermolecular collisions speed up the exploration of the whole conformational space, even for relatively short trajectories, and the infrared marker bands of the relevant stable structure are obtained with just one simulation.

Keywords: vibrational spectroscopy; quantum chemical simulations; ab-initio molecular dynamics; conformational potential; halogenated molecules;

I. Introduction

The characterization of several phenomena occurring at the nanoscale is a fundamental issue in materials science and chemical physics and to this aim a wide range of useful techniques have been developed. Among the most adopted, vibrational spectroscopy (IR and Raman) plays a very important role, due to the possibility to extract important information about the molecular structure but also about intramolecular and intermolecular interactions, which can drastically influence the properties of the system also at the macroscale. In this framework, computational approaches have become a very important and powerful tool to support the interpretation of the experimental spectra and to rationalize the physical effects taking place. Due to the need of a very accurate description of the vibrational force field (second derivatives of the molecular potential), classical molecular dynamics simulations cannot guarantee such an accuracy and quantum chemical calculations must be adopted. Despite the continuous improvements in hardware technology, the computational cost of these calculations is related to the choice of suitable models to represent the system under investigation and could be particularly demanding if large and flexible molecules are studied. The usual approach consists in starting from an input *guess* molecular geometry, running a structure optimization to search for a minimum in the potential energy surface and then computing the vibrational spectrum for the equilibrium structure obtained, through the calculation of the second derivatives of the potential energy (frequencies), the first derivative of the dipole moment (IR intensities) or of the polarizability tensor (Raman activities). This approach will be called here *static* since no information about large scale dynamical evolution of the system is taken into account, as for instance a jump over a potential barrier resulting in a change of the molecular conformation or intermolecular collisions in condensed phases.

It is quite evident that the *static* approach has some intrinsic weaknesses:

- 1) When more than one minimum of the intramolecular potential energy surface exists, we need to take into account each of these minima (or at least the lower energy ones), to compute the IR spectrum for each stable conformer and then to generate properly an average spectrum to be compared with the experimental one.
- 2) if the size of the molecule investigated exceeds the capability of the computational resources, suitable smaller molecular models should be chosen, to take into account the relevant effects having place for the real molecule.
- 3) no intermolecular effects are explicitly included (namely solvent effects, crystal field effects, interaction with other molecules often are neglected); no information about the external variables (temperature, pressure, external forces) are present in *static* calculations.
- 4) Spectra are computed in double harmonic approximations and thus anharmonic effects are lacking.

- 5) The spectrum profile is obtained from the computed IR transition probabilities (i. e. from the set of $|\partial\mu/\partial Q_i|^2$ values), assuming that each absorption band is characterized by a Lorentzian shape with fixed band width, described through a Γ_i parameter arbitrarily selected in order to obtain a good fit of the experimental features.

Methods have been developed to overcome some of the above limitations: for example calculations made on clusters of molecules can introduce the most relevant intermolecular effects; in the case of macromolecules or crystals, periodic boundary conditions allow to give a faithful description of the real crystal taking into account both intra and intermolecular interactions [1–4]; continuum methods (e.g. Polarizable Continuum Method (PCM) [5]) allow to introduce solvent effects; moreover, efficient methods have been recently implemented to compute anharmonic contributions [6–10].

However, other issues, such as the description of the different contributions to the spectra coming from all the relevant equilibrium structures co-existing at a given temperature is usually left to the intuition of the investigator. This often requires *ad hoc* procedures which can be partially arbitrary and cannot straightforwardly and automatically be extended to different cases. Furthermore, while increasing the dimension of the system under study, all these procedures become more and more cumbersome and computationally expensive. Indeed, the exploration of a multi-dimensional potential surface may become a complex task and the simulation of the real spectrum may require that a huge number of spectra (one for each stable structure) is calculated. Moreover, the description of vibrational motions in terms of small atomic displacements around some well-defined equilibrium geometry may become fully inadequate when large amplitude torsional motions occur, as indeed it happens in the case of flexible molecules at high temperature. On the other hand, the effect of the external variables is still completely lacking, or it should be introduced *a posteriori*.

Some of the limitations discussed above (e.g. correct sampling of the configuration space, description of intermolecular interactions in assemblies or large systems, dependence on temperature and pressure, effects of the anharmonicity) could be overcome by means of an *ab-initio* molecular dynamics approach.

In recent years, First Principles MD (FPMD) simulations have shown to be an intriguing alternative to standard *static* calculations for the prediction of the vibrational properties [11–14]. In this case, a quantum chemical approach, based on Density Functional Theory (DFT) calculations, is adopted for the solution of the electronic problem, thus opening the possibility to obtain an accurate evaluation of the vibrational force field while keeping all the advantages of a *dynamic* approach capable to describe in a realistic way the trajectory of the molecules in a given time interval. As described in the computational section, the IR spectrum is evaluated from the correlation function of the dipole moment, namely it is derived from the trajectory of the molecules in their configuration space, taking into account their different equilibrium structures, the evolution of intra and intermolecular interactions and the explicit dependence on the external variables, without the need of any

harmonic approximation. This approach seems to be very promising and it has been already applied successfully for several molecular systems [11–14].

In this paper we will illustrate a rather simple study case which allows to discuss pros and cons of *static* versus *dynamic* approaches for prediction of the IR spectrum of condensed phase systems made by weakly interacting, flexible organic molecules. To this aim we carried out computational investigation on the $(\text{ClCF}_2\text{CF}(\text{CF}_3)\text{OCF}_2\text{CH}_3)$ molecule, here referred to as N1 (see the sketch in Figure 1, where its lower energy conformation is shown).

N1 molecule is a partially halogenated ether with a quite flexible structure (5 torsional degrees of freedom, see Fig.1) and low energy barriers between its different equilibrium conformations.

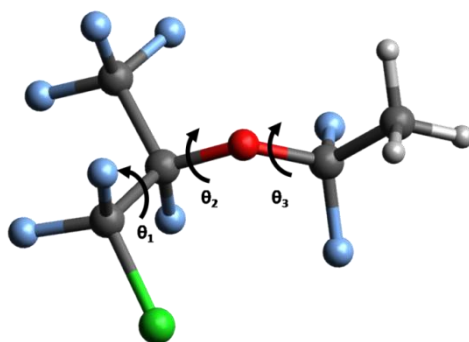


Fig.1 Structure of the N1 molecule ($\text{ClCF}_2\text{CF}(\text{CF}_3)\text{OCF}_2\text{CH}_3$). Carbon atoms are in grey, hydrogen atoms in white, oxygen atoms in red, fluorine atoms in blue and chlorine atoms in green.

At room temperature the molecule is able to explore a large portion of the potential surface and thus we expect that different conformers can co-exist and give a possibly different spectroscopic response.

N1 molecule has been already investigated in the past by some of the authors of this paper [15] and a good description of the IR spectrum (in gas phase) and of its temperature-dependence was obtained by using a sampling procedure of the conformational space, in the framework of the *static* approach. We want here to compare this procedure with the results obtained by computing the spectrum by means of FPMD simulations. The effect of intermolecular interactions in the liquid phase will be in this case explicitly considered and discussed in the light of new experimental data.

IIa. Experimental details

Synthesis of the molecules and its structural characterization are described in details in Refs. [15,16]. IR spectrum in liquid phase has been performed with a Thermo Nicolet 6700 FTIR instrument, in Attenuated Total Reflectance (ATR) mode, diamond crystal, single reflection (45°). Raw data has been corrected for ATR Intensity. Gas phase

spectrum has been acquired with a Nicolet 870 FTIR instrument, with a gas cell with 10 cm pathlength and 76 cm³ volume. Acquisition parameters for IR spectra were: 256 scans and a resolution of 2 cm⁻¹. Raman spectrum has been acquired with a FT-Raman module coupled with a Nicolet 870 FTIR spectrometer with a 1064 nm excitation and nominal power of about 200 mW on liquid sample. Acquisition parameters were 512 scans and a resolution of 4 cm⁻¹.

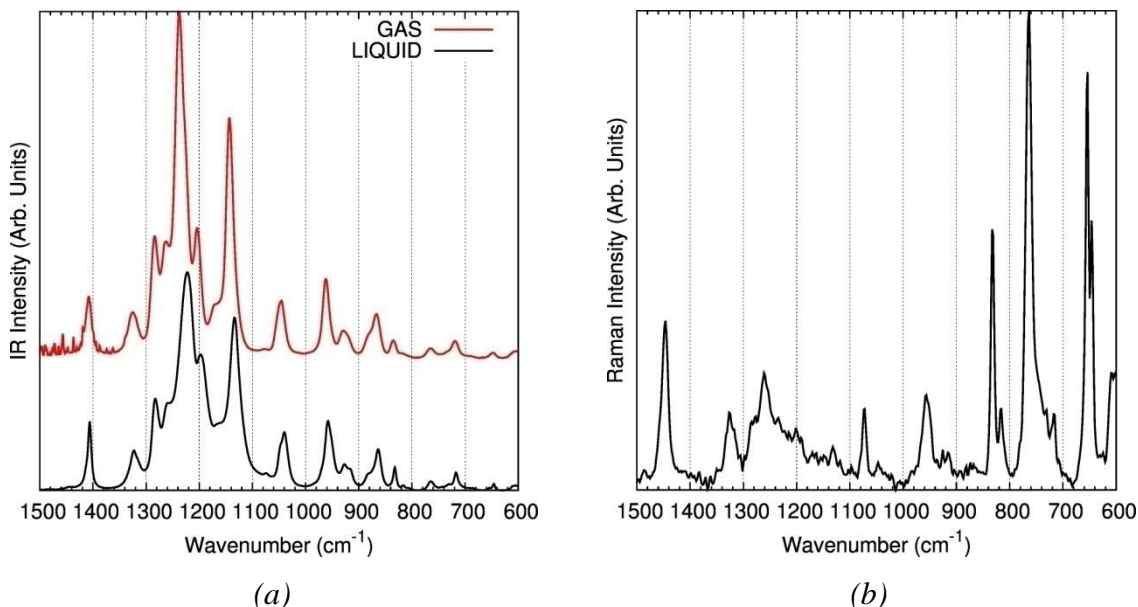


Fig.2 Experimental (a) IR spectra (liquid and gas phase), (b) Raman spectrum (liquid) of N1

IIb. Computational details

II.1 Static DFT calculations

In a previous paper about the N1 molecule [15], we developed an efficient method to identify the several stable conformers of N1 (predicted through simulations *in vacuo*) and to calculate its spectroscopic response at finite given temperatures. Starting from a given conformer, a large number ($3 \cdot 6^2 = 108$) of new input geometries were generated by successive and systematic change of θ_1 , θ_2 and θ_3 torsional angles (finite steps of 60° for θ_2 and θ_3 , of 120° for θ_1 , see Figure 1 for a definition of the torsional angles). In other words, we obtained a “grid” of structures mapping the conformational space of N1. However, some of these geometries were characterized by too close contacts between non-bonded atoms, making them unstable because of the sterical hindrance: to discard *a priori*

these unstable geometries a cutoff value was used to fix a minimal distance between pairs of non-bonded atoms (A,B), keeping only those structures which give rise to a non-bonded distance above a threshold value defined on the basis of van der Waals radii of A and B. By applying this procedure to N1 a final number of 62 starting geometries were identified and a geometry optimization run was carried out for all of them by using Density Functional Theory (DFT). B3LYP functional and 6-311G(d,p) basis set were adopted. However, since the present work is devoted to the comparison between *static* and *dynamic* approaches, we adopted here a different level of theory, because of the limitations encountered in the use of hybrid functionals in first-principle dynamics: both BLYP and PBE exchange-correlation functionals combined with TZVP basis set will be tested for the *static* calculations and to run the first-principles molecular dynamics simulations described in the next paragraph. *Static* calculations have been carried out by means of Gaussian09 code [17].

After geometry optimization of the many different guess geometries, usually a smaller number of final stable structures are observed; indeed different starting structures can reach the same minimum and, if the initial grid is suitably dense, all the minima of the potential energy surface can be located. In the present case, 26 and 24 minima are identified by means of PBE/TZVP and BLYP/TZVP calculations respectively.

As a second step, for all these minima a further run is carried out to predict the spectroscopic response (IR/Raman spectra) in double harmonic approximation, thus obtaining 26 (24) spectra associated to the different stable conformers. As a last step, in order to predict the spectroscopic response at different temperatures, a weight average spectrum can be generated by using Boltzmann distribution to take into account properly the contributions of the different at a fixed temperature.

The procedure adopted, based on calculations *in vacuo* allows to introduce the effects of the temperature, but still completely neglects the effects of the intermolecular interactions. While studying the gas phase, this is not considered a serious limitation, but in condensed phase intermolecular interaction are expected to play a non-negligible role. Remarkable spectral changes due to intermolecular interactions are often observed, especially when formation of molecular complexes occurs in condensed phases.

For this reason we expect that the static procedure based on calculations *in vacuo* will be able to reproduce nicely the gas phase experimental spectrum, but could show some weaknesses while dealing with the liquid one.

II.2 First principles molecular dynamics simulations

In order to overcome the intrinsic limitations of the *static* approach and to test the capability of a dynamic first principles approach, we decided to apply FPMD simulations to evaluate the IR spectrum of N1. The aim is to verify the ability of the dynamic approach to correctly sampling the potential surface and to quantify the contribution to the IR spectrum of the different conformers. Also, we want to evaluate the potentiality of the

dynamics in predicting the intermolecular interactions in condensed phase and their possible effects on the spectrum.

In the framework of first order perturbation theory, the IR intensity $I(\omega)$ can be written as [18,19]:

$$I(\omega) = \frac{2\pi\beta\omega^2}{3cV} \int dt \langle \boldsymbol{\mu}(t)\boldsymbol{\mu}(0) \rangle e^{i\omega t} \quad (1)$$

where $\boldsymbol{\mu}(t)$ is the instantaneous dipole moment of the system at the time t , $\beta = 1/kT$, ω is the frequency of the absorbed light, c is the speed of light in vacuum and V the volume of the system.

In Eq. (1) a quantum correction factor $\hbar\beta/(1 - \exp(-\beta\hbar\omega))$ has been introduced to correct the classical line shape [20–23]. Notice moreover that Eq. (1) does not require the introduction of any empirical parameter which account for the band width.

The correlation function of the dipole moment $\langle \boldsymbol{\mu}(t)\boldsymbol{\mu}(0) \rangle$ can be easily evaluated from a molecular dynamic simulation, for example by using the DFT based MD simulations here adopted. In this case, at each time step the nuclei are moving following the Newton classical equation, but the forces are evaluated by solving the electronic problem in the Born-Oppenheimer approximation, in the framework of DFT.

The simulations have been carried out by means of the CP2K code, adopting the BLYP and PBE functional in combination with different augmented Gaussian-plane waves basis set and GTH pseudopotentials. Moreover, Grimme D3 correction[24] has been introduced to provide a correct description of the Van der Waals interactions. On the basis of previous investigations, we adopted for all the cases a TZV2P gaussian basis set, while for the plane waves basis set we checked two different cutoff: 400Ry and 600Ry.

During a trajectory, the system is free to explore all the accessible points on the potential energy surface: different intramolecular (i. e. molecular conformations) and intermolecular structures (e.g. clusters) are automatically sampled and contribute to the total dipole correlation function. Therefore, by running only one calculation for a simulation time long enough, the IR spectrum computed according to Eq. (1) does contain the contribution of all the conformers explored during the trajectory. It should be noticed that no harmonic approximations is introduced according to the formalism adopted. Indeed Eq. (1) allowed to directly evaluate the IR spectrum.

For the N1 molecule, we carried out dynamic simulations for two cases:

- Case A: simulation of the liquid phase starting from a cubic box (13.33Å x 13.33 Å x 13.33Å) containing 8 molecules and adopting periodic boundary conditions. The size of the box has been chosen to reproduce the experimentally measured density [16] at 300 K (1.4947 g/cm³).
- Case B: simulation of the gas phase by computing the trajectory of single molecule in a cubic box (18.0 Å x 18.0 Å x 18.0 Å), large enough to avoid intermolecular interactions between N1 molecules in different cells.

In all the cases, we performed an equilibration dynamic (the details are reported in the following) followed by a 10 ps NVE production run for the prediction the spectra. For Case A, we explored also longer NVE trajectories (40 ps), obtaining negligible variations in the predicted spectra.

We chose a time step of 0.2 fs for the liquid phase and 0.4ps for the gas phase and the dipole moment was computed at each time step in the Berry phase formalism.

Two strategies have been adopted for the equilibration run of CASE A: i) first, we used the NVT ensemble to take into account temperature effects while keeping a fixed volume corresponding to the experimental density at room temperature (2 ps of dynamics); ii) second, we adopted an NpT ensemble to equilibrate also the density of the system.

In Case B, only an NVT equilibration was adopted (10 ps of dynamics).

In these NVT runs, we rescaled the velocity when the fluctuations in temperature fell outside a fixed range ΔT around the target temperature ($\Delta T = \pm 50$ K for the liquid phase, $\Delta T = \pm 100$ K for the gas phase).

Based on the results obtained with the NVT dynamics, we carried out NpT simulations only by choosing the PBE functional combined with the augmented Gaussian-plane waves basis set TZV2P- 600Ry and GTH pseudopotentials. Also in this case the D3 Grimme correction have been introduced.

To control the temperature and the pressure, the system was coupled with a thermostat (Nosè Hoover chain [26]) and a barostat (default implementation of CP2K [25,27]). Following the same strategy adopted by McGrath at al. [25], we chose a coupling time constant of 20 fs for the thermostat and 300 fs for the barostat.

One simulation of 30 ps, using a time step of 0.5 fs, has been run at 300 K while the pressure has been fixed to 1atm. Based on the NpT trajectory, we run the two NVE dynamic of 10 ps (0.2 fs time step), to predict the IR spectrum

III. Results

In Figure 2a the liquid and gas phase experimental IR spectra (at 300K) of the N1 molecule are compared. As expected, due to the weak intermolecular interactions that characterize this system, the spectra for the liquid phase and the gas phase don't show significant differences. In particular the main variation observed in the liquid phase is a redshift of the two strong bands at about 1240 cm^{-1} and 1140 cm^{-1} . Since the spectral pattern doesn't show a strong modulation by intermolecular interactions, in the first part of our discussion we will focus only on intramolecular effects; we will analyze the effect of the intermolecular interactions in section III.4.

III.1 *Static* calculations

In our previous paper about N1 molecule[15], we showed that the explicit introduction of the contributions of many conformers, obtained according to the *static* approach (see Section II.1) is mandatory to give a correct assignment of the IR spectrum and to follow

its evolution with temperature. The same procedure has been applied in the present study, adopting two other DFT functional and basis set (PBE and BLYP with TZVP basis set), chosen for consistency with FPMD simulations. In Figure 3, we report the comparison between the experimental IR spectrum at room temperature and the DFT computed spectra for the four lower energy conformers. In addition, Figure 3 shows the spectrum obtained as a Boltzmann-weighted sum (BWS) of the calculated spectra of all the equilibrium conformers (26 and 24 conformers for PBE and BLYP functional respectively).

As expected, our results are consistent with the previous ones (obtained at B3LYP/6-311G(d,p) level of theory), but show some non-negligible differences.

Both PBE and BLYP calculations (BWS) allow to predict the main spectra features experimentally observed, but peaks frequencies are systematically underestimated of about 100 cm^{-1} in the spectral range considered. This result was not found in the previous B3LYP calculations, which gave a very good prediction of peak frequencies, without any scaling procedure.

Instead, for PBE and BLYP calculations, the introduction of a scaling factor has been necessary for a better comparison with the experimental spectrum. Scaling of computed frequencies is a common and standard procedure in computational vibrational spectroscopy and it is usually motivated by the several approximations involved, as for instance the neglect of anharmonic effects, entropic contributions, zero-point vibrational energies etc. Moreover the choice of a DFT functional and the finiteness of the basis set are further source of possible errors. In this perspective, it will be interesting to compare the *static* spectra with those obtained by means of FPMD simulations also from the view point of the performances in the prediction of peaks frequency values.

In order to find a suitable scaling factor, the strong band observed at 1240 cm^{-1} in the experimental spectrum can be taken as a reference, allowing to determine a scaling factor of $f_1 = 1.0644$ and $f_2 = 1.0954$ for PBE/TZVP and BLYP/TZVP calculations respectively. Interestingly, the scaling factors obtained ($f_{1(2)} > 1$) are quite unusual, since in most of the cases DFT predictions give a systematic overestimation of the vibrational transition frequencies. This holds also for the two functionals adopted, namely the standard scaling factors reported in the literature for PBE and BLYP range from 0.987 to 0.995 and from 0.994 to 1 respectively [28].

On the other hand, the unusual behavior shown in the present case could be related to the presence of chlorine and fluorine atoms, as shown by frequency predictions for some small test molecules (see Supporting Information).

Looking at the individual IR spectra of the low energy conformers reported in Figure 3, it is clear that none of the spectra predicted for a given conformer is able to reproduce the whole pattern observed in the experimental spectrum.

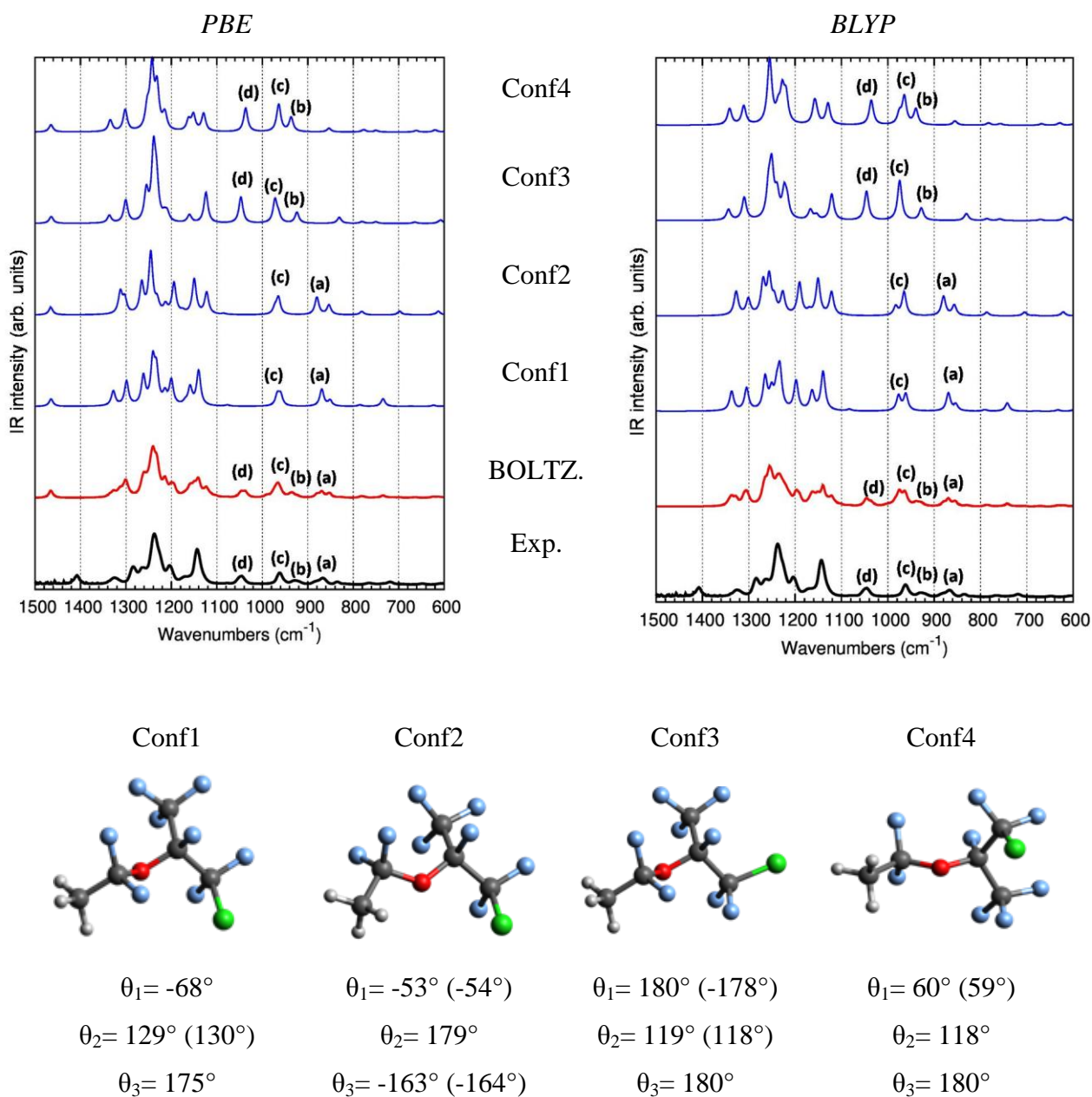


Fig. 3 Comparison of the predicted IR spectra (DFT static calculation) of the four lower energy conformers of N1 molecule and of the Boltzmann-weighted sum (BWS, see text) with the experimental spectrum in gas phase at 25 °C. The conformation-sensitive bands are marked by letters. The computed frequencies are scaled by a factor of $f_1 = 1.0644$ and $f_2 = 1.0954$ for PBE/TZVP and BLYP/TZVP calculations respectively.

In particular, focusing on the four marker bands (a-d labels in Figure 3) identified in the region $1100\text{ cm}^{-1} - 800\text{ cm}^{-1}$ (in the following discussion we will always refer to the experimental frequency values) we can observe that:

- i) the band observed at 870 cm^{-1} (band a) appears in the spectrum of conformers 1 and 2 but not for conformers 3 and 4;
- ii) the bands at 926 cm^{-1} (band b) and at 1045 cm^{-1} (band d) are predicted for conformers 3 and 4 but not for 1 and 2;
- iii) the band at 962 cm^{-1} (band c) is predicted for all the four lower energy conformers.

In fact, a nice prediction of the experimental spectrum at room temperature, including an accurate description of the pattern also in relative intensities, is reached only by means of a Boltzmann-weighted average (Figure 3). Obviously, especially in analytical applications where quantitative or semi-quantitative information is obtained from vibrational spectra, a detailed assignment and identification of the different species (conformers) occurring in the sample is an unavoidable prerequisite.

Analyzing more in details the predicted spectra some further observations can be done.

Comparing the spectra obtained by means of the two functionals, it can be seen that PBE functional gives a better description of the experimental pattern: the four marker bands are very well described in both relative positions and intensities; also the intensity pattern of the broad band in the region 1300 cm^{-1} - 1200 cm^{-1} is accurately predicted. As a minor discrepancy, the band at about 1150 cm^{-1} appears to be broader and weaker in the computed spectrum.

Considering BLYP predictions, the BWS computed spectrum is less accurate, even if the four conformation-sensitive bands are still correctly identified. However, according to BLYP prediction the (c) band is a doublet, while it appears to be a single band in the experimental and in PBE computed spectra; many overlapping bands are found in the region between 1000 and 1300 cm^{-1} , a complexity which is not observed in the experimental spectrum. Moreover, the gap between the band at about 1400 cm^{-1} and the group of bands around 1250 cm^{-1} is overestimated by both the functionals, but it is more significant in the case of BLYP.

Apart from the discrepancies illustrated above, it is clear that the procedure proposed can reproduce the relevant spectral features even when considering a conformational flexible molecule such as N1.

Moreover, in addition to the accurate prediction of the spectral pattern at room temperature in both frequencies and relative intensities, through the Boltzmann population of the conformers, it is possible to take into account the temperature dependence of the vibrational spectra.

In this way it has been possible to rationalize the experimentally observed systematic increase with the temperature of the intensity of 1045 cm^{-1} (d) and 926 cm^{-1} (b) bands compared to the 870 cm^{-1} (a) and 960 cm^{-1} (c) ones as due to the change in the relative conformers population while varying temperature [15].

Thanks to the availability of the Raman spectrum of N1 at room temperature (Figure 2), we can now validate the *static* approach by means of the comparison between the predicted BWS obtained from the computed Raman spectra of the stable conformers (Figure 4).

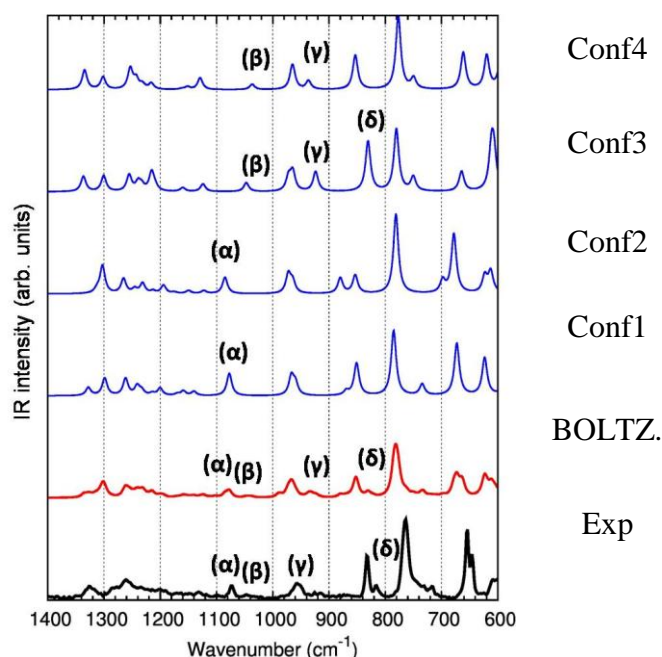


Fig. 4 Comparison of the predicted Raman spectra (DFT PBE/TZVP static calculation) of the four lower conformers of NI molecule and of the Boltzmann-weighted sum (BWS, see text) with the experimental spectrum in liquid phase at 25 °C. The conformation-sensitive bands are marked by letters. The computed frequencies are scaled by a factor of $f_1=1.0644$.

In this case we restricted our analysis to calculations carried out with PBE functional. Also in the Raman case it is possible to identify four marker bands:

- i) the band observed at 1070 cm^{-1} (band α) appears in the spectrum of conformers 1 and 2 but not for conformers 3 and 4;
- ii) the two bands observed at 1050 cm^{-1} (band β) and the one at 810 cm^{-1} (band δ) appears in the spectrum of the conformers 3 only;
- iii) the band at 960 cm^{-1} (band γ) predicted for conformers 3 and 4 but not for 1 and 2.

As expected, the BWS Raman spectrum nicely compares with the experimental one. Notice that the same scaling factor introduced in the case of IR determines a good agreement also in frequencies.

III.2 NVT + NVE dynamic simulations

We will now analyze the results obtained by means of FPMD simulations by using an NVT equilibration followed by an NVE production run: in Figure 5 we report the IR

spectrum of N1 molecule at 300 K between 1500 and 600 cm^{-1} predicted at different level of theory (BLYP and PBE).

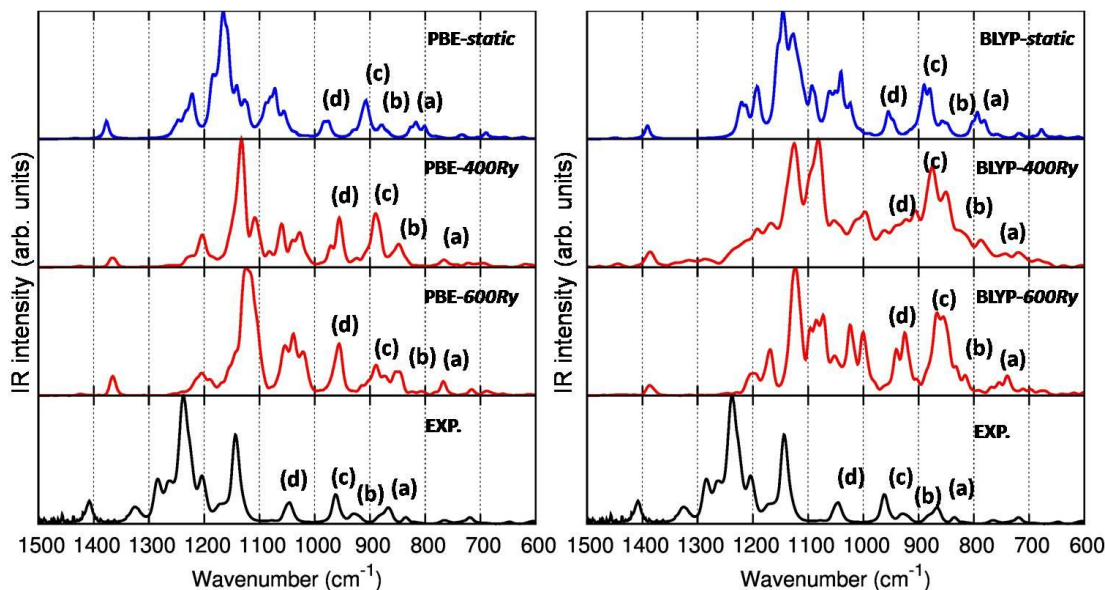


Fig. 5 Comparison of the FPMD predicted IR spectra (NVT+NVE) of N1 molecule in condensed phase with the experimental spectrum (gas phase at 25 °C). The conformation-sensitive bands are labeled by letters. No scaling factors have been adopted for computed frequencies.

The impressive result is that the four marker bands associated to the different conformation are now predicted, by means of one only dynamical calculations. This indicates that during the dynamics the configurations space is properly mapped and explored by N1 molecules. No selection of equilibrium geometries and no control on the structural evolution is required in FPMD simulations, thus reducing any source of arbitrariness and bias from the procedure and making it more robust from this point of view.

Analyzing in details the unscaled predicted spectra reported in Figure 5, it can be noticed that also in FPMD calculations the predicted peak frequencies underestimate the experimental ones by more than 100 cm^{-1} , similarly but to a larger extent than the *static* spectra. During the MD simulation the trajectories of the molecules are fully described and the harmonic approximation is not introduced, so the additional shift toward lower frequencies obtained through MD could be ascribed to the effect of anharmonicity. Moreover, in the FPMD simulations of the liquid phase intermolecular interactions could be responsible for this lowering of the frequency values, since eight interacting N1 molecules are present in the simulation box. These effects will be further considered in Section III.4 where we will compare the spectrum predicted by a FPMD in the condensed phase with the one predicted *in vacuo*. On the other hand, the remarkable underestimation of the peak frequencies obtained both in the *static* and *dynamic* approaches, confirms that

the main issue is the weakness of the functional/basis set in describing chlorine and flourine atoms.

In any case, after a proper frequency scaling all the main experimental feature of the spectrum in the region of interest are recognizable in the predicted FPMD spectra, even if sometimes wrong relative band intensities are predicted.

These inaccurate absorption intensities could be attributed to several factors in addition to the intrinsic approximations related to the choice of the DFT functional, pseudopotential and basis set. Indeed we used an NVT ensemble without cell optimization and the sampling of the conformational space could be inaccurate due to an incomplete equilibration or a not equilibrated density of the system; moreover the trajectory could be too short.

It should be noted that BLYP spectra are very noisy and increasing the plane wave cutoff from 400 to 600Ry only slightly improves the prediction. On the other hand, PBE functional gives quite good results already with a 400Ry cutoff.

For these reasons and for the sake of conciseness, from now on we will concentrate on the PBE computed spectra, and in particular on those obtained by using a 600Ry cutoff.

As already observed, with only one trajectory we are able to predict all the four bands that we previously identified as markers of different conformers and we can account for the relevant features of the whole experimental spectrum. The main discrepancies are related to band shapes: DFT computed spectra and in particular the FPMD ones show sometimes structured bands, with several components not observed experimentally. Increasing the length of the simulations could lead to a simplification of the computed spectra because of a better averaging of the contributions of the microstates described during the simulation, thus enhancing the similarity between prediction and experiment.

On the other hand, based on of the results so obtained, we can state that FPMD simulations proved to be a promising method to obtain a comprehensive description of the IR spectra of flexible molecular systems, where the structure of the molecules can modify strongly during time and thus modulating the spectroscopic response. These finding pave the way to several interesting applications in molecular sciences and chemical physics.

However, such goal requires a systematic exploration of the behavior of different methods (choice of the functional, basis sets and pseudopotentials) and of the computational setup to shed further light on the potentialities and limitations of FPMD simulations in vibrational spectroscopy.

III.3 NpT + NVE dynamic simulations

In this Section we will discuss in details the effect of the NpT equilibration on the spectral pattern. An implicit limitation of the previous MD simulations is indeed related to the fact that the density of the system has been fixed to the experimental value and no cell size optimization has been carried out for a complete optimization of the system. Therefore, in order to judge the importance of a full equilibration in both T and p for the N1 system, also NpT equilibration dynamics have been carried out before the NVE production run.

NpT simulations are not a standard choice in the field of ab-initio MD because they are quite computational expensive.

The NpT trajectories here obtained (30 ps) are not long enough for the volume fluctuations to fully converge. On the other hand, the average volume starts to converge already after 20 ps and we analyzed the last 5 ps of the trajectory to evaluate the size of the box at the equilibrium. The predicted value for the box size is bigger compared to the experimental value (13.33 Å), namely we obtained a size of 13.426 Å at 300K, indicating that when we set the density value at the room temperature experimental value, we are artificially compressing the system.

Also in this case, the experimental pattern is reproduced and the four marker bands (a), (b), (c) and (d) are recognizable in both spectra.

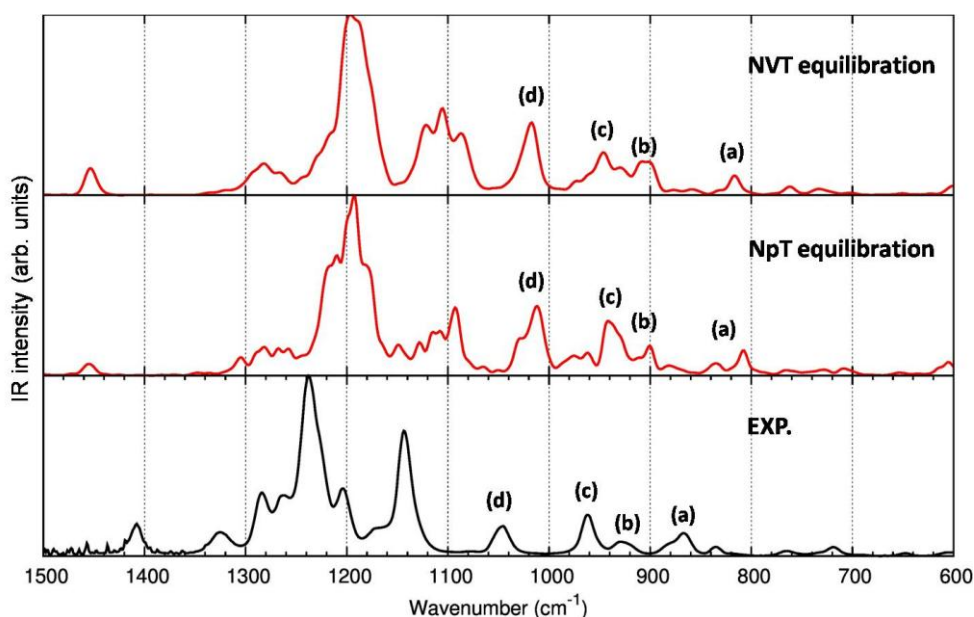


Fig. 6 Comparison of the FPMD PBE/TZVP predicted IR spectra of NI molecule in condensed phase using the NVT or the NpT equilibration. The computed frequencies are scaled by a factor 1.0644.

Interestingly, we should note that the peaks frequency underestimation already observed for the other predicted spectra is still present, proving that this behavior is not due to the compression of the system in NVT runs but it is an intrinsic feature of the computational model (choice of the functional and basis set) and related approximations.

Even if NpT equilibration certainly affects the simulated spectral pattern, the quality of the simulations in terms of band shapes and intensity does not show any clear improvement, if compared with the experimental features. For this reason our results do not allow to extract guidelines about the need of NpT equilibration in the prediction of the vibrational spectra.

III.4 FPMD simulations: gas phase vs. condensed phase

In Figure 7 we compared the spectrum predicted by FPMD simulations for the liquid phase (Case A) and for an isolated molecule *in vacuo* (Case B, see section II.2 for the details). Indeed, due to the good results obtained by static DFT simulations on an isolated molecule model, it is quite important from the methodological perspective to verify if also for FPMD simulations the gas phase model is enough in the N1 case for a reliable prediction of the spectra.

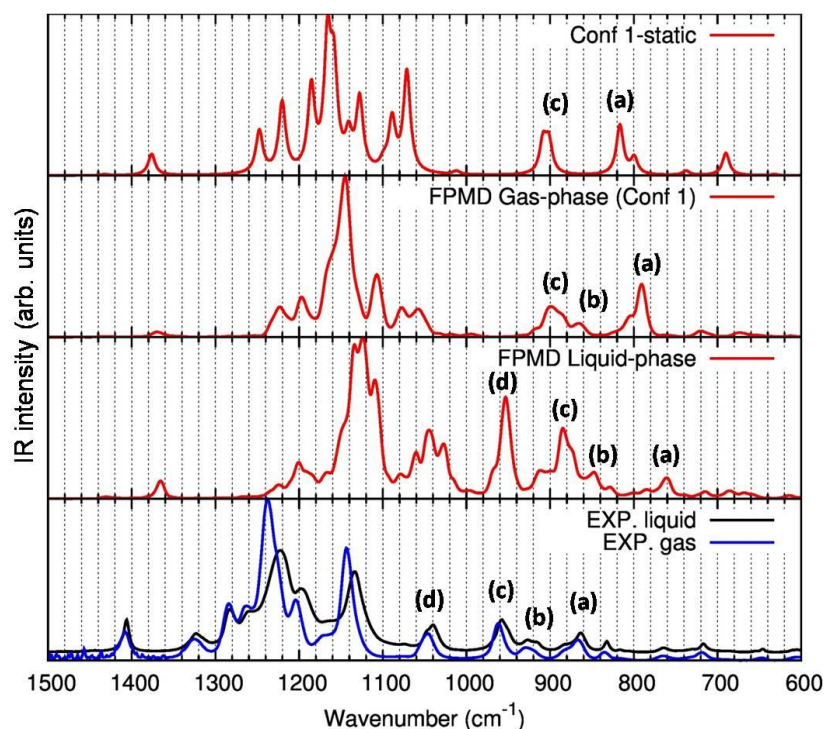


Fig. 7 Comparison of the experimental spectra of the liquid and the gas phase N1 molecule, FPMD computed IR spectra on the liquid phase and on the gas phase and by static calculations on the lowest energy conformer. The conformation-sensitive bands are labeled by letters. No frequency scaling factors have been adopted for all the computed spectra.

In FPMD simulations on the isolated molecule we considered different possible starting geometries for the equilibration run. Since the behavior observed is similar for all these cases, in Figure 7 we reported only the spectrum obtained starting from the lowest energy conformer (see the Supporting Information for the other cases).

A surprising result is found since a single FPMD run on an isolated molecule cannot predict all the four conformation-sensitive markers bands, contrary to FPMD simulations on the liquid phase. Indeed, as an example, starting from the lowest energy conformer the simulation doesn't predict the band (d), associated to a different conformation. This

finding indicates that, in a single run, the conformational space is not mapped properly, thus losing most of the important information about the system. One reason for this behavior can be the relative short length of the simulations (10 ps) or the fact that the fixed total energy of the isolated, non-interacting molecule does not allow to overcome the torsional energy barriers between different conformations. On the opposite, the FPMD for the condensed phase is able to predict all the marker bands, with a relatively short trajectory, of 10 ps. It should be noticed that also in the liquid phase simulation, we start with eight molecule in the lowest energy conformation. In this case however the molecules can easily exchange energy during the dynamics: this can promote changes of the conformation and allows to explore properly the whole configuration space. In conclusion, in the case of N1, a model system describing the isolated (gas phase) molecule seems to be much more critical than the apparently more complex liquid phase model.

By inspection of the spectra reported in Figure 7 a further result is found: as already pointed out, due to the weak intermolecular interaction between N1 molecules, the experimental spectra for the liquid phase and the gas phase are similar. The only one remarkable change is the frequency downward shift in the liquid of the two strong bands around 1240 cm^{-1} and 1140 cm^{-1} . FPMD spectra of the isolated molecule and of the liquid phase reproduce indeed this trend: regardless of the starting geometry chosen for the isolated molecule simulations (see the Supporting Information), all the predicted gas phase spectra shows the main features at 1240 cm^{-1} and the 1140 cm^{-1} occurring at higher frequencies with respect to the case of the liquid.

This result suggests that the effect of intermolecular interactions occurring in the condensed phase is correctly described by FPMD simulation.

IV. Summary and Conclusions

The results reported above allow to draw some conclusions about the reliability of *static* and *dynamic* calculations for the computation of the spectroscopic response of molecular systems, such as N1 molecule.

FPMD simulations shows to be a promising technique in the study of the spectroscopic response of flexible molecules in disordered condensed phases. Indeed, we have been able to predict the four marker bands sensitive to the conformers populations, previously identified on the basis of a rather complex analysis of many equilibrium molecular structures and associated spectra.

On the other hand, in the case of *dynamic* calculations, the computed IR spectrum is often quite noisy and it is very dependent both on the functional adopted and on several computational parameters (e.g. plane wave cutoff).

At least in principle, the use of NpT equilibration instead of NVT-NVE simulations, should improve the description of the spectra and better capture the correct temperature evolution, but the spectra modulation obtained according to this approach is still far from experimental observation. For this reason it has been impossible to assess the performances of this approach for spectra simulation; this still remains very important

issue in the perspective of future studies, especially considering the increase of the computational costs and the times required for NpT simulations.

At the present state of the art, we can conclude that the *static* calculations are the better choice in terms of accuracy and computational cost, provided that i) the conformational space is correctly sampled and ii) it is reasonable to model the spectrum as a weighted sum of contributions coming from isolated conformers (calculations are made *in vacuo*).

A deep analysis of the results here obtained by means of the *static* approach reveal however that the temperature evolution of the system is not reproduced in details by simply introducing a Boltzmann statistic applied to non interacting conformers; moreover, since the final spectrum is the weighted sum of the spectra associated to the different conformers, inaccuracies due to the choice of the method, such as the DFT functional, are reflected by the sum spectrum. For instance, we showed that BLYP computed spectra are not accurate enough to reproduce the experimental one, even if the contributions of the different conformers are anyway predicted correctly.

Considering that the *static* approach completely neglects intermolecular interactions and the number of structures required for an accurate exploration of the conformational space increases very rapidly with the number of torsional angles, it is clear that its application could be limited to a system made by quite small, weakly interacting molecules. This approach has been applied successfully for peculiar polymer systems according to an *oligomer approach* [29] but in any case its use should be evaluated case by case and it is far from being generally applicable. When then intermolecular interactions are very important (e.g. hydrogen bonded systems) or condensed phase effects (solvent effects, crystalline field) are relevant, the application of the *static* approach is even harder and/or not possible.

In these grounds FPMD should be regarded as an alternative powerful tool which can give at least a qualitative description of the vibrational spectra in presence of such a large variety of effects and variables. Their application to condensed phase systems has not yet explored in details; however, based also on the present results, we believe that there is wide room for further studies and potential applications of these computational methods in many different fields of chemistry, chemical physics and materials science. As an example, the interpretation and the characterization of the inter-molecular interactions taking place among macromolecules in their solid state and/or in solutions or the behavior of biological systems are just two topics where the joint application of computational and experimental spectroscopic techniques are expected to give a very important contribution for the rationalization of the properties of the material.

References

- [1] D. Galimberti, A. Milani, Crystal Structure and Vibrational Spectra of Poly(trimethylene terephthalate) from Periodic Density Functional Theory Calculations, *J. Phys. Chem. B.* 118 (2014) 1954–1961. doi:10.1021/jp411560r.
- [2] D. Galimberti, C. Quarti, A. Milani, Polymorphism of even nylons revisited through periodic quantum chemical calculations, *Polymer.* 67 (2015) 167–173. doi:10.1016/j.polymer.2015.04.060.
- [3] D. Galimberti, C. Quarti, A. Milani, L. Brambilla, B. Civalleri, C. Castiglioni, IR spectroscopy of crystalline polymers from ab initio calculations: Nylon 6,6, *Vib. Spectrosc.* 66 (2013) 83–92. doi:10.1016/j.vibspec.2013.02.005.
- [4] A. Milani, D. Galimberti, Polymorphism of Poly(butylene terephthalate) Investigated by Means of Periodic Density Functional Theory Calculations, *Macromolecules.* 47 (2014) 1046–1052. doi:10.1021/ma402602f.
- [5] J. Tomasi, B. Mennucci, R. Cammi, Quantum mechanical continuum solvation models, *Chem. Rev.* 105 (2005) 2999–3094.
- [6] S. Califano, *Vibrational States*, John Wiley & Sons Ltd, London; New York, 1976.
- [7] V. Barone, Anharmonic vibrational properties by a fully automated second-order perturbative approach, *J. Chem. Phys.* 122 (2005) 014108. doi:10.1063/1.1824881.
- [8] V. Barone, A. Baiardi, M. Biczysko, J. Bloino, C. Cappelli, F. Lipparini, Implementation and validation of a multi-purpose virtual spectrometer for large systems in complex environments, *Phys. Chem. Chem. Phys.* 14 (2012) 12404. doi:10.1039/c2cp41006k.
- [9] J. Bloino, V. Barone, A second-order perturbation theory route to vibrational averages and transition properties of molecules: General formulation and application to infrared and vibrational circular dichroism spectroscopies, *J. Chem. Phys.* 136 (2012) 124108. doi:10.1063/1.3695210.
- [10] M. Cossi, N. Rega, G. Scalmani, V. Barone, Energies, structures, and electronic properties of molecules in solution with the C-PCM solvation model, *J. Comput. Chem.* 24 (2003) 669–681. doi:10.1002/jcc.10189.
- [11] M.-P. Gageot, M. Sprik, Ab Initio Molecular Dynamics Computation of the Infrared Spectrum of Aqueous Uracil, *J. Phys. Chem. B.* 107 (2003) 10344–10358. doi:10.1021/jp034788u.

- [12] M.P. Gaigeot, R. Vuilleumier, M. Sprik, D. Borgis, Infrared Spectroscopy of N-Methylacetamide Revisited by ab Initio Molecular Dynamics Simulations, *J. Chem. Theory Comput.* 1 (2005) 772–789. doi:10.1021/ct050029z.
- [13] M.-P. Gaigeot, M. Martinez, R. Vuilleumier, Infrared spectroscopy in the gas and liquid phase from first principle molecular dynamics simulations: application to small peptides, *Mol. Phys.* 105 (2007) 2857–2878. doi:10.1080/00268970701724974.
- [14] M.-P. Gaigeot, Theoretical spectroscopy of floppy peptides at room temperature. A DFTMD perspective: gas and aqueous phase, *Phys. Chem. Chem. Phys.* 12 (2010) 3336. doi:10.1039/b924048a.
- [15] M. Tommasini, C. Castiglioni, A. Milani, G. Zerbi, S. Radice, P. Toniolo, et al., Molecular conformations of a partially halogenated ether: A study based on infrared spectroscopy and density functional theory calculations, *J. Fluor. Chem.* 127 (2006) 320–329. doi:10.1016/j.jfluchem.2005.12.015.
- [16] C. Tonelli, A. Di Meo, R. Picozzi, M. Bassi, New hydrofluoropolyethers II: Physico-chemical characterization, *J. Fluor. Chem.* 132 (2011) 356–362. doi:10.1016/j.jfluchem.2011.03.013.
- [17] M.J. Frisch, G.W. Trucks, J.R. Cheeseman, G. Scalmani, M. Caricato, H.P. Hratchian, et al., Gaussian 09, n.d.
- [18] D.A. McQuarrie, *Statistical Mechanics*, University Science Books, 2000.
- [19] R. Kubo, M. Toda, N. Hashitsume, *Statistical Physics II*, Springer Berlin Heidelberg, Berlin, Heidelberg, 1991. <http://link.springer.com/10.1007/978-3-642-58244-8> (accessed November 18, 2015).
- [20] H. Ahlborn, B. Space, P.B. Moore, The effect of isotopic substitution and detailed balance on the infrared spectroscopy of water: A combined time correlation function and instantaneous normal mode analysis, *J. Chem. Phys.* 112 (2000) 8083–8088. doi:10.1063/1.481408.
- [21] M.-P. Gaigeot, M. Sprik, Ab Initio Molecular Dynamics Computation of the Infrared Spectrum of Aqueous Uracil, *J. Phys. Chem. B.* 107 (2003) 10344–10358. doi:10.1021/jp034788u.
- [22] R. Iftimie, M.E. Tuckerman, Decomposing total IR spectra of aqueous systems into solute and solvent contributions: A computational approach using maximally localized Wannier orbitals, *J. Chem. Phys.* 122 (2005) 214508. doi:10.1063/1.1908950.

- [23] R. Ramírez, T. López-Ciudad, P.K. P, D. Marx, Quantum corrections to classical time-correlation functions: Hydrogen bonding and anharmonic floppy modes, *J. Chem. Phys.* 121 (2004) 3973–3983. doi:10.1063/1.1774986.
- [24] S. Grimme, J. Antony, S. Ehrlich, H. Krieg, A consistent and accurate ab initio parametrization of density functional dispersion correction (DFT-D) for the 94 elements H-Pu, *J. Chem. Phys.* 132 (2010) 154104. doi:10.1063/1.3382344.
- [25] M.J. McGrath, I.-F.W. Kuo, J.I. Siepmann, Liquid structures of water, methanol, and hydrogen fluoride at ambient conditions from first principles molecular dynamics simulations with a dispersion corrected density functional, *Phys. Chem. Chem. Phys.* 13 (2011) 19943. doi:10.1039/c1cp21890e.
- [26] G.J. Martyna, M.L. Klein, M. Tuckerman, Nosé–Hoover chains: The canonical ensemble via continuous dynamics, *J. Chem. Phys.* 97 (1992) 2635–2643. doi:10.1063/1.463940.
- [27] J. Schmidt, J. VandeVondele, I.-F.W. Kuo, D. Sebastiani, J.I. Siepmann, J. Hutter, et al., Isobaric–Isothermal Molecular Dynamics Simulations Utilizing Density Functional Theory: An Assessment of the Structure and Density of Water at Near-Ambient Conditions, *J. Phys. Chem. B.* 113 (2009) 11959–11964. doi:10.1021/jp901990u.
- [28] J.P. Merrick, D. Moran, L. Radom, An Evaluation of Harmonic Vibrational Frequency Scale Factors, *J. Phys. Chem. A.* 111 (2007) 11683–11700. doi:10.1021/jp073974n.
- [29] A. Milani, J. Zanetti, C. Castiglioni, E. Di Dedda, S. Radice, G. Canil, et al., Intramolecular and intermolecular OH...O and OH...F interactions in perfluoropolyethers with polar end groups: IR spectroscopy and first-principles calculations, *Eur. Polym. J.* 48 (2012) 391–403. doi:10.1016/j.eurpolymj.2011.11.022.
- [30] T. Shimanouchi, *Tables of Molecular Vibrational Frequencies Consolidated Volume I*, (1972) 1–160.

Supporting information

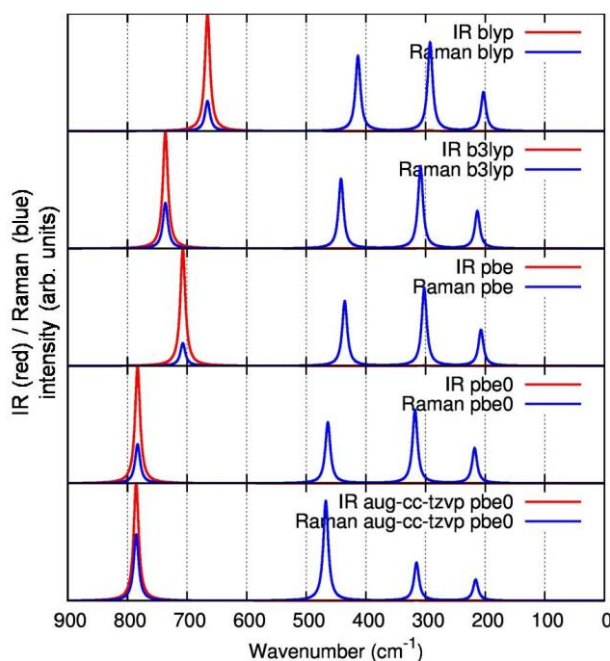


Fig S1. Comparison of the IR (red) and Raman (blue) spectra of CCl_4 molecule predicted at different level of theory.

Tab S1. Comparison of the vibrational frequencies of the CCl_4 molecule predicted at different level of theory with the experimental value [30]. The IR and Raman activity (Yes/No) is also reported.

mode	IR activity	Raman activity	Exp. Freq [cm ⁻¹]	blyp/tzvp [cm ⁻¹]	b3lyp/tzvp [cm ⁻¹]	pbe/tzvp [cm ⁻¹]	pbe0/tzv p [cm ⁻¹]	pbe0/aug-cc-tzvp [cm ⁻¹]
1 (doble degenerate)	N	Y	218	202	213	207	218	216
2 (triple degenerate)	Y	Y	314	292	309	302	317	315
3	N	Y	459	413	441	436	463	467
4	Y	Y	776	665	736	707	783	785

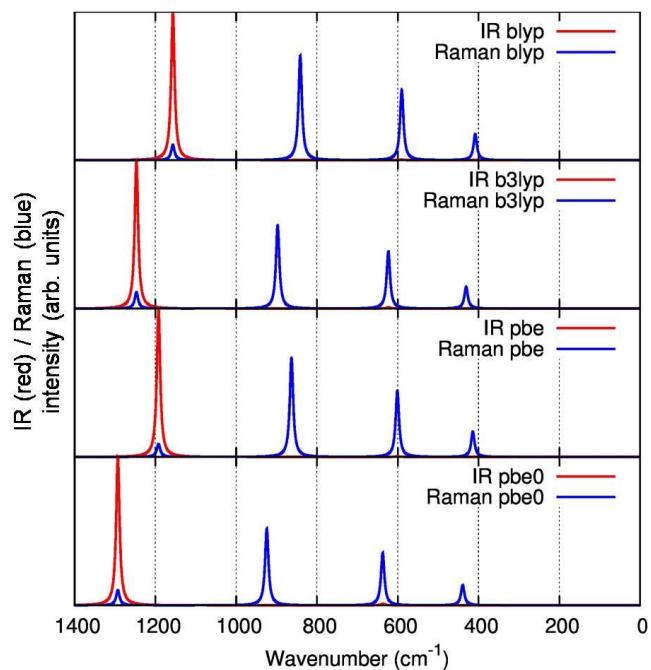


Fig S2. Comparison of the IR (red) and Raman (blue) spectra of CF_4 molecule predicted at different level of theory.

Tab S2. Comparison of the vibrational frequencies of the CF_4 molecule predicted at different level of theory with the experimental values[30]. The IR and Raman activity (Yes/No) is also reported.

mode	IR activity	Raman activity	Exp. Freq [cm ⁻¹]	blyp/tzv p [cm ⁻¹]	b3lyp/tzvp [cm ⁻¹]	pbe/tzvp [cm ⁻¹]	pbe0/tzvp [cm ⁻¹]
1 (double degenerate)	N	Y	435	408	431	414	439
2 (triple degenerate)	Y	Y	632	590	623	601	637
3	N	Y	909	841	897	863	924
4 (triple degenerate)	Y	Y	1281	1157	1247	1192	1293

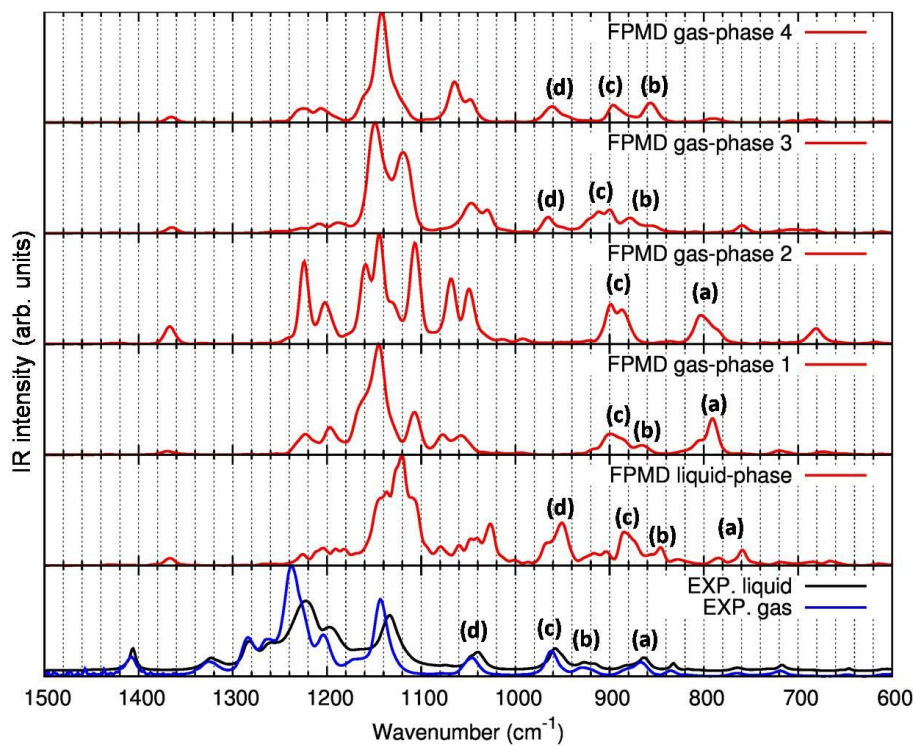


Fig S3. Comparison of the IR spectrum of N1 isolated molecule predicted starting for the equilibration run carried out with different input geometries.

4.2 Combining static and dynamic approaches for the determination of the infrared absorption intensities

4.2.0 Introduction:

As we have already seen in Sections 4.0 and 4.1, the usual method for the prediction of the IR spectrum of a system from a molecular dynamics run, is based on the calculation of the Fourier transform of the dipole autocorrelation function [2,3].

$$I(\omega) \propto \int dt e^{i\omega t} \langle \boldsymbol{\mu}(t) \boldsymbol{\mu}(0) \rangle$$

There are many examples in the literature where this method has been applied successfully for the prediction of the IR spectrum of molecules in gas phase by means of First-principle MD simulations [5–8]. However, this procedure is not free from some limitations and there are still a few critical points:

1) Evaluation of the dipole moment

First-Principle molecular dynamics programs, such as the CP2K and CPMD codes, work in periodic boundary conditions and the correct definition of the dipole moment of an infinite periodic system is not trivial and unambiguous. Different solutions have been proposed in literature: the Berry phase approach and the localization of the wave function by means of Wannier functions are most frequently used.

The Berry phase method [9,10] allows to predict the dipole moment of the system up to a phase factor, in a relatively cheap computational way. However, only the total dipole of the system can be evaluated, and it is not possible to split the partial contributions, for example, from a molecule and from its solvent.

Within the Wannier function formalism [11–14] the electron wave function is localized, at each step of the dynamics, according to an appropriate transformation. The expectation value of the vector position \mathbf{r}_i on the localized Wannier orbital, is interpreted as the site where an electron pair is located: in this way a set of points with formal electronic charge $q_i = -2e$ (or $q_i = -1e$ in an open shell approach) is provided. After the localization of the electronic wave function, the total dipole system can be then evaluated as:

$$\boldsymbol{\mu}(t) = -2e \sum_i \mathbf{r}_i + e \sum_j Z_j \mathbf{R}_j$$

where \mathbf{R}_j and Z_j are respectively the nuclear positions and atomic numbers.

The Wannier localization is a far more expensive method compared to the Berry phase one, but it is usually adopted because it is possible to separate different local contributions and their vibrational contribution.

2) IR spectrum bands assignment

In the usual *static* quantum chemical calculations carried out in double harmonic approximation, the bands of the IR spectrum can be easily assigned on the basis of the computed normal modes eigenvectors: indeed the vibrational frequencies are obtained evaluating the eigenvalues of the vibrational problem, where the normal modes are described by the relative eigenvectors.

Within the molecular dynamics approach, the prediction of the vibrational spectrum is based on a different formalism that does not exploit the calculation of the normal modes, which are defined only in harmonic approximation.

Usually, the assignment of the bands in the dynamic approach, is based on the Vibrational Density Of States (VDOS) obtained from the velocities correlation function, sometimes restricted to a given group of atoms, or from the correlation functions of the internal coordinates.

However, both methods do not distinguish between infrared active or non-active modes, because they don't take into account any information about dipole transitions. Moreover, in the case of delocalized complex vibrational motions, the assignment can be uncertain and ambiguous.

Different models have been presented in the literature [15–20] to overcome this limitation, but they are anyway quite complex and often not adequate as a practical tools for spectroscopic analysis.

To approach problems 1) – 2), we started from the work done by M.P. Gaigeot et al. [21,22] to develop an alternative method for the calculation of the vibrational spectrum: the correlation function of the dipole moment is not used anymore; the spectrum is predicted by the correlation function of the atomic polar tensors (i.e. Cartesian first derivatives of the dipole moment).

In particular, as explained in more detail in Section 4.1.1, the spectrum is predicted by:

$$I(\omega) \propto \sum_{x,y,z} \sum_{m=3N} \sum_{l=3N} \int dt e^{i\omega t} \langle P_{um}(t)v_m(t)P_{ul}(0)v_l(0) \rangle$$

This choice is motivated by the following facts:

1. In the case of *static* calculations in double harmonic approximation, the absolute absorption IR intensities are computed from the Atomic Polar Tensor (APT), so the APTs are easily available since they are printed in the output of standard calculations of the vibrational spectra.
2. As reported by different authors in the literature [23] the APTs can be easily transferred among different molecules, sharing the same chemical groups. Thus it is possible to deal with small model systems (at a high level of theory), and then transfer the APTs to larger and complex systems.
3. The APTs have a partially local character: in fact each APT is associated to displacements of a given atom in the molecule. Therefore, on the basis of the APTs involved, it is relatively easy to separately evaluate the contributions due, for

example, to a solute molecule or to the solvent molecule (Section 4.2.1). Moreover it allows to easily assign the bands in the spectrum (see Section 4.2.3 for details).

4. Using our model, it is possible to decouple the calculation of the velocities correlation function (and hence the vibrational frequencies) from the calculation of atomic polar tensors (see Section 4.2.1). The need to evaluate during the dynamics both the dipole moment and its derivatives forces the employment of FPMD simulations and tight convergence criteria. The possibility to evaluate separately the electronic response and the velocities, should allow to use less stringent convergence criteria for the FPMD. Moreover, usually the VDOS is well described by trajectories much shorter than those required for the prediction of a reliable good spectrum from the correlation function of the dipole moment. Separating the two contributions we are able to predict the spectra with shorter trajectory, without losing in accuracy. The model proposed could be adopted also in the framework of classical dynamics, which may allow to evaluate the velocities evolution in time at reduced computational cost, while keeping separately the description of the APTs at an high quantum level.

In summary the model illustrated below has two main outcomes:

- It allows to study bigger systems
- It makes possible to run longer trajectories

In the 4.2.1 - 4.2.2 - 4.3.3 Sections, we will illustrate the analytical derivation and some applications of this method. The results so far obtained indicate that this approach is very promising and is worth to be further developed and tested in future investigations.

4.2.1 Theory

It has been demonstrated within the time-correlation function formalism [2,3] that the absorption spectrum of an isotropic system is equal to:

$$I(\omega) = \frac{2\pi\beta\omega^2}{3cV} \int dt e^{i\omega t} \langle \boldsymbol{\mu}(t) \boldsymbol{\mu}(0) \rangle = \frac{2\pi\beta}{3cV} \int dt e^{i\omega t} \left\langle \frac{d\boldsymbol{\mu}(t)}{dt} \frac{d\boldsymbol{\mu}(0)}{dt} \right\rangle \quad (4.2)$$

or equivalently:

$$I(\omega)/k_1 = \int dt e^{i\omega t} \left\langle \frac{d\boldsymbol{\mu}(t)}{dt} \frac{d\boldsymbol{\mu}(0)}{dt} \right\rangle$$

where:

$$k_1 = \frac{2\pi\beta}{3cV}$$

Note that in Eq. (4.2) and all subsequent equations, according to the definition of correlation function, we should replace the symbol $\boldsymbol{\mu}(t)$ (used for sake of simplicity) by $\delta\boldsymbol{\mu}(t)$:

$$\delta\boldsymbol{\mu}(t) = \boldsymbol{\mu}(t) - \langle \boldsymbol{\mu} \rangle$$

where $\langle \boldsymbol{\mu} \rangle$ is the average value of $\boldsymbol{\mu}(t)$.
Similarly

$$\delta\left(\frac{d\boldsymbol{\mu}(t)}{dt}\right) = \frac{d\boldsymbol{\mu}(t)}{dt} - \left\langle \frac{d\boldsymbol{\mu}}{dt} \right\rangle$$

If we call μ_u the $u = x, y, z$ component of $\boldsymbol{\mu}$, Eq. (4.2) become:

$$I(\omega)/k_1 = \sum_{u=x,y,z} \int dt e^{i\omega t} \left\langle \frac{d\mu_u(t)}{dt} \frac{d\mu_u(0)}{dt} \right\rangle \quad (4.3)$$

Introducing the vector $\boldsymbol{\xi}$ that collects the $3N$ cartesian coordinates of the N atoms of the system

$$\boldsymbol{\xi} = \begin{bmatrix} x_1 \\ y_1 \\ z_1 \\ x_2 \\ y_2 \\ z_2 \\ \vdots \\ x_N \\ y_N \\ z_N \end{bmatrix}$$

In absence of an external field, $\frac{d\mu_u(t)}{dt}$ can be expanded as:

$$\frac{d\mu_u(t)}{dt} = \sum_{m=3N} \frac{\partial \mu_u(t)}{\partial \xi_m} \frac{\partial \xi_m(t)}{\partial t}$$

We can recognize that $\frac{\partial \xi_m(t)}{\partial t} = v_m(t)$ is the m^{th} Cartesian velocity while $\frac{\partial \mu_u(t)}{\partial \xi_m}$ is the um element of the APT $\mathbf{P}(t)$.

$$\frac{\partial \mu_u(t)}{\partial \xi_m} = P_{um}(t)$$

such that:

$$\frac{d\mu_m(t)}{dt} = \sum_{m=3N} P_{um}(t) v_m(t) \quad (4.4)$$

Substituting (4.4) in (4.3)

$$\begin{aligned} I(\omega)/k_1 &= \sum_{u=x,y,z} \int dt e^{i\omega t} \langle \sum_{m=3N} P_{um}(t) v_m(t) \sum_{l=3N} P_{ul}(0) v_l(0) \rangle \\ &= \sum_{u=x,y,z} \sum_{m=3N} \sum_{l=3N} \int dt e^{i\omega t} \langle P_{um}(t) v_m(t) P_{ul}(0) v_l(0) \rangle \end{aligned} \quad (4.5)$$

While the value of the velocities of all the atoms are easily available at each step of the trajectory, it would be too much expensive to evaluate also the $\mathbf{P}(t)$.

If the "electrical harmonic" approximation holds, $\mathbf{P}(t)$ can be assumed to be independent on the time during the trajectory, provided that it is referred to a "molecular fixed" reference system.

This is supported by the fact that, usually, the velocity correlation function has stronger fluctuations on the small time scale, while the dipole moment derivatives correlation functions is almost constant.

This behaviour can be exploited to reduce the computational cost for the evaluation of (4.5). In this work many approximations have been tested. While, in principle, the same methodology introduced below can be applied to any kind of systems (isolate molecules, condensed phase...), for simplicity we will report the equation referring just to a single molecule.

- **Case A**

If the trajectory is not too long we can assume that the atomic polar tensor does not change at all:

$$P_{um}(t) \sim P_{um}(0)$$

This approximation is severe and can hold only at very low temperature or in solid phase, where no rigid rotations of the molecule or conformational transitions take place.

- **Case B**

For liquid or gas phase dynamics of a single molecule, the molecule can rotate during the trajectory. Accordingly, the internal reference system of the molecule rotates with respect to the external reference system. In order to follow the rotation of the molecule during the trajectory - translations are not considered since $\mathbf{P}(t)$ is translational invariant - we can apply a rotation matrix to the $P_{um}(0)$, which is assumed to be constant in the molecular fixed system.

$$\mathbf{P}(t) = \mathbf{R}(0 \rightarrow t)\mathbf{P}(0)$$

If we call $\mathbf{X}(t)$ the $3 \times 3N$ matrix that collects the Cartesian coordinates of the N atoms of the molecule in the center of mass reference system, $\mathbf{R}(0 \rightarrow t)$ is the rotation matrix describing the best superimposition between $\mathbf{R}(0 \rightarrow t)\mathbf{X}(0)$ and $\mathbf{X}(t)$. To evaluate \mathbf{R} , in this work, we used a quaternion fit as implemented in the TINKER code [24,25] that minimizes the sum of the squared distances between corresponding atoms. In the case of flexible molecules and to avoid the noise generate by fast vibrating atoms (like the H atoms of a CH_3 rotor), the use of an appropriate subset of atoms for the definition of the positions vectors \mathbf{X} , can be a smart choice for the quaternion fit.

Another possible strategy to determine $\mathbf{R}(0 \rightarrow t)$, is to evaluate $\mathbf{P}(0)$ in the principal axis reference system: $\mathbf{R}(0 \rightarrow t)$ can be then estimated as the rotation matrix at the instant t between the laboratory reference system and the principal axis reference system.

For both cases, the \mathbf{R} matrix has to be calculated at each time step of the simulation (usually 0.1 fs - 0.5 fs).

As a conclusion, we must stress again that both the strategies proposed do not take into account the effects of the deformations of the molecular geometry. However it reasonable to assume that, for small displacements (deformations due to vibrational motions), this error is negligible.

- **Case C**

While the method proposed in Case B can take into account of the rotation of the molecules as a rigid bodies, it can't describe internal rotations i.e changes in the molecular conformation. Considering as example the Ala-Ala-H⁺ molecule (discussed in more detail in Section 4.2.2), this molecule has two stable conformers at room temperature separated by a low energy barrier. During a simulation both conformations are explored: the APT changes are usually non-negligible between the two minimum structures and we cannot consider a constant $\mathbf{P}(t)$ for both of them.

To take in consideration jumps among different equilibrium conformations during the trajectory, instead of using a single APT, we can approximate the $P_{um}(t)$ with a step function. The trajectory is divided in intervals $\Delta t_i = (t_{i+1} - t_i)$, and for each interval Δt_i we assume

$$P_{um}(t) = P_{um}(t_i) \quad \text{if} \quad t_i < t < t_{i+1}$$

or alternatively

$$P_{um}(t) = P_{um}\left(t_i + \frac{\Delta t_i}{2}\right) \quad \text{if} \quad t_i < t < t_{i+1}$$

The maximum length of the Δt_i intervals required to take into account the variations of $\mathbf{P}(t)$, is strongly dependent on the dynamic of the system under study. Slow evolving systems, like rigid molecules at low temperature (see the NMA cis example in

Section 4.2.2), will require Δt_i of the order of the picoseconds, while other system with a fast dynamics might demand more than one 1 APT each 100 fs of simulation. Obviously the transformation of Case B can still be applied: in each "macro" interval Δt_i , we can rotate at each time step $\mathbf{P}(t_i)$ to follow the rotation of the molecule (Case B + Case C approximation, in Section 4.2.2).

$$\mathbf{P}(t) = \mathbf{R}(t_i \rightarrow t)\mathbf{P}(t_i) \quad \text{if} \quad t_i < t < t_{i+1}$$

Indeed in many case this allows to increase greatly Δt_i (so less APTs to compute) without loss of accuracy (See, for example, the NMA trans and the Ala-Ala-H+ case in Section 4.2.2).

- **Case D**

With case C, using the proper time interval Δt_i between the evaluation of different APTs, we should be able to get a reliable description of internal rotation due to changes in the molecular conformation or to large amplitude vibrations. However, there are cases (for example in presence of fast rotating CH_3 groups) in which the required time interval would be too small and so the calculation of too many APTs is required. To avoid this problem, we propose a further approach to evaluate $\mathbf{P}(t)$. Considering again a single molecule that during a trajectory can change conformation one or more times, a reasonable hypothesis is that $\mathbf{P}(t)$ at an instant t , can be properly described by a linear combination of atomic polar tensors \mathbf{P}_j^{ref} of a set of appropriate reference structures $\{j\}$.

$$\mathbf{P}(t) = \sum_j w_j \mathbf{R}_j(0 \rightarrow t)\mathbf{P}_j^{ref}(0)$$

The matrix $\mathbf{R}_j(0 \rightarrow t)$ must be introduced in the equation to ensure the consistency of the internal reference system of the $\{j\}$ structure with the one of the molecule at the time t . The reference structures can be chosen following different strategies. For example it is possible to use the stable conformations of the molecule, if available, or the stable conformations with the addition of some transition points along the torsional potential barrier (see the Cl⁻ methanol example in Section 4.2.2). Another possibility is to choose randomly some structures along the trajectory and to use them as a reference. To evaluate the weights of the combination w_j , we followed a strategy similar to the one propose by Mathias et. al. [17]. We assumed a Gaussian distribution around the reference structures:

$$w_j(t) = \frac{\exp\left(-\frac{d_j}{2\sigma_c}\right)}{\sum_j \exp\left(-\frac{d_j}{2\sigma_c}\right)}$$

where d_j is a properly defined distance measuring the difference between the geometry of the molecule at instant t and the reference structure j and σ_c is the width of the Gaussian.

One possibility is to use a Cartesian distance like $\|\mathbf{R}(0 \rightarrow t)\mathbf{X}_j^{ref} - \mathbf{X}(t)\|$. However this choice can generate numerical noise: changes of all the internal coordinates are considered in this way, and, for example, bond and angle vibrational displacement can be treated as a change in the conformation. To avoid this problem we introduce a different distance, simply based on the torsional angles:

$$d_j(t) = \sqrt{\sum_k^{N_t} \theta_k(t) - \theta_k^j}$$

where $\theta_k(t)$ is the k -th torsional angle of the molecule at the step t , θ_k^j is the corresponding torsional angle value of the reference structure j . In most of the case a small number N_t (even one) of torsional angles allow to univocally characterize the different reference structures.

Rotational contributions Eq. (4.5) generate the whole absorption spectrum, which, in principle, include both the contribution of vibrational transitions and of the associated rotational structure, as well as rotational transitions. However, often the rotations are not well sampled by the trajectory and so can generate artefacts in the spectrum. For this reason it is often advisable to keep out rotational contributions from the predicted spectra.

Different strategies can be adopted:

- Remove the rotations contribution to the velocity:
We can substitute in Eq. (4.5) the instantaneous velocity, with an approximated vibrational velocity

$$\mathbf{v}_i^{vib}(t) = \mathbf{v}_i(t) - \mathbf{v}_{CM}(t) - \boldsymbol{\omega}(t) \wedge \mathbf{r}_i^{CM}(t)$$

where $\mathbf{v}_{CM}(t)$ is the velocity of the center of mass and $\mathbf{v}_i^{CM}(t)$ is the velocity of the i -th atom and $\boldsymbol{\omega}(t)$ is the angular velocity related to the rigid rotation of the molecule.

- Remove the rotational contributions directly from the APT:
The atomic polar tensor \mathbf{P} can be decomposed in two contribution: one related to vibrations, the other instead related to variation of the dipole moment due to rigid rotation of the molecule.

$$\mathbf{P} = \mathbf{P}^{vib} + \mathbf{P}^{rot}$$

\mathbf{P}^{vib} is the contribution of the vibrations to the change of the dipole moment expressed in Cartesian coordinates and it is the only necessary term to generate the vibrational IR spectrum:

$$I(\omega)/k_1 = \sum_{u=x,y,z} \sum_{m=3N} \sum_{l=3N} \int dt e^{i\omega t} \langle P_{um}^{vib}(t) v_m(t) P_{ul}^{vib}(0) v_l(0) \rangle$$

One possible way to evaluate \mathbf{P}^{vib} is to calculate \mathbf{P}^{rot} , that can be expressed as a function of the static dipole moment $\boldsymbol{\mu}_0$ and of the inertia moment \mathbf{I} [23].

$$\mathbf{P}^{rot} = \mathbf{P}_\rho \cdot \boldsymbol{\beta}$$

where $\mathbf{P}_\rho = \mathbf{P}_\rho(\boldsymbol{\mu}_0, \mathbf{I})$ and $\boldsymbol{\beta}$ is defined by the Eckart-Sayvetz conditions and it defines the rotational and translational collective coordinates. When $\boldsymbol{\mu}_0$ is not known with the required accuracy, a second possibility is to project \mathbf{P} on the vibrational subspace by using a set of coordinates, for example the internal coordinates \mathbf{R} , that is complete for the description of the vibrational sub-space but exclude the rotations.

In this case:

$$\mathbf{P}^{vib} = \mathbf{P} \cdot \mathbf{A} \cdot \mathbf{B}$$

$$\text{where } B_{ij} = \frac{\partial R_i}{\partial \xi_j} \text{ and } A_{ml} = \frac{\partial \xi_m}{\partial R_l}.$$

In this work we use this second method to remove the rotational contribution. In particular we adopted the Wilson definition of internal coordinate [26] to describe the vibrational subspace and the transformation \mathbf{A} and \mathbf{B} matrices, defining the relationships between internal and Cartesian displacements coordinates.

4.2.2 Results

Before the discussion of our results, we must underline that all the test cases analyzed are molecules with a sufficiently high moment of inertia such that rotational transitions do not appear in the infrared absorption spectrum. For this reason, for all the cases here presented, it is not necessary to introduce corrections aimed at the removal of the rotational contribution from ATPs or velocities (see Section 4.2.1).

As first step, it is important to verify if our model is able to predict IR spectra comparable to those obtained from the correlation function of the dipole moment. To this aim, we used the same FPMD simulations to predict the spectra both through dipole correlation function and according to our models.

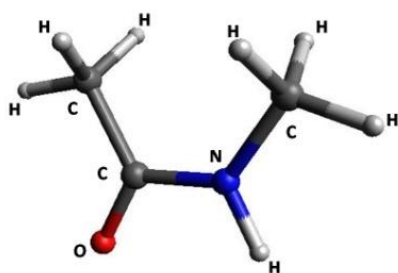
The systems tested were selected among previously published cases, for which the IR spectrum obtained with the "standard" FPMD method, nicely reproduced the experimental spectrum.

We decided to evaluate the ATPs by means of the Gaussian code. For consistency with the FPMD simulations, the functional BLYP [27,28] has been adopted, together with the 6-

311++G** basis set, chosen as a compromise between the required accuracy [29] and the need to limit the computational cost.

We already pointed out that one of the advantages of our method is the possibility to calculate velocities and the electronic response at different levels of the theory. In these grounds additional tests with different functionals and basis sets, both for the computation of the MD trajectory and for the APT's evaluation, will be required in the next future.

N-Methylacetamide(NMA) cis isomer at 20 K



Trajectory info:

Number of steps: 25000

Time steps: 0.4 fs

Trajectory length: 10 ps

T=20 K

BLYP/TZV2PX-MOLOPT-GHT + 340Ry

REF.[5,21]

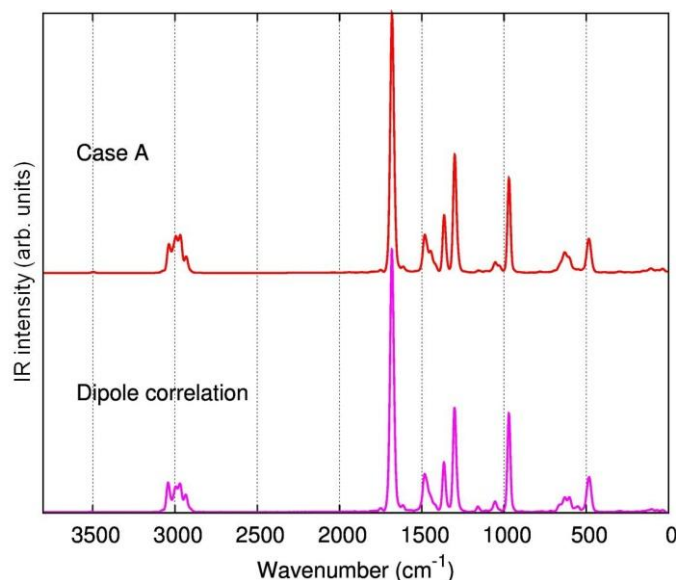
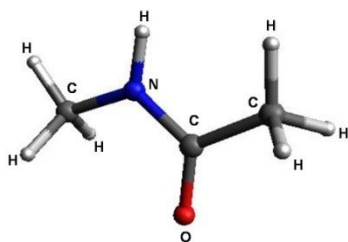


Fig. 4.1 Computed infrared spectrum of the N-Methylacetamide(NMA) cis isomer at 20 K.

In this case, at 20 K the molecule can only vibrate around the equilibrium geometry and conformational changes are inhibited. Therefore, as shown in Figure 4.1, our model in its simplest version (Case A) already predicts a spectrum practically superimposable to the one evaluated with the dipole correlation function.

N-Methylacetamide(NMA) trans isomer at 300 K



Trajectory info:

Number of steps: 25000

Time steps: 0.4 fs

Trajectory length: 10ps

T=300 K

BLYP/TZV2PX-MOLOPT-GHT+340Ry

REF:[5,21]

For this case there are two critical features to take into account:

- The NMA molecule doesn't change conformation during the trajectory, but it can rotate.
- During the trajectory, large amplitude motions involving the CH₃ groups, namely rotations around the CC bond, are active and they are coupled mechanically to all the other vibrational motions.

Before analyzing the results, it is worth to point out that, in the case of the B correction (see paragraph 4.2.1 for details), the rotation matrix $\mathbf{R}(t_0 \rightarrow t)$ has been evaluated without considering the H atoms of the CH₃ groups in the subset of atoms for the quaternion fit, in order to avoid spurious effects due to vibrational displacements.

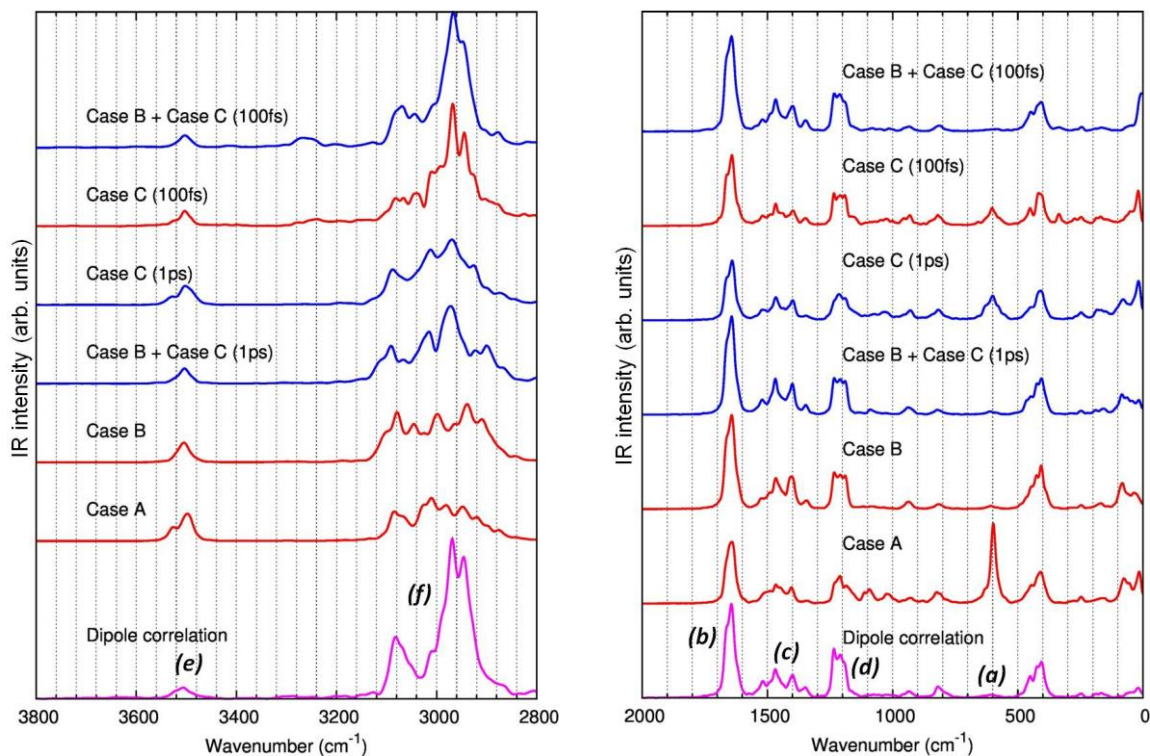


Fig. 4.2 Computed infrared spectra of the N-Methylacetamide(NMA) trans isomer at 300 K.

From Figure 4.2 it is immediately evident that Case A approximation fails to give a correct description of the vibrational spectrum. For example the band (a), at 600 cm^{-1} , is strong in the spectrum of Case A, but very weak in the reference spectrum (from dipole correlation). This band, related to skeleton modes of the molecule, is very sensitive to the effects of the rotation of the whole molecule, and less sensitive to the torsions of the CH_3 groups. Therefore it is better described by using a single APT rotated to follow the trajectory (case B), rather than using a new APT, not rotated, each $\Delta t_i = 100\text{ fs}$ (case C). Indeed it can happen that in a time interval of 100 fs the molecule rotates in a non-negligible way.

A similar behaviour is found for the band (b) at 1650 cm^{-1} (amide I band), underestimated in intensity in all cases in which B correction is not used.

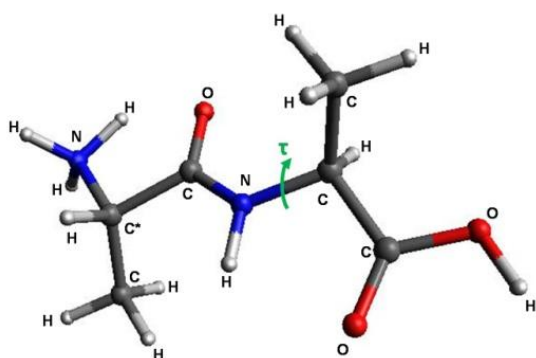
Let now consider the group of bands between 1600 and 1300 cm^{-1} (c), related to the CH_3 bendings: In this case approximation B is necessary for a proper description of the spectrum; however the relative intensities of this group of bands is better predicted by using many APTs to calculate the spectrum (B + C). This is due to the large amplitude torsional motions of the CH_3 , which are coupled with the bending modes. Similar arguments can be applied to the convolution of bands at 1200 cm^{-1} (d) associated to the NH-bending, mechanically coupled to the torsional motions of the CH_3 .

However, while (c) is not very sensitive to the different points of the torsional potential surface of CH_3 (just one APT each $\Delta t_i = 1\text{ ps}$ is required), for a correct description of the shape of (d) it is necessary to use a least one new APT each $\Delta t_i = 100\text{ fs}$.

Finally, consider the high frequencies region. The NH stretching band at 3500 cm^{-1} (e) is decoupled from the torsional motions of the CH_3 and is therefore well described already using a unique APT, provided to correct the rotation effects (case B).

On the other hand, the CH-stretching modes (bands between $3100 - 2800\text{ cm}^{-1}$) are coupled to the CH_3 torsional motions and only the combination B + C with an APT each $\Delta t_i = 100\text{ fs}$ is able to predict the correct shape of the bands.

Protonated Alanine Dipeptide (Ala-Ala-H⁺) trans conformers at 300 K



Trajectory info:

Number of steps: 30000

Time steps: 0.5 fs

Trajectory length: 15 ps

T=300 K

BLYP/DZVP-GHT + 320Ry

REF. [5,30,31]

As demonstrated in Ref. [30], at room temperature this molecule shows a continuous isomerization between two conformers TransA1 and TransA2. These two conformers are

characterized by a different value of the torsional angle τ (-C-N-C-COOH): $\tau = 201.5^\circ$ for TransA1 and $\tau = 279.5^\circ$ for TransA2 (from Gaussian BLYP/6-311++G** geometry optimization).

This continuous isomerization is due to the fact that the potential surface has a small barrier between TransA1 and TransA2 (See Figure 4.3).

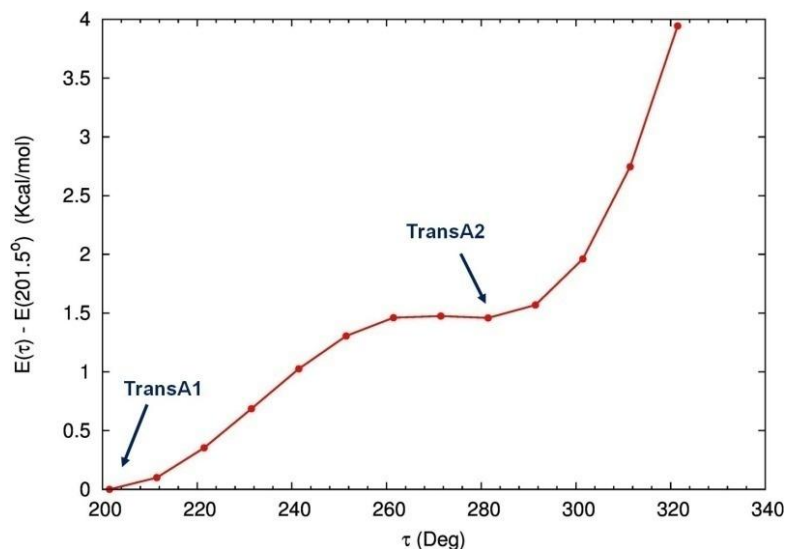


Fig. 4.3 Potential energy scan along the τ torsional angle (-C-N-C-COOH) of (Ala-Ala-H+).

Moreover, while the energy difference between the two conformers at 0 K is about 1.5 kcal/mol (Gaussian calculations BLYP/6-311++G**), at 300 K entropic contributions lower the free energy difference to 0.3 Kcal/mol (see Ref. [30] for details).

Before going into the details of the analysis, note that, given the greater total mass of the Ala-Ala-H+ molecule, rotational motions are present, but they are less relevant than in NMA trans isomer. Despite this, the B correction will be crucial.

Another difference, compared to NMA trans isomer, is that the CH_3 large amplitude torsional motions are not active for the Ala-Ala-H+ at 300 K.

Therefore, Ala-Ala-H+ is the ideal choice for discussing how conformational changes are described by the different approximations proposed in paragraph 4.2.1.

It should be noticed that due to the computational costs, the evaluation of the APT has been carried out each $\Delta t_i = 250$ fs in case C.

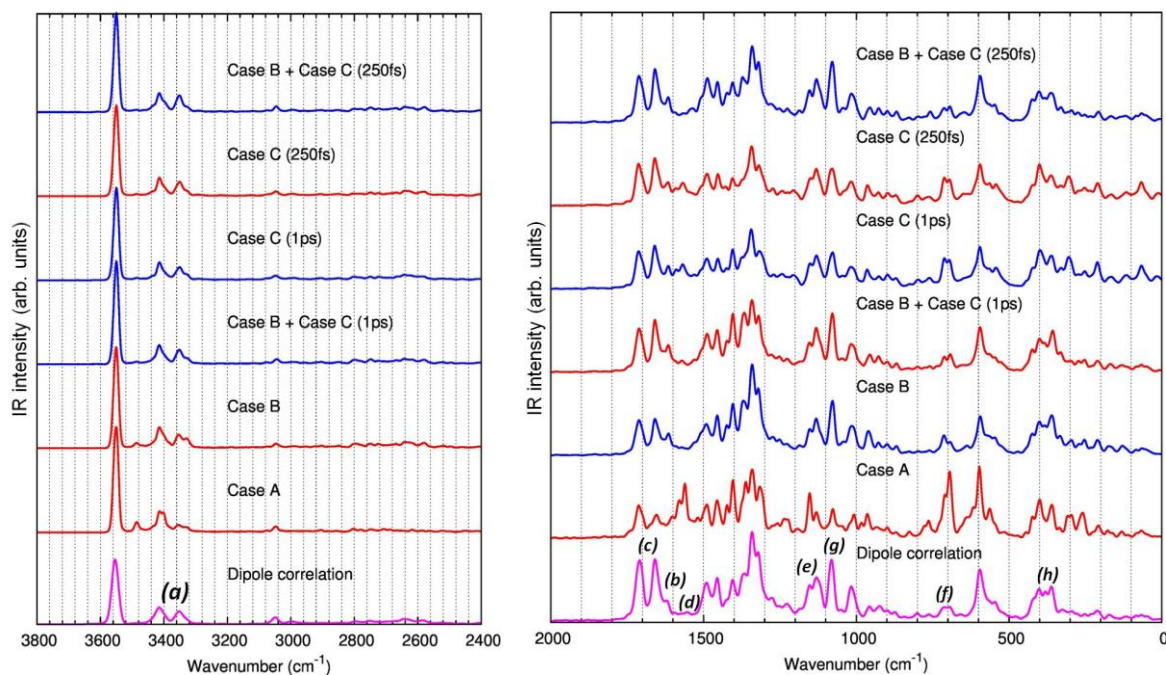


Fig. 4.4 Computed infrared spectra of the Protonated Alanine Dipeptide (*Ala-Ala-H⁺*) *trans* conformers at 300 K.

Let's consider first the region of the spectrum above 3000 cm^{-1} (Figure 4.4): given the large inertia of the molecule and the short length of the trajectory, the effects of the rotation are small. Changing an APT each $\Delta t_i = 1$ ps (Case C), without any further correction of type B, a spectrum that reproduce accurately the one obtained from the dipole correlation, is predicted. On the contrary, if we correct the rotation (Case B) and we employ a single APT for the whole trajectory and therefore we do not consider the conformational changes, a spurious band (related to the OH-stretching of the COH) appears around 3500 cm^{-1} (a).

In the spectral region below 2000 cm^{-1} (Figure 4.4), we can see that the effects of the rotation are not negligible, although the molecule rotates less than the *trans*-NMA. The spectrum predicted for case A is clearly inadequate and therefore it will not be taken into account for further consideration.

Let's focus now on the group of bands between 1600 cm^{-1} and 1700 cm^{-1} . The shoulder at 1611 cm^{-1} (b), related to the bending of the CH_3 group bonded to the carbon C^* , is slightly sensitive to rotations of the molecule and not sensitive to changes in conformation; for this reason it is predicted with almost the same shape and intensity by all the approximations. On the other hand, the two bands (c), at 1714 cm^{-1} (C = O stretching of the acid group), and 1663 cm^{-1} (amide I band), are predicted with the right shape in all cases, but their predicted intensity is generally weaker than in the reference spectrum.

In particular, only with the B+C correction and a calculation of new APTs each $\Delta t_i = 250$ fs, the intensity ratio with respect to the group of bands in the region under the 1500 cm^{-1} is correctly reproduced. This is due to the fact that both groups of bands are sensitive to the changes of conformation.

The region between 1600 cm^{-1} and 1500 cm^{-1} (d), related to NH bending of both the amide group and the NH_3 , gives a further demonstration of the importance of the B correction. Indeed, this region is well-predicted just by using Case B with a single APT, while it is too noisy when employing C also using APTs computed each $\Delta t_i = 250\text{ fs}$.

The same behaviour is shown by the two bands (e) between 1200 cm^{-1} and 1100 cm^{-1} . Since these bands are due to CH and NH bending of the NH_3 and CH_3 groups bonded to carbon 3, they are not affected by changes in conformation.

Another example of this behaviour is the doublet at 700 cm^{-1} (f), related to skeleton vibration (in particular to torsion on the amide group), which is too intense if the B correction is not adopted.

Considering instead the structured region between 1500 cm^{-1} and 1300 cm^{-1} , related to the CH and NH bending, we found that this group of bands is very sensitive to both the rotation of the molecule and conformational changes. Therefore the spectral pattern and intensity ratios with respect to the other region of the spectrum can be predicted only using B + C and with the APTs computed each $\Delta t_i = 250\text{ fs}$. Similar considerations can be applied to the band at 400 cm^{-1} (h), related to skeleton vibrations.

Therefore, up to now, we have demonstrated that some bands can be well predicted by using only B + C and changing the APTs each $\Delta t_i = 250\text{ fs}$. This procedure, however, is expensive from the computational viewpoint: in the case here under consideration we had to evaluate 50 different APTs.

We therefore decided to test an alternative route described, namely Case D in Section 4.2.1.

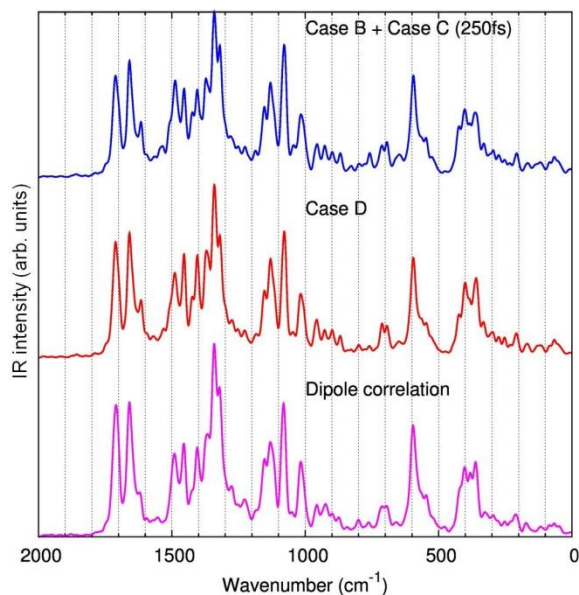
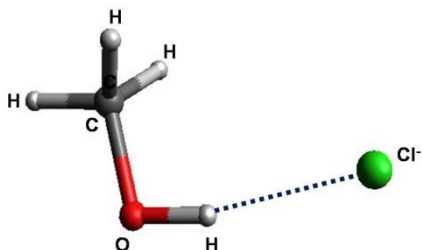


Fig. 4.5 Computed infrared spectra of the Protonated Alanine Dipeptide (Ala-Ala-H⁺) trans conformers at 300 K: Case D tests.

We evaluated the APT of the two conformers at the equilibrium geometry and built the APT at each step of the trajectory as a weighted average of only these two contribution, according to the procedure reported in paragraph 4.2.1.

The spectrum thus obtained (Figure 4.5) shows the same accuracy as the one calculated by the case B + C ($\Delta t_i = 250$ fs), at cost which is 1/25 (i.e. it uses 2 ATPs instead of 50)! This findings indicates that case D, when an appropriate number of reference geometries are used, can take into account correctly the evolution in the conformation of the molecule and its influence on the spectral pattern.

Cl⁻-Methanol ionic complex at 100 K



Trajectory info:

Number of steps: 11823

Time steps: 0.4 fs

Trajectory length: 4.5ps

T=100K

BLYP/aug-TZV2P-GHT+360Ry

REF:[32]

The Cl⁻Methanol cluster allowed to test the ability of the D correction to predict the spectrum of a molecule in the presence of a large amplitude torsional motions. Indeed at 100K the CH₃ group rotates practically freely around CC bond.

We tested two possible choices for the D correction:

- Using only the APTs corresponding to the three minima positions of torsional potential surface of the CH₃: Case D(min)
- Including also of the contribution of transition geometries (maximum of the torsional potential surface) between two minima: Case D (min + max)

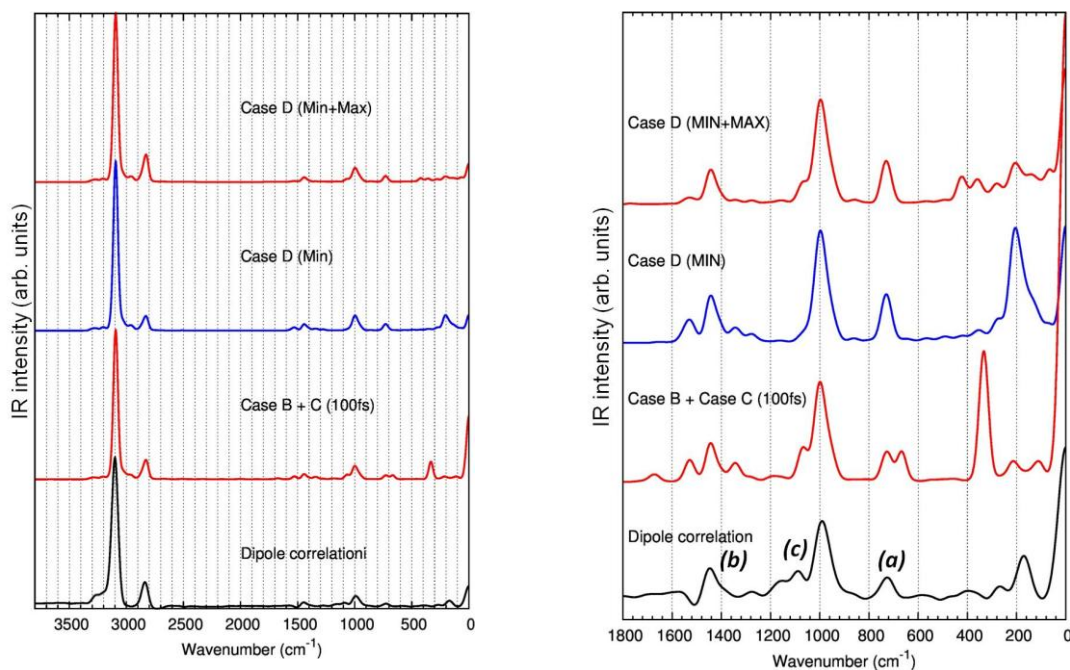


Fig. 4.6 Infrared spectra of the Cl⁻ Methanol ionic complex at 100 K

As reported in Figure 4.6, even by employing the correction B + C with a frequency of $\Delta t_i = 100$ fs, the calculated spectrum shows spurious bands compared to the reference (spectrum from the dipole correlation). The doublet around 750 cm^{-1} (a) of the spectrum B + C, is described as single band in the reference spectrum. This band, related to the CH_3 torsional motions, is well described by Case D, already considering a weighted average of the APTs relative to the minimum points of the torsional potential only.

On the other hand, for the bands between 1400 cm^{-1} and 1500 cm^{-1} (b), it is necessary to take into account the contribution of the transition points (case D (min+max)). Indeed, this region of the spectrum is related to the CH_3 and C-OH bending, which is strongly mechanically coupled with the CH_3 torsional motions (see also paragraph 4.2.3).

Let's consider now the convolution of two bands around 1000 cm^{-1} (c): the stronger band, due to the CO stretching, is well described by all the cases; on the other hand the shoulder around 1100 cm^{-1} , due to the CH_3 bending, is well described only by C + B (100 fs) or D (min + max). If we use the D correction, taking into account only the minimum geometry (D (min)), the intensity is underestimated.

Finally, let's analyze the region below 400 cm^{-1} : this region, related to the "intermolecular" vibrations (e.g. between the Cl^- ion and the molecule of methanol), is very sensitive to the description of the CH_3 torsional contributions. It is therefore described correctly only in case D, by using both the minimum and the maximum points. However, the prediction also in this case does not perfectly reproduce the reference spectrum. It must be noticed that, at such low frequencies, rotational transitions could make a contribution to the infrared spectrum.

As a conclusion, we can state that the results of the Cl^- Methanol cluster, together with those of the Ala-Ala-H+, indicate that the D method allow to predict an accurate spectrum both in case of flexible molecules characterized by more than one stable conformations and/or by large amplitude motions; the key point is taking into account enough geometries to build up the different APTs suitable for an accurate description of the electrical contribution along the whole trajectory. The Cl^- Methanol cluster shows that in some cases also the transition states between two stable conformations could give important contributions. Even if further investigations are required to better evaluate this feature, the computational cost of case D is still limited, and much lower respect of other choices and we believe that it is the most promising model for the implementation of our method.

4.2.3 Band assignment

As explained in the introduction, the assignment of the bands of the IR spectrum, obtained from MD simulations, is usually done on the basis of the vibrational density of states. The velocity correlation function and the correlation function of internal coordinates, however, do not contain any information about the intensities and therefore do not distinguish between active and inactive modes, and among strong and weak bands. Also in the case of non-localized vibrational motions, the assignment is a tricky task.

To solve these problems, starting from the equation (4.5), M.P. Gaigeot et al. [22], proposed a method to project the trajectory on the normal modes (evaluated by *static* calculations), then

assigning the bands of the spectrum on this basis. This method does possess some disadvantage anyway: it is necessary to evaluate at each step of the trajectory the transformation from Cartesian coordinates to normal modes, in addition the description of the Cartesian velocity in the normal mode reference system is required. These features make the method expensive and not straightforward to be applied and implemented.

In this contest, we decided to develop an alternative method, which allows to work with Cartesian velocities as obtained from the molecular dynamic simulation.

As already explained in paragraph 4.2.1

$$\mathbf{P} = \mathbf{P}^{vib} + \mathbf{P}^{rot}$$

To predict the vibrational spectrum we need only to \mathbf{P}^{vib} while \mathbf{P}^{rot} can be neglected. We have already shown that

$$\mathbf{P}^{vib} = \mathbf{P} \cdot \mathbf{A} \cdot \mathbf{B}$$

and the generic ij element of the \mathbf{P}^{vib} matrix can be written as:

$$P_{ij}^{vib} = \left(\frac{\partial \mu_i}{\partial \xi_j} \right)^{vib} = \sum_T \frac{\partial \mu_i}{\partial R_T} \frac{\partial R_T}{\partial \xi_j}$$

It is therefore always possible to consider separately the contributions of the different internal coordinates to vibrational atomic polar tensor \mathbf{P}^{vib} in Cartesian coordinates.

In particular, it is possible to set to zero all the contributions of internal coordinates different from a selected one, R^* ($\frac{\partial \mu_i}{\partial R_T} = 0$ if $R_T \neq R^*$). Accordingly we can substitute the $\mathbf{P}^{vib,*}$ so obtained in Eq. (4.5) and evaluate the contribution of the only R^* coordinate to the whole IR spectrum. If the procedure is repeated by selecting in turns each internal coordinate, we can obtain information about the relevant internal coordinates which contributes to the IR activity of each band.

An alternative procedure makes use of a set of normal coordinates \mathbf{Q} which indeed form a complete set of coordinates in the vibrational space; normal coordinates are obtained solving the vibrational problem in harmonic approximation. The following relationships hold:

$$P_{ij}^{vib} = \left(\frac{\partial \mu_i}{\partial \xi_j} \right)^{vib} = \sum_s \frac{\partial \mu_i}{\partial Q_s} \frac{\partial Q_s}{\partial \xi_j} = \sum_s \frac{\partial \mu_i}{\partial Q_s} L_{js}$$

Note that standard codes such as Gaussian provide the eigenvector matrix (\mathbf{L}) needed for the analysis. Also in this case we can select a given Q^* and evaluate its contribution to APTs in order to predict the whole IR spectrum, according to MD. Compared to an assignment based on VDOS or on the correlation function of internal coordinates, the proposed method has the advantage of taking into account only IR active vibrational modes.

As a last remark, it is important to underline that the method here proposed is based on the **contribution** of the different vibrational coordinates **to the intensities** of the bands.

Coordinates carrying small or vanishing IR activity will show no contribution in the whole spectrum. For this reason the resulting band assignment can be slightly different from that usually adopted in the framework of the *static* approach in double harmonic approximation, based on the analysis of vibrational eigenvectors. Indeed, vibrational eigenvectors provide information on the internal coordinates involved in the motion, irrespective of the fact that they give rise to large or vanishingly small dipole changes.

To demonstrate the reliability and usefulness of our method we propose two examples.

In Figure 4.7 the spectrum of the NMA *cis* isomer (already described in the Section 4.2.2) is compared to the spectrum predicted by considering the sole contributions to the atomic polar tensor of C=O bond stretching and of the C=O stretching normal mode.

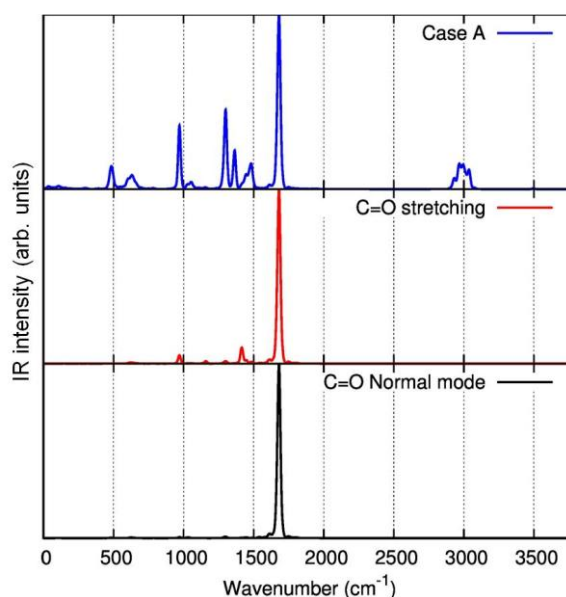


Fig. 4.7 Infrared spectrum of the N-Methylacetamide (NMA) cis isomer at 20 K. Upper panel: complete spectrum. Central and lower panel: C = O bond stretching and C = O normal mode contribution to the spectrum

Both "partial" spectra describe perfectly the band located at about 1700 cm^{-1} , where CO stretching mode is expected to occur. If one works with internal coordinates, while considering $R^* = R_{C=O}$ the predicted spectrum highlight also the (minor) contributions of this coordinate to other vibrational motions, at lower frequency.

As a second case we analyzed the complex Cl^- Methanol.

We already discussed, the importance of the CH_3 rotation (i.e. the torsional vibration $R^* = \tau$) to the IR spectrum, and how this motions is mechanically coupled to other vibrations.

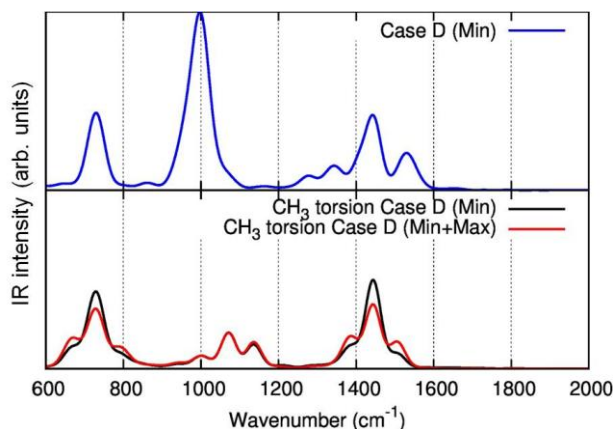


Fig. 4.8 Infrared spectra of the Cl-Methanol ionic complex at 100 K. Top panel: spectrum predicted from contribution of the whole APTs. Lower panel: CH₃ torsion contribution to the spectrum.

In Figure 4.8 we evaluated the contribution of the torsional motion of CH₃ to the vibrational spectrum: the two bands at 600 cm⁻¹ and 1500 cm⁻¹, well described only by D method, receive contributions from the CH₃ torsional motions, explaining why the other approximations, from Case A to Case C, fail.

With these two examples we have shown the usefulness of our method for the assignment of the bands in the IR spectrum. However, it is important to emphasize that we illustrated here only some preliminary tests. Further investigations will be needed to check the ability of this method to describe more subtle features, such as for example the coupling of vibrational modes, related to anharmonic effects.

4.2.4 Conclusions

The "standard" method for the prediction of the spectrum from FPMD simulations, although powerful, does possess some limitations due to the high computational cost.

Starting from previous works by M. Gaigeot et al. [21,22], we have developed and implemented a model to compute the IR spectrum from the correlation function of velocities and from the suitable APTs contributions, instead of the correlation function of the total dipole moment of the system.

Different strategies have been proposed to make the calculation computationally feasible and reliable. In particular the combination B + D (compensation of the rotational motion of the molecule + use of a weighted average of few APTs, calculated in correspondence of selected different molecular structures) allows to obtain a spectrum which is in good agreement with the reference spectrum, namely the spectrum obtained through the correlation function of the dipole moment.

For example, compared to the method proposed in Ref. [15] that requires the evaluation of a new set of APTs for each step of about $\Delta t_i = 1$ fs, our model allowed to predict a fairly good IR spectrum of Ala-Ala-H⁺ trans isomers with only two APTs, for 15 ps of trajectory. In addition, we proposed a relatively simple method for the assignment of the vibrational bands of the IR spectrum based on internal coordinates or harmonic normal modes.

As in the model proposed in Ref. [22], our method takes into account the contribution to absorption intensity of a given vibration, contrary to the VDOS analysis.

The method here proposed has the further advantage of working almost entirely in the Cartesian coordinates space. It does not require to calculate the velocities of the internal coordinates/ normal modes along the whole trajectory, thereby increasing the accuracy and reducing the computational weight.

In this chapter we illustrated a preliminary study on the applications of this model. Further works will be needed in the future to clarify some aspects:

- Is it possible to overcome the accuracy of the standard method in reproducing experimental spectra, by suitably selecting the level of theory for the calculation of the trajectory and of velocities, and for the evaluation of the APTs?
- Does this model also work properly for solid state systems?
- How much can we relax the convergence criteria of the FPMD to obtain reliable velocities? Can we use classical dynamics simulations?
- What is the minimum length of a trajectory for a reliable prediction of the spectrum?
- Is the method proposed for the band assignment suitable to detect anharmonic couplings and for the assignment/interpretation of overtones/combination features?

Despite the open issues here outlined, the results obtained, even if not exhaustive, indicate that the path undertaken is promising.

4.3 Applying FPMD to crystalline polymers: the PE test case

4.3.0 Introduction

As demonstrated by our investigation on the N1 molecule (Section 4.1), and by the several studies published in the literature [5–8], First Principles Molecular Dynamics proved to be a very powerful and promising tool for the prediction of the vibrational spectra of complex systems.

However the investigations proposed up to now with this technique focused mainly on gas-phase or liquid-phase systems: therefore, in collaboration with M.P. Gaigeot (University of Evry), we decided to extend FPMD simulations to the case of crystalline molecular materials, and in particular to polymer systems. Up to our knowledge, this is an almost unexplored field in computational materials science.

We demonstrated in Chapter 2 that DFT-*static* calculations, can provide important information for the characterization of polymers and for the understanding of their structure-properties correlations. On the other hand in static calculations the effects due to the environment (solvent, temperature, pressure, strain...), which play a relevant role also from the technological point of view, cannot be introduced so easily in the calculations. In this context, we decided to explore the potentialities of molecular dynamics: an MD approach allows indeed to evaluate the effects of intra- and intermolecular interactions on the supramolecular organization of molecular materials including the effects of a real environment and external variables and all the phenomena affecting bands shape of the vibrational spectrum.

The high computational cost of FPMD simulations is justified since spectroscopic properties are the focus of our investigation, aiming at a detailed description of both frequencies and intensities which is not guaranteed at all by using simulations based on classical dynamics with standard force fields.

As an example of this, the study proposed by Mavrantza et al. [33] is particularly significant: by using the COMPASS force field, the authors predicted the vibrational frequencies in the IR spectrum of polyethylene shifted only of 10-20 cm^{-1} with respect to the experimental data, and they correctly described the behavior of the CH-stretching frequencies as a function of temperature. However, in the deformation region below 1600 cm^{-1} the bands show similar absorption intensity, or even greater, with respect to the CH-stretching region. This doesn't agree with the experimental data, which show a ratio of 1/14 between the intensities of the CH-stretching and the deformation regions (see Section 2.4 for details). Moreover the CH_2 wagging band, not observed in the experimental spectrum, it is the most intense band in the predicted spectrum of ref. [33]!

Since, as demonstrated by our *static* DFT calculations (see Section 2.4), a quantum-chemical approach is mandatory and fully suitable for a correct description of the IR absorption intensities, we can expect that FPMD simulations could give the correct description of the band shapes, while considering environmental factors.

We decided to focus on the case of polyethylene (PE): PE is not a particularly innovative and novel material but can be considered an ideal test case, because of its structural simplicity and

high symmetry. Moreover PE has been widely studied in the past both experimentally and by means of theoretical approaches. Despite its importance in many applications, some features still required a deeper understanding: in particular the peculiar T/p behaviour is not completely unravelled. Since the CP2K code [4] has never been applied before for crystalline polymer, a significant part of our work focused on the determination of the best computational protocol for FPMD simulations of the structure and vibrational spectra in terms of DFT functional, basis sets, parameters for the MD run etc. required for a reliable simulation.

4.3.1 Computational details

As in the case of the N1 system (Section 4.1), the IR spectra of the polyethylene crystal have been predicted in the framework of first order perturbation theory [2,3]:

$$I(\omega) = \frac{2\pi\beta\omega^2}{3cV} \int dt e^{i\omega t} \langle \boldsymbol{\mu}(t)\boldsymbol{\mu}(0) \rangle \quad (4.6)$$

where $\boldsymbol{\mu}(t)$ is the instantaneous dipole moment of the system at the time t , $\beta = 1/kT$, ω is the frequency of the absorbed light, c is the speed of light in vacuum and V the volume of the system.

The simulations have been carried out by means of the CP2K code [4], adopting the BLYP functional in combination with different augmented Gaussian-plane waves basis set [34] and GTH pseudopotentials [35–37] (as implemented in the QuickStep [38] module of CP2K). PBE functional has been also tested. The results obtained by using the two functionals do not show significant difference for the purposes of this investigation and from now on we will focus only on the BLYP calculations.

The Grimme D2 correction [39,40] has been introduced to provide a correct description of the Van der Waals interactions (20 Å cutoff) and its parameters have been chosen, based on the results obtained in previous work for periodic DFT simulations [41–44] (see also Chapter 2).

Grimme D3 correction [45] have been also tested, but it showed negligible changes in the predicted spectrum which do not justify the higher computational cost.

In all cases presented here, we have adopted the dzvp-molop-short-range [46] gaussian basis set: the tests showed indeed that for such a large and symmetric system the use of a more extended and long-range Gaussian basis set is inadvisable both for much larger computational cost, basis set linear dependence problems and the instabilities of the SCF algorithms.

Regarding the plane waves part of the basis set, we will show in the following the results obtained by using two different cutoff: 300Ry and 600Ry.

In all the cases, we performed an equilibration run followed by an NVE run to compute the spectra (Eq.(4.6) is defined for the microcanonical ensemble).

A time step of 0.4 fs was chosen and the dipole moment was evaluated at each time step, following the Berry phase formalism [9,10] as implemented in CP2K code.

Two strategies have been adopted for the equilibration run: firstly we used NVT simulations to take into account temperature effects at a fixed volume. In the NVT simulations (1 ps

long) we rescaled the velocities when the temperature deviated over a fixed temperature range ΔT around the 300 K target temperature ($\Delta T = \pm 50$ K). Second, we adopted an NpT ensemble to equilibrate also the density of the system.

As it is well known from classical dynamics simulations, for the evaluation of the equilibrium properties (and vibrational properties in particular) of polymeric crystals, it is fundamental to get a system fully equilibrated, both for the temperature and the pressure. The choice of a volume based only on the experimental data could be not enough since it does not imply that the system is close to the minimum energy configuration obtained by a complete optimization.

NPT ensemble requires in general to adopt large model systems for a reliable prediction of the volume. In the case of crystalline polymers the situation is even more critical because the system is intrinsically anisotropic: along the chain axis strong covalent bonds play a dominant role, while in the other 2 directions only intermolecular interactions are present.

Based on the results of the NVT dynamics, we carried out NpT simulations by choosing only the augmented Gaussian-plane waves basis set - 600Ry plus GTH pseudopotentials.

To control the temperature and the pressure, the system has been coupled with a Nosé Hoover thermostat [47] and the default barostat of CP2K [48,49]. We chose a coupling time constant of 50 fs for the thermostat and 50 fs for the barostat based on the results of some tests made with classical MD, and as a compromise to get a fast equilibration and so reduce the computational cost.

4.3.2 NVT equilibration with 300Ry plane wave basis set

The crystalline structure of polyethylene is well known in the literature and has been the subject of many investigations focusing on the structural evolution both as function of temperature and pressure. At room temperature (or lower) all authors [50–52] agree in predicting an orthorhombic cell with two chains per cell possessing a transplanar conformation (Figure 4.9).

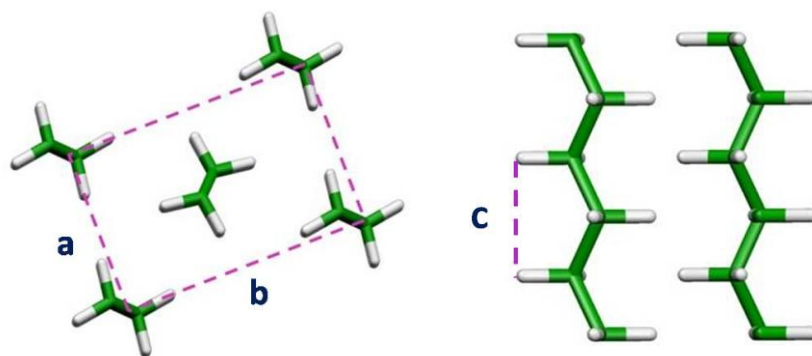


Fig. 4.9 Crystalline structure of polyethylene

The unit cell of the polyethylene is thus very small (12 atoms per cell) and a proper supercell is mandatory to run an MD simulations: it's indeed well-known from classical dynamics that,

in order to obtain good equilibrations in temperature and/or pressure, the thermostats and barostats needs simulation box of considerable size (few thousand of atoms in some cases). Indeed it the model system should be large enough to mediate the effects of the temperature and local volume fluctuations and to promote a reliable behaviour of thermostats/barostats. As already noticed, in the case of crystalline polymers the situation is even more complicated since the system is strongly anisotropic and molecular interactions of very different strength are found in different directions. On the other hand, increasing the number of atoms and the size of simulation box makes the calculation very expensive from the computational perspective, rapidly reaching the current limits in the available resources and facilities. The model systems normally adopted for the classical molecular dynamics are indeed totally out of the possibility for FPMD.

Therefore, in order to find a good compromise between the computational cost and the need of a suitable simulation box, we worked with a systems of about 450 atoms (the current limit of national Tier-1 supercomputers).

Classical dynamic investigations [53] also suggest to avoid a further anisotropy of the simulation box in addition to the intrinsic anisotropy of the system in order to reduce the problems with the thermostats/barostat.

Hence, we chose a supercell 3x2x6 of the unit cell to have an almost cubic box of 432 atoms. The values of the cell parameters of the unit cell have been fixed according to two different options:

- **Case 1:** We started from the experimental values proposed in the literature, in particular from those suggested by Bunn [50], based on the X-ray diffraction data at 300K. In this case the unit cell has dimensions 4.93 Å x 7.40 Å x 2.534 Å, and thus the supercell 14.79 Å x 14.80 Å x 15.204 Å.
- **Case 2:** We considered the values proposed in literature by Avitabile et al. [52], based on the neutron scattering data at 4 K (7.121 Å x 4.851 Å x 2.548 Å). Starting from experimental values, we relaxed the simulation box with a cell optimization (hereafter referred as “0K *static* calculation”) and then we evaluated the coefficient of thermal expansion from the ratios between the experimental cell parameters at 4 K and 300 K, and used it to correct the predicted cell parameters at 300 K. We used these values (unit cell: 7.479 Å x 4.887 Å x 2.570 Å, supercell: 14.661 Å x 14.958 Å x 15.420 Å) as starting point for the MD.

The spectra predicted for these two options, with trajectories of the same length, provide to be very similar, thus granting the correct stability and convergence of the calculations starting from different input structures. Therefore, we will show the results of Case 2 only.

At first, according to some geometry optimization tests (*static* calculation with CP2K) and based on the previous experience with FPMD, we decided to adopt 300Ry basis set.

We performed an NVT equilibration dynamic, followed by an NVE production run to compute the spectra (see Section 4.3.1 for details).

During the 7.5 ps trajectory, a non physical diffusion of the chains along the chain axis is observed, which can be recognized as an artefact of the simulation. A similar behaviour has been reported by Pagliai et al. [7] in the case of CPMD molecular dynamics applied to the

naphthalene crystal: they explained the phenomenon as due to the small size of the cell, combined with its anisotropy, leading to an incorrect balance of forces.

In the case of polyethylene, the phenomenon is even more marked because the covalent interactions along the chain axis are remarkably different from the VdW interactions in the other two directions and the anisotropy is more effective.

In order to confirm that this is not a specific problem of our approach but that it is a general behaviour, we did some tests by means of classical MD simulations: for simulation box below the 30 Å in the direction of the chain axis, the diffusion is observed again, thus showing that this is a general artefact of MD simulations.

In Section 2.4, we showed that the spectrum of the crystalline PE differs from that of an all-trans isolate chain, not so much in frequency, but for the lack of the band splitting and the intensity ratio between the CH-stretching region and the deformation region.

During the trajectory, despite the chain diffusion, the inter-chain distance is kept (the volume of the simulation box does not change), as also the average orientation of the chains in the *ab* plane. A partial effect of the crystal field is then preserved. So we expect that the FPMD is able to reproduce the main features of the PE spectrum. However the mismatch of the chains in the chain axis directions, due to the diffusion, could lead to an incorrect prediction of the intensity ratios between the CH-stretching region and the deformation region (region of the deformation modes, see Section 2.4 for details), or the magnitude of splitting.

Despite its intrinsic weakness (e.g. diffusion), the dynamics here analysed, allows to critically test the computational setup, which can then be used for the simulations of large systems (accessible only with European projects).

In the details, in Figure 4.10 we report the spectrum predicted from the NVE trajectory.

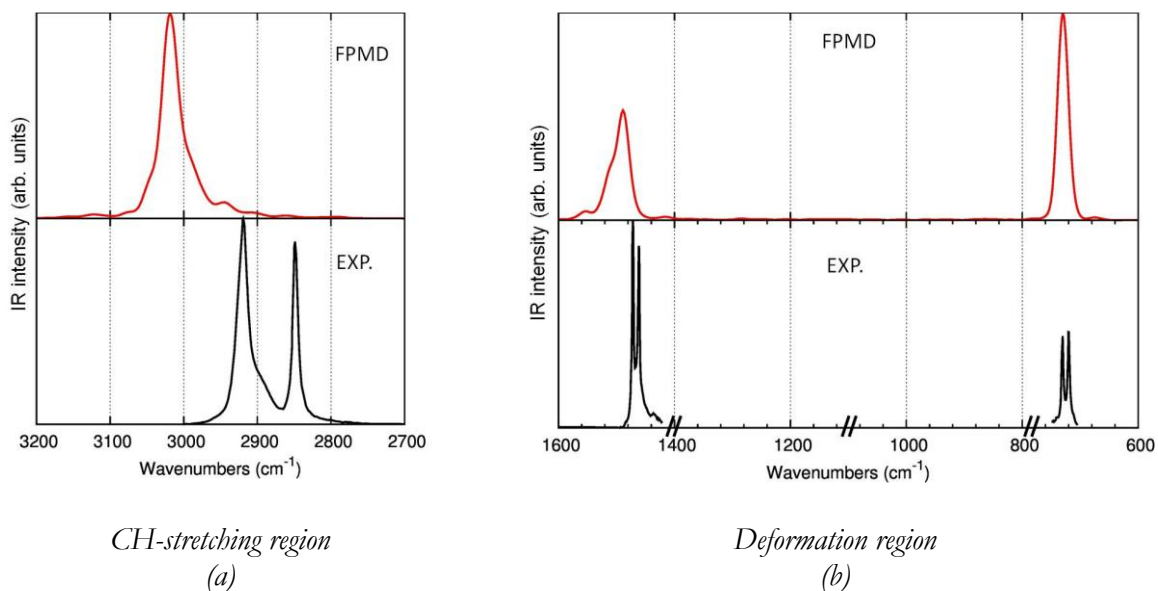


Fig. 4.10 Comparison between the infrared spectrum predicted by FPMD using a 300Ry plane waves basis set (NVT equilibration) and the experimental spectrum [54] of the crystalline polyethylene

The FPMD spectrum correctly predicts three regions of non-negligible intensity in the IR spectrum: the region of the CH stretching, at high frequency, the one of the CH₂ scissoring, around 1500 cm⁻¹, and the one of the rocking, around 700 cm⁻¹ (see Chapter 2 for details on the assignments). Indeed the CH₂ wagging modes are silent, as found in the experimental spectra, while the spectra obtained by classical dynamics [33] usually predict an intense band in this region (1300 -1000 cm⁻¹).

It has been demonstrated [55] that the CH₂ wagging bands have actually a negligible intensity in the case of all-trans chain due to a mutual cancellation of the contribution of equilibrium charges on hydrogen atoms and the charge fluxes along CC bonds.

Classical dynamics simulations, where fixed charges are used to predict IR intensities, cannot take into account charge fluxes; on the contrary FPMD simulations does not possess this limitation and can give a good description of electronic charge fluctuations.

In the deformation region there are some discrepancies that could indicate deficiencies in the simulation: the intensity ratios and characteristic splitting of the bands are indeed not well predicted. This might be due to the diffusion of the chains or to the too short trajectory, which can lead to a poor quality of the spectrum and to an incomplete sampling of the modes [6].

Further problems are found in the CH-stretching region.

First of all the CH-stretching region is blue shifted in frequency with respect to the experiment.

Such a behaviour cannot be easily interpreted: from one hand, we cannot exclude effects related to the functional/basis set choice or overcorrection of the Grimme approach; on the other hand, effects such as the lack of volume equilibration should be also take into account.

In order to shed light on this behaviour, we first considered the spectrum predicted by periodic *static* DFT-periodic calculation (CRYSTAL14 code [56]).

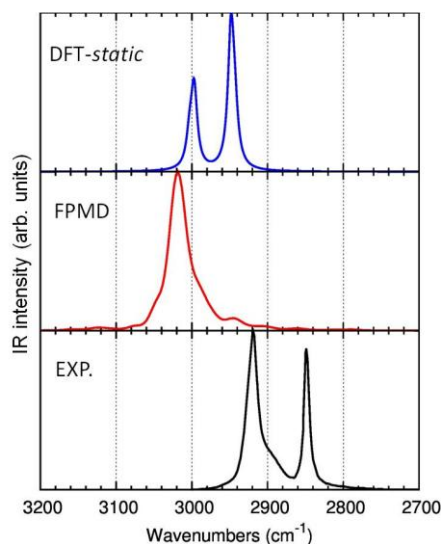


Fig. 4.11 Comparison between the infrared spectrum predicted by a static DFT-calculation (by means of CRYSTAL code), by a 7.5 ps FPMD using a 300Ry plane waves basis set (NVT equilibration) and the experimental spectrum [54] of the crystalline polyethylene

The *static* spectrum has been predicted at BLYP/6-31G(d,p) level, with the same D2 Grimme correction used for the CP2K dynamics. The unit cell of the PE has been optimized and then the IR spectrum has been predicted in double harmonic approximation on the equilibrium geometry so- obtained (with the same procedure of used in Chapter 2). Despite the difference in the basis set adopted, the *static* simulation can give anyway some indication about the effects of the quantum-chemical method and Grimme correction.

As reported in Figure 4.11, the DFT-*static* spectrum is blue shifted compared to the experimental spectrum.

The blue shift of the computed spectra with respect to the experimental one is a well-known fact in quantum chemistry. This motivated the inclusion of a suitable method-dependent scaling factor, which are usually justified due to the neglect of the anharmonicity (*static* calculation are carried out in double harmonic approximations). If this would be true, such effect should be smaller for FPMD simulations, where anharmonicity is partially taken into account.

However, the blue shift of 80 cm^{-1} predicted for *static* calculations appear to be too large to be attributed only to harmonic approximation. Also the result from FPMD was unexpected: CH stretching bands are predicted at even higher frequencies (of about 20 cm^{-1}) with respect to the *static* spectrum: since anharmonic effects are taken into account in FPMD a better agreement with the experimental spectrum would be expected.

It seems thus that the blue shift could be related to functional/basis set/Grimme correction effects and further studies should be required to better assess this behaviour. Note that the same effect as been found also in the N1 case (see Section 4.1) and reported by authors [6].

Figure 4.10 highlights another very important issue: one of the two CH-stretching bands appear to be missing, that is either the intensities of symmetric and antisymmetric stretchings are completely wrong or their relative frequencies are very badly described.

These results point out the existence of some serious problem in the FPMD simulations.

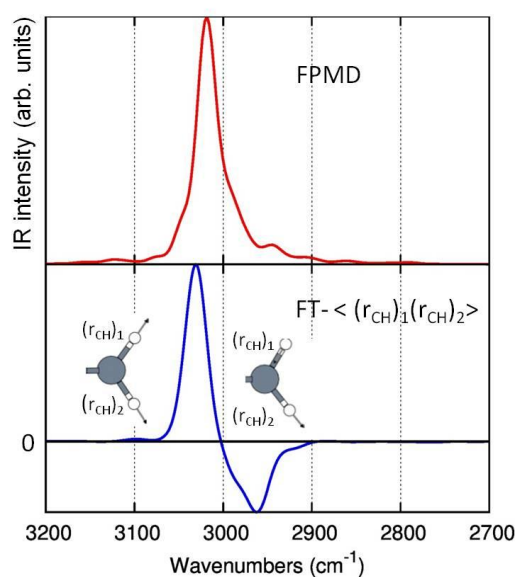


Fig. 4.12 Fourier transform of the $\langle (r_{CH})_1 (r_{CH})_2 \rangle$ correlation function of the r_{CH} bond length in the same CH_2 unit ($FT-\langle (r_{CH})_1 (r_{CH})_2 \rangle$ in the plot).

A further evidence of this issue is the results of the Fourier transform of $\langle (r_{CH})_1 (r_{CH})_2 \rangle$ correlation function which refers to the r_{CH} bond length of two CH belonging to the same CH_2 unit (Figure 4.12): this function indeed is positive when the two bond are stretching in phase, while it is negative when they possess an opposite phase.

The in phase vibration (d+) is predicted at the higher frequencies, while the out-of-phase mode (d-) is predicted at lower frequency, contrary to what is usually found (see Section 2.4).

As a first check, we verified if these discrepancies are due to a too short trajectory by extending the dynamic to 11 ps.

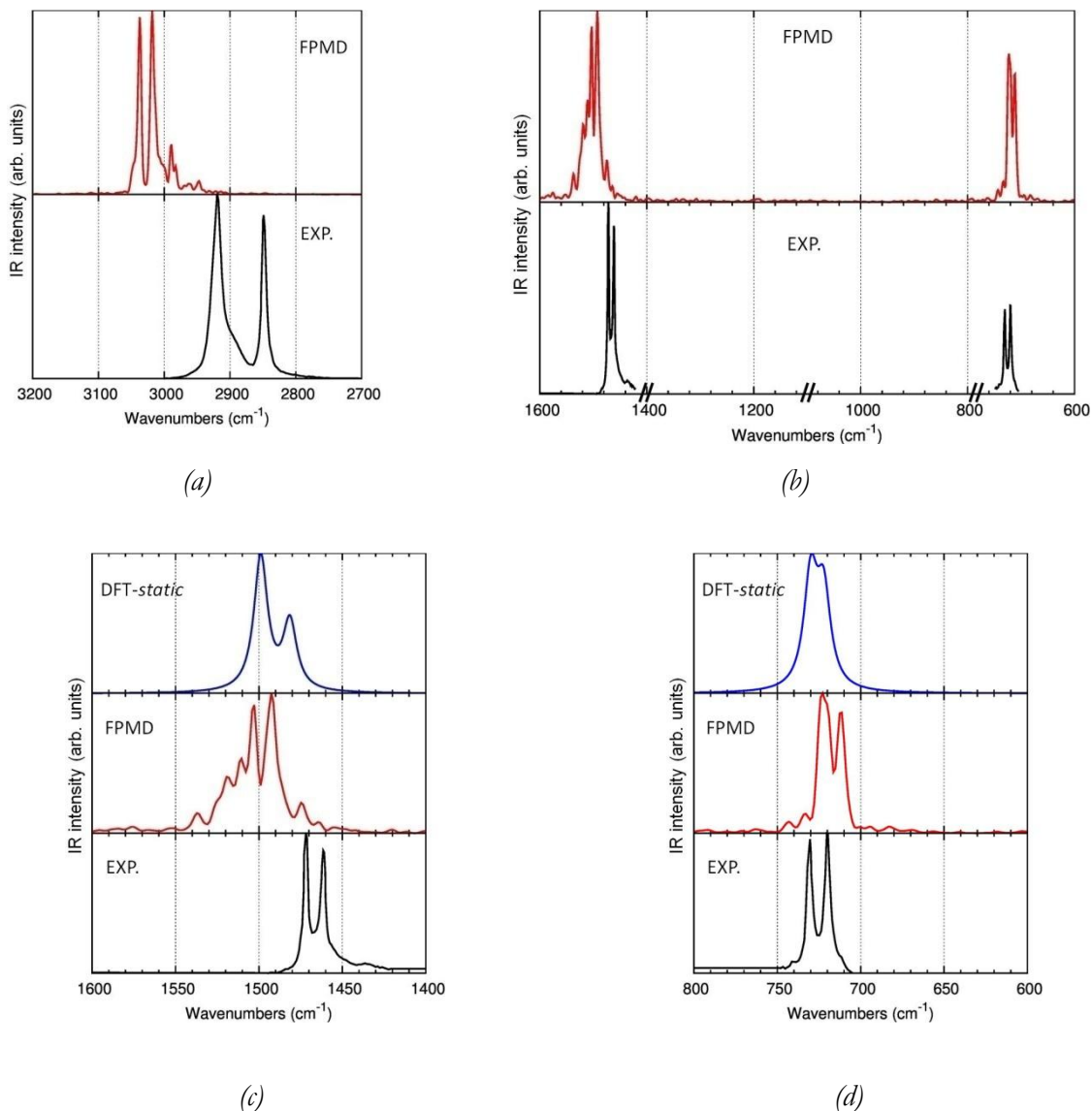


Fig. 4.13 Comparison between the infrared spectrum predicted by a 11 ps FPMD using a 300Ry plane waves basis set (NVT equilibration) and the experimental spectrum [54] of the crystalline polyethylene

As expected, a longer trajectory improves the results, in particular in the deformation region: the intensity ratio between the scissoring and the rocking bands is now better predicted and the splitting of these bands are now evident.

On the other hand, the CH-stretching region is still very badly predicted by FPMD and the CH₂ scissoring band is significantly broadened.

Therefore, even if a longer dynamic allows to obtain a better description, further approaches should be explored to obtain acceptable results. Two aspects in particular should be verified: the adequacy of the level of theory and the correct description of the volume of the system, as presented in the next sections.

4.3.3 NVT equilibration with 600Ry plane wave basis set

We will first focus on the adequacy of the level of theory, by testing the performance of our simulations when adopting a larger plane waves basis set with a cutoff of 600Ry.

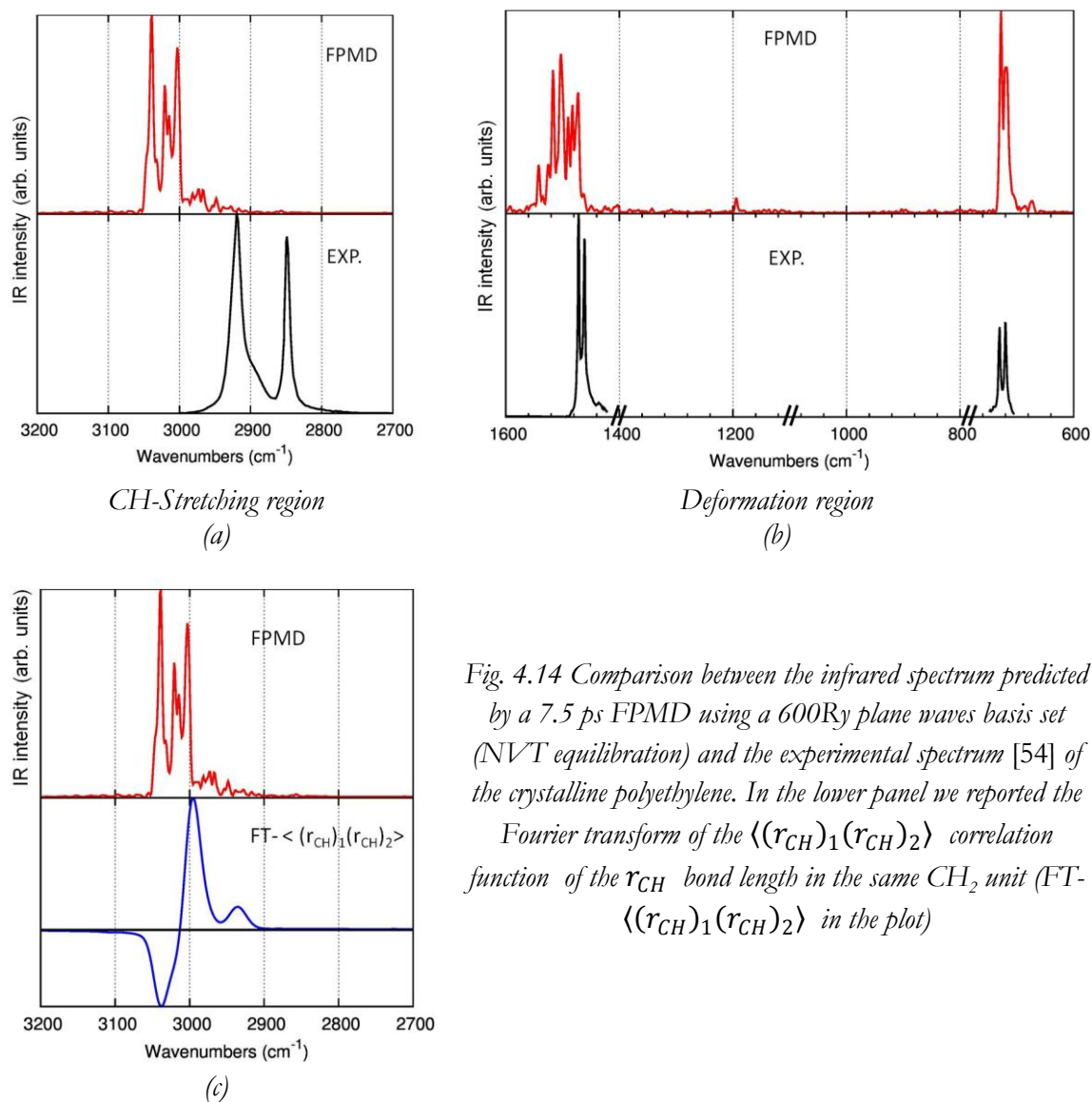


Fig. 4.14 Comparison between the infrared spectrum predicted by a 7.5 ps FPMD using a 600Ry plane waves basis set (NVT equilibration) and the experimental spectrum [54] of the crystalline polyethylene. In the lower panel we reported the Fourier transform of the $\langle (r_{CH})_1 (r_{CH})_2 \rangle$ correlation function of the r_{CH} bond length in the same CH₂ unit (FT- $\langle (r_{CH})_1 (r_{CH})_2 \rangle$ in the plot)

The spectrum predicted by a 7.5 ps trajectory is shown in Figure 4.14. The region of CH stretching shows now a better agreement since the d+ and d- bands are reasonably described and the $\langle(r_{CH})_1(r_{CH})_2\rangle$ correlation function shows correctly that the r- component occurs at higher frequency.

However, the separation in frequency between the two CH-stretching bands (40 cm^{-1}) is still widely underestimated with respect to the gap of 70 cm^{-1} observed in the experimental spectrum. Moreover, the FPMD predicted spectrum is still blue shifted with respect to the experimental one and to the spectrum obtained by *static* DFT calculations.

Furthermore, there is a series of spurious features between the r- and the r+ bands, and below r+.

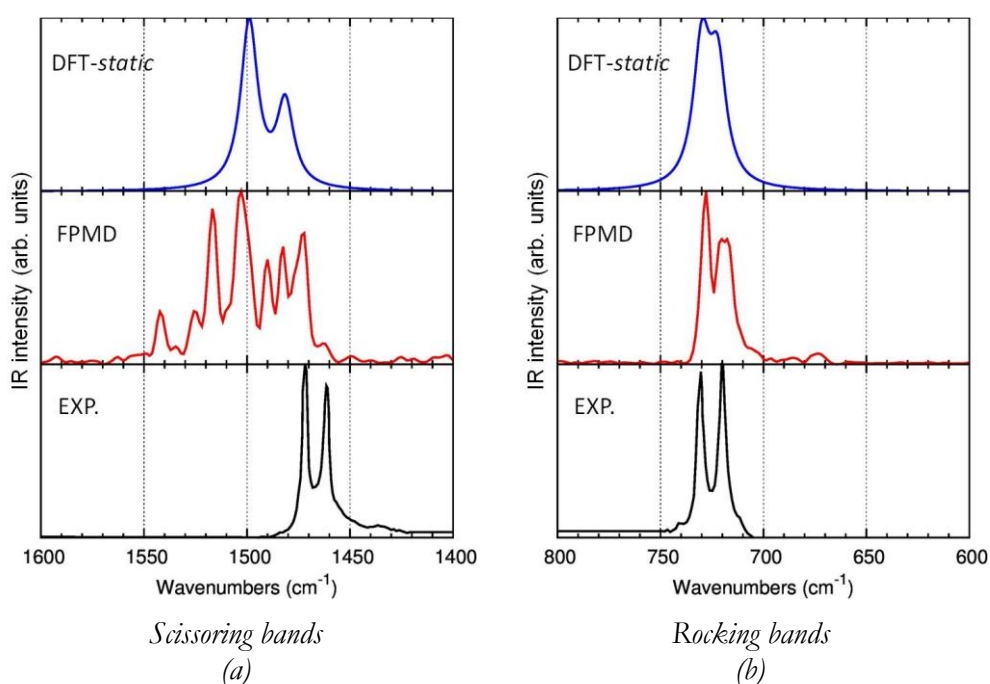


Fig. 4.15 Comparison between the infrared spectrum predicted by a static DFT-calculation (by means of CRYSTAL code), by a 7.5 ps FPMD using a 600Ry plane waves basis set (NVT equilibration) and the experimental spectrum [54] of the crystalline polyethylene: scissoring (a) and rocking(b) bands.

Moving to the other spectral regions, it is interesting to notice that 600Ry simulation is able to predict the splitting of the scissoring and the rocking bands already with a 7.5 ps trajectory, while for the 300Ry case 11 ps were needed (Figure 4.15). However, a too large broadening is predicted for the scissoring bands; even increasing to 1200Ry the plane waves basis set cutoff, adopting the D3 Grimme correction [57] no significant improvements are found. These results suggest that indeed a 600Ry cutoff is the minimum requirement for a reliable simulation, but this parameter is not the only one which determines the accuracy of the simulation. In particular the simulation could be influenced by the lack of equilibration of the volume resulting in a non-physical compression of the system which could affect the vibrational properties.

Due to the extreme sensitivity of the CH stretching bands to the intra and intermolecular environment, we can thus expect such a volume effect on the CH stretching frequencies. Moreover, the presence of conformational defects cannot be ruled out in our simulations and it is well-known that these defects do possess significant markers in the spectra [58]. To better explore conformational effects, we considered a 1x1x24 supercell model with a simulation box of two chains of 48 carbon atoms each, still adopting periodic boundary conditions, as in the case of DFT-periodic *static* calculation. In this case the chains are long enough to allow conformational transitions already during short trajectories: indeed after about 5 ps localized defects take places in the trans chains. To demonstrate that the occurrence of these defects is not due to deficiencies of the calculations (e. g. prediction of a too low trans-gauche barrier), we considered an isolated molecule of octane and we evaluated the energy profiles while varying the central torsional angle $-C-C-C-C-$ (CP2K BLYP-D2/dzvp-molop-SR/600Ry *static* calculation).

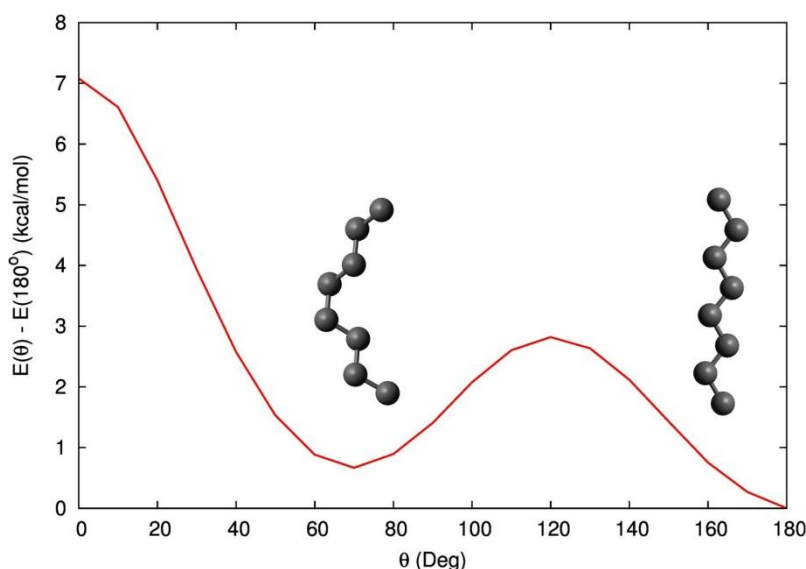


Fig. 4.16 Energy profile as a function of the central torsional angle $-C-C-C-C-$ (θ) of an octane molecule (CP2K BLYP-D2/dzvp-molop-SR/600Ry *static* calculation)

The barrier is about of 3 kcal/mol (Figure 4.16) which is a reasonable value for alkanes, thus confirming the reliability of the calculation.

Thanks to the larger chain length of the molecules in the 1x1x24 supercell, we considered the transplanar portion of the chains to calculate a more accurate value of the c parameter to be adopted; this allowed to estimate that a relaxed c parameter in the calculation should have a value between 2.77 Å and 2.86 Å.

The value of 2.57 Å, adopted in the previous NVT simulations, is out of this range, and clearly shows that, at least in the direction the chain axis, the cell is compressed and the intramolecular geometry is far from the equilibrium. This can be indeed at the origin of errors and poor quality of the simulated spectra. In summary, the above results confirms that for a reliable prediction of the spectra the equilibration of volume is mandatory.

4.3.4 NpT equilibration

In order to equilibrate the volume, NpT simulations are required (see paragraph 4.3.1 for details). Very few experience has been documented in the literature for FPMD NpT simulations [48,49] and to this aim, many tests have been necessary to determine the best set up for the simulations.

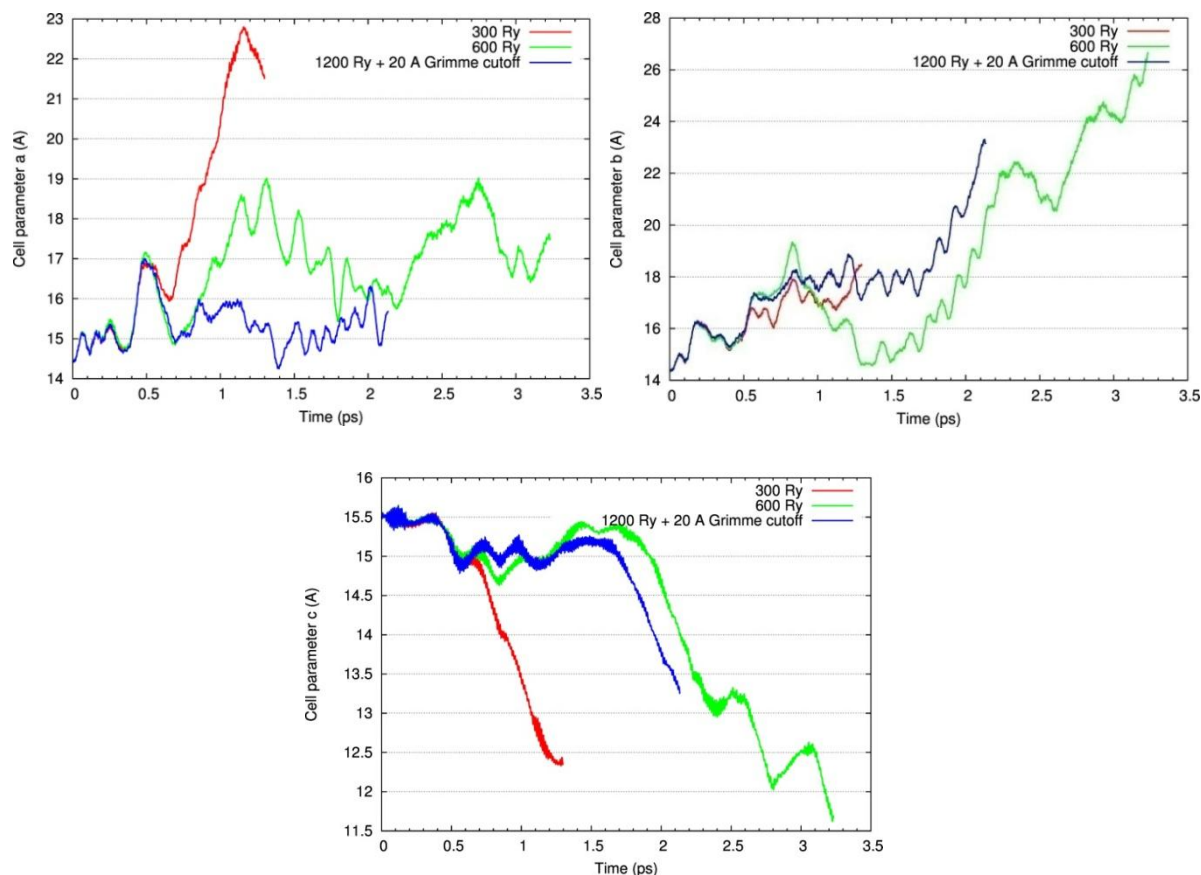


Fig. 4.17 Cell parameters evolution during the NpT simulations. The results for three different plane waves basis set (300Ry, 600Ry, 1200Ry and 40 Å cutoff for the Grimme correction) are reported.

Figure 4.17 shows the evolution of the cell parameters for increasing length of the NpT run. It is known that the correct behavior of the barostat in NpT simulations requires quite large supercells (even a few thousands of atoms as a rule of thumb) in order to accommodate correctly volume fluctuations and reach convergence in cell parameters for as complete equilibration. Clearly this appear not to be the case of our current simulation and the supercell 3x2x6 appears too small to this aim, regardless of the plane waves basis set adopted (300Ry, 600Ry, 1200Ry and 40 Å cutoff for the Grimme correction).

In all the cases the cell collapses in less than 3.5 ps and the value of the c parameter in particular (chain axis direction) evolves from the 15.420 Å less than 13 Å. This decrease, together with the increase found for a and b cell parameters (b doubles in the case of the 600Ry simulations, from 14.958 Å to more than 26 Å), is in accordance with the generation of conformational defects in the chains and to the loss of the all-trans conformation.

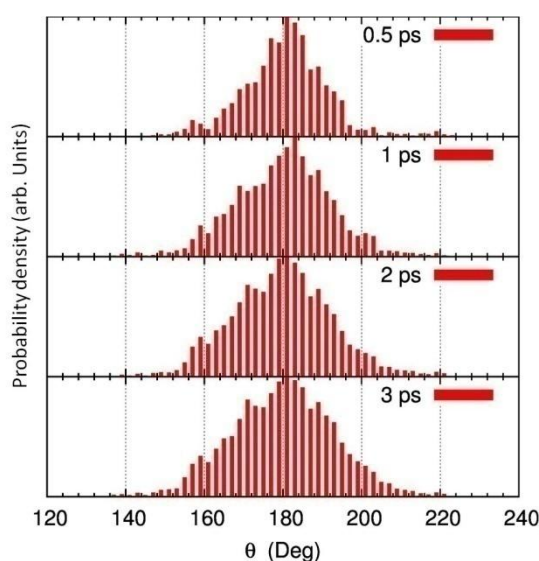


Fig. 4.18 Distribution of the -CCCC- torsional angles of a chain increasing duration of the NpT run (600Ry plane waves basis set).

In Figure 4.18, we reported the statistical distribution of the -C-C-C-C- torsional angles of a chain for increasing duration of the NpT run, focusing on the simulation with the 600Ry cutoff. The other two simulations (300Ry, 1200Ry + 40 Å Grimme cutoff) show negligible difference and so they will not be shown here.

Starting from an all-trans conformations, the chain conformation is largely distorted already after 0.5ps. In the next time intervals the distribution widely broadens showing a non-negligible amount of chains with torsional angles that differ about 40 degrees from the initial value of 180 degrees.

This behavior is due to the fact that the simulation box is too small and unphysical conformational transitions are generated.

We made some tests by means of classical MD simulations verifying that the correct behavior of the barostat needs a system of minimum 3500, up to 7000 atoms to work properly.

Using a longer time constant for the barostat to reduce the volume fluctuation is not a possible solution! Indeed, longer time constants would require longer equilibrations: unfortunately the time cost for time step (around 25s x MD step at 128 cores) and the limited scalability of the code make a simulation of hundreds of ps out of reach of the FPMD.

As explained in the following, some promising prospective are opened in this context, and imply the availability of European computational facilities, as we verified with preliminary and exploratory test simulations and projects.

4.3.5 Conclusions and future perspectives

The work presented in this chapter focused on the application of FPMD simulations to crystalline polymers, with the aim of predicting their spectroscopic response in particular. These kind of simulations have been never adopted to polymeric crystals and constitutes a very challenging topic in current computational material science.

Our main objective has been that of exploring the potentialities, the protocols and the model required to carry out these simulations, to pave the way for future investigations.

To this aim, we decided to consider the case of PE, as benchmark of typical polymeric materials.

We considered, at first, an NVT equilibration run on a system of 432 atoms (14.661 Å x 14.958 Å x 15.420 Å cell): by means of several tests we found the combination of simulation parameters that would guarantee a correct description of the wave function of the system, the stability of the algorithms during the calculation while maintaining an accessible computational cost (available on national Tier-1 supercomputers).

The spectrum, evaluated from the correlation function of the dipole moment, shows features clearly related to those observed experimentally, both in the CH-stretching region and in the deformations region. In particular several features which cannot be correctly described by molecular classical dynamics [33] simulations are taken into account by FPMD simulations.

On the other hand, the correspondence between the predicted spectrum and the experimental one is not accurate enough and needs to be significantly improved. Several tests suggest that to solve this problem an accurate equilibration of the volume, by means of NpT simulations is mandatory.

This is a further proof of the sensitivity of the vibrational spectra to the description of the intra and intermolecular structure of the system and of the fact that no constraints on the geometry (such a fixed volume) should be present for a reliable computation of the spectra by means of FPMD.

The 3x2x6 supercell, the largest that we can afford with usual resources (Tier-1 supercomputers), demonstrated to be too small to carry out stable NpT simulations and much larger cells of 3500-700 atoms proved to be necessary.

FPMD dynamics of such systems can be carried out only on the very powerful supercomputer available within European projects: indeed our estimation is that a single trajectory of 10 ps on a system 3500 atoms would require 10 days with 2000 core and a computational time of 1.5 million core-hours.

A PRACE project has been devoted to test the feasibility of these calculations: indeed such a large system has never been treated before by ab-initio approaches (without the use of linear scaling algorithms) and with this project we have been able to select the algorithms that ensure the stability of the simulation.

We tested different European machines and we have shown that the computational resources currently available allow to complete the simulation for both the 3500 and 7000 atoms systems.

On the basis of this exploratory project we prepared and submitted a proposal (12th PRACE project access call) to gain the access to European computational facilities required to conclude our simulations.

In addition to such a challenging and onerous approach, we also identified possible alternative to be explored in future investigations:

- The use of a first classical MD NpT equilibration, with an appropriate FF, to shorten the FPMD NpT simulation.

- The employment of an NVT FPMD simulations on small models to relax the polymer chain along the chain axis, to gain a more reliable description of the geometry at least for the intramolecular degree of freedom.
- The employment of the method developed in Section 4.2, that is the combination of APTs evaluated with high level DFT calculations with a FPMD at lower level of theory (e.g. small basis set, low convergence criteria for the SCF...) or with a classical MD.

As a general conclusion, we can state that our work constituted a meaningful preliminary investigation which can address further application of FPMD simulations on polymeric materials. These investigations, while still being extremely challenging, are however affordable with current Tier-0 supercomputer and will provide significant new tools for the applications of molecular computational techniques in materials science and technology.

4.4 Summary and Conclusions

In the field of computational materials science and quantum chemistry modelling for vibrational spectroscopy, FPMD simulations are a promising tool to complement and/or overcome more standard *static* calculations. Since their applications in this field is still limited or even lacking, we decided to evaluate the advantages and limitations of FPMD approach on some peculiar test cases.

First, we simulated the liquid phase spectra of a partially halogenated ether, which shows a large number of relevant conformers at room temperature. Both the *static* and the *dynamic* methods were able to predict all the marker bands of the IR spectrum of this molecule even if the *static* method, in the case of small, weakly interacting molecules, appears to be still the better choice in terms of accuracy and computational cost.

On the other hand, the *dynamic* method provides a good prediction of the spectral response by means of a single simulation, carried out directly on the condensed phase, while in the *static* method multiple runs on different equilibrium structures were needed, after a proper and accurate investigation of the potential energy surface.

Moreover, in the *static* approach no intermolecular interactions (i.e. description of the condensed phase) is introduced to keep an appropriate computational cost.

This single molecule model, however, is restricted to a limited number of cases: in the case of strong intermolecular bonds, such as for example H-bonding, condensed phase effects cannot be neglected, and the solvent should be explicitly included in the simulation.

For increasing size of the system, because of the need of the accurate exploration of the conformational space (whose dimension increases very rapidly with the number of molecules and of torsional angles) the *static* method becomes unfeasible.

Based on our tests on N1 molecule, FPMD proved to be a powerful alternative which can give at least a qualitative description of the vibrational spectra and which can also be extended to complex system with many degrees of freedom.

On these bases, in collaboration with Marie-Pierre Gaigeot (Evry university), the same technique has been also applied to the very challenging case of crystalline polymer systems: simulations on this kind of systems has never been done before and many tests have been required to select the parameters suitable for the simulations.

We have done several tests on the polyethylene crystal and found the combination of level of theory and simulation parameters that would guarantee a correct description of the wave function of the system, the stability of the algorithms during the whole calculation, while keeping an accessible computational cost (at least on national Tier-1 supercomputers).

Even if our results are still preliminary, we have however demonstrated for the first time that FPMD simulations by means of CP2K code can be applied and extended also to the case of crystalline polymers.

Due to the large facilities required, we also explored an alternative route by developing and implementing a new methodology for the prediction of FPMD IR spectra, which exploits the prediction of Atomic Polar Tensors (APT's) and of the velocity correlation function, instead of the computation of dipole correlation function.

Using our model, it is possible to partially decouple the calculation of the velocity correlation function (i.e. frequencies) from the electronic response (intensities), allowing to use less strict convergence criteria for the FPMD run. This approach would significantly reduce the computational cost, paving the way to the analysis of bigger systems and longer trajectories by using computational facilities more easily available.

The preliminary results are encouraging: the spectra predicted from the APT and velocity correlation functions are of the same quality as those of calculated from the dipole correlation function.

Another advantage of the use of APTs is that Equilibrium Charge Charge Fluxes (ECCF) model can be adopted for APT parameterization (see Chapter 3), thus providing a tool for the study of the electron charge distribution in molecules and for the interpretation of their IR absorption intensity.

In general, thanks to the work here presented, we can conclude that FPMD simulations for the prediction of the spectra of complex system are now an actual possibility for computational materials scientists. The great potentialities of this technique surely will constitute a further step in the employment of quantum chemical modeling for a large variety of systems and properties of interest in materials science, thus paving the way to a countless number of possible applications.

Even if there are still many open issues that require a detailed investigation and improvements, our preliminary results show that FPMD deserves at least the same attention and consideration which is paid to *static* quantum-chemical calculations and classical molecular dynamics simulations.

Bibliography

- [1] J. Tomasi, B. Mennucci, R. Cammi, Quantum mechanical continuum solvation models, *Chem. Rev.* 105 (2005) 2999–3094.
- [2] D.A. McQuarrie, *Statistical Mechanics*, University Science Books, 2000.
- [3] R. Kubo, M. Toda, N. Hashitsume, *Statistical Physics II*, Springer Berlin Heidelberg, Berlin, Heidelberg, 1991. <http://link.springer.com/10.1007/978-3-642-58244-8> (accessed November 18, 2015).
- [4] J. Hutter, M. Iannuzzi, F. Schiffmann, J. VandeVondele, CP2K: atomistic simulations of condensed matter systems, *Wiley Interdiscip. Rev. Comput. Mol. Sci.* 4 (2014) 15–25.
- [5] M.-P. Gaigeot, Theoretical spectroscopy of floppy peptides at room temperature. A DFTMD perspective: gas and aqueous phase, *Phys. Chem. Chem. Phys.* 12 (2010) 3336–3359. doi:10.1039/b924048a.

- [6] M. Thomas, M. Brehm, R. Fligg, P. Vöhringer, B. Kirchner, Computing vibrational spectra from ab initio molecular dynamics, *Phys. Chem. Chem. Phys.* 15 (2013) 6608. doi:10.1039/c3cp44302g.
- [7] M. Pagliai, C. Cavazzoni, G. Cardini, G. Erbacci, M. Parrinello, V. Schettino, Anharmonic infrared and Raman spectra in Car–Parrinello molecular dynamics simulations, *J. Chem. Phys.* 128 (2008) 224514. doi:10.1063/1.2936988.
- [8] M. Sulpizi, M. Salanne, M. Sprik, M.-P. Gaigeot, Vibrational Sum Frequency Generation Spectroscopy of the Water Liquid–Vapor Interface from Density Functional Theory-Based Molecular Dynamics Simulations, *J. Phys. Chem. Lett.* 4 (2013) 83–87. doi:10.1021/jz301858g.
- [9] R.D. King-Smith, D. Vanderbilt, Theory of polarization of crystalline solids, *Phys. Rev. B.* 47 (1993) 1651–1654. doi:10.1103/PhysRevB.47.1651.
- [10] D. Vanderbilt, R.D. King-Smith, Electric polarization as a bulk quantity and its relation to surface charge, *Phys. Rev. B.* 48 (1993) 4442–4455. doi:10.1103/PhysRevB.48.4442.
- [11] B. Kirchner, J. Hutter, Solvent effects on electronic properties from Wannier functions in a dimethyl sulfoxide/water mixture, *J. Chem. Phys.* 121 (2004) 5133–5142. doi:10.1063/1.1785780.
- [12] N. Marzari, D. Vanderbilt, Maximally localized generalized Wannier functions for composite energy bands, *Phys. Rev. B.* 56 (1997) 12847–12865. doi:10.1103/PhysRevB.56.12847.
- [13] P.L. Silvestrelli, M. Parrinello, Water Molecule Dipole in the Gas and in the Liquid Phase, *Phys. Rev. Lett.* 82 (1999) 3308–3311. doi:10.1103/PhysRevLett.82.3308.
- [14] P.L. Silvestrelli, M. Parrinello, Structural, electronic, and bonding properties of liquid water from first principles, *J. Chem. Phys.* 111 (1999) 3572–3580. doi:10.1063/1.479638.
- [15] A. Strachan, Normal modes and frequencies from covariances in molecular dynamics or Monte Carlo simulations, *J. Chem. Phys.* 120 (2004) 1–4. doi:10.1063/1.1635364.
- [16] G. Mathias, M.D. Baer, Generalized Normal Coordinates for the Vibrational Analysis of Molecular Dynamics Simulations, *J. Chem. Theory Comput.* 7 (2011) 2028–2039. doi:10.1021/ct2001304.
- [17] G. Mathias, S.D. Ivanov, A. Witt, M.D. Baer, D. Marx, Infrared Spectroscopy of Fluxional Molecules from (ab Initio) Molecular Dynamics: Resolving Large-Amplitude Motion, Multiple Conformations, and Permutational Symmetries, *J. Chem. Theory Comput.* 8 (2012) 224–234. doi:10.1021/ct2006665.
- [18] M. Schmitz, P. Tavan, Vibrational spectra from atomic fluctuations in dynamics simulations. I. Theory, limitations, and a sample application, *J. Chem. Phys.* 121 (2004) 12233–12246. doi:10.1063/1.1822914.
- [19] M. Schmitz, P. Tavan, Vibrational spectra from atomic fluctuations in dynamics simulations. II. Solvent-induced frequency fluctuations at femtosecond time resolution, *J. Chem. Phys.* 121 (2004) 12247–12258. doi:10.1063/1.1822915.

- [20] M. Martinez, M.-P. Gaigeot, D. Borgis, R. Vuilleumier, Extracting effective normal modes from equilibrium dynamics at finite temperature, *J. Chem. Phys.* 125 (2006) 144106. doi:10.1063/1.2346678.
- [21] M.P. Gaigeot, R. Vuilleumier, M. Sprik, D. Borgis, Infrared Spectroscopy of N-Methylacetamide Revisited by ab Initio Molecular Dynamics Simulations, *J. Chem. Theory Comput.* 1 (2005) 772–789. doi:10.1021/ct050029z.
- [22] M.-P. Gaigeot, M. Martinez, R. Vuilleumier, Infrared spectroscopy in the gas and liquid phase from first principle molecular dynamics simulations: application to small peptides, *Mol. Phys.* 105 (2007) 2857–2878. doi:10.1080/00268970701724974.
- [23] W.B. Person, G. Zerbi, *Vibrational intensities in infrared and Raman spectroscopy*, Elsevier Science Ltd, 1982.
- [24] J.W. Ponder, others, TINKER: Software tools for molecular design, Wash. Univ. Sch. Med. St. Louis MO. 3 (2004). <http://chem.skku.ac.kr/~wkpark/tutor/chem/tinker/doc/license.pdf> (accessed January 3, 2016).
- [25] S.K. Kearsley, On the orthogonal transformation used for structural comparisons, *Acta Crystallogr. A.* 45 (1989) 208–210. doi:10.1107/S0108767388010128.
- [26] J.E.B. Wilson, J.C. Decius, P.C. Cross, *Molecular Vibrations: The Theory of Infrared and Raman Vibrational Spectra*, New edition edition, Dover Publications, New York, 1980.
- [27] A.D. Becke, Density-functional exchange-energy approximation with correct asymptotic behavior, *Phys. Rev. A.* 38 (1988) 3098–3100. doi:10.1103/PhysRevA.38.3098.
- [28] C. Lee, W. Yang, R.G. Parr, Development of the Colle-Salvetti correlation-energy formula into a functional of the electron density, *Phys. Rev. B.* 37 (1988) 785–789. doi:10.1103/PhysRevB.37.785.
- [29] A. Milani, C. Castiglioni, Modeling of Molecular Charge Distribution on the Basis of Experimental Infrared Intensities and First-Principles Calculations: The Case of CH Bonds, *J. Phys. Chem. A.* 114 (2010) 624–632. doi:10.1021/jp908146d.
- [30] D.C. Marinica, G. Grégoire, C. Desfrancois, J.P. Schermann, D. Borgis, M.P. Gaigeot, Ab Initio Molecular Dynamics of Protonated Dialanine and Comparison to Infrared Multiphoton Dissociation Experiments, *J. Phys. Chem. A.* 110 (2006) 8802–8810. doi:10.1021/jp062114o.
- [31] G. Grégoire, M.P. Gaigeot, D.C. Marinica, J. Lemaire, J.P. Schermann, C. Desfrancois, Resonant infrared multiphoton dissociation spectroscopy of gas-phase protonated peptides. Experiments and Car–Parrinello dynamics at 300 K, *Phys. Chem. Chem. Phys.* 9 (2007) 3082–3097. doi:10.1039/B618094A.
- [32] J.P. Beck, A. Cimas, J.M. Lisy, M.-P. Gaigeot, O–H anharmonic vibrational motions in Cl⋯(CH₃OH)_{1–2} ionic clusters. Combined IRPD experiments and AIMD simulations, *Spectrochim. Acta. A. Mol. Biomol. Spectrosc.* 119 (2014) 12–17. doi:10.1016/j.saa.2013.05.073.

- [33] I.-E. Mavrantza, D. Prentzas, V.G. Mavrantzas, C. Galiotis, Detailed atomistic molecular-dynamics simulation of the orthorhombic phase of crystalline polyethylene and alkane crystals, *J. Chem. Phys.* 115 (2001) 3937–3950. doi:10.1063/1.1386912.
- [34] B.G. LIPPERT, J. HUTTER, M. PARRINELLO, A hybrid Gaussian and plane wave density functional scheme, *Mol. Phys.* 92 (1997) 477–488. doi:10.1080/002689797170220.
- [35] S. Goedecker, M. Teter, J. Hutter, Separable dual-space Gaussian pseudopotentials, *Phys. Rev. B.* 54 (1996) 1703–1710. doi:10.1103/PhysRevB.54.1703.
- [36] C. Hartwigsen, S. Goedecker, J. Hutter, Relativistic separable dual-space Gaussian pseudopotentials from H to Rn, *Phys. Rev. B.* 58 (1998) 3641–3662. doi:10.1103/PhysRevB.58.3641.
- [37] M. Krack, Pseudopotentials for H to Kr optimized for gradient-corrected exchange-correlation functionals, *Theor. Chem. Acc.* 114 (2005) 145–152. doi:10.1007/s00214-005-0655-y.
- [38] J. VandeVondele, M. Krack, F. Mohamed, M. Parrinello, T. Chassaing, J. Hutter, Quickstep: Fast and accurate density functional calculations using a mixed Gaussian and plane waves approach, *Comput. Phys. Commun.* 167 (2005) 103–128. doi:10.1016/j.cpc.2004.12.014.
- [39] S. Grimme, Accurate description of van der Waals complexes by density functional theory including empirical corrections, *J. Comput. Chem.* 25 (2004) 1463–1473. doi:10.1002/jcc.20078.
- [40] S. Grimme, Semiempirical GGA-type density functional constructed with a long-range dispersion correction, *J. Comput. Chem.* 27 (2006) 1787–1799. doi:10.1002/jcc.20495.
- [41] C. Quarti, A. Milani, B. Civalleri, R. Orlando, C. Castiglioni, Ab Initio Calculation of the Crystalline Structure and IR Spectrum of Polymers: Nylon 6 Polymorphs, *J. Phys. Chem. B.* 116 (2012) 8299–8311. doi:10.1021/jp303715v.
- [42] D. Galimberti, C. Quarti, A. Milani, L. Brambilla, B. Civalleri, C. Castiglioni, IR spectroscopy of crystalline polymers from ab initio calculations: Nylon 6,6, *Vib. Spectrosc.* 66 (2013) 83–92. doi:10.1016/j.vibspec.2013.02.005.
- [43] D. Galimberti, A. Milani, Crystal Structure and Vibrational Spectra of Poly(trimethylene terephthalate) from Periodic Density Functional Theory Calculations, *J. Phys. Chem. B.* 118 (2014) 1954–1961. doi:10.1021/jp411560r.
- [44] A. Milani, D. Galimberti, Polymorphism of Poly(butylene terephthalate) Investigated by Means of Periodic Density Functional Theory Calculations, *Macromolecules.* 47 (2014) 1046–1052. doi:10.1021/ma402602f.
- [45] S. Grimme, J. Antony, S. Ehrlich, H. Krieg, A consistent and accurate ab initio parametrization of density functional dispersion correction (DFT-D) for the 94 elements H-Pu, *J. Chem. Phys.* 132 (2010) 154104. doi:10.1063/1.3382344.
- [46] J. VandeVondele, J. Hutter, Gaussian basis sets for accurate calculations on molecular systems in gas and condensed phases, *J. Chem. Phys.* 127 (2007) 114105. doi:10.1063/1.2770708.

- [47] G.J. Martyna, M.L. Klein, M. Tuckerman, Nosé–Hoover chains: The canonical ensemble via continuous dynamics, *J. Chem. Phys.* 97 (1992) 2635–2643. doi:10.1063/1.463940.
- [48] J. Schmidt, J. VandeVondele, I.-F.W. Kuo, D. Sebastiani, J.I. Siepmann, J. Hutter, et al., Isobaric–Isothermal Molecular Dynamics Simulations Utilizing Density Functional Theory: An Assessment of the Structure and Density of Water at Near-Ambient Conditions, *J. Phys. Chem. B.* 113 (2009) 11959–11964. doi:10.1021/jp901990u.
- [49] M.J. McGrath, I.-F.W. Kuo, J.I. Siepmann, Liquid structures of water, methanol, and hydrogen fluoride at ambient conditions from first principles molecular dynamics simulations with a dispersion corrected density functional, *Phys. Chem. Chem. Phys.* 13 (2011) 19943. doi:10.1039/c1cp21890e.
- [50] C.W. Bunn, The crystal structure of long-chain normal paraffin hydrocarbons. The “shape” of the CH_2 group, *Trans. Faraday Soc.* 35 (1939) 482–491.
- [51] S. Kavesh, J.M. Schultz, Lamellar and interlamellar structure in melt-crystallized polyethylene. I. Degree of crystallinity, atomic positions, particle size, and lattice disorder of the first and second kinds, *J. Polym. Sci. Part -2 Polym. Phys.* 8 (1970) 243–276. doi:10.1002/pol.1970.160080205.
- [52] G. Avitabile, R. Napolitano, B. Pirozzi, K.D. Rouse, M.W. Thomas, B.T.M. Willis, Low temperature crystal structure of polyethylene: Results from a neutron diffraction study and from potential energy calculations, *J. Polym. Sci. Polym. Lett. Ed.* 13 (1975) 351–355. doi:10.1002/pol.1975.130130607.
- [53] T.L. Phillips, S. Hanna, Simulations of the mobile phase of polyethylene, *Polymer.* 46 (2005) 11035–11050. doi:10.1016/j.polymer.2005.09.019.
- [54] S. Abbate, M. Gussoni, G. Masetti, G. Zerbi, Infrared and Raman intensities of polyethylene and perdeuteropolyethylene by electro-optical parameters. Single chain, *J. Chem. Phys.* 67 (1977) 1519–1531. doi:10.1063/1.435036.
- [55] C. Castiglioni, M. Gussoni, G. Zerbi, Charge mobility in σ -bonded molecules: The infrared spectrum of polymethylene chains in the solid and liquid phases, *J. Chem. Phys.* 95 (1991) 7144–7149. doi:10.1063/1.461391.
- [56] R. Dovesi, V.R. Saunders, C. Roetti, R. Orlando, C.M. Zicovich-Wilson, F. Pascale, et al., *CRYSTAL14 User’s Manual*, University of Torino, Torino, 2014.
- [57] S. Grimme, J. Antony, S. Ehrlich, H. Krieg, A consistent and accurate ab initio parametrization of density functional dispersion correction (DFT-D) for the 94 elements H-Pu, *J. Chem. Phys.* 132 (2010) 154104. doi:10.1063/1.3382344.
- [58] G. Zerbi, Vibrational spectroscopy of very large molecules, *Adv. Infrared Raman Spectrosc.* 11 (1984) 301.

Chapter 5

Conclusions

In this thesis, we explored the potentialities and the reliability of different state-of-the-art computational techniques for the investigation of the structural and vibrational properties of complex macromolecular materials. In particular we wanted to verify if some powerful computational tools, seldom adopted in polymers science, could be employed to make a further step in quantum chemical modelling of molecular and polymeric materials, also in connection with practical, technological issues.

In this context, three tasks have been accomplished: i) the application of periodic DFT calculations through the CRYSTAL code to crystalline polymers ii) the development of theoretical models to investigate the molecular charge distribution, in the framework of the Equilibrium Charges and Charge Fluxes (ECCF) model, iii) the application of First-Principles Molecular Dynamics (FPMD) simulations for the description of small molecules in condensed phase and polymers.

An unambiguous and very accurate description of the structural and vibrational properties of several molecular and polymeric materials has been obtained, showing, in particular, that DFT calculations can be applied confidently to interpret the experimental data and to characterize in details complex molecular phenomena, such as, for example, polymorphism. The development of structure-properties correlations, the understanding of the behaviour of the material also in terms of its macroscopic properties and the rationalization of several physicochemical effects, require a molecular viewpoint which can be fully exploited by means of the proposed computational approach. In such a perspective intra- and intermolecular effects can be unrevealed and analyzed in details, and connected to macroscopic properties, as for example the polymorphism of even nylon or mechanical-induced transitions in PBT.

As a first outcome, our work demonstrated that DFT periodic calculations are a mature, well established and reliable technique, whose applications extend also to technological applications.

On the other hand, the study of the molecular dynamics by means of FPMD simulations should allow a more realistic description of the behaviour of molecular materials, paving the way toward a countless number of applications in the field of polymers science and characterization. Our investigation moved a first step in this direction, even if many open issues are still unsolved. Our results show that FPMD starts to be an intriguing choice for materials scientists. In particular, the possibility of taking into account external variables (e.g.

temperature, pressure...) is promising for future applications. In this context, we explored the application of this technique to molecular systems almost never approached before with FPMD; moreover we proposed some strategies to overcome some of the current limitations. The outcome of this thesis is two-fold. In the context of fundamental research we verified the potentialities of new methods and simulations tools never applied in some fields of materials science, such as polymers science. These tools allowed the description of some molecular properties (e.g. solid state packing, environmental effects...) which are mandatory to understand the behaviour of materials and which cannot be investigated by usual computational approaches.

On the other hand, our results open many perspectives in applied research and technology: quantum chemical calculations are finding more and more room in the industrial environment for their ability to give both a detailed interpretation of the experimental data, and also for possible design purposes. Indeed, the use of computational techniques to give a *priori* information useful for the design of new materials, is not only a future hope, but a real possibility and a few papers started to appear in the literature. Indeed, the high accuracy and reliability obtained, make quantum chemical methods suitable techniques for preliminary studies of newly designed materials, before their synthesis. For instance, the theoretical results can help to focus on the most promising molecules, inside a set of guess structures, thus lowering the costs associated to a time expensive experimental exploration on a wide variety of different chemical compounds.

In conclusion, we believe that the results reported in this thesis will contribute to practical applications in current technology, paving the way to an increasing employment of quantum chemical modelling in chemical and materials engineering.